INL/EXT-07-13078

HyPEP FY-07 Annual Report: A Hydrogen Production Plant Efficiency Calculation Program

C. H. Oh, INL
E. S. Kim, INL
S. R. Sherman, INL
R. Vilim, ANL
Y.J. Lee, KAERI
W.J. Lee, KAERI

September 2007

The INL is a U.S. Department of Energy National Laboratory
operated by Battelle Energy Alliance

INL/EXT-07-13078

HyPEP FY-07 Annual Report: A Hydrogen Production Plant Efficiency Calculation Program

C. H. Oh, INL
E. S. Kim, INL
S. R. Sherman, INL
R. Vilim, ANL
Y.J. Lee KAERI
W.J. Lee, KAERI

September 2007

Idaho National Laboratory
Idaho Falls, Idaho 83415

Prepared for the
U.S. Department of Energy
Under DOE Idaho Operations Office
Contract DE-AC07-05ID14517

ABSTRACT

The Very High Temperature Gas-Cooled Reactor (VHTR) coupled to the High Temperature Steam Electrolysis (HTSE) process is one of two reference integrated systems being investigated by the U.S. Department of Energy and Idaho National Laboratory for the production of hydrogen. In this concept the VHTR outlet temperature of 900 °C provides thermal energy and high efficiency electricity for the electrolysis of steam in the HTSE process. In the second reference system the Sulfur Iodine (SI) process is coupled to the VHTR to produce hydrogen thermochemically.

In the HyPEP project we are investigating and characterizing these two reference systems with respect to production, operability, and safety performance criteria. Under production, plant configuration and working fluids are being studied for their effect on efficiency. Under operability, control strategies are being developed with the goal of maintaining equipment within operating limits while meeting changes in demand. Safety studies are to investigate plant response for equipment failures. Specific objectives in FY07 were (1) to develop HyPEP Beta and verification and validation (V&V) plan, (2) to perform steady state system integration, (3) to perform parametric studies with various working fluids and power conversion unit (PCU) configurations, (4) the study of design options such as pressure, temperature, etc. (5) to develop a control strategy and (6) to perform transient analyses for plant upsets, control strategy, etc for hydrogen plant with PCU.

This report describes the progress made in FY07 in each of the above areas. (1) The HyPEP code numeric scheme and Graphic User Interface have been tested and refined since the release of the alpha version a year ago. (2) The optimal size and design condition for the intermediate heat exchanger, one of the most important components for integration of the VHTR and HTSE plants, was estimated. (3) Efficiency calculations were performed for a variety of working fluids for this reference design. (4) Efficiency improvements over the reference VHTR/HTSE plant were investigated for an alternative design that directly couples a High Temperature Steam Rankin Cycle (HTRC) to the HTSE process. Integration of the VHTR with SI process plants was begun. (5) Plant control studies showed that inventory control in the VHTR plant and flow control in the HTSE plant is effective in maintaining hot-side temperatures near constant during load change. (6) Dynamic calculations showed that thermal transients arising in the chemical plant are strongly damped at the reactor resulting in a stable combined plant.

CONTENTS

HyPEP FY-07 Annual Report: A Hydrogen Production Plant Efficiency Calculation Program

1. INTRODUCTION

1.1 Project Description

The Next Generation Nuclear Plant (NGNP), a very High temperature Gas-Cooled Reactor (VHTR) concept, will provide the first demonstration of a closed-loop Brayton cycle at a commercial scale of a few hundred megawatts electric and hydrogen production. The power conversion system (PCS) for the NGNP will take advantage of the significantly higher reactor outlet temperatures of the VHTR to provide higher efficiencies than can be achieved in the current generation of light water reactors. Besides demonstrating a system design that can be used directly for subsequent commercial deployment, the NGNP will demonstrate key technology elements that can be used in subsequent advanced power conversion systems for other Generation IV reactors. In anticipation of the design, development and procurement of an advanced power conversion system for the NGNP, the system integration of the NGNP and hydrogen plant was initiated to identify the important design and technology options that must be considered in evaluating the performance of the proposed NGNP. This study is part of DOE's Nuclear Hydrogen Initiative (NHI) Program and is intended to provide DOE with key information to support the process of making research and procurement decisions for the NGNP system integration.

The objective of the FY-07 study is (1) to develop HyPEP Beta, (2) to optimize PCU configurations, (3) parametric studies with various working fluids, (4) study of design options such as pressure, temperature, etc. (5) to develop control strategy and (6) to perform transient analyses for plant upsets, control strategy, etc for hydrogen plant with PCU.

HyPEP computer program will have the capability to model and to calculate the electrical generation efficiencies of a Brayton or Rankine cycle, and the hydrogen production efficiencies of the high temperature electrolysis and the S-I thermo-chemical cycles. The primary application of HyPEP will be for the VHTR (Very High Temperature Reactor) coupled to hydrogen production plant such as Nuclear Hydrogen Development and demonstration (NHDD). The principal applications for HyPEP are in the scoping analyses on plant configurations, and the optimizations on various design and operating parameters. HyPEP will be developed to enhance user friendliness. HyPEP will be available to support analyses for both the United States and Korean governments.

1.2 Background

The abundant cheap fossil energy resources such as oil and coal fuelled the great technological advances of the 19th and 20th that have dramatically improved the quality of human life. However, the massive use of fossil fuels has brought serious problems in pollution and global warming. In particular, if the current rate of oil usage is continued, the oil is forecasted to be depleted in the 21st century. The supply of high quality energy at a reasonable price is essential to maintain and improve the quality of life, and there is an urgent need to develop energy resources to replace oil.

Hydrogen is being promoted as the future energy-carrier under the proposed "hydrogen economy" scheme. Hydrogen is proposed to replace oil primarily in the transportation sector. Hydrogen may be burned in an Internal Combustion Engine (ICE) or oxidized in fuel cells to provide the motive power. Hydrogen is environmentally clean as the byproduct of hydrogen burn or oxidation is pure water.

Although hydrogen is the most abundant element in the universe, hydrogen in molecular form (H_2) does not exist in appreciable quantities on earth. Thus, it is necessary to produce molecular hydrogen from base materials such as water or methane using energy from such primary sources as coal, solar, wind or nuclear energy.

The Nuclear Hydrogen Initiative (NHI) calls for the demonstration of hydrogen production technologies utilizing nuclear energy. The goal is to demonstrate hydrogen production compatible with nuclear energy systems by ways of scaled demonstrations, and then to couple a commercial-sized demonstration plant with a Generation IV demonstration facility by approximately 2015. The process of producing the hydrogen from water is highly energy intensive and the efficiency of the process depends on different factors for different process. The high temperature electrolysis and the thermo-chemical cycles can produce hydrogen from water and these processes are being developed.

For the demonstration of hydrogen generation using nuclear power, the INL (Idaho National Laboratory) in the US, and KAERI (Korea Atomic Energy Research Institute) in the Republic of Korea have proposed the development of the VHTR (Very High Temperature Reactor) and the NHDD (Nuclear Hydrogen Development and Demonstration), respectively. The potential layouts of the VHTR and NHDD are shown in Figure 1 and Figure 2.

Both plants use the VHTR (Very High Temperature Reactor) to supply the power, while they are designed to use two different hydrogen production processes; the high temperature electrolysis and the S-I thermo-chemical process. The VHTR is used because the high temperature is essential in maximizing the hydrogen production efficiencies for both electrolysis and the thermo-chemical process.

In order to optimize the design of such plant systems as VHTR and NHDD, it is necessary to be able to evaluate the operating parameters and production efficiencies of various design layouts. The presently proposed project aims to develop a computer program HyPEP to easily and quickly evaluate the efficiencies and the operating parameters.

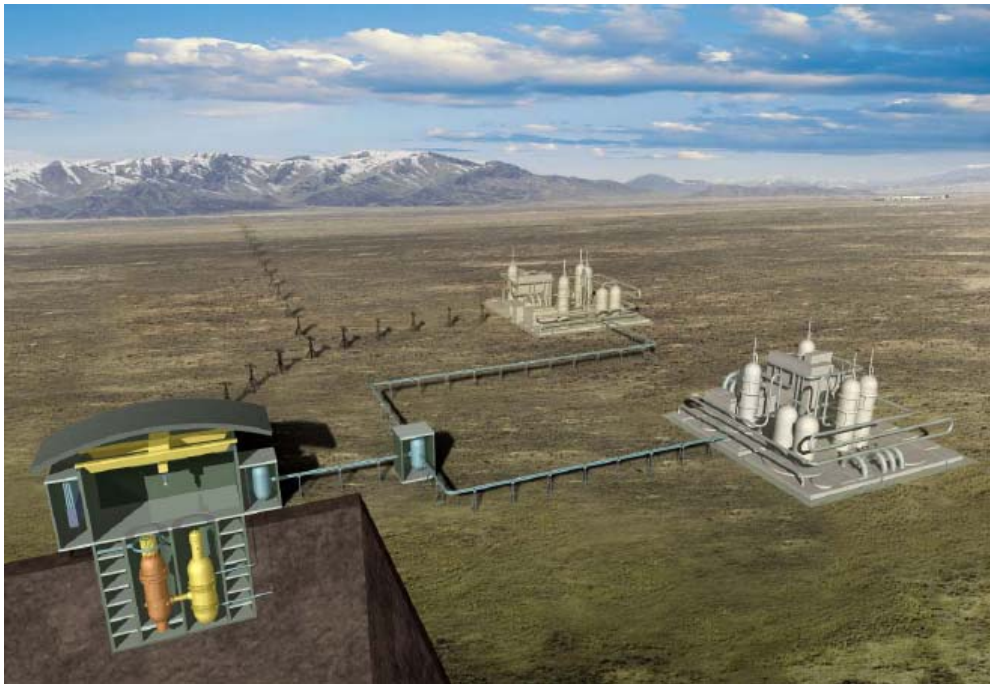

Figure 1 Potential Layout of VHTR for Hydrogen Production.

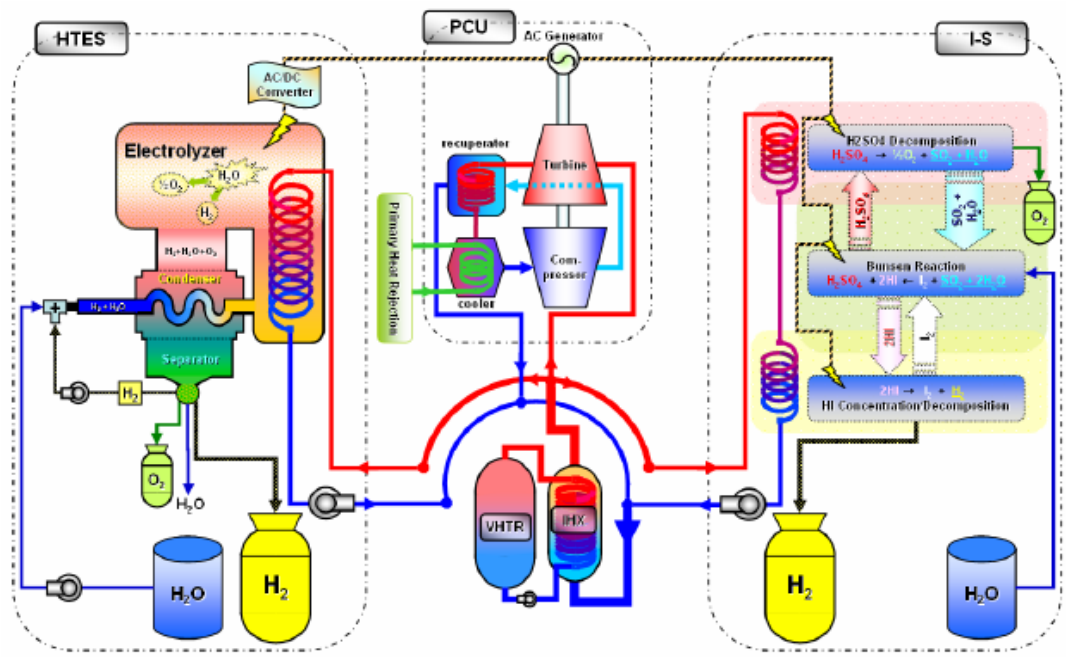

Figure 2 Potential Layout of Proposed NHDD Plant.

2. HyPEP BETA DEVELOPMENT

2.1 Overview

The HyPEP (Hydrogen Production Efficiency Calculation Program) is conceived to calculate the hydrogen production efficiencies for different hydrogen production facility layouts. HyPEP aims to rapidly evaluate the overall hydrogen efficiencies for plant configurations that are built on-screen by the user.

The final version of the HyPEP will have simplified models and components with sufficient sophistication to allow build-up of complex plant layouts with multiple hydrogen producing systems configured in parallel or in series. In addition, a basic cost-analysis and the component sizing models will be incorporated to allow rudimentary estimation of the hydrogen production cost.

The HyPEP is being developed in three stages, and the three stages are represented by HyPEP alpha, HyPEP beta, and the HyPEP V1.0 versions. The alpha version is basically the test bed for the program developers and it is very limited in capability. Main purpose of the alpha version is to 1) examine whether the overall program structure is sound, 2) design the Graphic User Interface (GUI) and the T/H system build up logic of the HyPEP code, and 3) provide the platform on which to develop and test the conceptual numerical scheme and 4) provide the platform on which the model developers can test their numerical models. The development of the alpha version of HyPEP concluded successfully at the end of September 2006.

Following the HyPEP alpha, the next development version is the HyPEP beta. In the HyPEP beta, the major developmental effort are; 1) bug-fixing and refinement of the GUI, 2) further development of the algorithms to accomplish the system on-screen build-up, 3) ascertain and demonstrate the capability of the HyPEP GUI to correctly model the system, 4) the installation of numerical solution scheme for the flow-network. The HyPEP beta is expected to be completed in the October, 2007.

The HyPEP beta will be used, in the final year (2007.10 ~ 2008.10), as the platform to 1) refine and finalize the numerical solution scheme, 2) carry out modeling of the hydrogen production plant system to calculate the hydrogen production efficiencies, 2) test numerical performance through Verification & Validation, 3) provide platform on which to incorporate the component sizing model and the cost analysis model.

The final version of HyPEP will be capable of:

1) The evaluation of:
   - - hydrogen production efficiency of the thermo-chemical processes
   - - hydrogen production efficiency of the electrolysis processes
   - - electricity generation efficiency
2) The assessment of the component sizing for major components of the plant.
3) The estimation of the plant construction cost.

The primary application area of HyPEP will be the scoping analysis for plant layout optimizations. The HyPEP is not conceived to be used for applications in plant transient analyses.

The HyPEP is being designed in such a way to allow flexible modeling of the hydrogen production plant layouts. For the Input/Output interface, major emphases are placed on the use of the GUI features to make the HyPEP a very user-friendly application program. The user will be able to construct most of the desired simulated plant system ‘on-screen’ using the plant system canvas of the HyPEP. For this, the GUI

will provide various component/system palettes consisting of multiple pages of basic and pre-made components or sub-systems. The conceptual schematic layout of the canvas and the component/sub-system layout are shown in Figure 2-1.

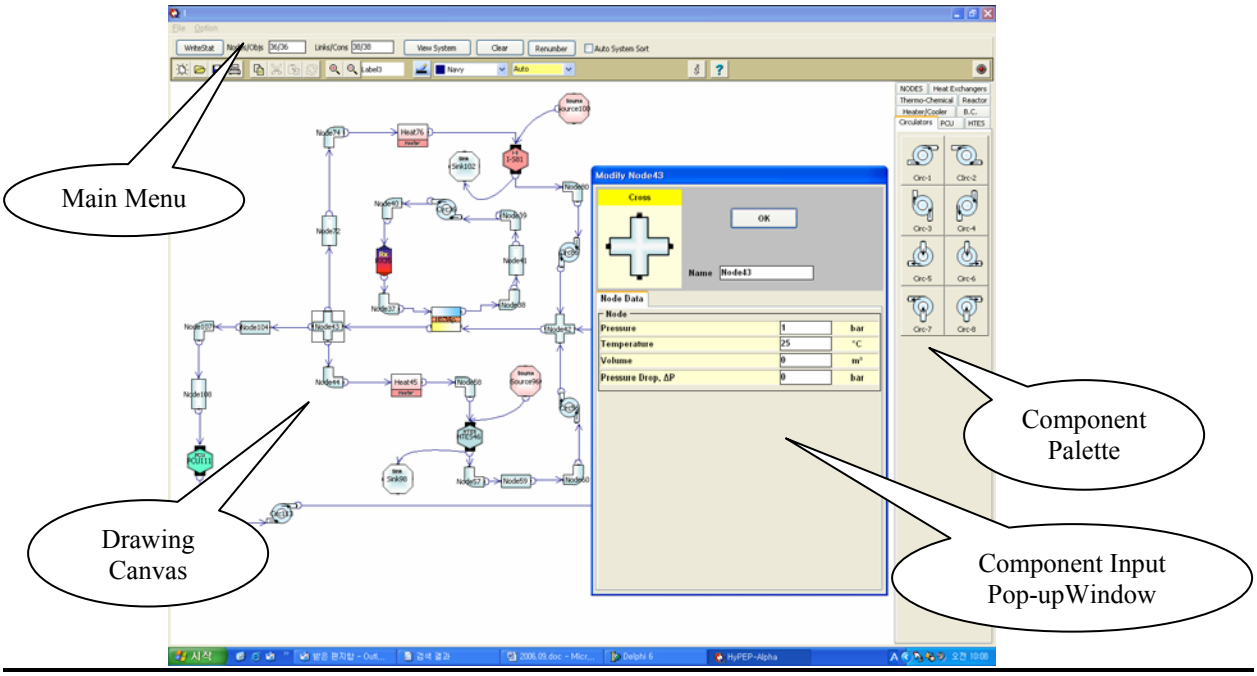

Figure 2-1. Basic Layout of the HyPEP Program.

2.2 Formulation of Flow Network

In order to calculate the hydrogen production and the hydrogen production efficiencies of a plant, it is necessary to first evaluate the thermo-dynamic states of, and the flows between the components that make up the plant system. Thus it becomes necessary to setup the flow network representing the system under evaluation.

The basic concepts for the thermal hydraulic formulation for the HyPEP program were established during the HyPEP alpha development. In the HyPEP, the flow network is used to establish the thermo-dynamic conditions and the flow conditions of the components that make up the system. In order to establish these conditions, the thermo-dynamic equations expressing the conservations in the mass, energy and the momentum need to be set-up.

These equations are then discretised to evolve a numerical solution scheme suitable for programming. The models for the flow network of multi-species fluid systems have also been incorporated by making the single phase fluid to be a mixture of a number of fluids. The flow network itself is made up of systems and components.

The numerical scheme of the HyPEP has been formulated based on the node-link-heat block component system. These components are the basic building block to construct the numerical representation of the Flow/Heat Network of the plant systems. The node component represents the thermal-hydraulic volume with scalar properties such as volume, mass, molar or mass fraction of fluid specie, energy, pressure, temperature, and pressure drops. To handle the chemical reactions that can occur in a node, specialized node components which is derived from the normal node component, is used? The link component

represents the flow path between nodes and has such properties as mass flow rate, pressure drop, and scalar properties of the donor-node. The heat block component represents the solid structures that conduct or generate heat. The heat block component also provides the solid-to-fluid boundaries where convection occurs.

The basic equations consider the steady-state mass and energy transport of reactive single species fluid mixtures. The equations have been setup to conserve mass and energy. A simplified momentum balance equation is also used. For the hydrogen production systems, the HyPEP needs to consider mass and energy conservation of multi-species fluid that undergoes chemical reactions. Thus the equations are extended to multi-species by incorporating the fluid composition make-up in the form of molar-fractions in the properties (variables) of the node component object. In the HyPEP beta, the mixture properties are evaluated using the property routines. The thermo-dynamic tables for the fluid mixtures have been setup for the following fluids:

Hydrogen	(gas)
Water	(liquid)
Steam	(gas)
Oxygen	(gas)
Carbon dioxide	(gas)
Air	(gas)
Nitrogen.	(gas)

With the basic equations, the numerical scheme has been devised to ensure conservation of the mass and energy of the systems and components. The numeric solver has been developed principally for the steady-state operation but with the provisions for further extension that may include mild transient calculations.

The flow net of HyPEP contains most major components associated with the hydrogen generation facility. The user can build the electronic representation of the flow net using the Flow Net Builder which processes the user-specified component data and the boundary conditions.

The Solution Matrix Generator, then, utilizes the electronic flow net and produces the solution matrix which is determined by the discretized form of the flow governing equation. The temporal part of the discretized governing equation is able to characterize the transient behavior of the flow net. However, for the steady-state condition, the flow net is solved by using solely the spatial part. The Solution Matrix Generator is able to generate both the temporal and the spatial parts from the information of the electronic flow net. The Flow Net Solver employs solving techniques which can be categorized by: 1. the iteration of the solution matrix 2. the direct inversion of the solution matrix 3. the iteration with minor flow modifiers.

The diagonal dominance of the solution matrix, therefore, should be checked before choosing the solution strategy. Most of flow net with simple topology will exhibit diagonal dominance. For the flow net of complex topology, the iterative method may not be used. When the solution matrix does not show diagonal dominance, the Solution Strategy Chooser will pick the direct inversion or the iterative method with minor flow modifier.

After all the thermodynamic conditions are calculated, the production and the consumption in each component for hydrogen, electricity and the heat are evaluated to assess the plant hydrogen production efficiency.

2.2.1 Conservation Equations

The HyPEP beta uses the following set of continuity equations as the basic field equations :

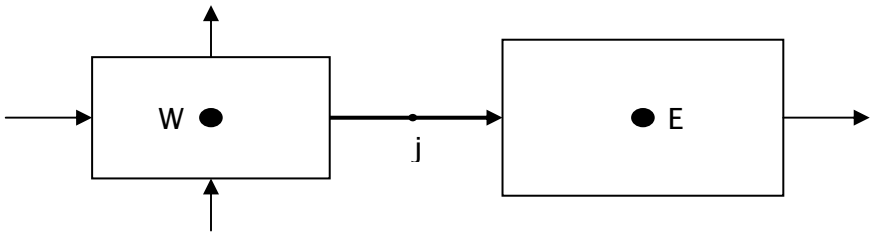

Mass Continuity (for node)

$$V\frac{\partial \rho}{\partial t} = \sum_{j=1}^{N_j} \tilde{\rho}_j A_j \, u_j + S_m V \tag{2-1}$$

Energy Continuity (for node)

$$V\frac{\partial (\rho h)}{\partial t} = \sum_{j=1}^{N_j} \tilde{\rho}_j \tilde{h}_j A_j \, u_j + S_h V \tag{2-2}$$

Momentum Balance Equation (for link j);

$$\frac{\partial (\rho u)}{\partial t} + \frac{\partial (\rho u^2)}{\partial x} + \frac{\partial P}{\partial x} = \Delta P_{K,source} + \Delta P_{extra} - \frac{f_T \, \rho_j \, \tilde{u}^2}{2 \cdot \Delta x} \tag{2-3}$$

where

V = *volume of node* (m^3)

u = *fluid velocity* (m/s)

ρ = *density* (kg/m^3)

$\tilde{\rho}$ = *density of donor node* (kg/m^3)

h = *enthalpy* $(Joule/kg)$

$\tilde{h}$ = *enthalpy of donor node* $(Joule/kg)$

f_T = *total flow resistance* $(form + friction + drag + ...)$

$\Delta P_{K,source}$ = *pressure source such as from pumps or circulators*

ΔP_{extra} = *other pressure gain (or loss) e.g. gravity*

A_j = *flow area of link* (m^2)

N_j = *Total number of links connected to a given node* $(N_j > 0)$

S_m = *volumetric mass generation rate* $(kg/m^3/s)$

S_h = *volumetric enthapy generation rate* $(kg/m^3/s)$

In the HyPEP alpha a simple flow relationship equation had been proposed to be used. However, during the numerics testing, it was found that the particular numeric formulation resulted in frequent program failure due to "division by zero" error. This error was traced to be caused by the velocity term in the denominator having the value of zero. Thus the momentum balance equation for a single phase gas has been re-written to follow the momentum conservation format and adopted for the HyPEP beta in place of the simple flow relation equation used in the HyPEP alpha.

2.2.2 Numerical Solution Scheme

A numerical solution for the HyPEP is based on simultaneously solving the mass, energy and momentum continuity or conservation equations. The 3 continuity equations are set up for a compressible fluid working well below the critical flow regimes. Also, the fluid should not change its phase through boiling or condensation. Thus, the fluid in HyPEP is basically a gas-like fluid which is compressible.

Three conservation equations are setup and the number of unknowns are 4 variables which are the pressure P, enthalpy h, velocity u, and density ρ . The thermodynamic relationship of the fluid is used to correlate the density ρ in terms of pressure and enthalpy.

The conservation equations are discretised into numerically more convenient forms. At present, the temporal terms are retained and the numerical derivations preserve the temporally changing terms. The solution is actually carrying out the transient calculations until a steady-state is achieved. This was adopted because of the possibility of expanding the HyPEP into a transient capable program. The density ρ is linearly expanded using the Taylor expansion.

The equations are manipulated to eventually yield a system of linear equations, in a matrix form, with the pressures of the nodes as the variable to calculate. The coefficients of the pressure matrix are evaluated in the 'old time step' to eliminate complexities arising from having an implicit solution scheme.

The detailed account of the HyPEP numerical scheme is described in the following.

Firstly, the mass continuity equation 2-1 is discretized as follows where subscript index i represents the node and the j the link connected to the node:

$$\frac{V_i}{\Delta t}\left(\rho_i^{n+1}-\rho_i^n\right)=\sum_{j=1}^{N_j}\tilde{\rho}_j^n A_j\, u_j^{n+1}+S_{m,i}^n V_i \tag{2-4}$$

The energy continuity equation 2-2 is discretized as:

$$\frac{V_i}{\Delta t}\rho_i^n\left(h_i^{n+1}-h_i^n\right)+\frac{V_i}{\Delta t}h_i^n\left(\rho_i^{n+1}-\rho_i^n\right)=\sum_{j=1}^{N_j}\tilde{\rho}_j^n\tilde{h}_j^n A_j\, u_j^{n+1}+S_{h,i}^n V_i \tag{2-5}$$

Taylor expansion of the density ρ in terms of pressure P and enthalpy h, and approximate to first order terms gives :

$$\rho_i^{n+1} = \rho_i^n + \left(\frac{\partial \rho}{\partial h}\right)_i^n \left(h_i^{n+1} - h_i^n\right) + \left(\frac{\partial \rho}{\partial P}\right)_i^n \left(P_i^{n+1} - P_i^n\right) \tag{2-6}$$

Substituting the Taylor expanded density of Equation 2-6 into the mass continuity Equation 2-4 gives :

$$\frac{V_i}{\Delta t}\left[\left(\frac{\partial \rho}{\partial h}\right)_i^n \left(h_i^{n+1} - h_i^n\right) + \left(\frac{\partial \rho}{\partial P}\right)_i^n \left(P_i^{n+1} - P_i^n\right)\right] = \sum_{j=1}^{N_j} \tilde{\rho}_j^n A_j \, u_j^{n+1} + S_{m,i}^n V_i$$

Rearranging the above equation gives :

$$\frac{V_i}{\Delta t}\left(\frac{\partial \rho}{\partial h}\right)_i^n \delta h_i^{n+1} + \frac{V_i}{\Delta t}\left(\frac{\partial \rho}{\partial P}\right)_i^n \delta P_i^{n+1} = S_{m,i}^n V_i + \sum_{j=1}^{N_j} \tilde{\rho}_j^n A_j \, u_j^{n+1} \tag{2-7}$$

where

$$\delta h_i^{n+1} = h_i^{n+1} - h_i^n$$

$$\delta P_i^{n+1} = P_i^{n+1} - P_i^n$$

Carrying out the similar substitution in Equation 2-5 and re-arranging gives :

$$\frac{V_i}{\Delta t}\rho_i^n \delta h_i^{n+1} + \frac{V_i}{\Delta t} h_i^n \left(\left(\frac{\partial \rho}{\partial h}\right)_i^n \delta h_i^{n+1} + \left(\frac{\partial \rho}{\partial P}\right)_i^n \delta P_i^{n+1}\right) = S_{h,i}^n V_i + \sum_{j=1}^{N_j} \tilde{\rho}_j^n \tilde{h}_j^n A_j \, u_j^{n+1}$$

$$\text{or, } \frac{V_i}{\Delta t}\left[\rho_i^n + h_i^n \left(\frac{\partial \rho}{\partial h}\right)_i^n\right] \delta h_i^{n+1} + \frac{V_i}{\Delta t} h_i^n \left(\frac{\partial \rho}{\partial P}\right)_i^n \delta P_i^{n+1} = S_{h,i}^n V_i + \sum_{j=1}^{N_j} \tilde{\rho}_j^n \tilde{h}_j^n A_j \, u_j^{n+1} \tag{2-8}$$

The equations 2-7 and 2-8 represent the numerically convenient equation form as used in the HyPEP code and these Equations are expressed in a Matrix form as follows :

$$\begin{bmatrix} a_{11} & a_{12} \\ a_{21} & a_{22} \end{bmatrix} \bullet \begin{bmatrix} \delta h_i^{n+1} \\ \delta P_i^{n+1} \end{bmatrix} = \begin{bmatrix} S_1 \\ S_2 \end{bmatrix} + \sum_{j=1}^{N_j} \left\{ \begin{bmatrix} C_{1j} \\ C_{2j} \end{bmatrix} u_j^{n+1} \right\} \tag{2-9}$$

where

$$a_{11} = \frac{V_i}{\Delta t}\left(\frac{\partial \rho}{\partial h}\right)_i^n, \qquad a_{12} = \frac{V_i}{\Delta t}\left(\frac{\partial \rho}{\partial P}\right)_i^n$$

$$a_{21} = \frac{V_i}{\Delta t}\left[\rho_i^n + h_i^n \left(\frac{\partial \rho}{\partial h}\right)_i^n\right], \qquad a_{22} = \frac{V_i}{\Delta t} h_i^n \left(\frac{\partial \rho}{\partial h}\right)_i^n$$

$$S_1 = S_{m,i}^n V_i, \qquad S_2 = S_{h,i}^n V_i$$

$$C_{1j} = \tilde{\rho}_j^n A_j, \qquad C_{2j} = \tilde{\rho}_j^n \tilde{h}_j^n A_j$$

Equation 2-9 can be re-written as

$$[A]\bullet\begin{bmatrix}\delta h_i^{n+1}\\ \delta P_i^{n+1}\end{bmatrix}=\begin{bmatrix}S_1\\ S_2\end{bmatrix}+\sum_{j=1}^{N_j}\left\{\begin{bmatrix}C_{1j}\\ C_{2j}\end{bmatrix}u_j^{n+1}\right\} \tag{2-10}$$

Find inverse of [A] and multiplying both sides :

$$\begin{bmatrix}\delta h_i^{n+1}\\ \delta P_i^{n+1}\end{bmatrix}=[A]^{-1}\bullet\begin{bmatrix}S_1\\ S_2\end{bmatrix}+\sum_{j=1}^{N_j}\left\{[A]^{-1}\bullet\begin{bmatrix}C_{1j}\\ C_{2j}\end{bmatrix}u_j^{n+1}\right\}$$

$$or,\quad \begin{bmatrix}\delta h_i^{n+1}\\ \delta P_i^{n+1}\end{bmatrix}=\begin{bmatrix}\sigma_1\\ \sigma_2\end{bmatrix}+\sum_{j=1}^{N_j}\left\{\begin{bmatrix}\phi_{1j}\\ \phi_{2j}\end{bmatrix}u_j^{n+1}\right\} \tag{2-11}$$

where

$$[A]^{-1}=\begin{bmatrix}\alpha_{11} & \alpha_{12}\\ \alpha_{21} & \alpha_{22}\end{bmatrix},\qquad \begin{bmatrix}\sigma_1\\ \sigma_2\end{bmatrix}=[A]^{-1}\bullet\begin{bmatrix}S_1\\ S_2\end{bmatrix},\qquad \begin{bmatrix}\phi_{1j}\\ \phi_{2j}\end{bmatrix}=[A]^{-1}\bullet\begin{bmatrix}C_{1j}\\ C_{2j}\end{bmatrix}$$

Collecting pressure terms only,

$$\delta P_i^{n+1}=\sigma_2+\sum_{j=1}^{N_j}\left\{\phi_{2j}\,u_j^{n+1}\right\} \tag{2-12}$$

Now Equation 2-3 can be discretized and re-written as

$$\begin{aligned}u_j^{n+1} &= u_j^n+\frac{\Delta t}{\Delta x_j}\left[P_{from,j}^{n+1}-P_{to,j}^{n+1}\right]+\frac{\Delta t}{\Delta x_j}\left[\Delta P_{from,source,j}+\Delta P_{extra,j}-(1+f_T)\frac{\rho_j\,\tilde{u}^2}{2}\right]\\ &= \frac{\Delta t}{\Delta x_j}\left[(P_{from,j}^{n+1}-P_{from,j}^{n})-(P_{to,j}^{n+1}-P_{to,j}^{n})\right]\\ &\quad +u_j^n+\frac{\Delta t}{\Delta x_j}\left[(P_{from,j}^{n}-P_{to,j}^{n})+\Delta P_{from,source,j}+\Delta P_{extra,j}-(1+f_T)\frac{\rho_j\,\tilde{u}^2}{2}\right]\\ &= \eta_j(\delta P_{from,j}^{n+1}-\delta P_{to,j}^{n+1})+\theta_j\end{aligned} \tag{2-13}$$

where

$$\eta_j=\frac{\Delta t}{\Delta x_j}$$

$$\theta_j=u_j^n+\eta_j\left[(P_{from,j}^{n}-P_{to,j}^{n})+\Delta P_{from,source,j}+\Delta P_{extra,j}-(1+f_T)\frac{\rho_j\,\tilde{u}^2}{2}\right]$$

Substitute Equation 2-13 into Equation 2-12 gives Pressure Equations for a node :

$$\delta P_i^{n+1}=\sigma_{2i}+\sum_{j=1}^{N_j}\left\{\phi_{2j}\left(\eta_j(\delta P_{from,j}^{n+1}-\delta P_{to,j}^{n+1})+\theta_j\right)\right\}$$

$$or, \quad \delta P_i^{n+1} - \sum_{j=1}^{N_j} \left\{ \phi_{2j} \eta_j (\delta P_{from,j}^{n+1} - \delta P_{to,j}^{n+1}) \right\} = \sigma_{2i} + \sum_{j=1}^{N_j} \phi_{2j} \theta_j \tag{2-14}$$

Using Equation 2-14, setup (n x n) Pressure Matrix and solve for pressure.
then, use Equation 2-13 to calculate new velocity as :

$$u_j^{n+1} = \eta_j (\delta P_{from,j}^{n+1} - \delta P_{to,j}^{n+1}) + \theta_j \tag{2-15}$$

With new velocity and Equation 2-12, calculate new enthalpy :

$$\delta h_i^{n+1} = \sigma_1 + \sum_{j=1}^{N_j} \left\{ \phi_{1j} \; u_j^{n+1} \right\} \tag{2-16}$$

All unknown variables have been calculated for the new time step.
Using new variables, thermal hydraulic states at the new time step can be calculated.

The time step calculations are repeated until satisfactory convergence in pressure and enthalpy are achieved. The single fluid equations are used/extended to multi-specie fluid equation by considering the molar fractions and the partial pressures.

2.3 Component Models

2.3.1 Overview

The HyPEP program has been designed and written with hierarchical program and the data structures. The major systems and components of hydrogen productions had been identified and these were categorized during HyPEP alpha development as shown in Figure 2-2. The categorization was used to establish the hierarchical system and component structure which defines the thermal-hydraulic processes and phenomena that need to be considered in HyPEP. Thusly, the basis of the plant modeling of HyPEP has been established and the established modeling basis has been used to design the component/system palette.

The hierarchical form of program/data structure is well suited to take advantages of the Object Oriented Programming (OOP) techniques described by Bertrand Meyer [1997], and from the beginning the HyPEP has been programmed with the OOP techniques. In the development of HyPEP beta, the categorized components and the systems have been incorporated into the program structures in such a way that the components and the sub-systems of the simulated plant system are represented one-to-one by the ‘objects’ in the program.

For the nuclear hydrogen production facility, the major system components that form the top-tier hierarchical group were identified and included the Reactor System for the generation of nuclear power, Power Conversion Unit (PCU) for the electricity generation, and the High Temperature Electrolysis System (HTES) and Thermo-Chemical System (TCS) for the hydrogen generation.

The top-tier components contain sub-systems and/or components. The Reactor system includes as its sub-systems and components, the pebble type VHTR, prismatic type VHTR, Intermediate Heat Exchanger (IHX), and gas circulator. The PCU system includes the Brayton cycle, Rankine cycle, and electricity generator. The Brayton cycle includes gas compressors, gas turbines, a recuperator and coolers. The Rankine cycle includes steam generator, steam turbine, condenser, pump, reheating and superheating

circuits. The HTES will include heat exchangers, electrolyser, AC-DC converter, condenser, separator, gas circulator, and water pump. For the current project, the TCS will only consider the I-S thermo-chemical process. The I-S thermo-chemical process will include the H_2SO4 decomposition unit, Bunsen reaction unit, HI concentration/decomposition unit, gas circulator, water pump and heat exchangers.

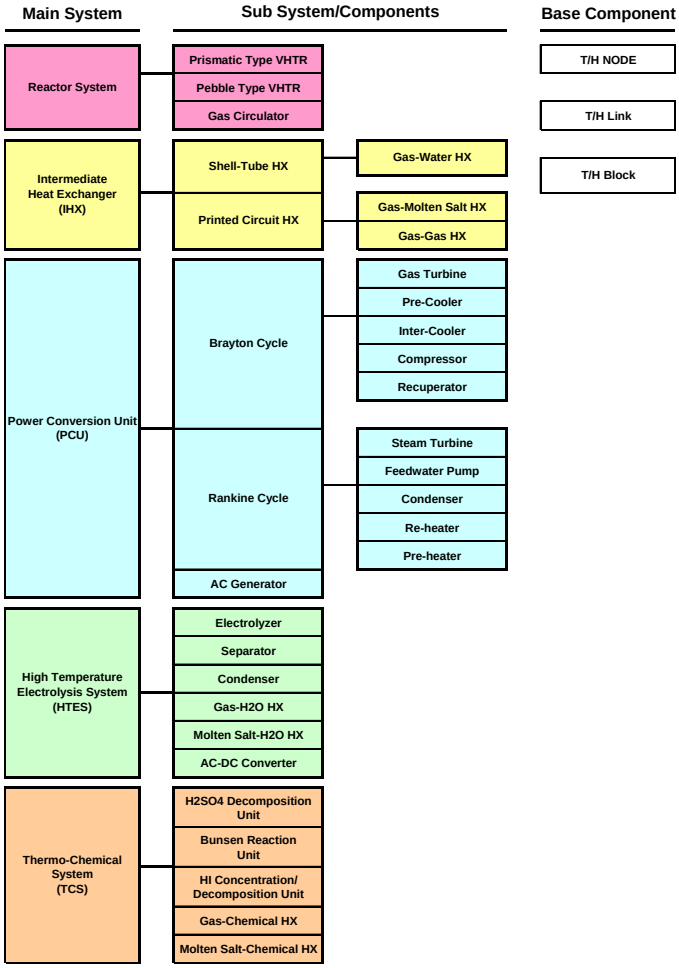

Figure 2-2 The Hierarchy of Components and System Models of HyPEP.

One of the major functional requirements for the HyPEP is the flexible system build up, and thus, the HyPEP beta has been developed with the emphasis on easy and flexible plant system layout modeling. To facilitate the user friendly and flexible plant configuration modeling, the HyPEP has been programmed with extensive GUI (Graphic User Interface) features such as; 1) the provision of the drawing canvas on-which user can build-up the system graphically on-screen, 2) the functionality of drag-dropping the components onto the drawing canvas for easy system build-up, 3) the provision of on-screen GUI based input templates for easy input entry and modification whilst minimizing the input error, 4) on-screen connection of components to eliminate the connection errors that commonly occur in the text-based input, etc. The foundations for the GUI features of HyPEP program was established during the HyPEP alpha development, and during the beta development, mostly the bug-fixing has been carried out.

With these GUI features of the HyPEP beta, the user can select components or sub-systems from the palettes to build up the plant configuration using the drag/drop/connect feature. The components are designed to have a hierarchical structure, for example, the top-tier palette may contain VHTR, IHX, PCU,

HTES and I-S components. These top-tier components will each be able to contain sub-components such as circulators, heat exchangers, electrolyzer, etc. General purpose components such as heat exchangers, nodes, links, and blocks will also be provided. The program will employ a graphic user interface extensively to enhance the user friendliness in modeling the system, preparing the input and to view the results. The system will be built by drag-dropping a component from the palette to the drawing canvas and then connecting them using the link component. Each primitive component (TNode and TLink) will have, associated with it, an on-screen input window to configure the component in detail.

The main work is to develop detailed thermal-hydraulic models for the components and to incorporate these into the model palette for the drag-drop-connect scheme to work. In order to realize such scheme, the OOP language was deemed best suited resulting in the selection of the Delphi programming language for the HyPEP development. The inheritance and the polymorphism features of the OOP language has greatly facilitate the creation and development of the hierarchical component system for numerics as well as the GUI.

2.3.2 Basic Components

The basic components represent the simplest components that have the necessary modeling capabilities. Thus, a simple thermo-dynamic system can be constructed using only the base components. These include the node, link and the heat block components. These base components are the top-most ancestor to other 'derived' components.

A. Node component (TNode)

A node component represents a volume of fluid having scalar properties such as the pressure, temperature, density, enthalpy, molar composition, etc. Physical modeling of a node is defined by the volume, length, the in-flows, the out-flows, and the heat input and outputs from heat blocks.

In the program, the node component is modeled using the TNode class in the OOP language. The TNode component contains the properties and the methods needed in the thermo-dynamic calculations as well as for the GUI manipulation.

The node object class is derived from the object class 'TdxfcObject' by inheritance. TdxfcObject is a member object of the Drawing Canvas object and it presents the basic graphic building blocks of a flow network. Each TdxfcObject can have its own location, size, shape, color, bitmap image, text and font in the drawing canvas. Any TdxfcObject can be linked with other TdxfcObjects via TdxfcConnection object. Thus, building the GUI system with TNode results in the 'automatic' creation of visual graphical object (as TdxfcObject) in the drawing canvas whose properties and methods can be accessed as the intrinsic properties and methods of the TNode object. At the same time a thermo-dynamic node is also created. This way of deriving the node object from the GUI was used effectively to ensure that 1-to-1 correspondence can be reliably made between the numerical T/H objects and the visual GUI objects.

More detailed descriptions are to be found in subsection 2.4.2 Component Object Class Definitions.

B. Link component (TLink)

A link component represents the flow paths between the node type components. The T/H properties of the link component include the fluid flow rates, and the pressure drop. The link component connects to the inlet or the outlet ports of the node-type components. The physical modeling of a link component is defined by the from-node, to-node, and the flow area. The fluid composition of the from-node and the to-node should be identical (i.e., no chemical reaction or heat exchanges in the link component).

The link component is modeled using the TLink class in the OOP language. TLink object class is derived from the 'TdxfcConnection' object of the drawing canvas by inheritance. TdxfcConnection object is a line that generally links two TdxfcObjects. Each connection can have its own line style and width, drawing style, color, and up to two arrow shapes. Additionally, it can have any number of intermediate points to build a line. Within the properties of a TLink object are the from-node (srcNode) and the to-node (destNode).

In the fashion similar to the TNode object, the TLink object has a 1-to-1 correspondence with the visual object in the drawing canvas. Thus, the visual and the T/H correspondence for the link component can be reliably made with minimum to no programming.

More detailed descriptions are to be found in subsection 2.4.2 Component Object Class Definitions.

C. Heat block component (THeatBlock)

A heat block component represents the solid structure that thermally interacts with the fluids. The heat exchanger tubes, reactor vessel walls, heaters, heat losses are represented by the heat block component. The heat block component is modeled using the THeatBlock class in the OOP language. The physical modeling of the heat block component includes the heat generated or taken away (all of which is given to the connected Node objects), temperature, connected node (2 nodes in the case of heat block of a heat exchanger), thermal conductivity, density, and specific heat capacity.

Unlike the TNode or the TLink objects, the THeatBlock object is not derived from any graphical object. Thus, there is no 1-to-1 correspondence between the Heat Block and graphical component, and such correspondence is not required. Because, in HyPEP program, heat block component is included in the TNode type components and their derivatives and there is no stand-alone single heat block component.

More detailed descriptions are to be found in subsection 2.4.2 Component Object Class Definitions.

D. TH System component (TSystem)

A TH System component represents the connected nodes and links that form a complete T/H system. A T/H system as defined in this regard is the collection of all the components (excluding the heat block and its derived components) that are connected fluid-wise and therefore share the fluid. The system component contains all the necessary fluid details to carry out the TH numerical calculations.

There may be more than one system in the overall plant, and any two systems may be thermally connected via the heat block component. As an example, the primary system of a reactor system can form the first TH system whereas the secondary system can form the second system. The two systems are connected via the Heat Exchanger (Steam Generators in PWRs, IHX in Gas Cooled Reactors). In numerical sense, each system forms a pressure solution matrix of size N×N where N is the total number of the node component in any given system.

In the HyPEP program, the TSystem object is created when a new T/H system is found. The TSystem component includes 1) an array of TNode components, 2) an array of TLink components, and 3) a pressure Matrix. The TSystem object in HyPEP beta has just 2 methods which are TSystem.SetupMatrix, and TSystem.Solve_P_Matrix. The two methods are used to setup and solve the system's pressure matrix. The part of the calculation of T/H parameters required in the matrix and the numerical schemes is carried out by the TNode and TLink components.

2.3.3 Other Components

A. Chemical node component (TChemNode)

A chemical node component models the components where chemical reaction can occur. The chemical node is modeled using the TChemNode class created by inheritance from the TNode class. Thus, TChemNode can be regarded as a special component of a node component able to model chemical reaction.

In the TChemNode component the mass and energy fractions of the fluid species are allowed to change. This component can be used to model such component/system as the electrolyzer of the high temperature electrolysis unit, and the Bunsen reaction, H2SO4 decomposition, and the HI decomposition units of the I-S thermo-chemical unit. The simplified sub-system components for the HTES and I-S components where specific models are pre-coded for can be used for major chemical reactions occurring in the hydrogen production.

In addition to the inputs required for the node component, the chemical reactions that occur in this component need to be defined and supplied by the user especially the chemical formulae and the energies of the reactions.

The development of this component has not been completed as of this writing.

B. Reactor component (TReactor)

The reactor component models the nuclear reactor and the component includes the specialized components for the pebble bed reactors and the prismatic reactors. For the hydrogen production efficiencies, the main differences of the reactor systems to consider are the core and vessel pressure drops. The pebble bed reactor component and the prismatic reactor component have the empirically derived correlations suitable to each design for estimating the core and vessel-wide pressure drops. The reactor component object 'TReactor' is derived from the TNode object using the inheritance and has a heatblock component as a member. Thus, it consists of a node component that represents reactor volume, and a heat block component to provide the nuclear power.

C. Gas circulator component (TGasCirculator)

The gas circulator component is a specialized model component with the empirical correlation to calculate the power requirements and the developed pumping head. The gas circulator component is described in the HyPEP program by the 'TGasCirculator' object. The TGasCirculator object is derived from the TNode component by inheritance

User inputs include the adiabatic efficiency of the circulator, the mass flow rates and others inputs needed for the estimation of the sizing and the cost.

The pumping work required for the gas-circulator can be given by the following simplified equation:

$$\dot{W}_{CP} = \frac{1}{\eta_{CP}} \dot{m} c_p T \left[\left(r_p^{CP} \right)^{\frac{\gamma - 1}{\gamma}} - 1 \right]$$

where $\dot{W}_{CP}$ required work for compressor

c_p specific heat at constant pressure
$\dot{m}$ mass flowrate
r_p^{CP} pressure ratio (= P_{out}/P_{in})
γ the ratio of specific heats (= c_p/c_v)
η_{CP} adiabatic efficiency of compressor

D. Heat Exchanger Components (THeatX)

A wide variety of heat exchanger types can be installed in a nuclear hydrogen production system. The 'THeatX' component is the base heat exchanger component and contains the data and the methods of a generic heat exchanger. The THeatX component consists of two node components representing primary and the secondary side volumes, and a heat block component. The primary and the secondary fluids may be different. Thus, Helium-Helium, Helium-CO2, CO2-Helium, etc. heat exchangers can be modeled.

In order to consider the sizing and cost correlations for the different types of heat exchangers, a list of following heat exchanger objects has been reserved in the HyPEP program

- Shell-Tube Type Heat Exchanger (TShellTubeHeatX)
  The 'TShellTubeHeatX' component is derived from THeatX object and will have thermo-dynamic empirical correlations, and the sizing and cost analysis models suitable for the shell-tube type heat exchangers.
- Plate Type Heat Exchanger (TPlateHeatX)
  The 'TPlateHeatX' component is derived from THeatX object and will have thermo-dynamic empirical correlations, and the sizing and cost analysis models suitable for the plate type heat exchangers.
- Printed Circuit Heat Exchanger (TPrintedCircuitHeatX)
  The 'TPrintedCircuitHeatX' component is derived from THeatX object and will have thermo-dynamic empirical correlations, and the sizing and cost analysis models suitable for the printed circuit type heat exchangers.
- Helical Heat Exchanger (THelicalHeatX)
  The 'THelicalHeatX' component is derived from THeatX object and will have thermo-dynamic empirical correlations, and the sizing and cost analysis models suitable for the helically coiled tube type heat exchangers.

E. PCU Components (TPCU)

The PCU component models the power conversion unit and includes Brayton cycle and the Rankine cycle components. Reheats and the superheating circuits may be modeled using the base components of HyPEP. However, user can design combined cycles and then save the layouts as a user-defined component. The PCU components calculate the electricity generation efficiencies.

Brayton Cycle (TBrayton)
The closed cycle Brayton cycle component is added as a sub-system component in HyPEP. The schematic layout of the Brayton cycle modeled in HyPEP is shown in Figure 2-3.

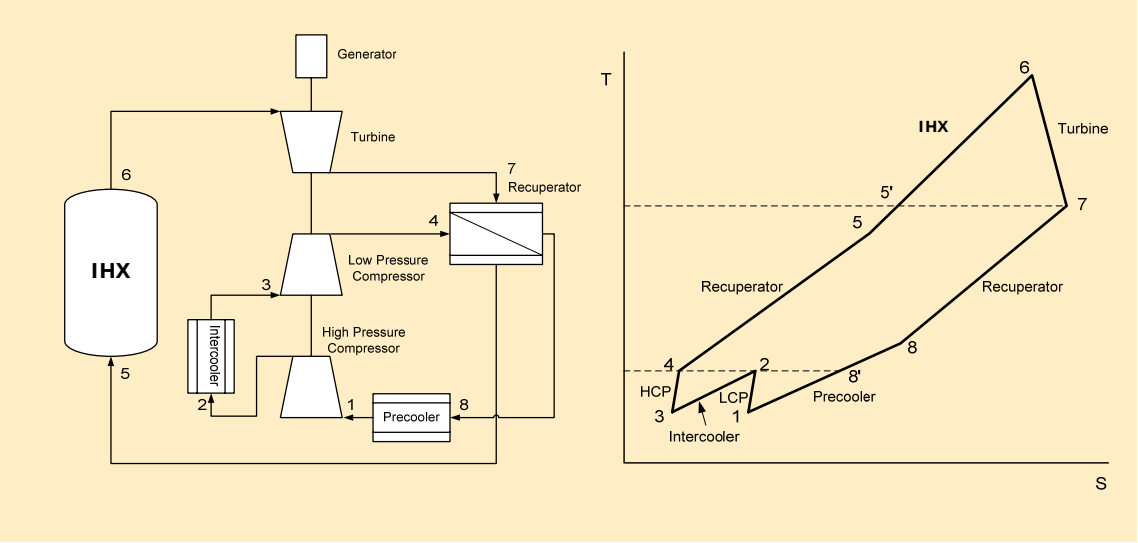

Figure 2-3 Diagram of a Typical Brayton Cycle modeled in HyPEP.

The component models the Brayton Cycle with the following sub-components :

- Gas turbine component (TBraytonGasTurbine)
- Compressor component(TBraytonCompressor)
- Pre-cooler component(TBraytonPreCooler)
- Inter-cooler component(TBraytonInterCooler)
- Recuperator component(TBraytonRecuperator)

Rankine Cycle (TRankine)

This component models the Rankine Cycle. At present, the Rankine cycle component modeling is not completed. However, Figure 2-4 shows the simplified Rankine cycle and the component, currently under design, will contain the following components :

- Steam generator component(TRankineSteamGenerator)
- Steam turbine component (TRankineSteamTurbine)
- Condenser component(TRankineCondenser)
- Pump component(TRankinePump)

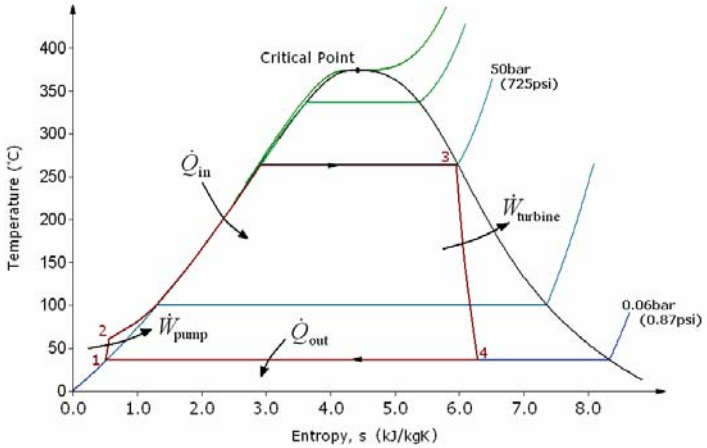

Figure 2-4 T-S Diagram of a Typical Rankine Cycle

F. HTES Components (THTES)

The HTES component is a highly simplified model of a High Temperature Electrolysis System consisting of models for the heat exchanger, the electrolyser, the condenser, the separator, the H_2 and water supplies, and the helium circulator, as shown in the schematically in Figure 2-5. The thermodynamic states of the mixture fluid are calculated from the property routines and the molar fractions are calculated according to the chemical reaction provided.

$$n_1\,H_2O + n_2\,H_2 = n_3\,H_2 + (n_1+n_2-n_3)\,H_2O + (n_3-n_2)/2\,O_2$$

This model is similar to that used in the NHDD program developed by KAERI.
The H_2 is re-circulated and the ratio of the re-circulated H_2 is determined by the global chemical balance equation. The global chemical balance equation has the following form and the user can vary the values of n_1, n_2 and n_3 via interactive input.

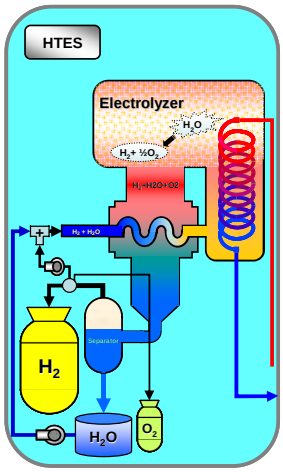

Figure 2-5 A Schematic Diagram of the Simplified HTES Component.

The water from water storage tank and the re-circulated H_2 are mixed and enter the condenser where the mixture recovers heat of the exiting hot mixture. The heated mixture then enters the heat exchanger where it is heated to the electrolysis temperature. The mixture enters the electrolyser where chemical reaction of takes place. The AC current from the PCU is converted to DC current and it is supplied to the electrolyser. The hot mixture from the electrolyser is cooled in the condenser by the feeding H_2 and water mixture. The cooled mixture then enters the separator where H_2, O_2 and residual water are separated. A portion of H_2 is re-circulated and the remaining H_2 is the final product.

An equi-potential table is used to determine the electric power and the heating requirements for the operating temperature of the electrolysis. The operating temperature of the electrolysis is determined after various temperature drops in the heater exchangers have been determined and deducted from the core outlet temperature.

The THTES component consists of further components listed below:

- Electrolyzer Components (THTESElectrolyzer) : This component models the electrolyzer. The chemical reactions of the electrolysis are modeled in this component.
- Separator Components (THTESSeparator) : This component models the separator and the model separates the various chemicals (hydrogen, oxygen and steam).

- Condenser Components (THTESCondenser) : This component models the separator and the model is used to model the condenser where heat is exchanged.

AC-DC Converter (TAC_DC) : This component models the conversion of AC current into DC needed by the HTES.

2.4 Program Structure

2.4.1 Overview

The HyPEP program has been designed to have a strong hierarchical structure, and with an emphasis on the program modularity and the use of a modern programming language with Object Oriented Programming (OOP) features. The modularity and the OOP features are considered to offer advantages in setting up the hierarchy, the program maintenance, the program clarity, and the program component re-usability. The inheritance, polymorphism, and encapsulation provided in OOP languages are well suited in modeling the hierarchical structure of the system and component models of HyPEP.

The programming language has great influence on the program style as the features of the programming languages can dictate the way a program is structured. For the Microsoft Windows® operating system, a number of excellent development environments with modern OOP languages exists. Examples are the Microsoft Visual Studio development environment for Visual C++ and Visual Basic, and Delphi® for the rapid application development environment. The factors considered in the language selection were;

1) Windows programming capability.
2) Ease-of-use in application of windows API (Application Program Interface) procedures.
3) Rapid program development environment.
4) Code reusability.
5) Code robustness and fault tolerance.
6) Code extensibility.
7) Amenability to interface with other program languages.

In the first year of the HyPEP development, the Delphi programming language, which is derived from the object Pascal language, was chosen after some considerations. The OOP programming techniques has been employed extensively in setting up the GUI and the numerical programs of the HyPEP.

2.4.2 Component Object Class Definitions

An object is defined via its class, which acts like a template, which defines and determines the properties and the methods about an object. The objects are the individual instances of a class. For example, an object named ‘helicalHX’ can be created (or “instantiated”) using the class “THeatX.” The “THeatX” class defines (by means of method and property definitions) what a heat exchanger object is, that is, its data structure and all the methods (or actions, functions) that a heat exchanger object can perform.

In programming the HyPEP, a hierarchy of program object classes matching the component/system structure has been established using the OOP techniques and feature. The inheritance and the polymorphism features of the OOP have facilitated easy derivation of other object-classes from the parent class. The inheritance feature of OOP allows easy creation of sub-classes (or children class) of an object-class. The polymorphism feature allows easy creation of variations of an object class.

For example, the “TPrintedCircuitHX” class can be created from the “THeatX” class using the inheritance feature of the OOP by adding properties (data) and methods (routines) specific to printed circuit heat exchanger to the generic a heat exchanger class “THeatX”. Whereas, the

“TPrintedCircuitHXwithSquareCrossSection” object class can be created by changing the heat transfer coefficient calculation routine (Object’s method) of the “TPrintedCircuitHX” class to that specific to square cross section.

At the base of the GUI program of the HyPEP is a Visual Component Library (VCL) called “Express Flowchart.” This VCL is developed by the Developer Express Company for Delphi and C++ builder, and it is commercially available.

The Express Flowchart VCL was developed to allow easy creation of applications that display charts, schemes, hierarchies, graphs, etc. In the HyPEP program, the ability of the Express Flowchart VCL to generate the flow chart has been used for the graphical creation of flow network.

The drawing canvas of HyPEP, where the flow network is created graphically by the user, is an object which is an instance of the ‘TdxFlowchart’ object class of the Express Flowchart VCL. The TdxFlowchart has, as its members (or properties), the TdxfcObject and the TdxfcConnection object classes. The TdxfcObject class is the basic graphic building blocks of a flow network. And the TdxfcConnection class is the graphic line that connects the TdxfcObject class objects. The TdxfcObject and the TdxfcConnection has sufficient functionalities to graphically build-up the system on-screen.

The node and the link which form the basic components of HyPEP are derived from the objects of the drawing canvas via object inheritance. This has been used to good effect in ensuring the 1-to-1 correspondence between the visual components of the drawing canvas and the numerical T/H components.

Other objects for HyPEP have been derived from the node and link objects.

The relationships between the object classes have been established and it is presented in the Figure 2-6.

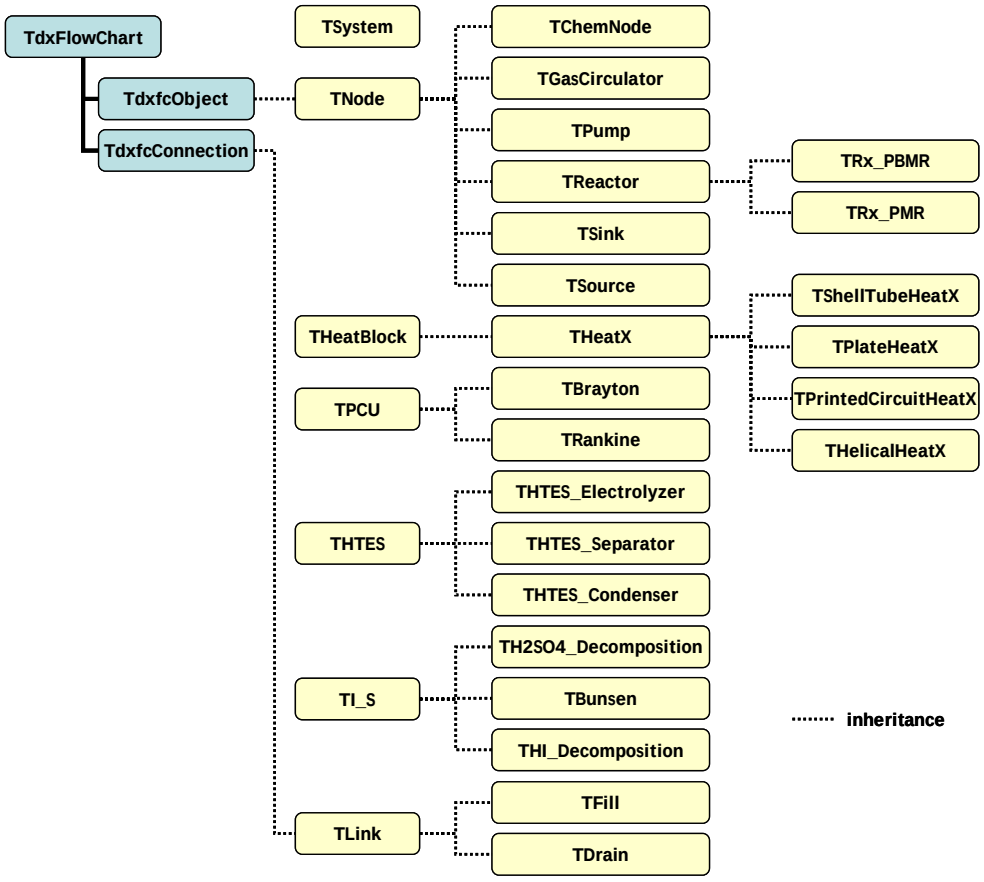

Figure 2-6 Object Classes of the HyPEP and Inheritance.

A. TNode (Object class for Node)

In the HyPEP program, the TNode object class is defined as shown in List 2-1. As can be seen, TNode is derived from the GUI object TdxfcObject through inheritance. Thus, a TNode object can be treated as a TdxfcObject and has all the graphical methods and properties of the TdxfcObject. The TNode object can also be typecasted as a TdxfcObject for the situations where TdxfcObject is needed as an argument of a function. Added in the TNode object class, there are a number of methods (procedures) and properties which are used mostly by the thermo-dynamic numerical solution parts.

The methods defined for the TNode object class are described in the following :

procedure NodeInfo (xList : TStrings)
This method writes the information relating to the node properties into a TStrings object, xList. The information is written to a TStrings object because the TStrings objects can be easily copied or used directly in such components as the TStringGrid (as row or column), TMemo, and TList object classes by object assignment.

procedure CalcTHState
This method calculates the various thermo-dynamic state parameters such as density, internal energy, entropy, enthalpy, and the derivatives $\partial\rho/\partial h$ and $\partial\rho/\partial P$ for the node. The thermo-dynamic calculations are carried out with the consideration for the molar-fraction of fluid species that are present in the node.

List 2-1 TNode Object Class Definition

```
TNode = class (TdxfcObject)
  private
  public
    Name       : string;
    papa       : TNode;     // Parent Node, if any
    BC_Node    : Boolean;

    // Index Specifications
    compIdx,                // Component Index
    ArrayIdx,               // Index for all Node array
    SysIdx,                 // Index Showing which System this Node belongs
    MatIdx    : Integer;    // Index showing the position in the P-solve Matrix Array

    // Link Specification section
    nInLink,                // Number of inlet  links
    nOutLink,               // Number of outlet links
    nTotLink   : integer;   // Total number of connected links
    InLinks,                        // Array of inlet  links
    OutLinks,                       // Array of outlet links
    TotLinks   : Array of TLink;    // Array of total  links

    // Block Specification
    nHBlock    : integer;
    moved      : boolean;
    HBList     : Array of THeatBlock;

    // Thermal hydraulic properties
    //
    subsFrac                  : recSubsFrac;
    P, T, h, s, u, v,{ Sm, Sh, }     // Obvious variables
    xt,                              // vol * dtime
    dP, P_old,                       // pressures (new & old)
    dP_src,                          // p-source used for pump/circulator/compressor
    dP_grav,                         // gravity turbines (?)
    dh, h_old,                       // enthalpy  (new & old)
    rho, rho_old,                    // net density
    vol, varea, vleng,               // physical volume (m3)
    drho_dP, drho_dh,                //
    Src_h,                           // enthalpy source (may be replaced by a function)
    Src_m,                           // mass source
    a11, a12, a21, a22,              // Matrix elements(during matrix operation)
    S1, S2,                          // Vector elements(during matrix operation)
    alp11, alp12, alp21, alp22,      // Inverse Matrix (during matrix operation)
    Sig1, Sig2           : extended; // Vector (during matrix operation)
    phi1, phi2           : Array of extended;

//    constructor Create(var dxCanvas : TdxFlowChart; Idx, x, y : Integer) : override;
//    destructor Destroy; override;
    procedure NodeInfo (xList : TStrings);
    procedure CalcTHstate;
    procedure Prepare_for_P_Matrix;
    procedure UpdatePressure (delP : extended);
    procedure get_T_from_P_h;
    procedure new_h;
    procedure explicit_rho;
    procedure explicit_h;
  published
  end;
```

procedure get_T_from_P_h

This method calculates the temperature with the calculated h. The thermo-dynamic calculations are carried out with the consideration for the molar-fraction of fluid species that are present in the node.

procedure UpdatePressure (delP : extended)

This method calculates the new pressure after the pressure matrix solution has been found.

procedure Prepare_for_P_Matrix
This method provides the coefficients of the systems pressure matrix for the solution of flow network. The equations 2-9 ~ 14 are solved in this method.

The 'procedure explicit_rho' and the 'procedure explicit_h' are used for the numeric scheme testing purpose only.

B. TLink (Object class for Link)

The TLink object class definition is shown in List 2-2.

List 2-2 TLink Object Class Definition

```
TLink = class (TdxfcConnection)
  private
  public
    Name                          : string;
    ArrayIdx, sysIdx, compidx     : Integer;
    vel, mass                     : extended;
    srcNode, destNode, DonorNode : TNode;
    massflow, jarea, jleng        : extended;
    moved                         : Boolean;
    u, u_old,               // velocities (new & old)
    Aj,                     // flow area
    fT,                     // total flow resistance
    rhoj,
    hj,
    dP_extra,
    etaj, thetaj                  : extended;
    BC_Link                       : Boolean;

//    constructor Create(Owner: TComponent) : override;
//    destructor Destroy; override;
    procedure LinkInfo (xList : TStrings);
    procedure UpdateVelocity;
    procedure CalcTH;
    procedure explicit_update;
  published
  end;
```

TLink is derived from the GUI object TdxfcConnection. In addition to the properties and methods of the TdxfcConnection object class, following methods (procedures) have been added :

procedure LinkInfo (xList : TStrings)
This method writes the information relating to the link properties into a TStrings object, xList. As with the TNode object class, the information is written to a TStrings object because the TStrings objects can be easily copied or used directly in such components as the TStringGrid (as row or column), TMemo, and TList object classes by object assignment.

procedure CalcTH
This method calculates the donor properties of the link. The thermo-dynamic properties of the link object are calculated to be either the properties of the source node (srcNode) or the destination node (destNode) depending on the value of link velocity. If the link velocity is positive or zero, the thermo-dynamic properties of the source node (srcNode) are used as the properties of the TLink object, otherwise the properties of the destination node (destNode) are used.

procedure UpdateVelocity

This method calculates the new velocity after the pressure matrix solution has been found using the momentum conservation equation.

The 'procedure explicit_update' is used for the numeric scheme testing purpose only.

C. THeatBlock (Object class for Heat Block)

The THeatBlock object class definition is shown in List 2-3. Unlike TNode or TLink object classes, the THeatBlock is a basic object class without any parent object class (other than basic TObject which defines that the class is an object). Thus it has no GUI component. It is possible to have no GUI component for the Heat Block because in HyPEP, there is no stand-alone heat block. HyPEP is designed in such a way that all heat blocks have at least one node component associated with it. Thus, in HyPEP the GUI information for the heat block is contained within the associated node component. The TNode component has a list of HeatBlock (HBList, nHBlock) and the THeatBlock has the associated node as a member (HBNode1, HBNode2, nHBNode), so that the heat block-to-node association information can be obtained easily.

Currently, there is no procedure or function for the THeatBlock component. However, a procedure to calculate a time-varying heat-fluid heat transfer may be added if the HyPEP code needs to be extended to transient calculations.

List 2-3 THeatBlock Object Class Definition

```
THeatBlock = class (TObject)
  private
  public
    HBType                    : HeatBlockTypes;
    Idx, nHBNode, compIdx     : Integer;
    delT, eff_th              : extended;
    HBNode1, HBNode2          : TNode;
    name                      : String;
    Heat_add                  : extended;
    t1, t2                    : extended;
    k                         : extended;
  published
  end;
```

D. TSystem (Object class for Heat Block)

The TSystem object class definition is shown in List 2-4. TSystem object class defines the thermodynamic system consisting of nodes and links that share the fluid by flows in the link object. There can be many different thermodynamic systems in HyPEP. Different thermodynamic systems may exchange heat via heat blocks. The numerical scheme of the HyPEP for the flow networks sets up the pressure matrix for each system. Therefore this object class has as its member the pressure matrix (MatP and RHS arrays).

MatP is a 2-dimensional pressure matrix and the RHS is a one-dimensional array representing the right hand side of the pressure matrix solution scheme.

The main members of the TSystem object class are the NodeList, LinkList and the subsList. The nNodeSys property defines the number of nodes in the system and the NodeList lists the nodes of the TSystem. Similarly, the nLinkSys property defines the number of links in the system and the LinkList lists the links of the TSystem. The subsList lists the substances (fluid species) considered in the TSystem.

At present, the subsList is fixed and consists of the 7 fluid species described in section 2.2. plus butane and the propane.

List 2-4 TSystem Object Class Definition

```
TSystem = class (TObject)
  Private
  Public
    nNodesys, nLinkSys        : Integer;
    MatP                      : Array of Array of Extended;
    RHS                       : Array of Extended;
    NodeList                  : Array of TNode;
    LinkList                  : Array of TLink;
    subsList                  : Array of recSubstance;
//    destructor Destroy;
    procedure Setup_Matrix;
    procedure Solve_P_matrix (var Max_P_error : extended);
  published
  end;
```

procedure Setup_Matrix

This method sets up the pressure matrix using equation 2-14. Using the equation, the pressure equations can be setup for each node of the system, and the appropriate entries in the MatP and the RHS arrays.

procedure Solve_P_matrix (var Max_P_error : extended)

This method solves the pressure matrix using a matrix solver. Although a number of matrix solvers have been coded, only the Gauss solver is actually implemented for HyPEP beta. The method returns the maximum pressure error defined as the ratio between the newly calculated pressure and the old pressure.

There has been some efforts to install the numerical matrix solvers of IMSL through Fortran-to-Delphi interface, but has experienced some technical difficulties in transferring the data.

2.4.3 Main Program Units

The HyPEP beta is programmed in a modular fashion and the program modules can be divided into main program units and the utility program units. The major functions of the main units are to carry out the system build-up and to perform the numerical solution schemes. The main program units:

- main.pas
- HyPEPComp.pas
- Solver.pas

A. Main.pas

This program unit is the main body of the HyPEP program and it contains the global variable definitions of the HyPEP program. The global variables defined in this program unit include a) the Nodes array variable which is the array of all the nodes, b) the Links array variable which is the array of all the links, c) the HeatBlocks array which is the array of all the heat blocks, and d) the Systems array which is the array of all the systems currently under calculation.

Other global variables defined in main.pas include the IconImageList which is an array of the TImageList of the VCL of Delphi and contains the bitmaps for the components. There are a total of 5 bitmaps corresponding to the 5 zoom levels.

The Major functions served in this program unit can be summarized as:

- GUI functions to perform the tasks such as
  - File load/save/import/print functions
  - Component drag-drop onto the Drawing Canvas

- Component addition/delete/copy
- Zoom-in/zoom-out
- Component template object creation
- Link connection selection
- Etc.

- Functions for the numerical scheme such as:
  - Build-up the thermodynamic system
  - Bookkeeping of the components and systems
  - Setting up the pressure matrix arrays
  - Etc.

B. HyPEPComp.pas

The main purpose of this program unit contains the object class definitions of the components. The definitions for the substances (in 'record' form) are also defined in this program unit. The record definitions of the fluid substances are shown in List 2-5, and the object class definitions of the important components are shown in List 2-6.

List 2-5 Structures Data Records of HyPEPComp.pas

```
//-------------------------------------------------------------------------
  recPvT   = Record
               alpha, gamma               : RType; // Data for P-v-T Eqn.
               A                          : Array [1..35] of RType;
               a_, b_, c_, d_             : RType;
               A0, B0, C0, D0, E0         : RType;
               Tau_c                      : RType;
             end;
  //-------------------------------------------------------------------------
  recPsat  = Record
               Tp                         : RType; // Data for P-v-T Eqn.
               F                          : Array [1..10] of RType;
               alpha, gamma, Tt, Pt       : RType;
             end;

  //-------------------------------------------------------------------------
  recCv    = Record
               cv,  u0, s0, T1, T2, beta  : RType;
               G                          : Array [1..17] of RType; // Data for Cv eqn.
             end;
  //-------------------------------------------------------------------------
  recRliq  = Record
               alpha                      : Rtype;
               D                          : Array [1..7]  of RType; // Data for Liq. Den.
Eqn.
             end;
//-------------------------------------------------------------------------
  recSubstance = Record
                   subsName               : string;
                   PvT_Index,  Psat_Index,
                   Cv0_Index,  Rliq_Index  : Integer;
                   // Ganeral Data
                   R, M, Tc, Pc, rhoc, T0  : RType;
                   PvTData                 : recPvT;
                   PsatData                : recPsat;
                   CvData                  : recCv;
                   RliqData                : recRliq;
                 end;
  //-------------------------------------------------------------------------
```

List 2-6 Object Classes of HyPEP (forward declaration list)

```
//---------------------------------------------------------------------
// Node Components
TNode                 = class;
TChemNode             = class;
// Link Component
TLink                 = class;
// Heat Block Component
THeatBlock            = class;
// Heat Exchanger Components
THeatX                = class;
TShellTubeHeatX       = class;
TPlateHeatX           = class;
TPrintedCircuitHeatX  = class;
THelicalHeatX         = class;
// Circulators and pump Components
TGasCirculator        = class;
TPump                 = class;
// Reactor Components
TReactor              = class;
TRx_PBMR              = class;
TRx_PMR               = class;
// PCU Components
TPCU                  = class;
TBrayton              = class;
TRankine              = class;
// HTES Components
THTES                 = class;
THTES_Electrolyzer    = class;
THTES_Separator       = class;
THTES_Condenser       = class;
// AC-DC Converter
TAC_DC                = class;
// Thermo-chemical Component
TI_S                  = class;
TH2SO4_Decomposition  = class;
TBunsen               = class;
THI_Decomposition     = class;
// TH System
TSystem               = class;

recFlowBC  = Record time, flow : extended end;
recPresBC  = Record time, p    : extended end;

recCopyList = record
                ncNode, ncLink : Integer;
                cNodes         : Array of TNode;
                cLinks         : Array of TLink;
                fpt, tpt,
                fnode, tNode   : Array of Integer;
              end;
```

2.4.3.1 Numerical Scheme Program

As previously described, the complex matrix coefficient calculations are carried out by the methods of the TNode and TLink components. Thus, the coding for the overall numerical solution in the main program becomes extremely simple with around 20 lines of coding as shown in List 2-7.

List 2-7 shows the top-most calculation scheme to numerically calculate the thermo-dynamic states of the flow-network of the systems. As can be seen in the List, the primary loop, with main function to obtain the satisfactory flow-network solution is a ‘repeat..until’ loop with max_P_error and max_Iter as the conditional variables with which to terminate the calculation loop.

Within the primary repeat loop are the secondary loops consisting of:

- A loop over all node components to evaluate the thermodynamic variables of the nodes
  - TNode.CalcTHState method is used.
- A loop over all link components to evaluate the thermodynamic variables of the links
  - TNode.CalcTH is used
- A loop over all node components to calculate the various coefficients to be used in setting up the pressure matrix
  - TNode.Prepare_for_P_Matrix is used
- A loop over all systems to setup and solve the pressure matrix.
  - TSystem.Setup_Matrix and TSystem.Solve_P_Matrix methods are used.
- A loop over all nodes to update parameters using the newly calculated pressure.
  - TNode.Update_Parameters method is used.

List 2-7 Numerical Solution Scheme Main Loop

```
Repeat
    MainForm.Caption := intToStr (nIter);
    SolverDisplay.Caption := MainForm.Caption;

    inc (nIter);

    satisfied := true;

    // =================
    // *** IMPORTANT ***
    // =====================================================
    //  Do not combine or change order of the following loops
    // =====================================================
       For n := 0 to nNode-1 do Nodes[n].CalcTHstate;
       For n := 0 to nLink-1 do Links[n].CalcTH;
       For n := 0 to nNode-1 do Nodes[n].Prepare_for_P_Matrix;
       For n := 0 to nSystem-1 do
       begin
         Systems[n].Setup_Matrix;
         Systems[n].Solve_P_matrix (Max_P_error);
         satisfied := satisfied and (Max_P_error < 1.0e-5);
       end;
      For n := 0 to nNode-1 do Nodes[n].Update_Parameters;
    // =====================================================
    // *** IMPORTANT end ***
    // =====================

    Plot_P_Trend (PlotPos);

  until satisfied or (nIter >= max_Iter);
```

2.4.3.2 GUI Program

The GUI program of the HyPEP is complex and most of the coding for the event-driven functions.

The GUI programs carry out the following functions:

- Detect events such as keyboard input or mouse click and produce event messages
- Interpret the event-created message and carry out the appropriate functions such as:
  - Create/destroy components
  - Showing/Hiding various windows
  - File open/close/import
  - Zoom in-out
  - Print the window form
  - Maintain the bookkeeping of component generation/destruction
- Build-up the systems of flow network.

Most of the GUI program coding resides in the main.pas with the utilities supported by the HyPEPUtil.pas. The main.pas has associated 'windows form' which is called the MainForm. The MainForm window acts as the main work area and is the container for most of GUI components. Detailed description of major GUI components of the MainForm is provided below.

A. *dxCanvas (TdxFlowChart)*

This is the drawing canvas of the HyPEP. The components are drag-dropped onto dxCanvas for the system build-up.

Major events of dxCanvas are:

- dxCanvasChange
  Occurs when a change occurs in the components of dxCanvas
- dxCanvasDblClick
  Occurs when the dxCanvas is double clicked, depending on whether a node or a link is clicked, a node or a link parameter modify wizard pops up
- dxCanvasDeletion
  Occurs when a node or a link is deleted.
- dxCanvasDragDrop
  Occurs when a drag-drop originating from the BitButton of the Template. The tag property of the bitbutton is used as the component type identifier and the appropriate components are created on the drawing canvas.
- dxCanvasKeyDown
  Occurs when a key is pressed (in down stroke). A total of 5 keys are recognized. The 4 keys (up, down, left, right) are used to move components, and the 'del' key is used for deleting a component. For the move keys, depressing the 'shift' key while moving makes large step move. Depressing the 'ctrl' key makes fine step move.
- dxCanvasMouseDown, dxCanvasMouseUp, dxCanvasMouseMove
  Occurs when the mouse is moved or clicked. The component move, select/deselect and various other functions are coded to respond to the mouse events.

B. *Template (TPageControl)*

This component holds several tabsheets which contains the BitButtons with component glyphs. The tabsheets are categorized according to the type of components that it contains such as nodes, heat exchangers, heater/cooler, etc. The bitbuttons are drag-dropped to make a component on the drawing canvas, dxCanvas.

C. *MainMenu1 (TMainMenu)*

This is the main menu and contains the following commands

- File : New, Load, Save, Save As, Open, Import, Print, Exit
- Option : Snap, Canvas Color, Show Stat

D. *PopupMenu1 (TPopupMenu)*

This is the popup menu which appears when the right mouse button is clicked on the drawing canvas, and contains the following commands

- Make Link, Add point to a link, Flip link connections
- Change line style of a link

- Component selection commands
- Zoom commands
- Copy (clone) and import commands
- Union Command
- Component z-order change commands (Bring to front, Send to back)

E. *OpenDialog (TOpenDialog), SaveDialog(TSaveDialog)*

These are the dialog components for the opening and saving the HyPEP files.

F. *Icon24, Icon32, Icon48, Icon72, Icon96 (TImageList)*

These contain the images of components used as the image of the TNode component on the dxCanvas. There are 5 different size images (24x24, 32x32, 48x48, 72x72, 96x96) corresponding to the 5 Zoom levels.

2.4.4 Utility Program Units

A number of program units provide functions and procedures for the HyPEP programs. The thermodynamic property calculation routines, the string handling routines, mathematics routines are categorized into this program units. used in HyPEPUtil.pas program unit.

2.4.4.1 Thermodynamic Property Routines

The HyPEP program needs to calculate the thermo-dynamic states of the nodes with good accuracy.

A. Water/Steam Thermodynamic Properties

The thermodynamic property calculation routines for water/steam have been developed using the 1967 IFC Formulation for Industrial Use in conformity with the 1963 International skeleton tables. In the 1967 IFC formulation, the property regions are divided into 6 sub-regions including a sub-region for the saturation line and a sub-region near the critical point. The correlations for the specific Helmholtz function, the specific Gibbs functions, the K-function for saturation line are provided in the formulation. These correlations have been coded in Pascal language for use in Delphi program environment which has been selected for the HyPEP development. The routines have been packaged as a Delphi unit in which several routines have been defined as the interface routines.

The Delphi interface routines are coded in ASME.pas and which is compiled to generate the ASME.dcu which essentially acts as a library which is callable from any Delphi program by including the ASME in the unit declaration of the calling program. The list of routines available in ASME.pas is as follows :

- *procedure calc_Prop (P, T, v, h, s, cp, e, c)*
  This routine calculates v, h, s, cp, e, c for given pressure P, and temperature T.
- *procedure T_sat_Prop (T, Psat, vf, vg, hf, hg, sf, sg, cpf, cpg, ef, eg, cf, cg)*
  This routine calculates Psat, vf, vg, hf, hg, sf, sg, cpf, cpg, ef, eg, cf, cg for a given temperature T.
- *procedure P_sat_Prop (P, Tsat, vf, vg, hf, hg, sf, sg, cpf, cpg, ef, eg, cf, cg)*
  This routine calculates Tsat, vf, vg, hf, hg, sf, sg, cpf, cpg, ef, eg, cf, cg for a given pressure P.
- *function SurTen (T) : real*
  This function returns surface tension for a given pressure P.
- *function satT (P) : real*
  This function returns saturation temperature for a given pressure P.

- *function satP (T) : real*
  This function returns saturation pressure for a given pressure T.
- *function th_k (P, T, ρ) : real*
  This function returns thermal conductivity for given pressure P, temperature T, and density ρ.
- *function visc (P, T, ρ) : real*
  This function returns dynamic viscosity for given pressure P, temperature T, and density ρ.
  where
  P = pressure, MPa
  T = temperature, K
  v = specific volume in m3/kg
  ρ = density, kg/m3
  h = specific enthalpy, J/kg
  s = specific entropy, J/kg/K
  c_p = specific heat capacity, J/kg/K
  e = expansivity
  c = compressibility
  subscript f = liquid water
  subscript g = gaseous steam
  subscript sat = saturation

The sub-regions of IFC formulations are as shown in Figure 2-7. As can be seen in the diagram, there are 6 sub-regions including the saturation line and near critical point line. The IFC formulation provides correlations for the 4 subregions (1 ~ 4). For the saturation line, the steam and the liquid properties are calculated using the appropriate sub-regions for the given temperature or the pressure.

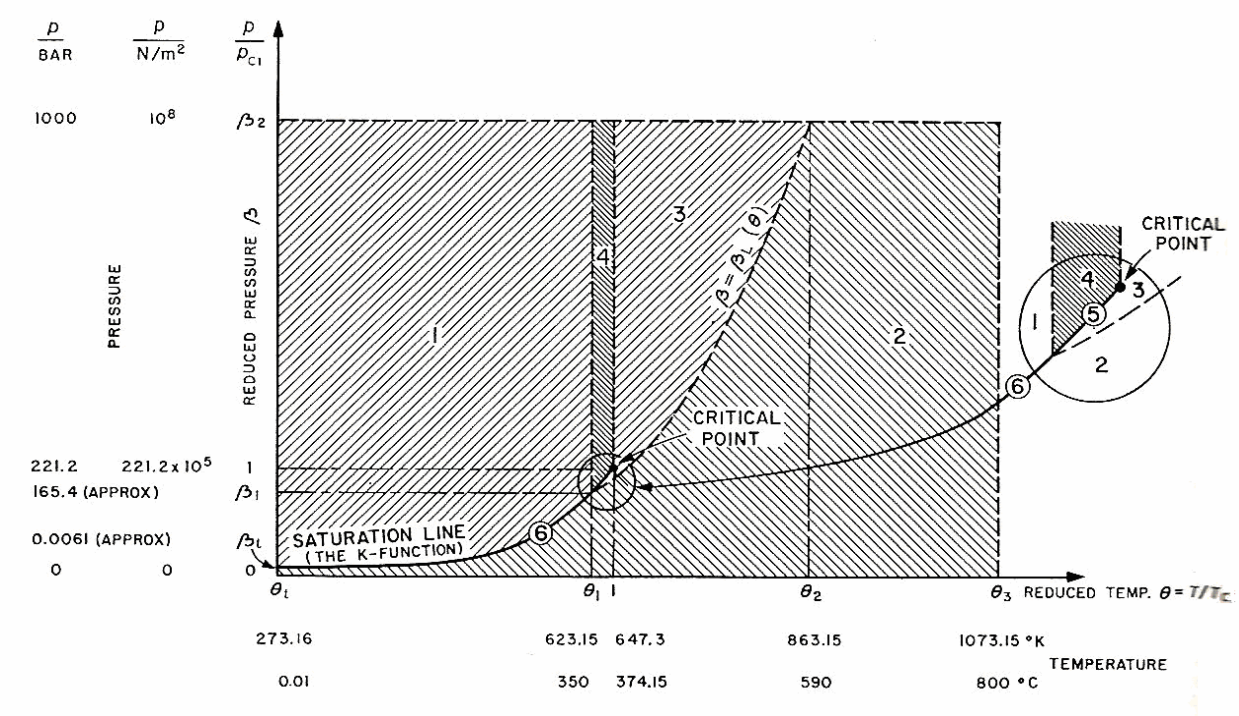

Figure 2-7 Sub-regions of IFC Formulations for Steam/Water Properties.

B. Gas Thermo-dynamic Properties

The thermodynamic property calculation routines for gas substances have been developed using the "Thermodynamic Properties in SI" by W.C. Reynolds Correlations where correlations for a total of 40 substances are provided. Of the 40 substances available, helium, hydrogen (para), nitrogen, oxygen, argon, carbon dioxide, butane, and propane have been coded in Pascal language for use in Delphi program environment. The correlations are based on the PVT relationships which are different for the different substances. The internal energy and the entropy values are derived from the PVT relations using the following relationships:

$$u = \int_{T_0}^{T} c_v^0(T)\,dT + \int_0^{\rho} \frac{1}{\rho^2}\left[P - T\left(\frac{\partial P}{\partial T}\right)_{\rho}\right] d\rho + u_0$$

$$h = u + pv$$

$$s = \int_{T_0}^{T} \frac{c_v^0(T)}{T}\,dT - R\ln\rho + \int_0^{\rho} \frac{1}{\rho^2}\left[\rho R - \left(\frac{\partial P}{\partial T}\right)_{\rho}\right] d\rho + s_0$$

More substances can be added by providing appropriate correlation constants. The gas mixture (e.g. air) properties are calculated by summing (using molar fraction) constituent substance properties.

These routines are programmed as the Delphi program unit, THProps.pas (THProps.dcu). Following interface routines are currently programmed in the THProps unit.

- *procedure AirProps (P, T, v, h, s, u)*
  This routine calculates v, h, s,u for given pressure P, and temperature T for air which is a mixture with molar composition of 78.29% Nitrogen, 20.95% oxygen, and 0.96% argon.
- *procedure GetProps (Substance, P, T, v, h, s, u)*
  This routine calculates v, h, s,u for given pressure P, and temperature T for the named "Substance". The "substance" should be a pure substance and not a mixture such as air. For air, the procedure AirProps is used.
- *function PvT_eqn (Substance, T, rho) : real*
  This routine returns pressure P for given temperature T and density ρ for the named "Substance."
- *function u_eqn (Substance, T, rho) : real*
  This routine returns energy u for given temperature T and density ρ for the named "Substance".
- *function s_eqn (Substance, T, rho) : real*
  This routine returns entropy s for given temperature T and density ρ for the named "Substance".
- *function dPdT_eqn (Substance, T, rho) : real*
  This routine returns dP/dT for given temperature T and density ρ for the named "Substance".
- *function dPdRho_eqn (Substance, T, rho) : real*
  This routine returns dP/dρ for given temperature T and density ρ for the named "Substance".
- *function rho_P_T (Substance, P, T) : real;*
  This routine returns density, ρ for given temperature T and density ρ for the named "Substance".
- *function Rliq_Eqn (Substance,T) : real;*
  This routine returns liquid density, ρ for given temperature T for the named "Substance".
- *function Psat_Eqn (Substance,T) : real;*
  This routine returns saturation pressure Psat for given temperature T for the named "Substance".

The substances are defined by the structured record defined as recSubstance. List 2-8 shows a sample substance definition (in this case Argon).

List 2-8 Sample Substance Definition File

```
//+++++++++++++++++++++++++++++++++++++++++++++++++++++++++++++
  Argon : recSubstance       // Argon
     =(subsname   : 'Argon';
       PvT_Index  : 3;
       Psat_Index : 2;
       Cv0_Index  : 0;
       Rliq_Index : 2;

       // General Data
       R    :  208.128;
       M    :   39.948;
       Tc   :   150.70;
       Pc   : 4.8649e6;
       rhoc :   513.00;
       T0   :     83.8;

       PvTData :
        (alpha : 0.0; gamma : 3.5e-6;
         A :( 1.9825921e-1, -8.1733119e1,  1.7777470e3,  -8.2406544e5,   3.1666098e7,
             -4.4202671e-5,  6.216142e-2,  1.1443248,     4.7797520e-7, -1.9645227e-4,
             -2.1572754e-10, 1.6544141e-7,-2.8142112e-11, 8.2532059e1,  -9.1538377e3,
             -1.8340752e6,  -3.3858136e-3, 1.5532886,    -6.7479568e1,   0.0,
              0.0,           0.0,          0.0,          0.0,           0.0,
              0.0,           0.0,          0.0,          0.0,           0.0,
              0.0,           0.0,          0.0,          0.0,           0.0);

         a_ : 0.0; b_ : 0.0; c_ : 0.0; d_ : 0.0;
         A0 : 0.0; B0 : 0.0; C0 : 0.0; D0 : 0.0; E0 : 0.0;
         Tau_c : 0.0);
       PsatData :
        (Tp : 100.0;
         F : (-5.340410,    -2.371280e-1,  -9.490142e-1,  1.187040,     -5.889895,
               5.627790,     2.674117e1,   -6.661814e1,   0.0,           0.0);
         alpha : 0.0;  gamma : 0.0; Tt : 0.0; Pt : 0.0);
       CvData   :
        (cv  : 312.192; u0 : 1.4935540e5;
         s0 : 2.2706700e3;  T1  : 0.0;     T2 :0.0;          beta : 0.0;
         G : ( 0.0,          0.0,          0.0,          0.0,          0.0,
               0.0,          0.0,          0.0,          0.0,          0.0,
               0.0,          0.0,          0.0,          0.0,          0.0,
               0.0,          0.0));
       RliqData :
        (alpha : 0.0;
         D : ( 5.1299940e2,  8.3581370e2,   1.1958780e3, -3.1968580e3,   4.5022760e3,
              -2.0863750e3,  0.0));
        );
```

2.4.4.2 Miscellaneous Routines

HyPEPUtil.pas program includes following routines for HyPEP program:

Graphic routine

- *function HSV2RGB(Hh, Ss, Vv : single) : TColor;*
  This function returns the RGB value corresponding to the Hue-Saturation-Value provided as input. The format of the returned value is the TColor which is the RGB format defined in the Delphi VCL. This function is used in the post-processors such as graph generating routines where the line colors or fill colors need to be changed.

Math functions

- *function Gauss (N:integer; var A:Matrix; var b, x:vector; var errmess : string):boolean;*
  This function carries out the simultaneous set of equations of $[A] \bullet \underline{x} = \underline{b}$. The inputs are the matrix A and the vector x. The Matrix is defined as a 2-dimensional array with the maximum size of 500x500.
- *function IntegSimpson (a, b : extended; nx : Integer; fx : Tfx) : extended;*
  This function carries out the numerical integration using the Simpson's rule. The function to be integrated is the function fx of type Tfx. Tfx is defined as 'Tfx = function (x : RType) : RType;' where the RType is defined as an extended real variable. The extended real variable is a real variable of 10 bytes (80 bits) in length. The variables a and b defines the integration region.
- *function IntegGauss_Quad (a, b : RType; fx : Tfx) : extended;*

This function carries out the numerical integration using the Gauss Quadrature method. The function to be integrated is the function fx of type Tfx. Tfx is defined as 'Tfx = function (x : RType) : RType;' where the RType is defined as an extended real variable. The extended real variable is a real variable of 10 bytes (80 bits) in length. The variables a and b defines the integration region.

Flowchart procedures

- *procedure ZoomCanvas (var dxCanvas : TdxFlowChart; xImages : TImageList; Zoomfactor : integer);*
  This function carries out the utility functions necessary for the zoom-in and zoom-out features of the drawing canvas. There are a total of 5 zoom levels, and this routine changes the image sizes of the GUI components to the appropriate size.
- *Procedure SetLinkPoints (var xLink : TLink; nPoint : Integer);*
  This function is used when the connecting points of the Link component need to be set or changed. Such situation occurs when a Link component is created or when it's shape is changed.
- *Procedure SnapCoord (var xx, yy : Integer; Snapsize : Integer);*
  This function carries out the utilities for the component snapping when the 'Snap' option is selected. The snapsize defines the snap grid size and it is set at 8. The snap option is found in the main menu of the main program.
- *Procedure MoveNode (var xNode : TNode; dx, dy : Integer; snapOn : Boolean; SnapSize : integer);*
  This function carries out the utilities necessary when a node component is moved. When the snap option is selected, the node is moved by 'SnapSize' increments.
- *Procedure Move_Link (var xLink : TLink; dx, dy : Integer; snapOn : Boolean; SnapSize : integer);*
  This function carries out the utilities necessary when a link component is moved. When the snap option is selected, the node is moved by 'SnapSize' increments.
- *Procedure Move_Node_Link (var xNode : TNode; dx, dy : Integer; snapOn : Boolean; SnapSize : integer);*
  This function carries out the utilities necessary when a node and the link components connected to the node are moved. When the snap option is selected, the node is moved by 'SnapSize' increments.
- *Procedure MoveNode_n_Link_Point (var xNode : TNode; dx, dy : Integer; snapOn : Boolean; SnapSize : integer);*
  This function carries out the utilities necessary when a node and the link components connected to the node are moved. This routine also moves the connection points of the links by dx and dy. This is necessary when the link has more than 2 connection points. When the snap option is selected, the node is moved by 'SnapSize' increments.
- *procedure getCopyList (var dxCanvas : TdxFlowChart; var xCopyList : recCopyList; x, y : Integer);*
  This function makes a list of components for duplication when the user needs to duplicate all or part of the system he is building. The List is saved to variable 'xCopyList' of type recCopyList. The recCopyList is a record type defined in the 'HyPEPComp.pas' with member variables consisting of an array of TNode, an array of TLink, and a number of integer variables defining the number of nodes, number of links etc. that are to be copied.
- *function GetPtCoords (var xNode : TNode; nPt : Integer) : TPoint;*
  This function returns the coordinates of the connection points of the node. nPt is an index defining the connection points. The connection points of the TNode are defined as shown in Figure 2-8.

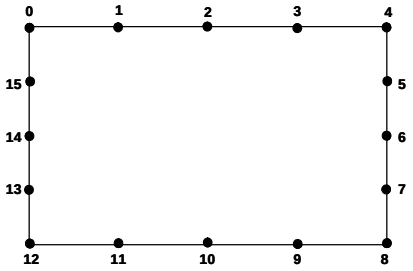

Figure 2-8 Connection point arrangement of a node.

- *function MakeANode (var dxCanvas : TdxFlowChart; idx, x, y, wid, heit : Integer) : TNode;*
  This function is invoked when a new node component is added to the drawing canvas. When a node component is drag-dropped onto the drawing canvas, the GUI routines of the main program unit detects the event and calls this routine to make a node component of size wid and heit at the location x, y.
- *function MakeALink (var dxCanvas : TdxFlowChart; var fObj, tObj : TdxfcObject; fpt, tpt : Integer; IdxStyle : Integer; xColor : TColor) : TLink;*
  This function is invoked when a new link component is added to the drawing canvas. When a link component is generated between two node type component, the GUI routines of the main program unit detects the event and calls this routine to make a link component. The two nodes to connect are defined by the fObj (from object) and the tObj (to object) variables. The node components need to be typecasted to TdxfcObject for this routine. The connection points are defined by fpt and tpt variables. The IdxStyle defines the connection type (whether it is curved, horizontally or vertically kinked etc.). The xColor defines the color of the newly created link.
- *function NodeAtXY (var dxCanvas : TdxFlowChart; x, y : Integer) : TNode;*
  This function returns the node at the coordinate x, y of the drawing canvas. If not, the function returns 'nil'.
- *function LinkAtXY (var dxCanvas : TdxFlowChart; x, y : Integer) : TLink;*
  This function returns the link at the coordinate x, y of the drawing canvas. If not, the function returns 'nil'.
- *function ConnectedNode (Node1, Node2 : TNode) : Boolean;*
  This function returns boolean value 'true' if node1 and node2 are connected by a link component. If not, the function returns boolean value 'false'.

TH Component Support

- *function Wa (nx, R, Ts, Ps, Pd, eff : extended) : extended;*
  This function calculates and returns the work performed by the gas circulator. The variable definitions are as follow:
  - nx : Polytropic index
  - R : Gas constant in (J/kg/K)
  - Ts : Suction temperature (K)
  - Pd : Discharge pressure
  - Ps : Suction pressure
  - eff : Polytropic efficiency
- *procedure Calc_gas_Pump_power (var Pump : TGasCirculator; R, mdot : extended);*
  This function calculates the electric and thermal power of gas circulator power given the mass flow rate. The other variables such as the suction, discharge temperatures ands pressure are defined in the Pump (TGasCirculator) variable.
- *procedure EquiPotential (T : extended; var dH, Tds, dG, EV : extended);*
  This function returns the equipotentials for the electolyzer.

2.5 Program Verification

As previously described, the verification and validation of HyPEP program is to be systematically carried out in the third and final year of the project after the completion of the HyPEP beta. In the final year of the project, the main emphasis will be on strengthening the numerical scheme, through verification and validation efforts, so that the HyPEP program is robust and sound, and can provide reliable results. In the development efforts leading to the HyPEP beta version, the main emphasis of the program verification is the verification related to the system build-up and the utility programs. Thus, some verification efforts have been carried out in the following areas:

- GUI verification to test whether the thermodynamic systems are properly setup
- Tests on thermodynamic property routines for gases
- Tests on numeric solution routines.

The current tests and verifications are not performed as part of the systematic program verification efforts but as improvised efforts to ascertain that the routines satisfy the basic functionality.

2.5.1 GUI Verification

The verification of HyPEP GUI has been carried out throughout the development of the HyPEP beta versions using the HyPEP alpha platform. The major activities of the verification of GUI program of HyPEP can be summarized as follow:

- Creation and destruction of components by drag-drop of the components from the component palettes.
- Component move and modification.
- On-screen connection of components using link component.
- File open, save, copy, print feature verification.
- Visual utility verification
- Verification of graphic options.
- Verification of 1-to-1 matching of a GUI component and a Thermodynamic Component.

In order to test the GUI results, a 'Layout Information' window has been added to HyPEP beta. Screen captures of the 'Layout Information' window is shown in Figure 2-9.

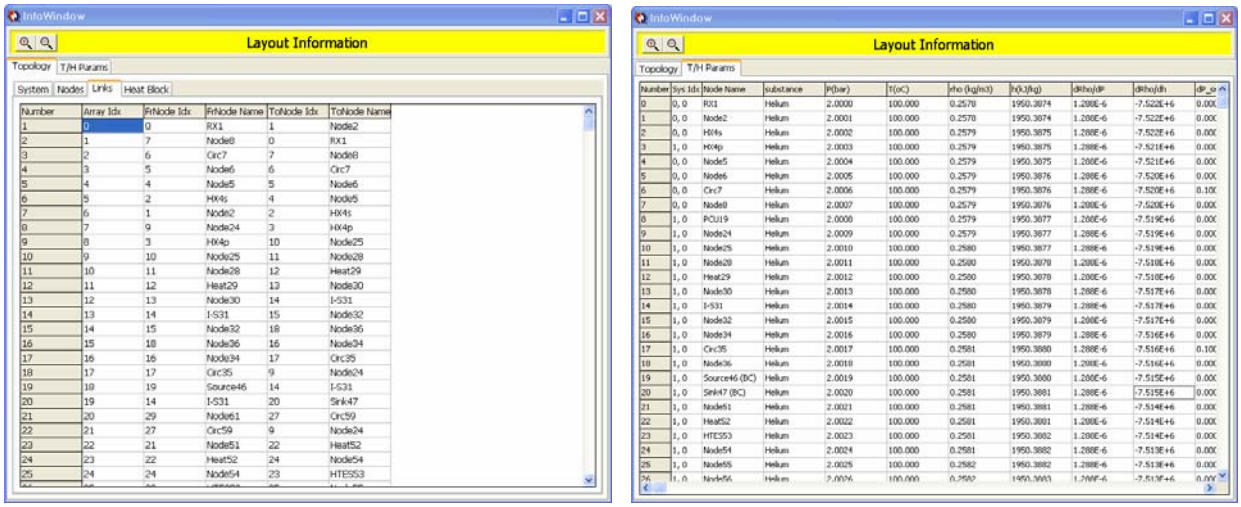

Figure 2-9 The Layout Information Window of HyPEP.

Details of the user-built-up systems are recorded in the 'StringGrids'. Information recorded is the System Topology information consisting of list of systems, nodes, links and heat blocks. The information on the system consists of System array index and the node list. And for each element of the node list, the node array index and the node name. The information on the nodes consists of the node name, node array index, system index for the node, number of inlets and the number of outlets. The information on the links consists of link array index, from-node index, from-node name, to-node index, and to-node name. The information on the heat-block consists of array index, heat-block name, node name at boundary 1, and node name and boundary 2. The T/H Params information shows the thermodynamic state of the nodes and includes such information as the substance, pressure, temperature, density, and others.

The creation of a component is accomplished by selecting the component from the component templates by holding down the left mouse-button and then drag and dropping it at the desired location of the drawing canvas. Upon releasing the left mouse-button, there should be a GUI component drawn on the drawing canvas and a component wizard appropriate for the drag-dropped component should pop-up. User enters the data as specified in the component wizard and then clicks the 'OK' button to finish the component creation. An example is shown in Figure 2-10. Then the HyPEP program should configure the various global variables to reflect the component creation.

In the tests, the GUI can be checked readily since the component should be visible as it is created. The system build-up logics were tested by examining the variables using the 'Layout Information' window. With the HyPEP alpha, the component creation was extensively tested for all the components of the palettes, and a number of program bugs have been detected and corrected.

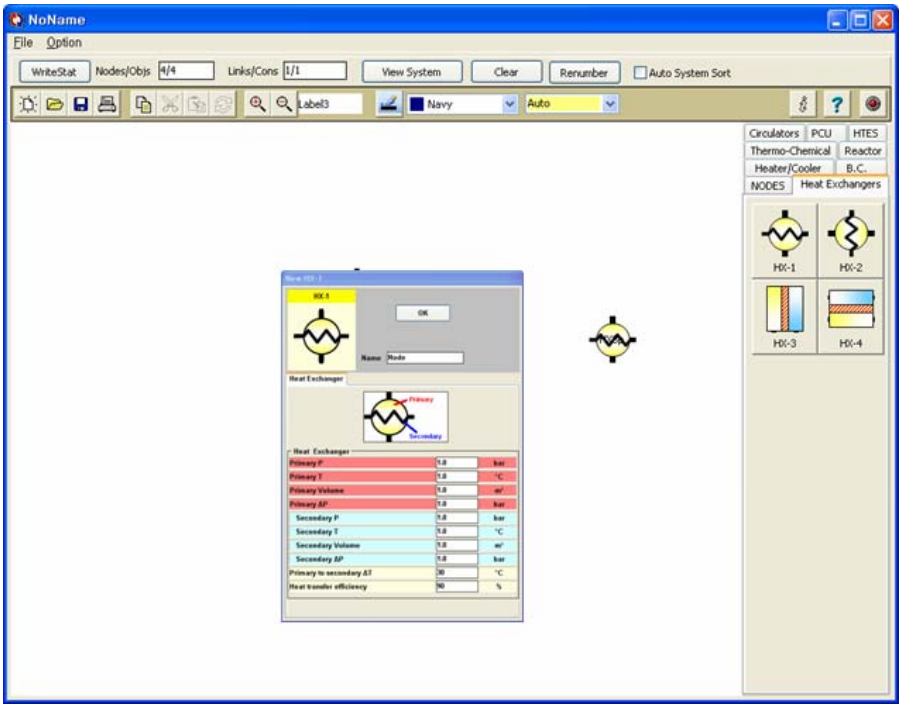

Figure 2-10 An example of a Component Creation and the Component Input Wizard.

The destruction of a component is much simpler to carry out then the component creation as all that is required is for the user to select the component and depress 'Del' key of on the keyboard. When the user depresses the 'Del' key a message window should pop up asking the user to confirm the deletion. When user confirms the deletion, the HyPEP carries out the logics to re-configure the system and various global

arrays. As in the case of component creation, the verification of GUI functionalities was simple as the functionalities could be checked visually. However, the resulting corrections to the arrays were checked by examining them through the 'Layout Information' window. Extensive tests were carried out for the component destruction, and some minor programming errors have been detected and corrected.

Verification of GUI component move and component modification was also carried out visually and interactively. The move of the component was shown to preserve the connections served by the link components. The modification of the component parameters were also checked to see that all the values are modified as intended.

On screen connections of the two node-type component using the link component was tested intensively as this has important consequences in the system build-up. Figure 2-11 shows the how the components are connected on-screen using the link specification wizard. In HyPEP, to prevent wrong connections, the from-component and the to-component show only the connection points which are valid. For example, in Figure 2-xx, the from-component is a reactor and the to-component is a gas circulator. Thus, for the link component connecting the two components, only the outlet of the reactor component and the inlet of the circulator components are available for the user to connect. The inlet of the reactor and the outlet of the gas circulator components are not available for this particular connection. This type of connection scheme was tested extensively for all the components in the palette of the HyPEP alpha and was found to be sound. In addition, by examining the information using the Layout Information window, the system build up was also checked extensively by connecting various components in various configurations and the HyPEP was found to correctly build-up the system.

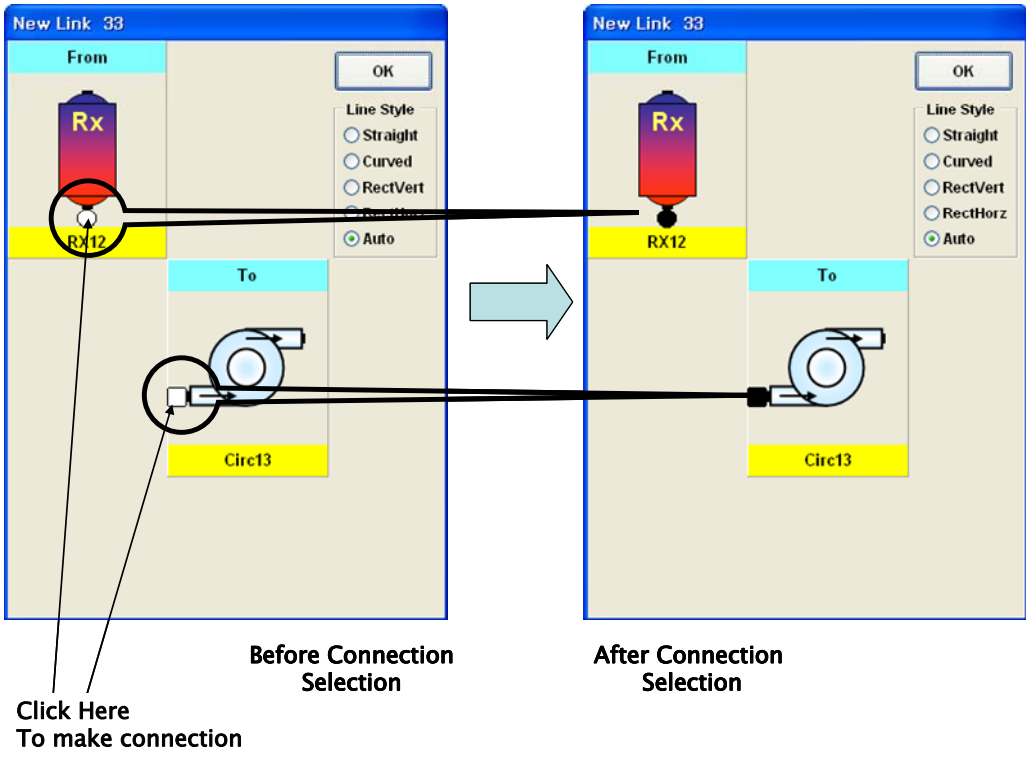

Figure 2-11 An Example of Component Connection with A Link Component.

File open/import/save commands of the main menu were tested using the sample inputs generated and using the HyPEP alpha version. These commands were found to perform as designed. The file saves and open saves the graphic information to a file with the extension of '.HyPEP' and the thermodynamic

information in the file with the extension of '.HyPEPdata'. When HyPEP opens the file with '.HyPEP' extension and if there is a file with same name with the extension of 'HyPEPdata' then it reads in the thermodynamic data. If not, the thermodynamic data need to be initialized or entered using the component modification feature. The file open/save features need to be continually updated as the HyPEP program evolves.

The test of the utilities such as the link style change, adding points to a link component, flipping of the from- and to- components of a link component, selecting and deselecting components, zoom in and zoom out, cloning (copying) of a system of components, changing z-order of the components (BringToFront and the SendToBack commands), were extensively tested and these were found to work as designed.

At present, some known GUI function bugs include the separation of primary and secondary side nodes of the heat exchanger when it is cloned and then copied onto the drawing canvas, occasional errors of the 'Save As' command resulting in fouled files, and others. These errors are expected to be resolved in the HyPEP beta and the final version.

2.5.2 Thermodynamic Properties of Gases

The thermodynamic property calculation routines of the gases for the HyPEP were tested for their robustness and the smoothness of the properties. An independent program was produced for the gas properties to draw the property surface diagrams for each of the substances in the property tables. More systematic verification/validation for the thermodynamic properties of gases is planned for the 3rd year of this project.

Following are the results of the tests for selected gas species.

Test for Helium

The test ranges for the Helium are as follows:

P (bar)	:	1	~	300
T (K)	:	200	~	1650
h (kJ/kg)	:	1050.9	~	8665
rho (m3/kg)	:	0.01488	~	28.90
s (kJ/kg/s)	:	30.24	~	85.25

The property surfaces are shown in Figure 2-12. As can be seen in the Figure, the surfaces of enthalpy, entropy and the density show smooth variation.

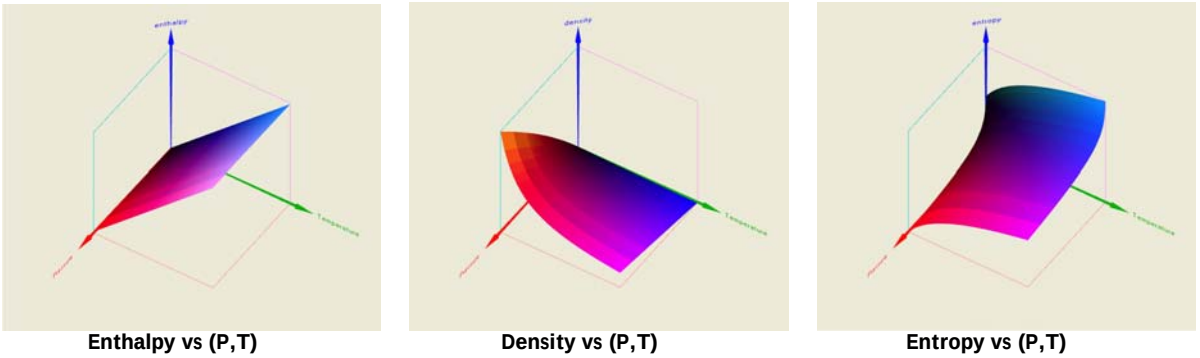

Figure 2-12 Helium Property Surfaces.

Test for H_2 Para

The test ranges for the H_2 Para are as follows:

P (bar)	:	1	~	300
T (K)	:	200	~	1650
h (kJ/kg)	:	2971	~	25207
rho (m3/kg)	:	0.01488	~	28.90
s (kJ/kg/s)	:	30.24	~	85.25

The property surfaces are shown in Figure 2-13. As can be seen in the Figure, the surfaces of enthalpy, entropy and the density show smooth variation.

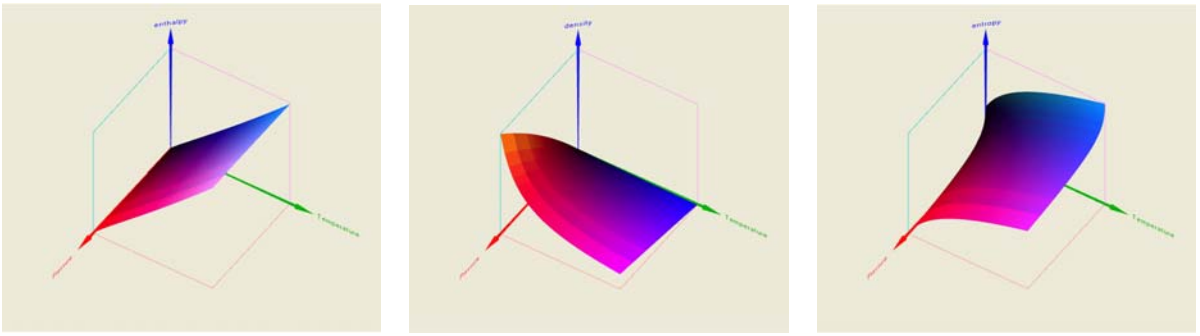

Enthalpy vs (P,T) Density vs (P,T) Entropy vs (P,T)

Figure 2-13 Hydrogen (Para) Property Surfaces.

Test for CO_2

The test ranges for the CO_2 are as follows:

P (bar)	:	1	~	300
T (K)	:	200	~	1650
h (kJ/kg)	:	288.6	~	2038.2
rho (kg/kg)	:	0.325	~	769.2
s (kJ/kg/s)	:	1.472	~	4.132

The property surfaces are shown in Figure 2-14. There are sudden drops occurring at low temperature region. This is because the Carbon Dioxide is near the triple point, and the thermodynamic routines are not valid in this region. In other regions, the surfaces of enthalpy, entropy and the density show smooth variation.

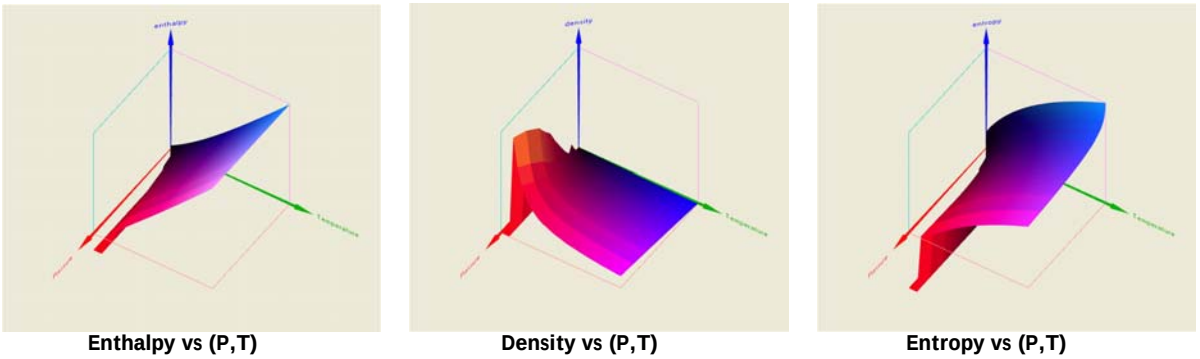

Enthalpy vs (P,T) Density vs (P,T) Entropy vs (P,T)

Figure 2-14 Carbon Dioxide Property Surfaces.

Test for Argon

The test ranges for the Argon are as follows:

P (bar)	:	1	~	300
T (K)	:	200	~	1650
h (kJ/kg)	:	154.2	~	996
rho (kg/kg)	:	0.295	~	833.3
s (kJ/kg/s)	:	1.386	~	8.45

The property surfaces are shown in Figure 2-15. As can be seen in the Figure, the surfaces of enthalpy, entropy and the density show smooth variation.

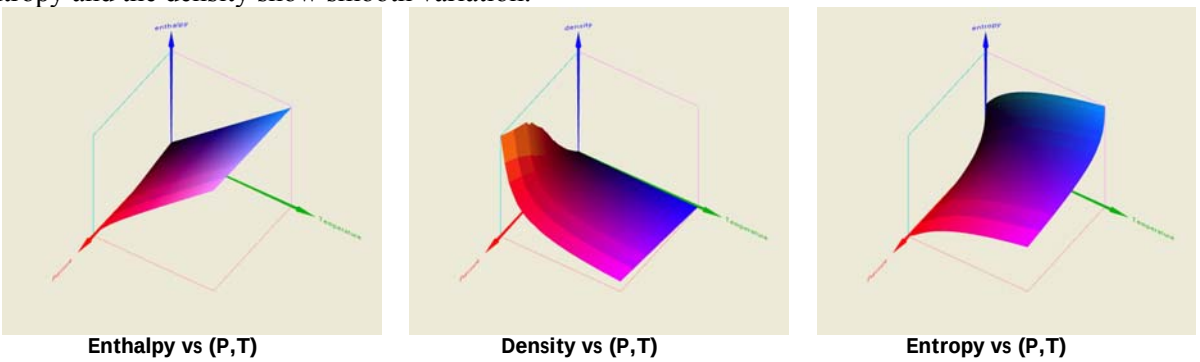

Figure 2-15 Argon Property Surfaces.

Test for Nitrogen

The test ranges for the Nitrogen are as follows:

P (bar)	:	1	~	300
T (K)	:	200	~	1650
h (kJ/kg)	:	272.6	~	2046.6
rho (m3/kg)	:	0.207	~	476.2
s (kJ/kg/s)	:	2.2152	~	6.31

The property surfaces are shown in Figure 2-16. As can be seen in the Figure, the surfaces of enthalpy, entropy and the density show smooth variation.

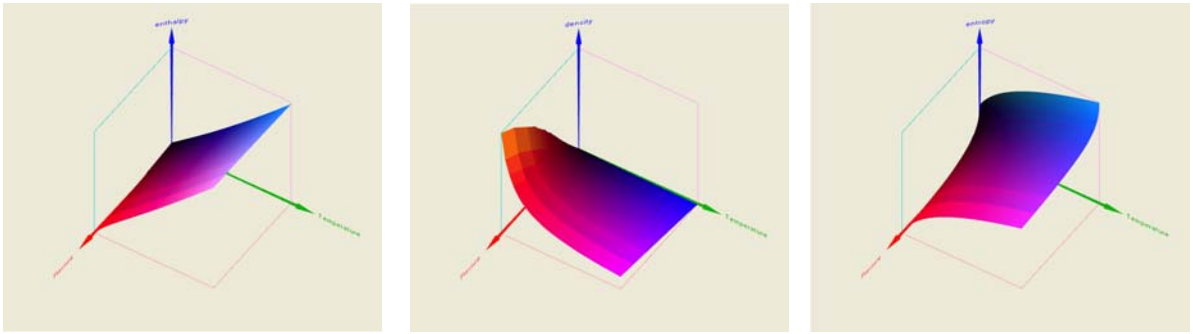

Figure 2-16 Nitrogen Property Surfaces.

Test for Oxygen

The test ranges for the Oxygen are as follows:

P (bar)	:	1	~	300
T (K)	:	200	~	1650
h (kJ/kg)	:	257.9	~	1928.4
rho (m3/kg)	:	0.236	~	714.3
s (kJ/kg/s)	:	1.0249	~	6.0729

The property surfaces are shown in Figure 2-17. As can be seen in the Figure, the surfaces of enthalpy, entropy and the density show smooth variation.

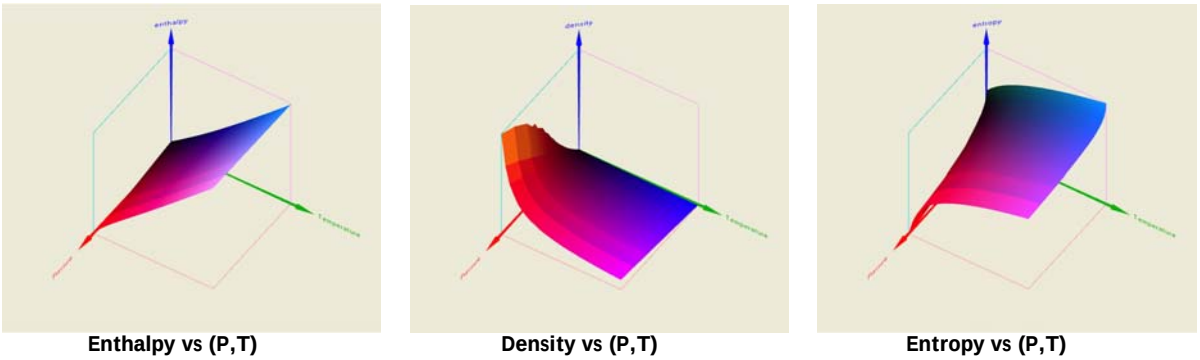

Enthalpy vs (P,T) Density vs (P,T) Entropy vs (P,T)

Figure 2-17 Oxygen Property Surfaces.

2.5.3 Numerics Test

At present, the HyPEP beta version is being developed with a view to completion in October 2007. The numerics of the HyPEP will not be completed until the final version is completed. In the third year, a systematic verification and validation is planned to be carried out. In the HyPEP beta, however, all the major elements of the numeric solution scheme have been installed and these are being tested for functionality.

In the first year, a set of equations for the numerical solution scheme for the flow network had been developed with the view to installation into the HyPEP beta. In the second year this numeric scheme had been installed into HyPEP program, but during the preliminary numeric testing, it was found that the simple flow relationship developed to replace the flow caused frequent 'division by zero' error caused by the velocity of the link becoming zero. Thus, in the beta version, a simplified momentum conservation equation has been installed into the HyPEP program as described in section 2.2. At present the modified scheme is being tested for the HyPEP beta.

The first major function in the HyPEP numerics scheme is the build-up of the system(s) of thermo-dynamic components built by user on-screen. The build-up of the systems is the responsibility of the GUI part of the HyPEP program and this part of the GUI has been extensively tested as described in the previous sections.

After the system(s) have been built-up, the numeric program part of HyPEP builds the pressure matrix for each of the thermodynamic system using the mass, energy and momentum continuity equations described in Section 2.2. The system pressure matrix is solved using a matrix solver based on Gauss elimination.

The test of the numerics were carried out to check the followings

- Correct pressure matrix set-up
- Accuracy of the matrix solution algorithm (function Gauss)

Test of pressure matrix set-up

In order to check the system build-up and the pressure matrix set-up, a program segment which shows the details of the system and the pressure matrix has been developed and imbedded into the HyPEP program. The program segment shows the information in a separate window named the 'SolverDisplay' which is shown in Figure 2-18.

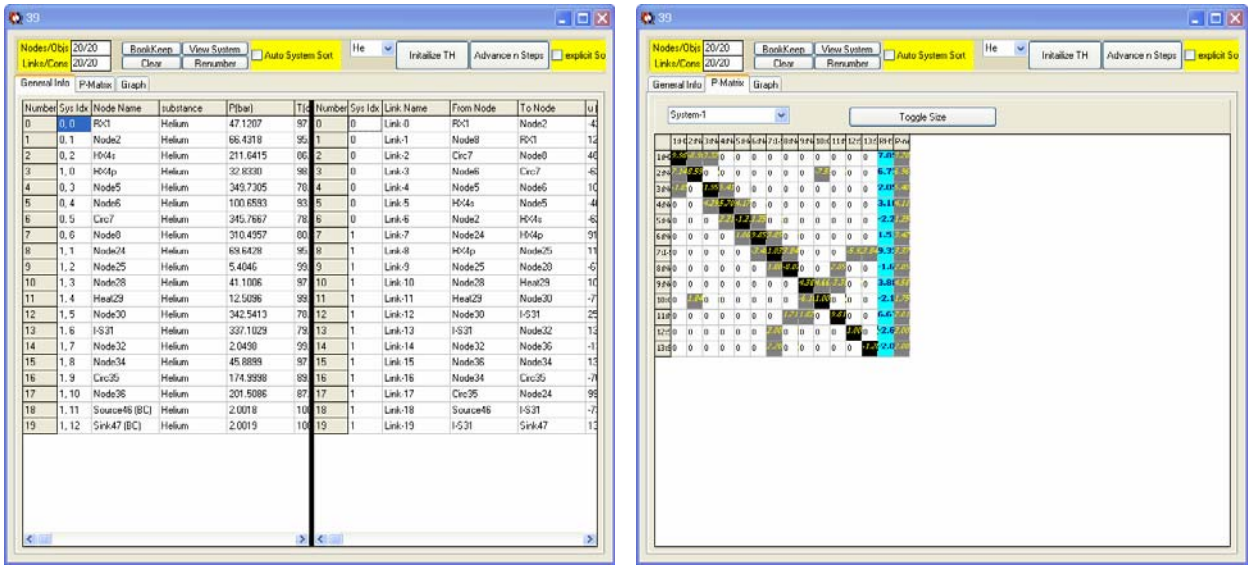

Figure 2-18 An example of SolverDisplay window showing the General information and the System Matrix.

The SolverDisplay shows the Pressure matrix for each system and it is possible to visually check the contents of the pressure matrices. The SolverDisplay is expected to be a useful tool. Using the SolverDisplay, a number of sample layouts built with the GUI were analyzed and the HyPEP has been tested to build the pressure matrix correctly.

Test of Gauss Matrix Solver Routine

A separate program was generated with the same Gauss matrix solver to test the accuracy of the Gauss elimination routine. The program was designed so that a system of ‘n’ linear equations is setup and then solved with known solution and then the answer is compared with the known solution.

This is accomplished by first generating a matrix of size n x n with random coefficients. Then a vector array of n random values is generated as the known solution. The n x n matrix and the ‘known’ vector are multiplied to calculate the vector b. The vector b and the "n x n" matrix are used as input to obtain the solution vector. The solution vector and the ‘known’ vector are compared to find the maximum error.

This test was repeated for 500 cases of 500x500 different random matrices and it was found that the maximum relative error was about 1.0^{-15} for the coded Gauss elimination scheme.

2.6 Summary

The HyPEP beta is being developed with the expected completion date of October 2007. Major development efforts have been and are being given to the development and installation of the numeric scheme for the flow network and the component model developments. Also, compared with the HyPEP alpha completed in October 2006, the HyPEP beta has more robust Graphic User Interface.

The numerical scheme developed during the 1st year has now been modified to include the simplified momentum conservation. And the HyPEP coding has been changed to reflect the change in the basic numerics formulation. Testing of various basic aspects of the numerical scheme are being carried out such as the test of correct system build-up and pressure matrix set-up, smoothness of the property calculation routines, and the accuracy of the matrix solver, etc. A number of independent programs, such as Gauss elimination accuracy testing program, and 3-dimensional gas property visualizer, and HyPEP imbedded programs such as SolverDisplay unit and the LayoutInformation unit have been developed. These programs will be useful in the verification and validation of HyPEP in the third year.

The component development has continued and now a set of object classes defining the various components necessary to model the hydrogen production plant has been established. The methods and the properties of the object classes are being developed and coded for these object classes such as the heat exchanger object, High Temperature Electrolysis System object, Brayton Cycle object for the PCU, etc.

The Graphic User Interface was functional with the HyPEP alpha, and in the HyPEP beta, the GUI is being improved and the some bug-fixes have been carried out. Currently all the major concepts for GUI have been explored, demonstrated and installed in the HyPEP program.

3. SYSTEM INTEGRATION I - Steady state system performance analysis

3.1 Introduction

The Next Generation Nuclear Plant (NGNP), a very High temperature Gas-Cooled Reactor (VHTR) concept, will provide the first demonstration of a closed Brayton cycle at a commercial scale of a few hundred megawatts electric and hydrogen production. The power conversion system (PCS) for the NGNP will take advantage of the significantly higher reactor outlet temperatures of the VHTR to provide higher efficiencies than can be achieved in the current generation of light water reactors. Besides demonstrating a system design that can be used directly for subsequent commercial deployment, the NGNP will demonstrate key technology elements that can be used in subsequent advanced power conversion systems for other Generation IV reactors. In anticipation of the design, development and procurement of an advanced power conversion system for the NGNP, the system integration of the NGNP and hydrogen plant was initiated to identify the important design and technology options that must be considered in evaluating the performance of the proposed NGNP.

The integrated system of a Very High Temperature Gas-Cooled Reactor (VHTR) and a High Temperature Steam Electrolysis (HTSE) process is one of systems being investigated by the U.S. Department of Energy and Idaho National Laboratory. This system will produce hydrogen by utilizing a highly efficient VHTR with an outlet temperature of 900 °C and supplying necessary energy and electricity to the HTSE process for electrolysis of high temperature steam.

In this section, we mainly focused on the steady-state efficiency analyses for the integration system between VHTR and HTSE system. Totally, 55 different system configurations were extensively investigated by a process analysis code, HYSYS. Besides, some alternative concepts for hydrogen generation were briefly considered. This section includes (1) efficiency analyses for various system configurations, (2) optimization of system efficiencies, (3) optimum sizing of heat exchangers and (4) parametric studies.

3.2 Methods

3.2.1 Plant Efficiency

The efficiency of each proposed configuration was estimated using HYSYS [Aspen Technology 2001], a process optimization code used in the chemical and oil industries.

The power conversion unit (PCU) cycle efficiency, η_{PCU}, used in this study is defined as [Oh et. al 2006a]:

$$\eta_{PCU} = \frac{\text{Electric power output}}{\text{Reactor themal power} - \text{H}_2 \text{ process power}} = \frac{\sum W_T - \sum W_C - W_S - \sum W_{CIR}}{Q_{th} - Q_{H2}} \qquad (3\text{-}1)$$

where $\sum W_T$ is the total turbine workload, $\sum W_C$ is the total compressor workload, W_S is the plant stationary load, $\sum W_{CIR}$ is the circulator workload in the primary, intermediate, and, if present, ternary loops and includes, for example, the recycle and make-up water pumps and the H_2 and sweep water circulators, Q_{th} is the reactor thermal power, and Q_{H2} is the thermal power supplied to the hydrogen

generating plant. For the efficiency calculations, we report the overall cycle efficiency, which is defined as

$$\eta_{overall} = \frac{\sum W_T - \sum W_C - W_S - \sum W_{CIR} - \sum Q_{HTSE} + Q'_{H2}}{Q_{th}} \quad (3\text{-}2)$$

where $\sum Q_{HTSE}$ is the electric power requirement for electrolysis and Q'_{H2} is the hydrogen production mass flow rate times the specific energy content of the hydrogen.

3.2.2 Optimization

For this calculation, the process optimization was carried out using HYSYS process modeling software. HYSYS has an optimization tool that is built in to integrate the simulation model of the system. The optimization program searches for the maximum value of a given objective function subject to a number of imposed constraints. Figure 3-1 shows a two-dimensional design space with defined regions. The goal is to maximize f (x1, x2, x3,...) where x1, x2, x3 are independent variables such as mass flow, pressure, temperature, etc. For the optimization, the x variables are manipulated within a specified range of a lower and upper bound. The regions in Figure 3-1 are defined by a feasible design space within functional constraints and an infeasible design space outside of the constraint boundaries [Mckellar 1992]. Functional constraints are material and energy balances, for example, positive pressure drop in every stream in the direction of flow, positive power in turbine and compressor, temperature requirements at the inlet and outlet of the heat exchangers, etc. The function, f, is the objective function which is defined as the overall plant efficiency above. Constant values of the objective function define contours on the design space. Figure 3-2 shows design space of 2-D design vector showing optimal design points. First, the initial calculation should be in the feasible design space and the search continues towards a direction in the design space until a maximum is reached. A new direction is found and the search continues in that direction as long as the objective function value increases. Once a maximum is reached, the search continues towards the optimal design point. However, if the optimal design point is outside of the feasible design space, the closest contour to the optimal solution that coincides with the constraint boundary can be the optimal solution within the constraints specified.

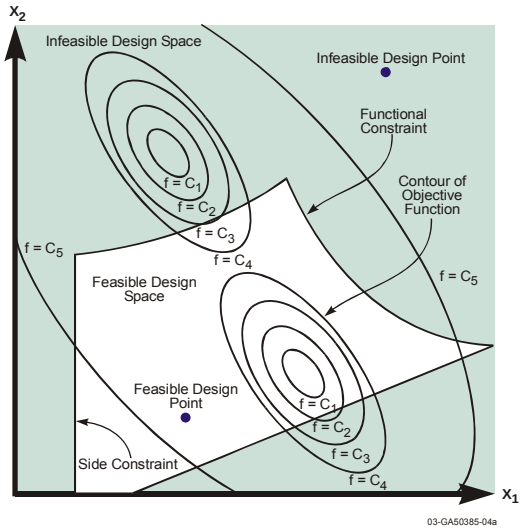

Figure 3-1 Design space with designed regions.

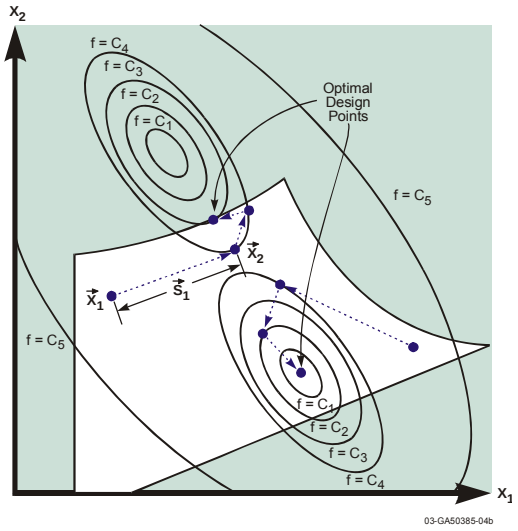

Figure 3-2 Potential optimal solutions.

In the electrolyzer model [Oh et al. 2006a], the oxygen stream produced at the anode is assumed to mix with a sweep gas stream that is introduced at the anode. The combined stream then exits the electrolyzer. The hydrogen stream produced at the cathode is assumed to mix with a feed stream that is introduced at the cathode. The feed stream is composed of water vapor to be electrolyzed, hydrogen gas for maintaining reducing environment, and possibly an inert gas, presently assumed to be nitrogen.

3.2.3 Electrolyzer Model for High Temperature Steam Electrolysis (HTSE)

Energy Equation

An energy balance on the electrolyzer gives

$$\sum_i \dot{n}_{P-i} H_{P-i}(T_P, P) = \sum_i \dot{n}_{R-i} H_{R-i}(T_R, P) + Q + W \tag{3-3}$$

where

$\dot{n}$	=	species mole flow rate,
H	=	enthalpy per mole,
Q	=	rate of heat transfer to the electrolyzer,
W	=	rate of electrical work supplied to the electrolyzer,
T	=	temperature,
P	=	pressure,

and where we have used subscripts *R* for reactants and *P* for products. Their mass flow rates are defined

$$\begin{aligned} & m_{H_2O-o-cath}\, h_{H_2O}(T_o, P) + m_{H_2-o-cath}\, h_{H_2}(T_o, P) + m_{N_2-o-cath}\, h_{N_2}(T_o, P) \\ & \quad m_{O_2-o-anode}\, h_{O_2}(T_o, P) + m_{sweep-o-anode}\, h_{sweep}(T_o, P) = \\ & \qquad m_{H_2O-i-cath}\, h_{H_2O}(T_i, P) + m_{H_2-i-cath}\, h_{H_2}(T_i, P) + m_{N_2-i-cath}\, h_{N_2}(T_i, P) \\ & \qquad\quad m_{O_2-i-anode}\, h_{O_2}(T_i, P) + m_{sweep-i-anode}\, h_{sweep}(T_i, P) + Q + W \end{aligned} \tag{3-4}$$

where

m	=	species mass flow rate (kg/s),
h	=	specific enthalpy (Joules/kg),

and where subscripts *i* and *o* represent inlet and outlet, respectively.

Species Mole and Mass Flow Rates

The species mole flow rates entering and leaving the electrolyzer are related to the current density through the relationships

$$\dot{n}_{H_2O-o-cath} = \dot{n}_{H_2O-i-cath} - \frac{iA}{2F}$$
$$\dot{n}_{H_2-o-cath} = \dot{n}_{H_2-i-cath} + \frac{iA}{2F}$$
$$\dot{n}_{O_2-o-anode} = \dot{n}_{O_2-i-anode} + \frac{iA}{4F} \qquad (3\text{-}5)$$
$$\dot{n}_{sweep-o-anode} = \dot{n}_{sweep-i-anode}$$
$$\dot{n}_{N_2-o-cath} = \dot{n}_{N_2-i-cath}$$

where

i	=	current density (amps/m^2),
A	=	electrode surface area, (m^2) and
F	=	Faradays constant.

The species mass flow rates and mole flow rates are related as follows: For an individual species

$$\dot{m}_{k-o} = A_k \ \dot{n}_{k-o} \text{ and } \dot{m}_{k-i} = A_k \ \dot{n}_{k-i} \ , \quad k = H_2O, H_2 , O_2, \text{ and } N_2. \qquad (3\text{-}6)$$

where A_k is the atomic weight of species, k in kg per mole, subscript o is the outlet and i is the inlet.

Cell Voltage and Electrical Work

The voltage drop across the electrolyzer is the sum of the electrode Nernst potential and the resistance of the cell. In estimating the resistance, the activation and the concentration overpotentials are lumped in with the cell internal resistance. The cell voltage is then assumed given by

$$V_{cell} = \overline{V}_{Nernst} + i \cdot ASR \qquad (3\text{-}7)$$

where

$\overline{V}_{Nernst}$	=	is the Nernst potential, and
ASR	=	is the area-specific cell resistance (ohms-m^2).

The electrical work done in the cell is

$$W = V_{cell} \cdot i \cdot A \ . \qquad (3\text{-}8)$$

The active species giving rise to the Nernst potential satisfy the chemical balance equation

$$H_2O\,(g) \rightarrow H_2\,(g) + \frac{1}{2}O_2\,(g)\,. \qquad (3\text{-}9)$$

The change in Gibbs free energy for this reaction carried out at temperature T and pressure P is

$$\Delta G(T,P) = \Delta G_f(T,P) + RT \ln\left[\frac{f_{H_2}\, f_{O_2}^{\frac{1}{2}}}{f_{H_2O}}\right] \tag{3-10}$$

where f is the molar fraction of a species and $\Delta G_f(T,P)$ is the Gibbs free energy in forming the products at temperature T and pressure P minus the same for the reactants, that is,

$$\Delta G_f(T,P) = G_{f-H_2}(T,P) + 1/2\, G_{f-O_2}(T,P) - G_{f-H_2O}(T,P)\,. \tag{3-11}$$

where $G_{f\text{-}i}(T,P)$ is the Gibbs free energy on a per mole basis of forming species i at conditions T and P. In turn $\Delta G_f(T,P)$ is written in terms of $\Delta G^0{}_f(T) = \Delta G_f(T,P_{STD})$ where P_{STD} = 0.101 MPa. Then setting the change in Gibbs free energy equal to the electrical work done the voltage developed by the cell is

$$\mathrm{V_{Nernst}} = \frac{-1}{2\mathrm{F}}\left[\Delta G_f{}^0(T) + RT \ln\left[\left(\frac{f_{H_2}\, f_{O_2}^{\frac{1}{2}}}{f_{H_2O}}\right)\left(\frac{P}{P_{STD}}\right)^{\frac{1}{2}}\right]\right] \tag{3-12}$$

where P_{STD} = 0.101 MPa and P is the cell pressure. Then the average value of $\mathrm{V_{Nernst}}$ was calculated using the following equation.

$$\overline{\mathrm{V}}_{\mathrm{Nernst}} = \frac{1}{2\mathrm{F}(\mathrm{T_P}-\mathrm{T_R})(\mathrm{y_{o,O2,A}}-\mathrm{y_{i,O2,A}})(\mathrm{y_{o,H2,C}}-\mathrm{y_{i,H2,C}})}\times \int_{\mathrm{T_R}}^{\mathrm{T_P}}\int_{\mathrm{y_{i,O2,A}}}^{\mathrm{y_{o,O2,A}}}\int_{\mathrm{y_{i,H2,C}}}^{\mathrm{y_{o,H2,C}}} \Delta\mathrm{G(T)} - \mathrm{RT}\ln\left(\frac{1-\mathrm{y_{H2}}-\mathrm{y_{N2}}}{\mathrm{y_{H2}}\,\mathrm{y_{O2}}^{1/2}}\right)\mathrm{dy_{H2}\,dy_{O2}\,dT} \tag{3-13}$$

The mole fractions at any point in the electrolyzer are related to the molar mass flow rates at that point through

$$f_{H_2O-cath} = \frac{\dot{n}_{H_2O}}{\dot{n}_{H_2O}+\dot{n}_{H_2}+\dot{n}_{N_2}} \qquad f_{H_2-cath} = \frac{\dot{n}_{H_2}}{\dot{n}_{H_2O}+\dot{n}_{H_2}+\dot{n}_{N_2}}$$
$$f_{O_2-anode} = \frac{\dot{n}_{O_2}}{\dot{n}_{sweep}+\dot{n}_{O_2}} \qquad f_{sweep-anode} = \frac{\dot{n}_{sweep}}{\dot{n}_{sweep}+\dot{n}_{O_2}}. \tag{3-14}$$

The current density and active cell area are then specified, yielding the total operating current. Care must be taken to insure that the specified inlet gas flow rates and total cell current are compatible. The minimum required inlet steam molar flow rate is the same as the steam consumption rate, given by:

$$\dot{N}_{i,H2O,\min} = \Delta\dot{N}_{H2O} = \frac{I}{2F}N_{cells} = \frac{i\,A_{cell}}{2F}N_{cells} = \Delta\dot{N}_{H2} \tag{3-15}$$

this is of course also equal to the hydrogen production rate.

Once the total and per-cell hydrogen production rates are known, the outlet flow rates of hydrogen and steam on the cathode side and oxygen on the anode side can be determined. The flow rates of any inert gases, the anode-side sweep gas, and any excess steam or hydrogen are the same at the inlet and the outlet. Once all these flow rates are known, the summations in Equation (3-3) can be evaluated. The product summation must be evaluated initially at a guessed value of the product temperature, T_P.

Matlab (Mathworks 2006) was used to calculate Equations (3-3) through (3-15). Figures 3-3 through 3-5 illustrate the calculated results. Figure 3-3 contains two curves. One curve shows the required electrical work with current density at a fixed total current. The other curve shows the required number of cells to obtain the current density. As shown in this figure, electrical work increases with current density because higher current density results in higher operating voltage as shown in Equation (3-8) and Figure 3-4. However, the number of cells is reduced by the increase of current density. Therefore, economically, the increase of current density increases the operating cost, but reduces the capital cost. Therefore, the operating condition of the current density should be carefully determined under various economic considerations. To obtain the optimal operating current density, further optimization analysis is recommended.

Figure 3-5 shows the variation of product temperature with total electric current. Basically, the water splitting process is an endothermic reaction. Therefore, without additional heat, the product temperature is reduced. In Figure 3-5, we can see the temperature reaches a minimum between 5 and 15 amperes. At the higher current density, we can see the temperature gradually turns upward. It is due to the ohmic heating by the cell internal resistance. The heating rate also increases with the current density causing the product gas temperature rise.

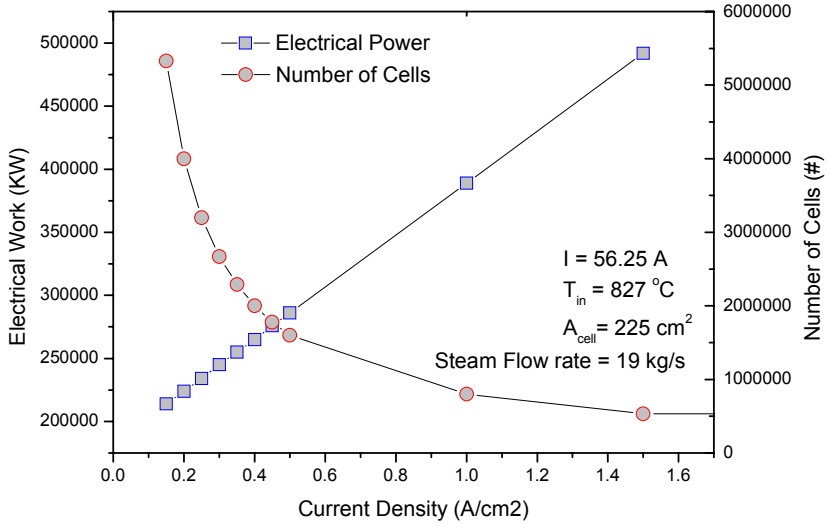

Figure 3-3. Required electrical work and number of cells with current density at the constant current.

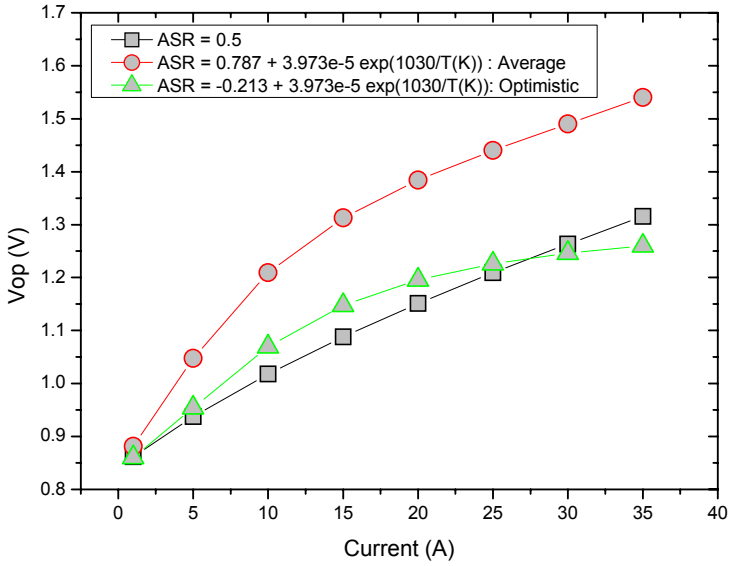

Figure 3-4. Variation of cell operating voltage with current for different stack area-specific resistance (ASR).

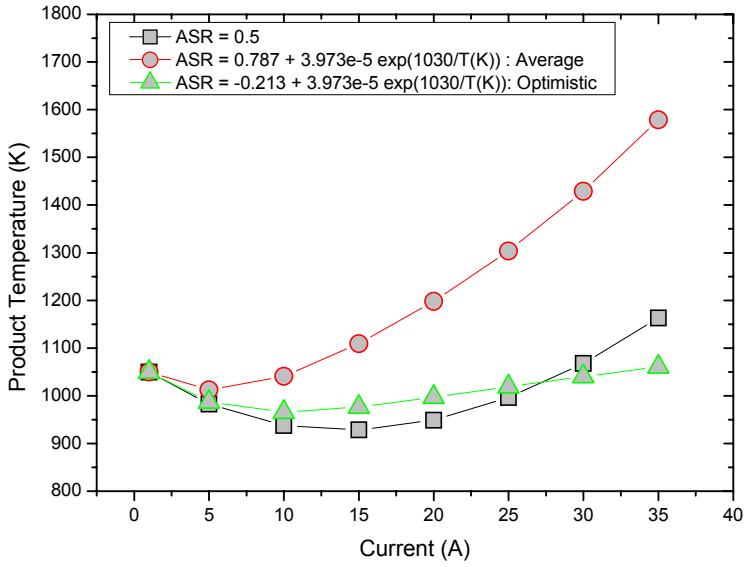

Figure 3-5. Variation of product temperature with current for different ASR.

3.3 Efficiency Analysis and Optimization for the Integrated Systems

3.3.1 Five configurations for the VHTR/HTSE integration

The current work is focused on the integration of the VHTR and the HTSE. In this system, the heat generated in the reactor core is transferred to the HTSE system through various heat exchangers that increase the steam temperature to more than 800 °C. The electrolyzer is made of Solid Oxide Fuel Cells that convert the heated steam into hydrogen and oxygen molecules. Approximately 10 percent of the total energy transferred is supplied by heat and the rest is supplied by electricity, which is generated in the PCU integrated in the VHTR system. The PCU is based on the widely-used closed-loop gas Brayton cycle, which shows high efficiency especially at higher temperatures. The reactor core and PCU are integrated in two different configurations; the direct cycle and the indirect cycle. In the direct cycle, the PCU is located in the primary system in series with the reactor core. In the indirect cycle, the primary system and PCU are separated by a heat exchanger resulting in a more complicated configuration and reduced efficiency. However, separating the reactor core from the PCU results in easier maintenance and should reduce the strong dynamic coupling between the core and PCU, which may improve safety. The Independent Technology Review Group [2004] has recommended an indirect cycle and the maximum VHTR outlet temperature of 900 ^{0}C, based in part on material problems associated with higher temperatures.

In the current study, the efficiency of VHTR/HTSE system has been estimated using HYSYS, a commercial process flowsheet analysis code that has been used in chemical and petroleum industry. The HYSYS code supports models for many basic system components and has a process optimization capability. Typical HYSYS components used in this study are a reactor, pump, compressor, heat exchanger, turbine, cooler, and vessel. VHTR system modules of various configurations are developed with these basic components.

Since HYSYS does not have a model for electro-chemical processes, an electrolyzer model was developed. This model was then integrated into the HYSYS model for the balance of the HTSE process. A HYSYS model for the VHTR system was then combined with the HTSE system to obtain the combined VHTR/HTSE plant simulation. The details of the models are described below.

System Configurations for Reference Designs

In this study, the following five different configurations of the integrated system are evaluated in terms of the overall hydrogen production efficiency.

(1) Configuration 1 - Indirect Parallel Cycle (Figures 3-6 and 3-7)
(2) Configuration 2 - Indirect Serial Cycle (Figure 3-8)
(3) Configuration 3 - Direct Serial Cycle (Figure 3-9)
(4) Configuration 4 - Steam Combined Cycle (Figure 3-10)
(5) Configuration 5 - Reheat Cycle (Figure 3-11)

Figure 3-6 illustrates the indirect parallel system. The flow in the secondary coolant system is divided, with most of the flow going towards the PCU and the remainder going through a secondary heat exchanger (SHX) that directs heat towards the HTSE plant. The flow through the hot side of the SHX is then mixed with the flow from the PCU to feed the cold side of the intermediate heat exchanger (IHX). However, some of the flow is diverted away from the PCU, which acts to decrease the efficiency of the cycle. There are three coolant loops. The primary coolant system contains the nuclear reactor, the hot side of the IHX, and a compressor. The secondary coolant system contains the cold side of the IHX, the

hot side of the SHX, the PCU, and connecting piping, which is assumed to be short. The intermediate heat transport loop connects the secondary coolant system to the HTSE plant through several process heat exchangers (PHXs).

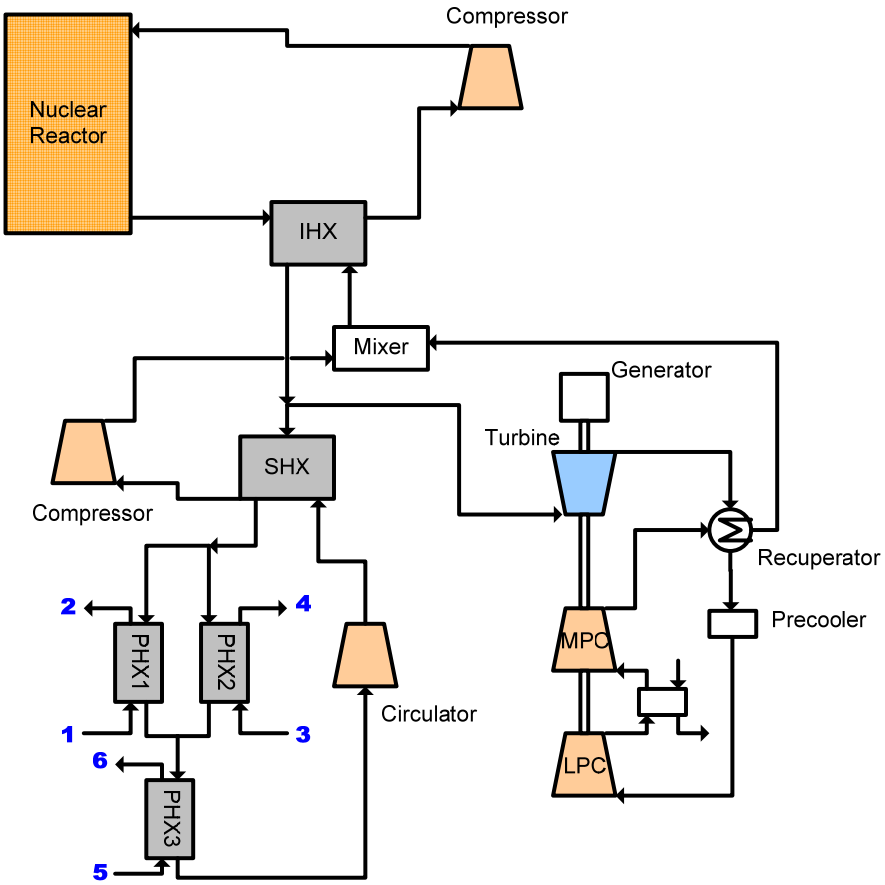

Figure 3-6. Configuration 1 - indirect parallel cycle.

For electrolysis, the steam is heated up to higher than 800 °C by the heat from SHX. The heated steam is converted into hydrogen and oxygen in the electrolyzer and discharged through the fuel and oxidizer outlet, respectively as shown in Figure 3-7. The heat of the discharged gases is recovered through three recuperators. Finally, the product gas in the fuel side contains hydrogen and steam, and the oxidizer outlet gas contains oxygen and steam. As shown in Figure 3-7, the discharged fuel steam is recycled to the inlet fuel stream, and the hydrogen gas is separated and collected in the separator. In the oxidizer outlet stream heat is first recuperated and then the stream is run through an expander to recover work. The oxygen and water components of the stream are then separated.

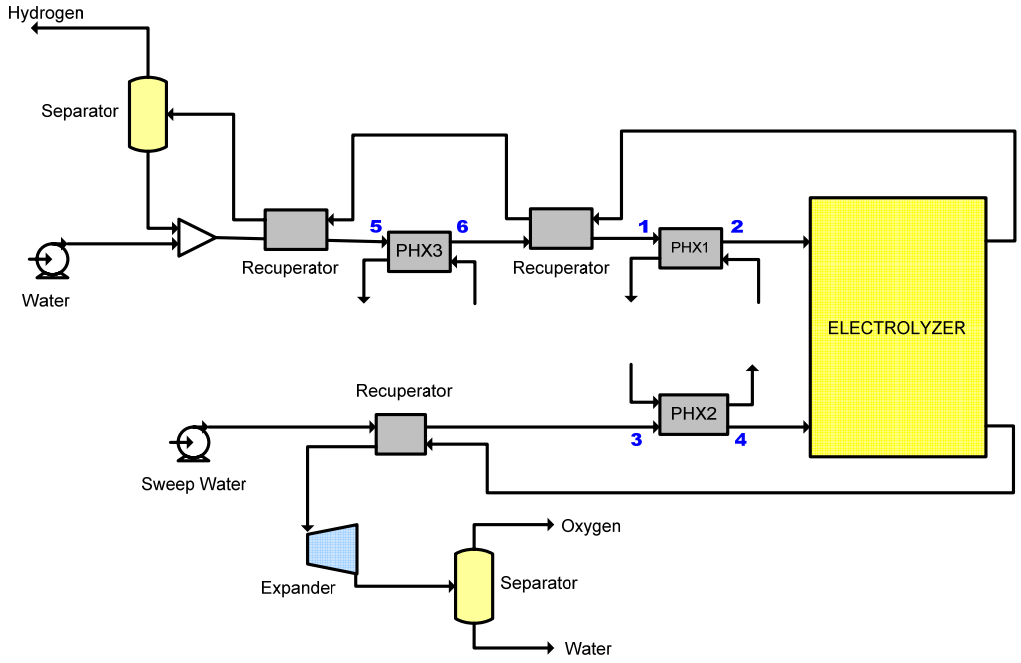

Figure 3-7. HTSE system.

Figure 3-8 illustrates the indirect serial configuration. In this configuration, SHX is located upstream of the IHX that is linked to the PCU. Therefore, the heat from the VHTR is firstly transferred to the HTSE system, and then it is transferred to the PCU. This configuration is able to supply higher temperature to the HTSE system, but decreases the PCU maximum temperature, resulting in a decreased PCU efficiency. However, in this configuration, the system is more controllable due to its less connectivity. The reduction in the number of circulators can reduce the cost and increase the overall efficiency. The same HTSE system configuration as shown in Figure 3-7 is used here in terms of coupling the VHTR and the HTSE.

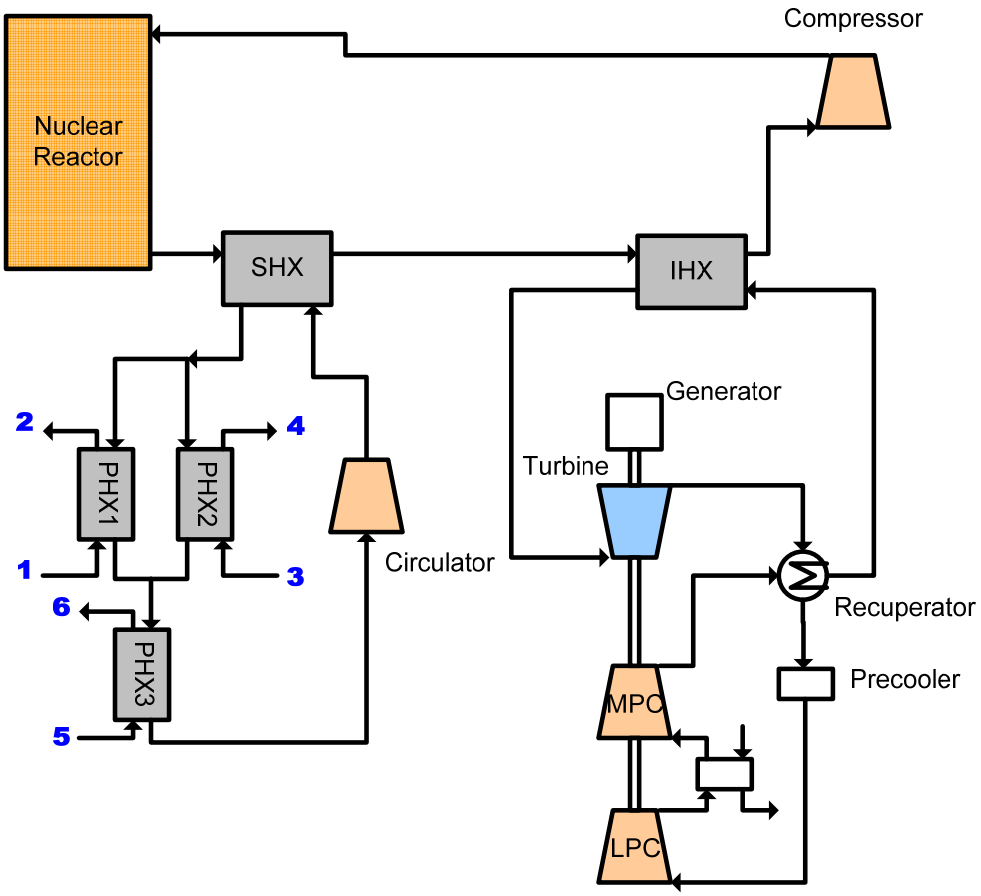

Figure 3-8. Configuration 2 - indirect serial cycle.

Figure 3-9 depicts Configuration 3, which is a direct serial cycle. The outlet stream of the VHTR flows through the SHX and then flows to the high pressure turbine. The system integration is very similar to the previous configurations in terms of utilizing heat through PHX1, PHX2, and PHX 3 that are linked to the HTSE via streams 1 to 6 as shown in Figure 3-9.

Even though the indirect configuration was recommended by the Independent Technology Review Group [2004], the direct cycle was also considered in this study due to its simplicity, high efficiency, and economics. In this configuration, the primary side is integrated with the PCU, which leads to the elimination of the large IHX between the core and the PCU and the circulator in the primary side. As a result, it increases the efficiency and will reduce the capital cost. However, on the other hand, there will be some possibilities of safety and maintenance problems. In this configuration, the HTSE system is connected to VHTR through the SHX. The HTSE system is the same as the previous configurations.

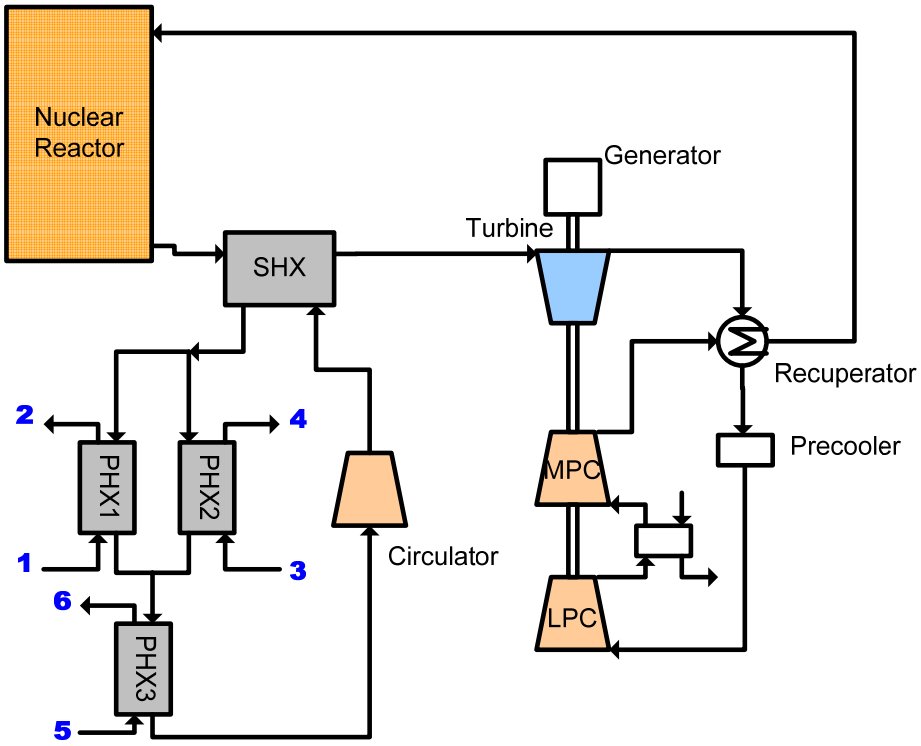

Figure 3-9. Configuration 3 - direct serial cycle.

Figure 3-10 illustrates the steam combined system. This configuration is basically the same as the Configuration 1 (indirect parallel cycle), but the recuperator is replaced with the steam turbine cycle. This configuration is commonly used to maximize the gas turbine efficiency and heat recovery in combined cycle power plants. The advantage of this configuration is due to the reduced pumping power for water in the Rankine cycle compared with that of the high pressure gas media.

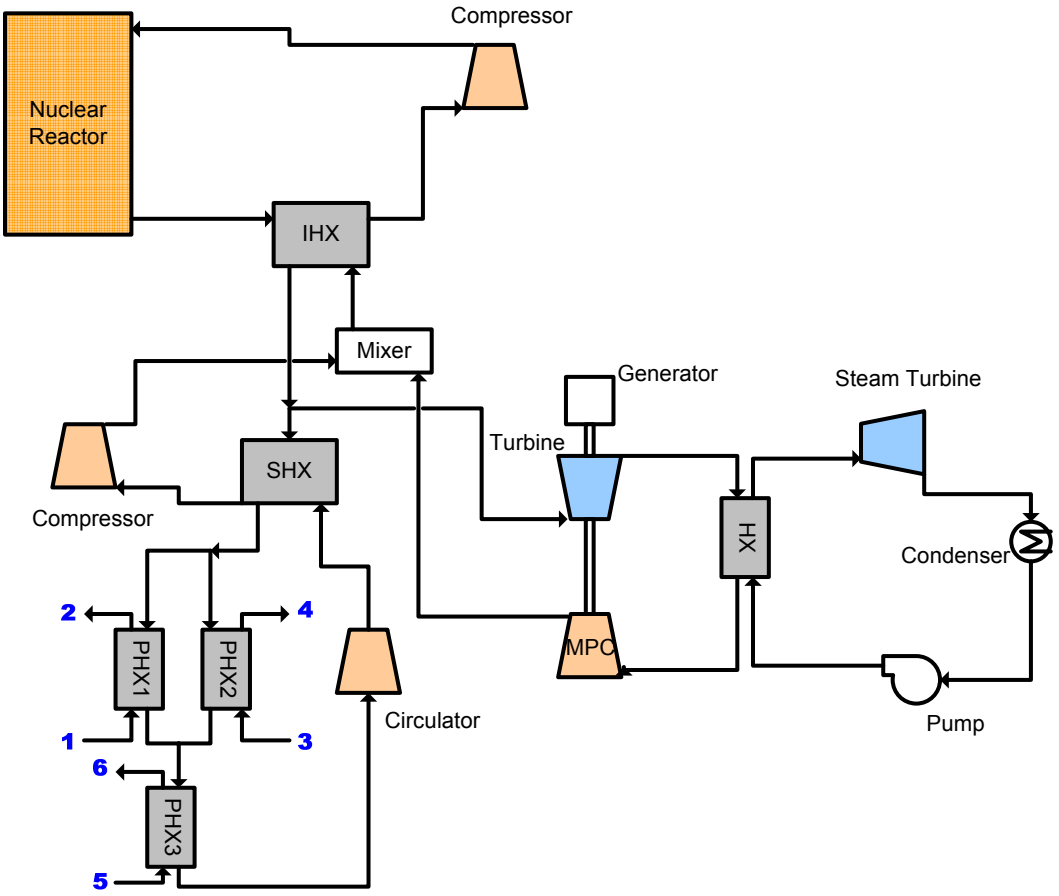

Figure 3-10. Configuration 4 - steam combined cycle.

Figure 3-11 illustrates the reheat cycle. This configuration is included to determine how much the reheat option can enhance the cycle efficiency and to investigate technical issues associated with the reheat option. For these calculations, a cycle with multiple preheaters and coolers was used. Molten salt is the coolant fluid on the primary side and helium in the Brayton cycle. Theoretically a combination of reheat and intercooling increases the cycle efficiency in a closed cycle, but the full implications have not been explored. Multiple-reheat is technically viable for closed gas cycles [Oh et al. 2007a]. For gas-cooled reactors, a multiple reheat option may not be practical due to higher-pressure loss associated with gases, i.e., helium, supercritical CO_2, and nitrogen. However, molten salt coolants can transport heat with low pumping power, which becomes very attractive without any consideration of material problems associated with molten coolants at high temperatures.

In this configuration, the discharged gas from a turbine is reheated and re-introduced to other turbines. This process usually leads to higher efficiency and power density. However, it requires more system components such as extra turbines and compressors resulting in higher capital cost. The size of turbines and compressors in this configuration will be smaller than those configurations with one turbine and one/two compressors because the total turbine and compressor work will be the same regardless of the number of turbomachines. The HTSE system is connected through the SHX and the configuration is the same as the previous systems.

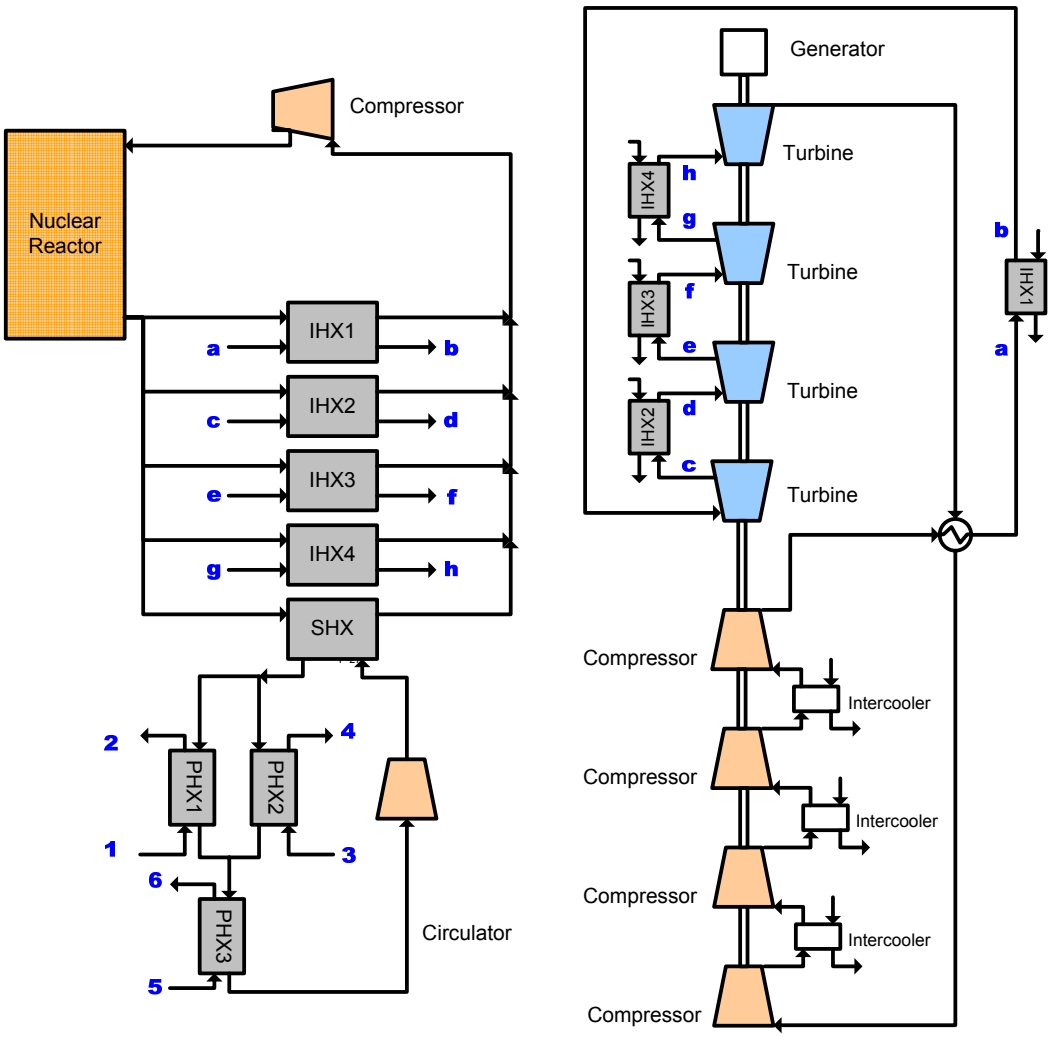

Figure 3-11. Configuration 5 - reheat cycle.

Working Fluids

In this work, the effect on efficiency of the following three coolants is estimated:

(1) Helium
(2) Supercritical carbon dioxide (S-CO_2)
(3) Flinak (LiF-NaF-KF)

Helium is the basic working fluid used in most VHTR designs. It can be used for all parts of the system; in the primary side for core cooling, the secondary side for Brayton cycle, and the ternary side for transferring heat to the HTSE. S-CO_2 can be used for the secondary and ternary sides, but not for the primary side because of its chemical reaction with the graphite materials installed in the primary core. Flinak is one kind of molten salt coolant and is very nearly incompressible. It can be used for primary core cooling and ternary heat exchange loop. However, it can not be used in the PCU because the

turbomachinery require a compressible substance. In this study, we organized all the possible combinations of working fluids, and performed efficiency optimization and analysis. Table 3-1 summarizes the physical properties for those coolant materials.

Table 3-1. Physical properties for working fluids (at 900°C, 7 MPa).

	Helium	S-CO_2	Flinak (LiF-NaF-KF)
Formula Wt (g/mol)	4.003	44.01	41.2
Melting Point (°C)	-	-	454
Density (kg/m3)	2.859	31.06	1528
Heat Capacity (kJ/kg-mol-°C)	20.78	1.285	88.35
Viscosity (Pa s)	2.703e-3	5.161e-5	1.963e-4
Thermal Conductivity (W/m-°C)	0.2517	0.07885	0.8612
Phase	Gas	Gas	Liquid

3.3.2 Parametric Study

In this section, the effects on the plant efficiency were estimated for various operating parameters. These parameters included reactor inlet temperature and turbine and compressor efficiencies. Note that the parametric studies on reactor inlet temperature were performed with the reactor outlet temperature fixed at 900 °C, which is assumed dictated by HTSE system requirements. The Configuration 1 system with He-He-He working fluids combination was selected as the reference case for analysis (refer to Table 3-2).

Figure 3-12 shows the effect of compressor efficiency and core inlet temperature on the overall system efficiency. As shown in this figure, the system efficiency increases with the compressor efficiency. The maximum efficiency ranges around the core inlet temperature of 600~700 °C. The reason for the efficiency increase with compressor efficiency is obvious because high compressor efficiency reduces irreversibility of the system. In our calculation, one percent increase of compressor efficiency results in about 0.3 ~ 0.6 percent increase of overall efficiency. Thus, improving the compressor efficiency is a very useful way to get a more efficient system. Of course, this also means that a decrease of the compressor efficiency during operation can cause the overall efficiency to decrease.

The effect of core inlet temperature is quite complicated. Core inlet temperature is closely related to PCU flow rate, and also directly to the flow rate in the primary side. As the core inlet temperature is raised, the PCU flow rate can also be increased, resulting in PCU efficiency increase. However, the increase of core inlet temperature requires higher flow rate in the primary side (since reactor power and outlet temperature are maintained constant), requiring higher circulation power. As shown in Figure 3-12, the overall efficiency increases with core inlet temperature below 500 °C from the increase of PCU flow rate, but above 600°C, the efficiency is reduced due to the increase of circulation power. Essentially, there is a break point where the decrease in efficiency from increased compressor losses is opposite and equal to the efficiency gain resulting from a higher average core temperature.

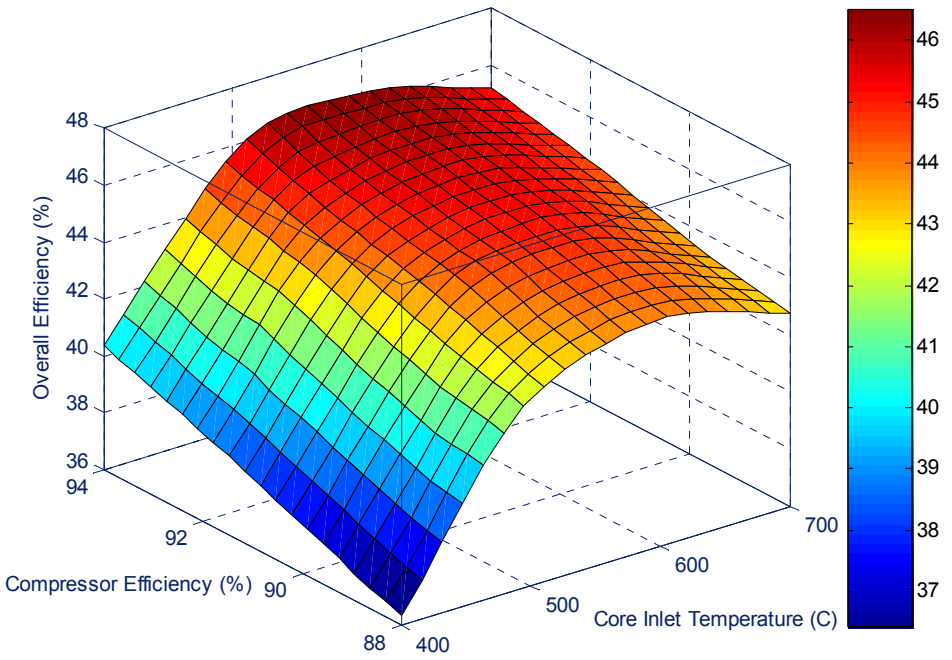

Figure 3-12. Effect of core inlet temperature and compressor efficiency on overall plant efficiency (He-He-He).

Figure 3-13 shows the effects of turbine efficiency and core inlet temperature on overall efficiency. The optimal temperature occurred around 650 °C. As expected, the overall efficiency was increased with turbine efficiency. One percent increase of turbine efficiency caused 0.5~0.9% increase of overall efficiency. However, the rate of increase decreased as the operating temperature approached the optimal temperature. In this study, the efficiency of turbine seems to affect the overall efficiency a little more than the efficiency of one compressor.

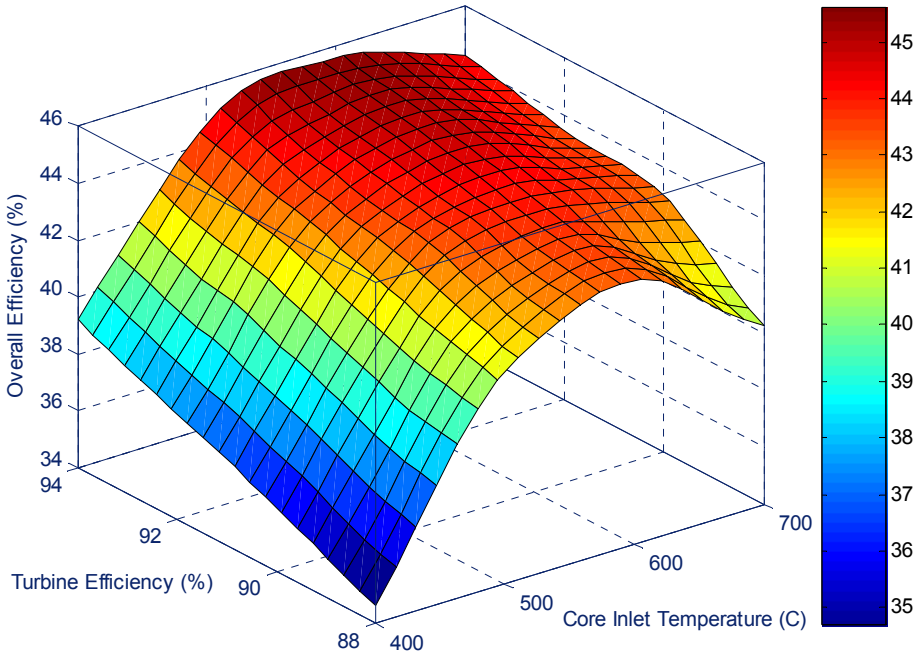

Figure 13. Effect of core inlet temperature and turbine efficiency on overall plant efficiency (He-He-He).

Figure 3-14 shows the effect of ternary loop (intermediate heat transport loop) flow rate on the overall efficiency. In this calculation, the overall efficiency is decreased as the flow rate is increased. It is because the lower flow rate requires less circulation power. However, the effect of ternary loop flow rate was nearly negligible around the optimal temperature, because the portion of ternary loop circulation power was too small compared with the other part. In this calculation, the effect of ternary loop flow rate seems very effective especially at a core inlet temperature below 500°C, since the low core inlet temperature results in low PCU flow rate, and the flow rate in turbine cycle is relatively decreased with the ternary flow rate. Therefore, it leads to the overall efficiency drop.

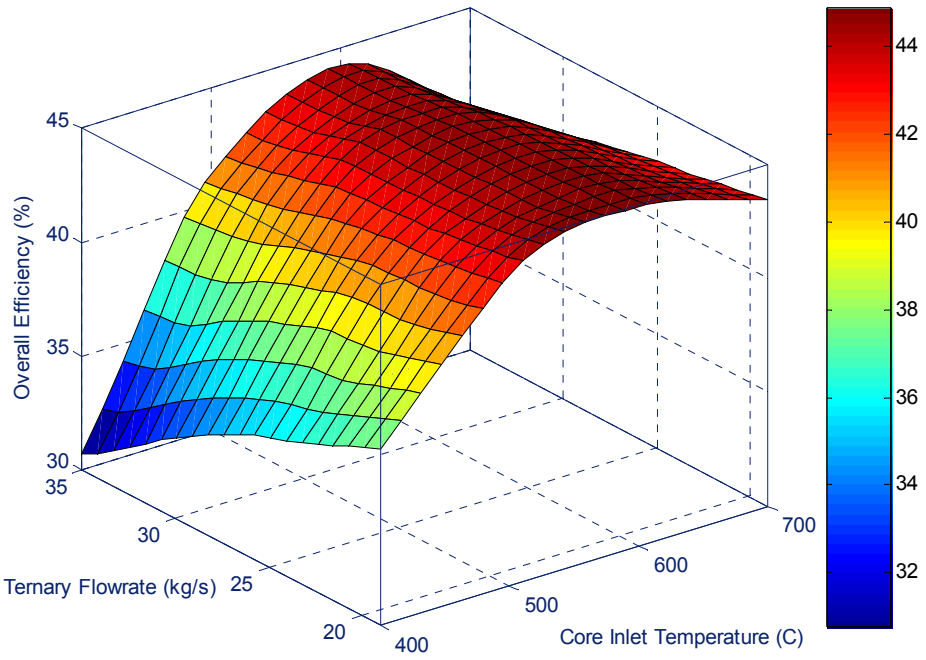

Figure 14. Effect of core inlet temperature and ternary flow rate on overall plant efficiency (He-He-He).

Figure 3-15 shows the effect of the medium pressure compressor (MPC) outlet pressure on the overall efficiency. The MPC outlet is the position where the highest system pressure is located. According to the figure, at low temperature, the efficiency is highly affected by the increase of the MPC outlet pressure, while it is only slightly affected around the optimal core inlet temperature. Figure 3-16 illustrates the variation of optimal pressure ratio along the MPC outlet pressure and the core inlet temperature. It shows the optimal pressure ratio increases significantly as the core inlet temperature decreases, while the variation by the MPC outlet pressure is very slight. It means the optimal pressure ratio is a sensitive factor to the PCU flow rate. Generally, PCU flow rate determines the PCU operating temperature range and it also determines the optimal operating pressure range.

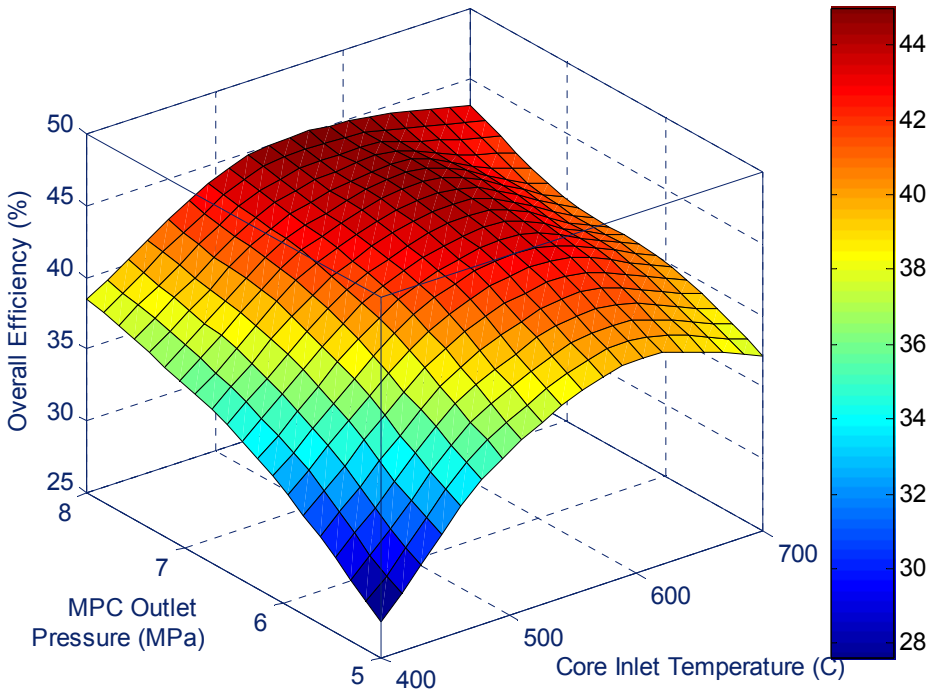

Figure 3-15. Effect of core inlet temperature and MPC outlet pressure on overall plant efficiency (He-He-He).

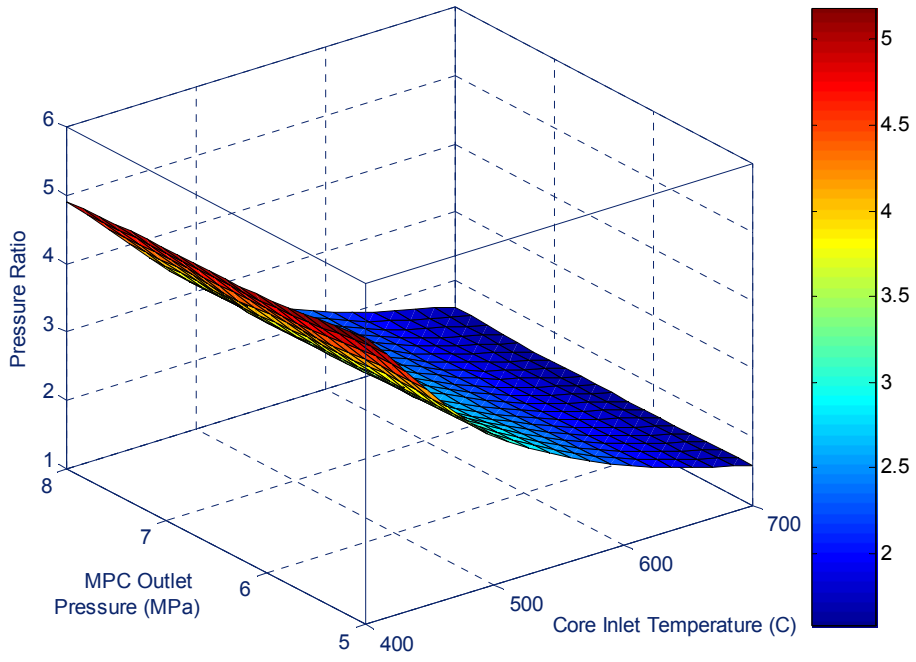

Figure 3-16. Effect of core inlet temperature and MPC outlet pressure on pressure ratio (He-He-He).

Finally, the effect of heat exchanger effectiveness on the overall efficiency was estimated. As shown in Figure 3-17, the efficiency increases with the heat exchanger effectiveness. These trends are similar at both low and high core inlet temperatures. As a result, one percent increase of heat exchanger effectiveness increases the overall efficiency by around 0.5~0.8 %. It means effective heat exchanger performance is a very important factor for achieving more effective system performance. Since the increase of the effectiveness usually requires larger effective surface area, which increases the heat exchanger size and the capital cost, an optimal VHTR system requires a heat exchanger with a very high effectiveness. In this study, the printed circuit heat exchanger (PCHE) is considered as the main heat exchanger in the VHTR, with a commonly accepted effectiveness of around 95%.

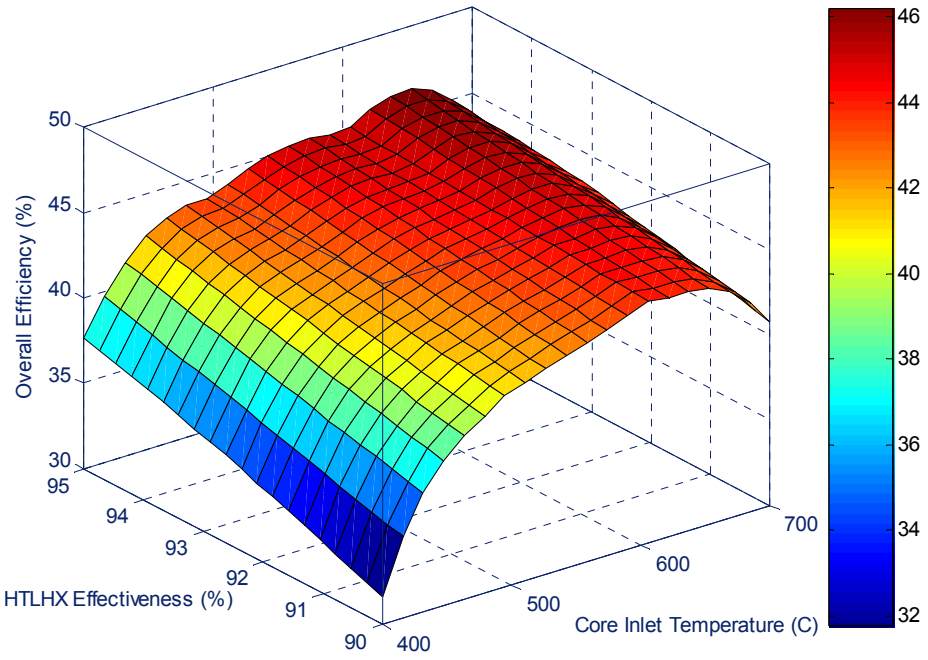

Figure 3-17. Effect of core inlet temperature and SHX effectiveness on overall plant efficiency (He-He-He).

3.3.3 Configuration 1 – Indirect Parallel Cycle

Table 3-2 summarizes the calculated system efficiencies for Configuration 1. In this table, the primary flow loop includes the reactor core and the hot side of the IHX while the secondary loop includes the PCU and the ternary loop contains the intermediate heat transport loop that connects the SHX and the HTSE system. As a primary working fluid, Helium and Flinak were evaluated, as a secondary fluid, Helium and S-CO_2, and as a ternary fluid, Helium, S-CO_2, and Flinak were evaluated. A total of twelve different combinations of working fluids were evaluated.

In this calculation, Flinak in the primary loop increased the overall efficiency by 1.4% on average compared to Helium. Essentially, liquid phase (Flinak) requires less circulation power than the high pressure gas phase (Helium). The highest efficiency using helium in the primary flow loop was achieved in Case 3 (He-He-Flinak) while Case 9 (Flinak-He-Flinak) resulted in the maximum overall efficiency.

With this configuration, the flow rate of Flinak, 1318 kg/s, is three times higher than the one of He, 478.4 kg/s, however, its circulation power is only 1/140 of He (Flinak: 104.7 kW, He: 14770 kW). This results in a slight efficiency increase with molten salt. Due to the higher density of the molten salt by a factor of 500 compared with that of Helium, we expect that Flinak system would require smaller core volume resulting in some economical advantages.

Table 3-2. Optimized efficiencies for Configuration 1.

Primary	Secondary	Ternary	Efficiency (%)
He	He	He	44.12
He	He	CO_2	44.47
He	He	Flinak	46.13
He	CO_2	He	43.35
He	CO_2	CO_2	43.5
He	CO_2	Flinak	43.41
Flinak	He	He	45.25
Flinak	He	CO_2	45.5
Flinak	He	Flinak	47.24
Flinak	CO_2	He	44.83
Flinak	CO_2	CO_2	45.06
Flinak	CO_2	Flinak	45.39

In the ternary loop, Flinak shows the highest performance due to the reduced pumping power compared with gas and as a result, approximately 0.5% of efficiency improvement was achieved on average. The reason why the improvement in the ternary loop is smaller than in the primary loop is that the circulation power of the ternary loop is much less than the primary loop.

From the above results, we could conclude that Flinak-He-Flinak system is the most effective working fluids in the primary, secondary and the ternary flow loop in terms of the overall system efficiency. The efficiency of this combination is 47.24%, the greatest of all combinations evaluated. Figures 3-18 and 3-19 illustrate the operating conditions for the optimized VHTR (Flinak-He-Flinak) and HTSE system, respectively. Figures 3-20 and 3-21 illustrate the P-V and T-S diagrams for the PCU in this system (Flinak-He-Flinak). These results will be benchmarked later with the HyPEP code.

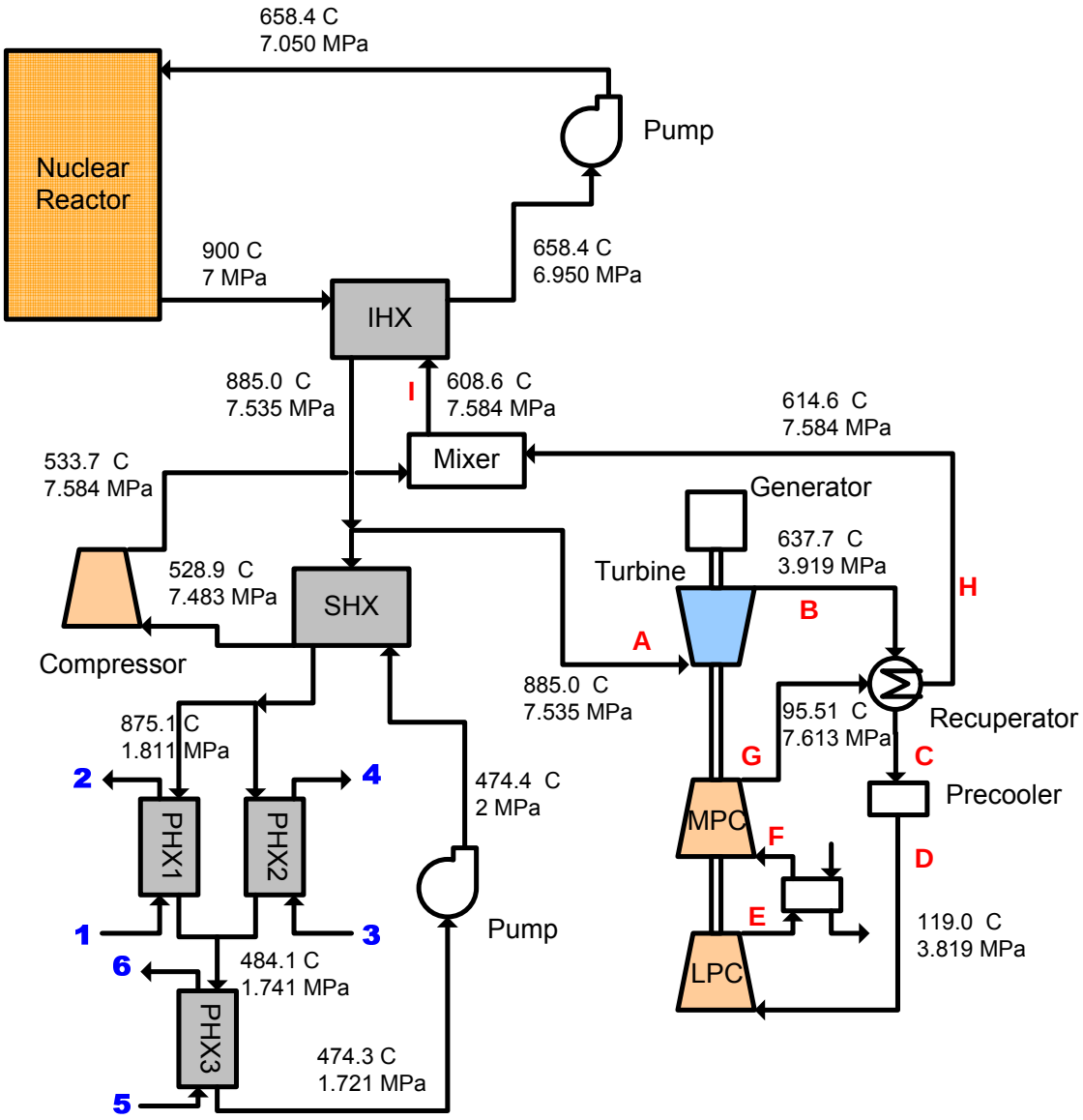

Figure 3-18. Plant operating conditions for Configuration 1 (Flinak – He – Flinak).

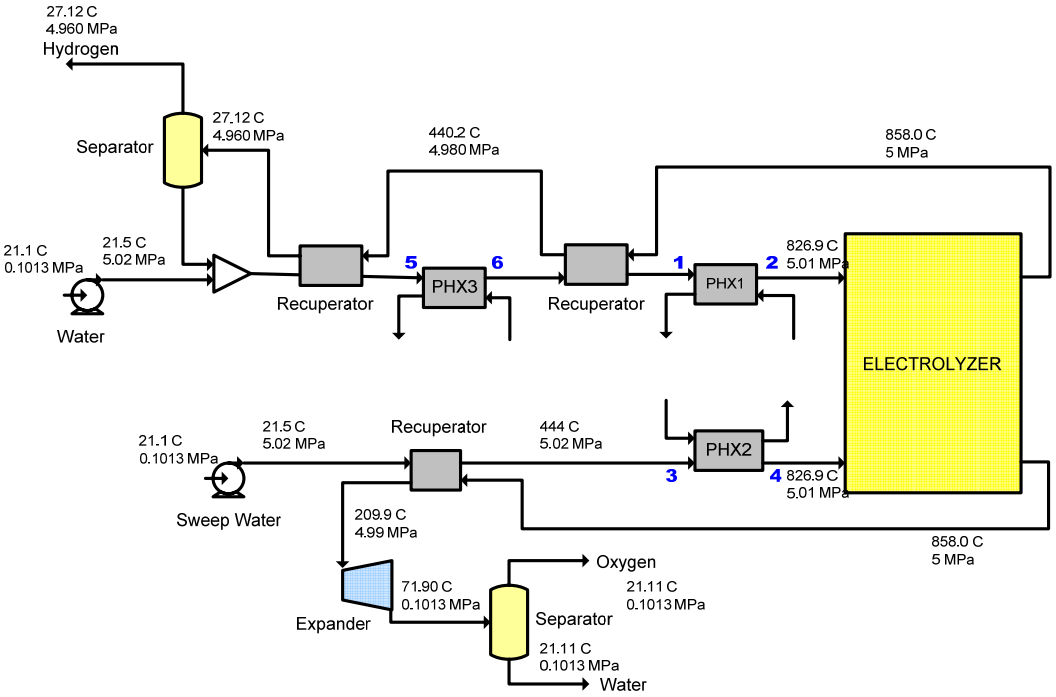

Figure 3-19. Operating conditions for the HTSE system.

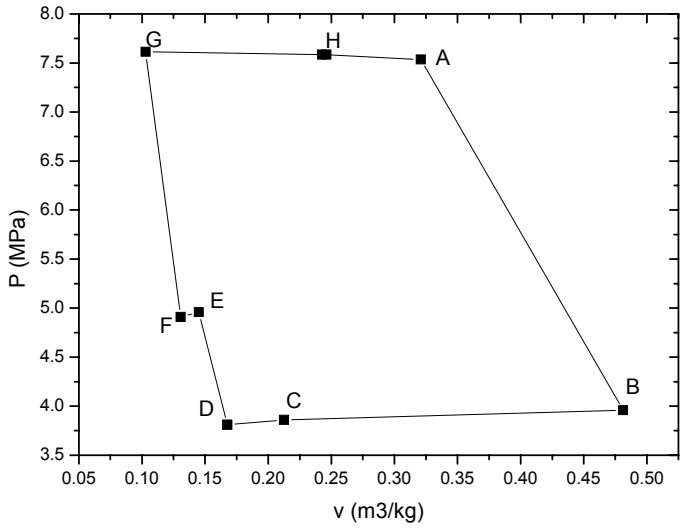

Figure 3-20. P-V diagram for Configuration 1 (Flinak-He-Flinak).

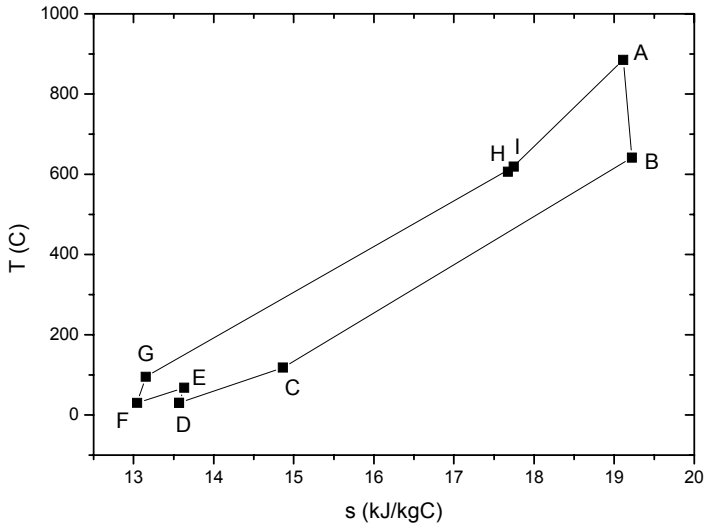

Figure 3-21. T-S diagram for Configuration 1 (Flinak-He-Flinak).

3.3.4 Configuration 2 – Indirect Serial Cycle

The optimized results for the indirect serial cycle are summarized in Table 3-3. Like Configuration 1, the primary, secondary and ternary loops contain the reactor, the PCU, and the intermediate heat transport loop, respectively.

Table 3-3. Optimized efficiencies for Configuration 2.

Primary	Secondary	Ternary	Efficiency (%)
He	He	He	46.26
He	He	CO_2	46.32
He	He	Flinak	46.32
He	CO_2	He	45.02
He	CO_2	CO_2	45.09
He	CO_2	Flinak	45.09
Flinak	He	He	48.13
Flinak	He	CO_2	48.3
Flinak	He	Flinak	48.38
Flinak	CO_2	He	46.9
Flinak	CO_2	CO_2	47.07
Flinak	CO_2	Flinak	47.15

The maximum efficiency (48.38 %) was obtained for Flinak-He-Flinak combination. It is due to the reduction of circulation power for the primary and the ternary side caused by liquid coolant. As a result, The overall efficiency for Configuration 2 is about 1% higher than for Configuration 1, even though the turbine inlet temperature is a little reduced. The increase in efficiency is due to the decreased number of

circulators. The elimination of one circulator and flow splitter is also expected to result in lower capital cost and higher controllability.

Figure 3-22 shows the optimized operating conditions for Configuration 2. Since the working fluid of the primary and the ternary loop is Flinak, the circulator in the original configuration (Figure 3-8) is changed to a pump. In the ternary loop, the minimum temperature is maintained above 454°C, the melting temperature of Flinak.

The core outlet temperature is maintained at 900 °C, and the optimal core inlet temperature is calculated to be 673.6 °C by the energy balance around the VHTR. The effectiveness of the IHX and SHX was used as 0.95. The turbine inlet temperature (870 °C) is little reduced compared with the Configuration 1 (885°C). At the optimal condition, the pressure ratio is 1.89. The operating conditions of the HTSE system are the same as for Configuration 1. Figures 3-23 and 3-24 illustrate the P-V and T-S diagrams for the optimized conditions (Flinak-He-Flinak).

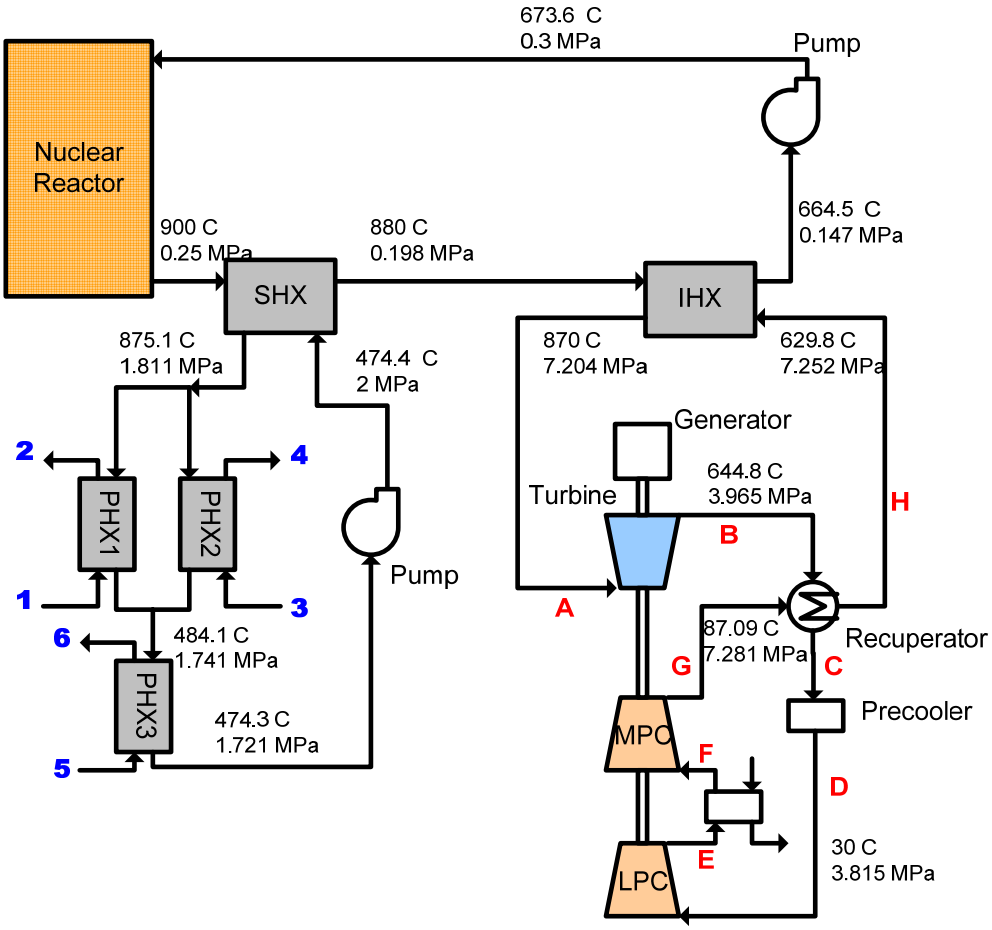

Figure 3-22. Optimized operating conditions for Configuration 2 (Flinak – He – Flinak).

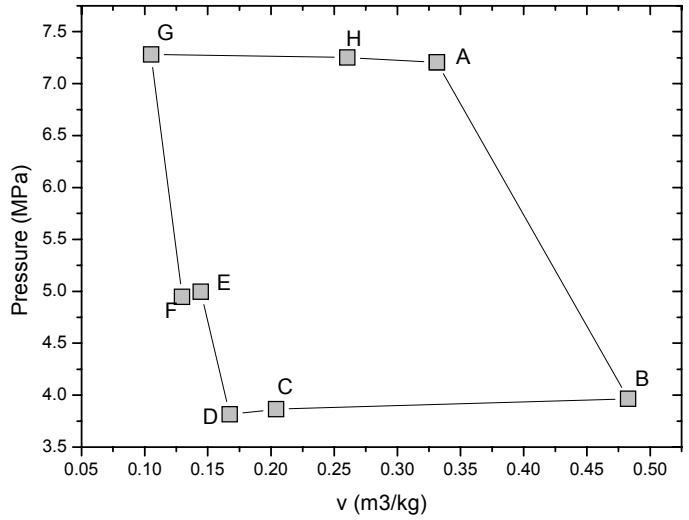

Figure 3-23. P-V diagram for Configuration 2 (Flinak-He-Flinak).

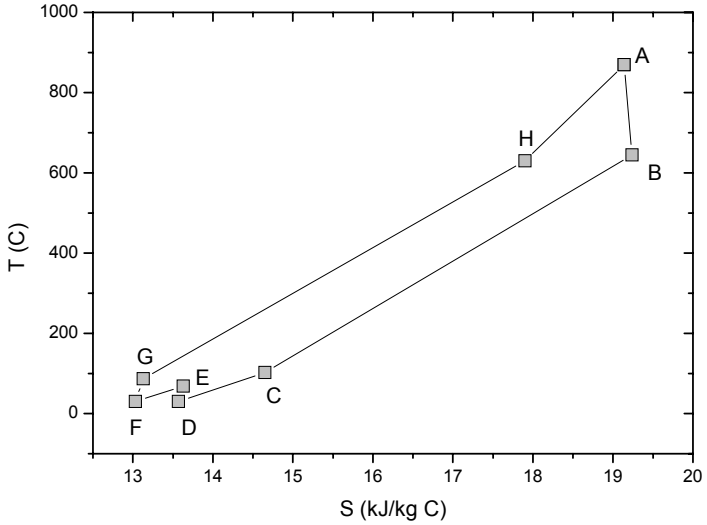

Figure 3-24. T-S diagram for Configuration 2 (Flinak-He-Flinak).

3.3.5 Configuration 3 – Direct Serial Cycle

Table 3-4 summarizes the estimated efficiencies for Configuration 3. This configuration is a direct cycle, so the PCU is in series with the reactor in the primary system. The reactor and PCU both use the same working fluid, which precludes the use of the molten salt as a coolant. At high temperatures, CO_2 will react with the graphite materials in the VHTR core. As a consequence the inert gas helium is used in this application to avoid chemical oxidation in the core. In the ternary loop (intermediate heat transport loop), three working fluids were evaluated: He, CO_2, and Flinak.

As mentioned above, the direct cycle has many benefits for efficiencies and cost effectiveness by eliminating the IHX and primary circulator. In our calculation, the maximum efficiency of Configuration 3 was found to be 48.96 %. Comparing this with Configuration 2, the maximum efficiency increase of Configuration 3 was only 0.5 %. This is attributed to the already low pumping power in the primary side of Configuration 2 as a consequence of Flinak coolant (185 kW).

Table 3-4. Optimized efficiencies for Configuration 3.

Primary	Secondary	Ternary	Efficiency (%)
He	He	He	48.48
He	He	CO_2	48.77
He	He	Flinak	48.96

Figure 3-25 illustrates the optimized operating conditions for Configuration 3. The core outlet temperature is maintained at 900 °C, and the optimal core inlet temperature is calculated to be 622.0°C. The SHX effectiveness was 0.95. The turbine inlet temperature (873.5°C) is reduced compared with the Configuration 1 (885°C), but it is little higher than the Configuration 2. At the optimal condition, the pressure ratio is 1.97. The operating conditions of the HTSE system are the same as the Configuration 1. Figures 3-26 and 3-27 illustrate the P-V and T-S diagram for the optimized conditions (He-He-Flinak).

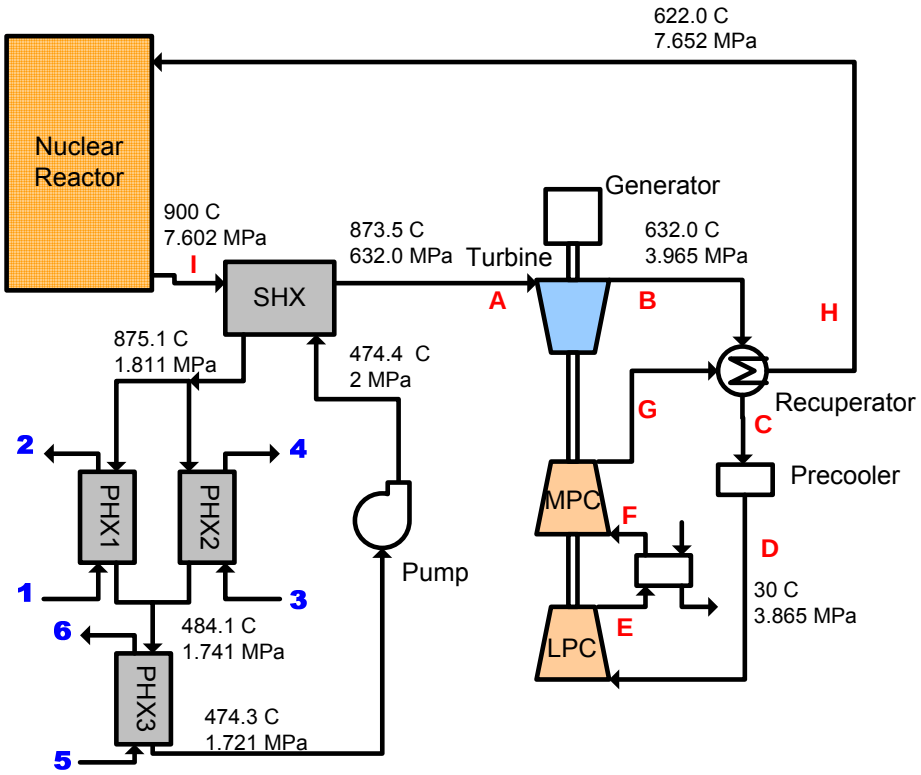

Figure 3-25. Optimized operating conditions for Configuration 3 (He-He-Flinak).

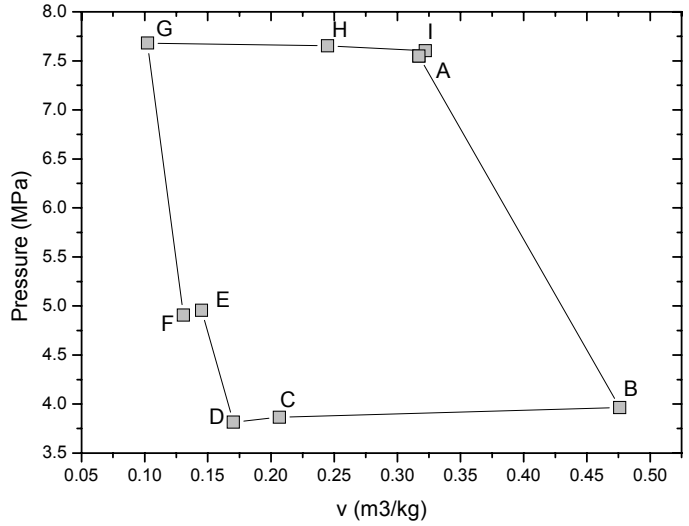

Figure 3-26. P-V diagram for Configuration 3 (He-He-Flinak).

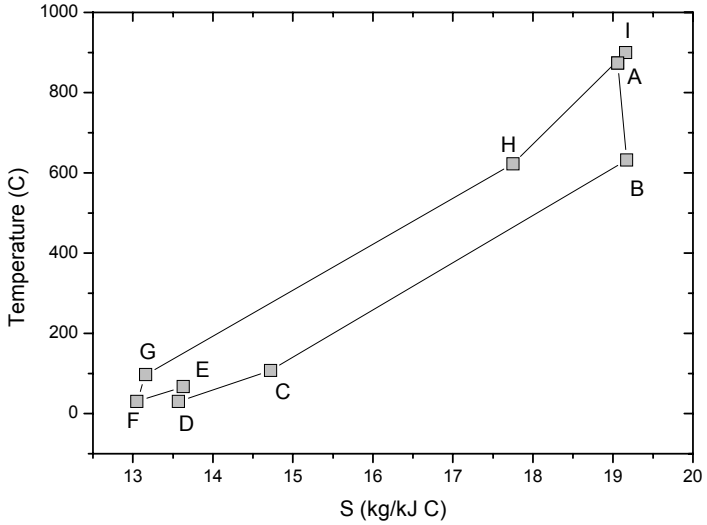

Figure 3-27. T-S diagram for Configuration 3 (He-He-Flinak).

3.3.6 Configuration 4 – Steam Combined Cycle

Configuration 4 is a steam combined cycle. In this system, a steam turbine system is utilized to recover the heat discharged from the turbine outlet instead of the recuperator. Usually, this kind of configuration gives higher efficiency than that of normal recuperation cycle. Table 3-5 summarizes the optimized efficiencies for Configuration 4. In our calculation, the maximum efficiency of 44.32 % was obtained for Flinak-CO_2-Flinak combination. This is significantly lower efficiency than those of the other configurations using Flinak. It means that the recuperation is more effective way to recover the heat at the

turbine outlet, because the temperature difference between the outlet of the turbine and the compressor is high. Essentially, the difference between average temperature of heat addition and average temperature of heat rejection is greater in the case of the recuperated gas reactor. As a consequence the Carnot efficiency is greater.

Figure 3-28 illustrates the optimized condition (Flinak-CO_2-Flinak). In this system, the heat generated in the core is transferred to the PCU loop through the IHX. The heated flow in the PCU is split into two streams, one for electricity generation by the turbine cycle and the other for transferring energy to the HTSE through the SHX. Configuration 4 is basically the same as the indirect parallel cycle (Configuration 1), but it has only one compressor. We think it is one of the main reasons of the resultant low efficiency of this configuration is due to a higher inlet temperature to the compressor with no intercooler.

The core outlet temperature is maintained at 900 °C, and the optimal core inlet temperature is obtained as 548.8 °C. The IHX and SHX effectiveness were 0.95. At the optimal condition, the pressure ratio is 8.76. The operating conditions of the HTSE system are the same as Configuration 1. Figures 3-29 and 3-30 illustrate the P-V and T-S diagram for the optimized conditions (Flinak-CO_2-Flinak).

Table 3-5. Optimized efficiencies for Configuration 4 (Steam combined cycle).

Primary	Secondary	Ternary	Efficiency (%)
He	He	He	42.09
He	He	CO_2	42.45
He	He	Flinak	42.77
He	CO_2	He	43.46
He	CO_2	CO_2	44.06
He	CO_2	Flinak	44.3
Flinak	He	He	42.79
Flinak	He	CO_2	42.98
Flinak	He	Flinak	43.29
Flinak	CO_2	He	44.32
Flinak	CO_2	CO_2	44.55
Flinak	CO_2	Flinak	44.88

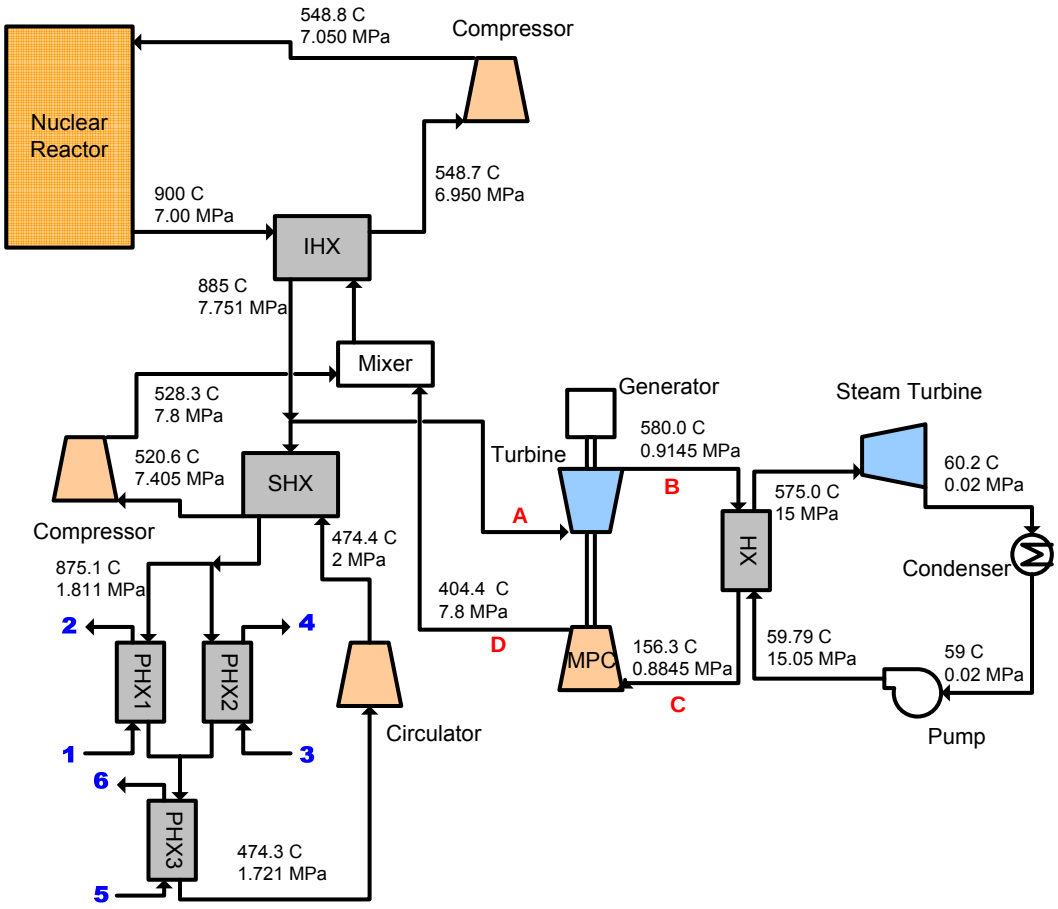

Figure 3-28. Optimized condition for Configuration 4 (Flinak-CO_2-Flinak).

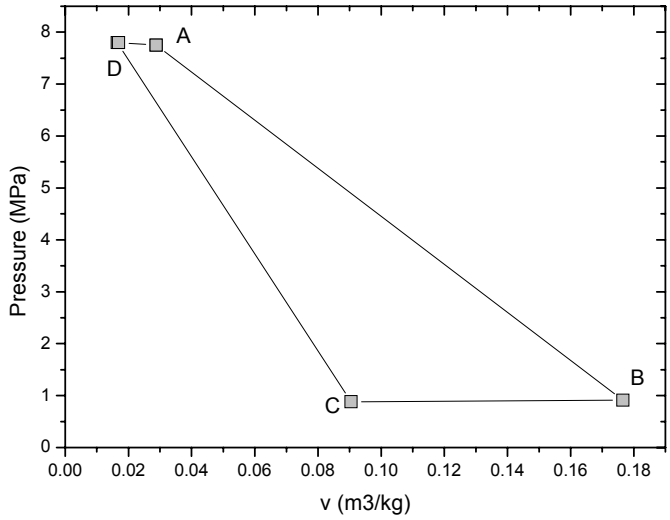

Figure 3-29. P-V diagram for Configuration 4 (Flinak-CO_2-Flinak).

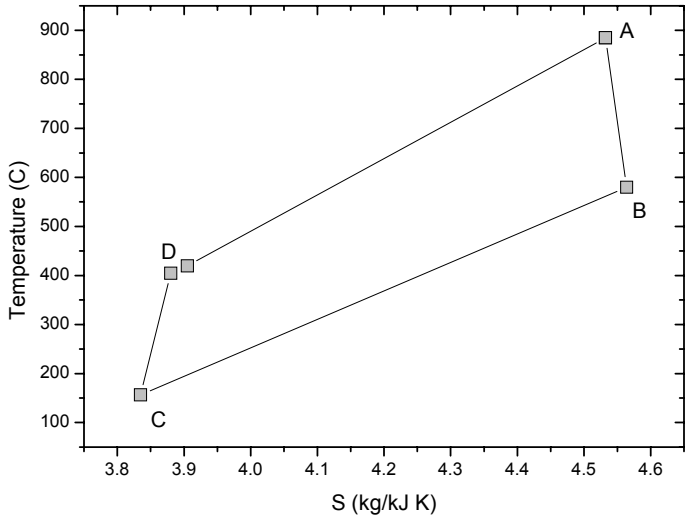

Figure 3-30. T-S diagram for Configuration 4 (Flinak-CO_2-Flinak).

3.3.7 Configuration 5 – Reheat Cycle

Configuration 5 is a reheat cycle. In this system, the stream discharged from a turbine is reheated by the primary side and regenerates the electricity through another turbine. In this configuration, four turbines and four compressors were used. Table 3-6 summarizes the calculated efficiencies for various combinations of working fluids. The maximum efficiency obtained was 50.64 % for the Flinak-CO_2-Flinak combination. Figure 3-31 shows the optimal condition for this system. The detailed conditions of each stream are shown in Figures 3-32 and 3-33, which are P-V and T-S diagrams, respectively.

The core outlet temperature is maintained at 900°C, and the optimal core inlet temperature is obtained as 793°C. The IHX and SHX effectiveness were 0.95. At the optimal condition, the pressure ratio is 9.314. The operating conditions of the HTSE system are the same as the Configuration 1.

Although the efficiency of this system is much higher than the other configurations, it requires extra components (heat exchangers, turbines and compressors) increasing capital cost. In addition, the greater system complexity may give rise to control problems or perhaps safety issues. The optimal efficiency of this system was obtained at full power conditions. One would also need to investigate how efficiency behaves at reduced power and during transient operation.

Table 3-6. Optimized efficiencies for Configuration 5.

Primary	Secondary	Ternary	Efficiency (%)
He	He	He	47.04
He	He	CO_2	47.2
He	He	Flinak	47.43
He	CO_2	He	47.4
He	CO_2	CO_2	47.49
He	CO_2	Flinak	49.52
Flinak	He	He	49.23
Flinak	He	CO_2	49.4
Flinak	He	Flinak	49.76
Flinak	CO_2	He	49.6
Flinak	CO_2	CO_2	49.77
Flinak	CO_2	Flinak	50.64

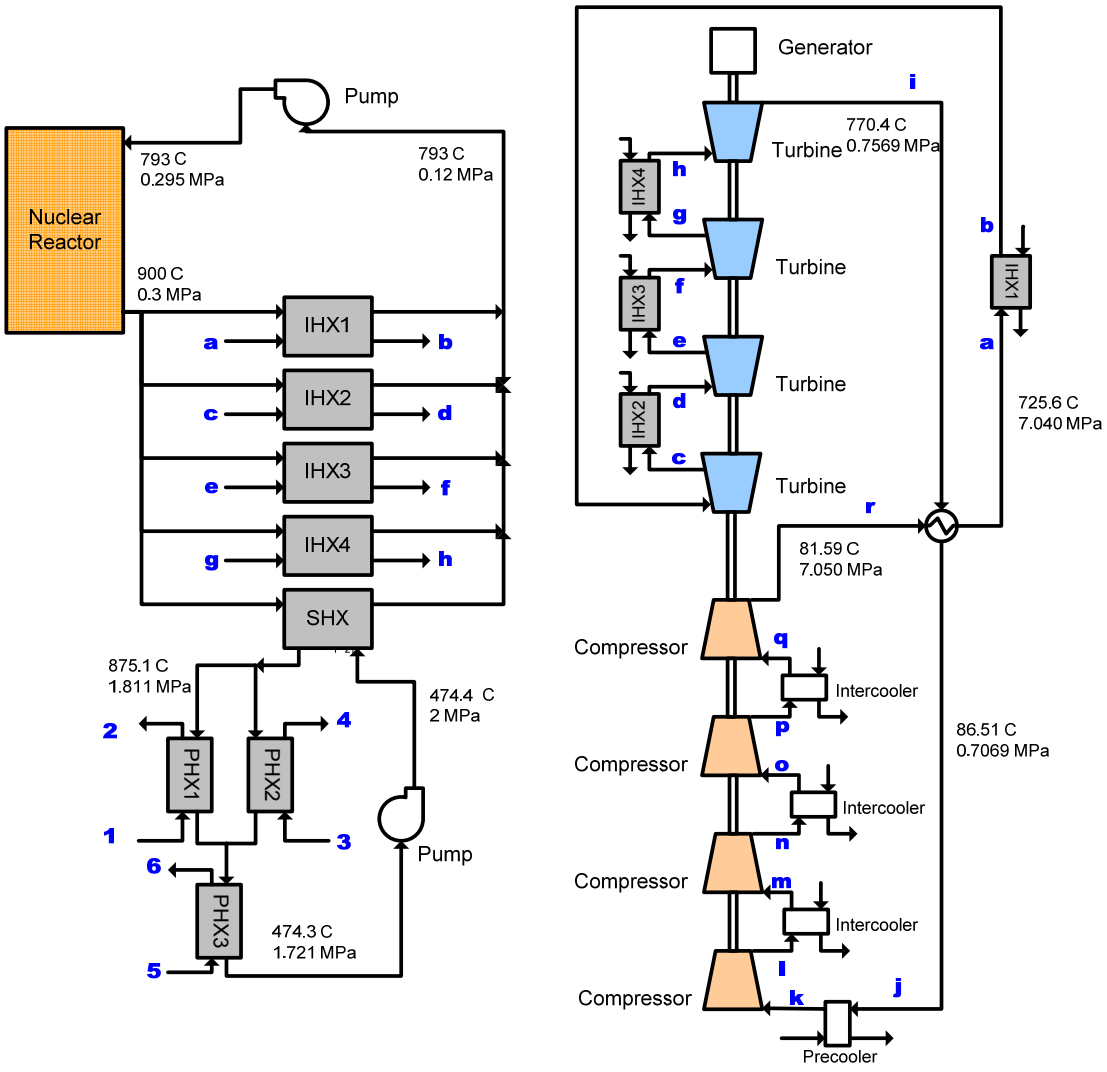

Figure 3-31. Optimized condition for Configuration 5 (Flinak-CO_2-Flinak).

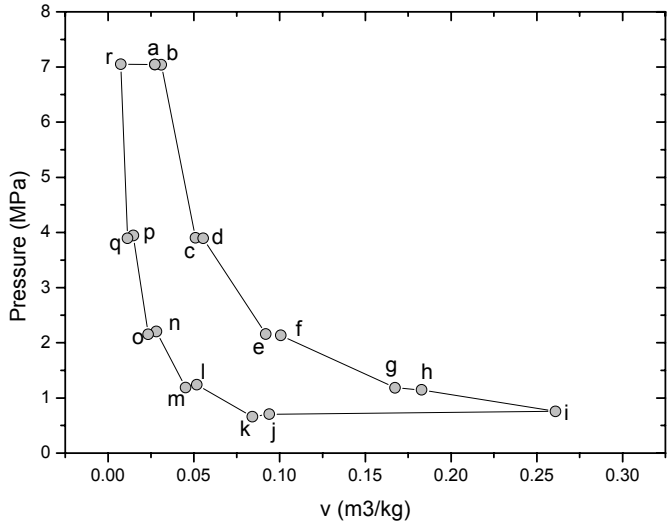

Figure 3-32. P-V diagram for Configuration 5 (Flinak-CO_2-Flinak).

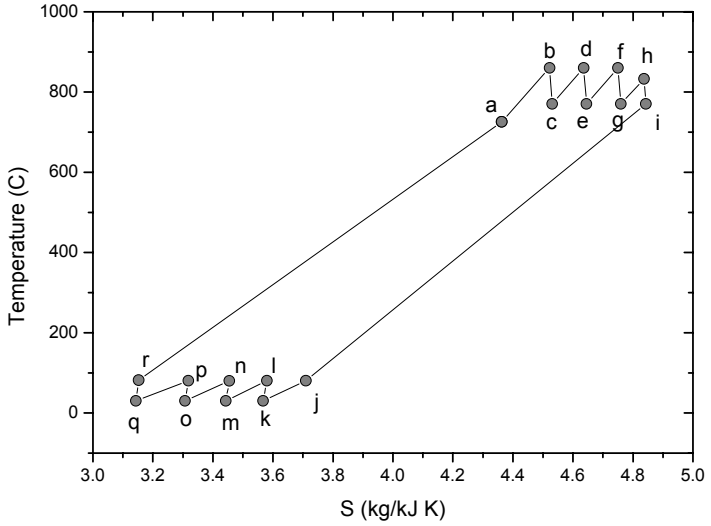

Figure 3-33. T-S diagram for Configuration 5 (Flinak-CO_2-Flinak).

3.3.8 Integration of high temperature Rankine cycle to HTSE

In HTSE system, 80 % of energy is provided by the process heat from VHTR and 20% by electricity. The overall efficiency is determined by the efficiency equation defined in Equation 3-2. Figure 3-34 shows two main thermodynamic cycle efficiencies with temperature; steam Rankine cycle and gas Brayton cycle. As shown in Figure 3-34, at low temperature less than 700 C, the steam Rankine cycle shows much higher efficiency than the gas Brayton cycle, but at high temperature above 700 ℃, the efficiency of gas turbine cycle is much higher. It means that the gas turbine cycle is a more suitable thermodynamic cycle

for hydrogen production, which requires very high temperature over 900 ℃ for good efficiency. Actually, at this temperature, the efficiency of the gas turbine system exceeds 50 %, which is much higher than the commercial PWR. In the current PWR technology, the efficiency is ranged just around 33 ~ 35 %. For this reason, all research on the nuclear reactor concerning with hydrogen production is now focused on the very high temperature gas cooled reactors.

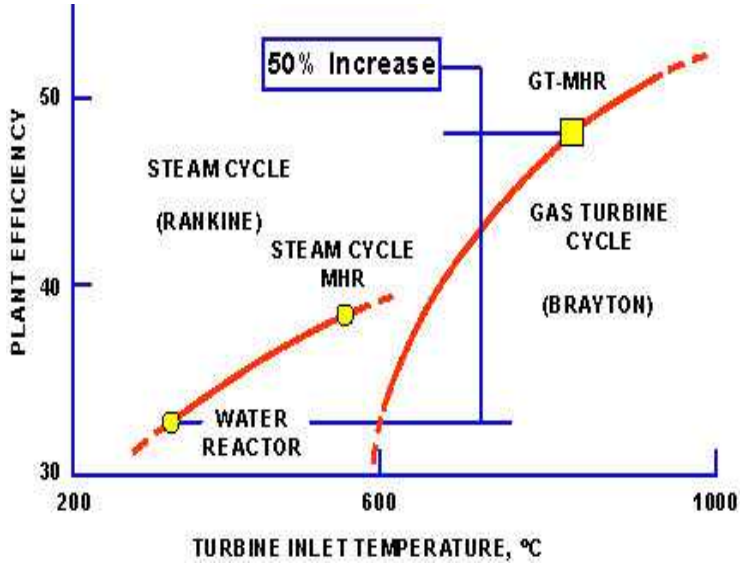

Figure 3-34. Cycle efficiency versus turbine inlet temperature.

In this study, the direct integration of the steam Rankin cycle and the HTSE was investigated because of some advantages we can obtain from this system. First of all, it requires no additional intermediate heat exchange loop like VHTR/HTSE system to generate process steam required for high temperature electrolysis because the steam generated in the PCU can be directly used in the electrolysis system by simple flow split method sharing the same coolant loop. Therefore, it will make the system configuration much simpler than the integration of VHTR and HTSE system. Secondly, the steam Rankine cycle is well-proven technology, which has been used for several decades in the most commercial nuclear reactors. It means that lots of design and operating experiences have been collected so far. It will significantly reduce the uncertainties for the newly developed system. For this reason, it is worth considering the Rankin cycle as a possible candidate for the application to the hydrogen production in spite of its lower theoretical efficiency compared with gas Brayton cycle. Ultimately the cost estimate is required to select the final design along with technical issues. In this study, we directly integrated the steam Rankin cycle with hydrogen production system and evaluated the overall system efficiency by using commercial process analysis tools.

System Configurations for Reference Designs

In this study, HTSE system is directly integrated with the steam Rankin cycle. Figure 3-35 shows the basic concept of the integration method. This system is a basically indirect cycle, in which the reactor primary side is separated with the secondary Rankin cycle by a heat exchanger. A key point of this system is, as mentioned in the previous section, that the generated steam in the secondary system can be directly used for an electrolyzer. Therefore, the hydrogen production and electricity generation system are sharing the same coolant loop as a one body.

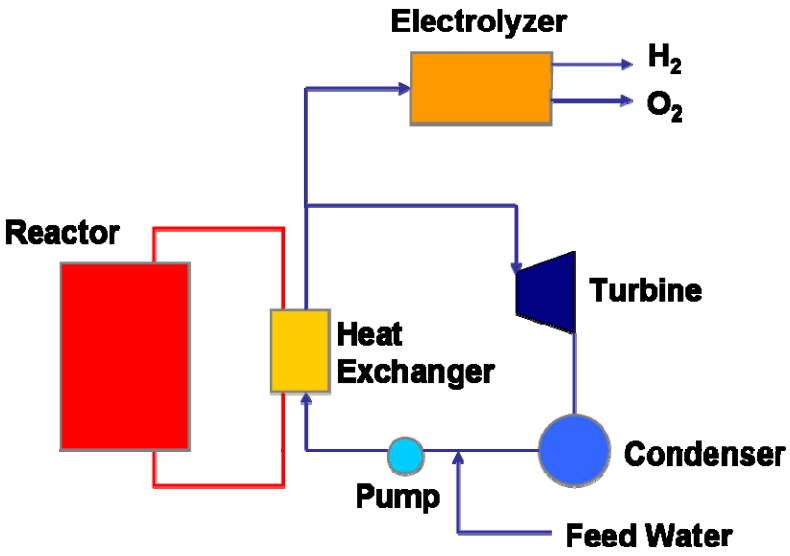

Figure 3-35. Concept of direct integration of HTRC and HTSE system.

We estimated five different configurations having different heat recovery methods by using HYSYS code. Figure 3-36 through 3-40 shows the configurations and their estimated efficiencies. In this calculation, the maximum efficiency was obtained to be 41.6 % at the configuration 2 shown in Figure 3-37. In this configuration, helium is used as primary coolant, and the maximum coolant temperature is fixed at 900 ℃. Two heat exchangers (IHX and IHX2) are used to transfer primary heat to the secondary side, and eventually generate superheated steam. Water is converted to the superheated steam at 880℃, and it generates electricity passing through the high pressure turbine. Then, the steam at the turbine outlet is reheated by IHX2 up to 860℃. After that, some amount of the steam is separated by a flow splitter and provided to an electrolyzer for generation of hydrogen. The rest of the steam is re-used for generation of electricity through the low pressure turbine. To recover the water consumed in the electrolyzer, some water is continuously injected at the condenser outlet, the minimum pressure point. Comparing with the VHTR/HTSE system (Figure 3-41), a favored candidate for hydrogen production, and this direct Rankine system looks much simpler. It is eventually expected to cause some capital cost reduction.

However, the following drawbacks are anticipated in this system.

a. Hydrogen system contamination

Since the secondary side and the hydrogen system are integrated as one loop, the radioactive materials can be easily released to the hydrogen production system. Tritium generated in the primary side will penetrate through the heat exchanger wall and directly mixed with the steam at the secondary side. To take care of this problem, some special measures are required at the secondary side.

b. Secondary steam discharge

In this system, the secondary working fluid is continuously released to the environment through hydrogen production system. We can put another intermediate exchange loop between primary and secondary side to prevent this situation, but it will make the system more complicated and reduce the efficiency.

c. Thermal stress

In this system, since the feed water temperature at the steam generator is too low (around 100℃), sharp temperature gradient in the heat exchanger is expected. It might cause continuous thermal stress on the heat exchanger causing some problems.

d. Steam corrosion

Usually, steam is much corrosive at high temperature. In this system, some components like turbines and heat exchangers are operated at around 900℃, so they are placed in the severely corrosive environment.

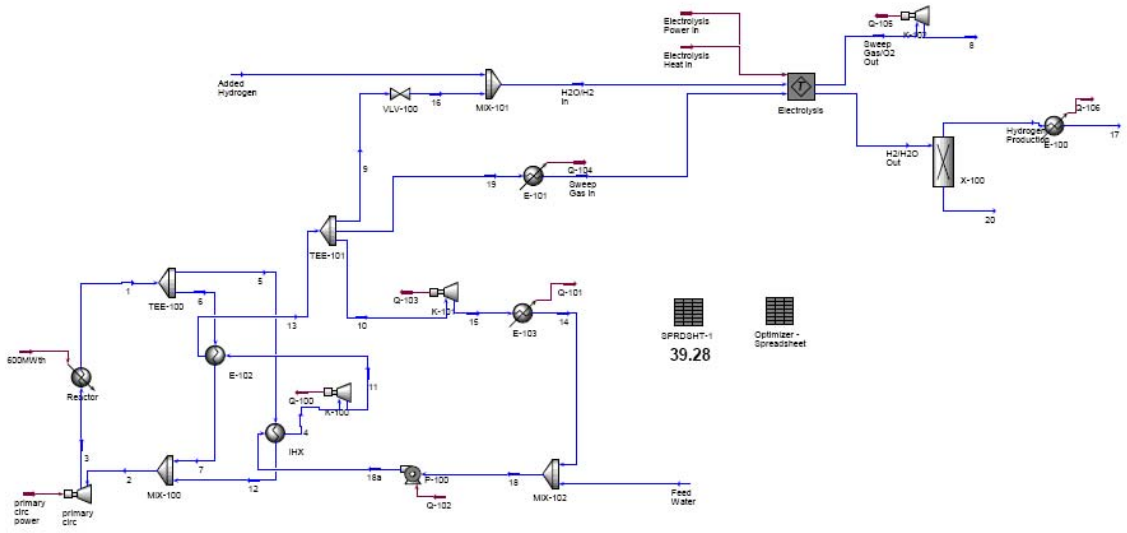

Figure 3-36. HTSR/HTSE Configuration 1 (39.28%).

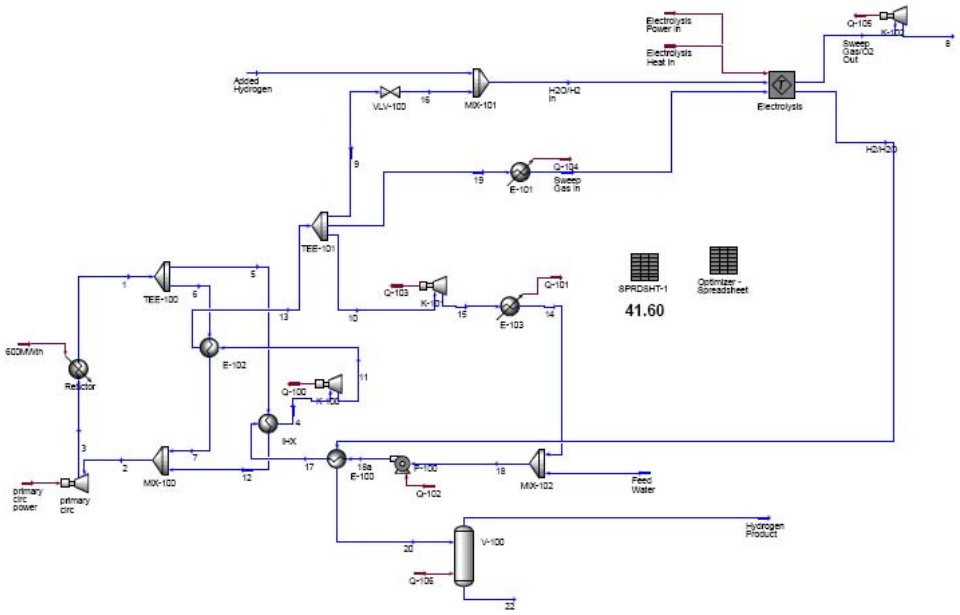

Figure 3-37. HTSR/HTSE Configuration 2 (41.60%).

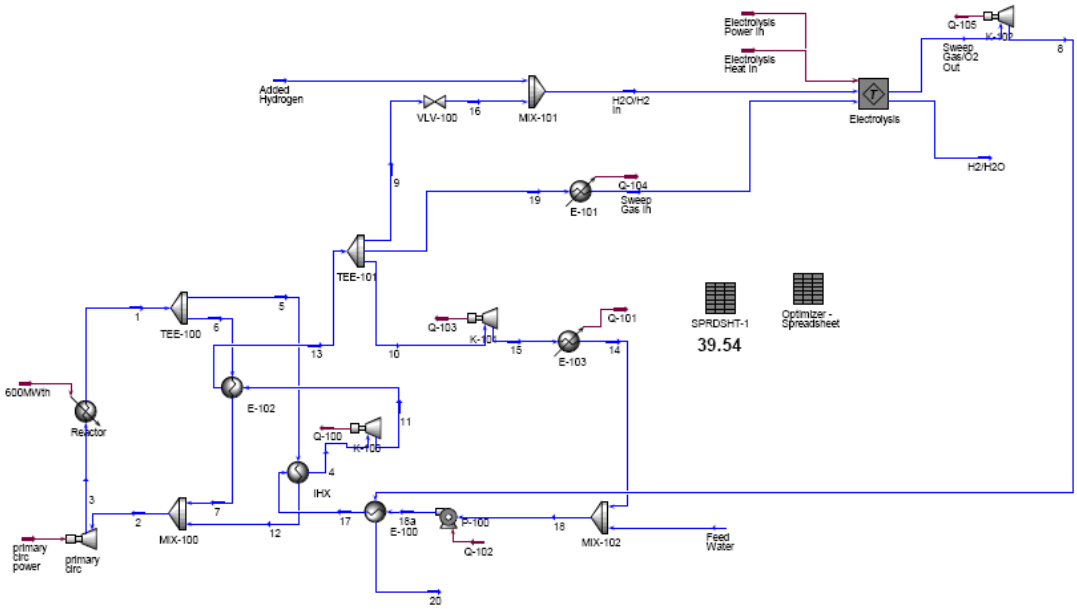

Figure 3-38. HTSR/HTSE Configuration 3 (39.54%).

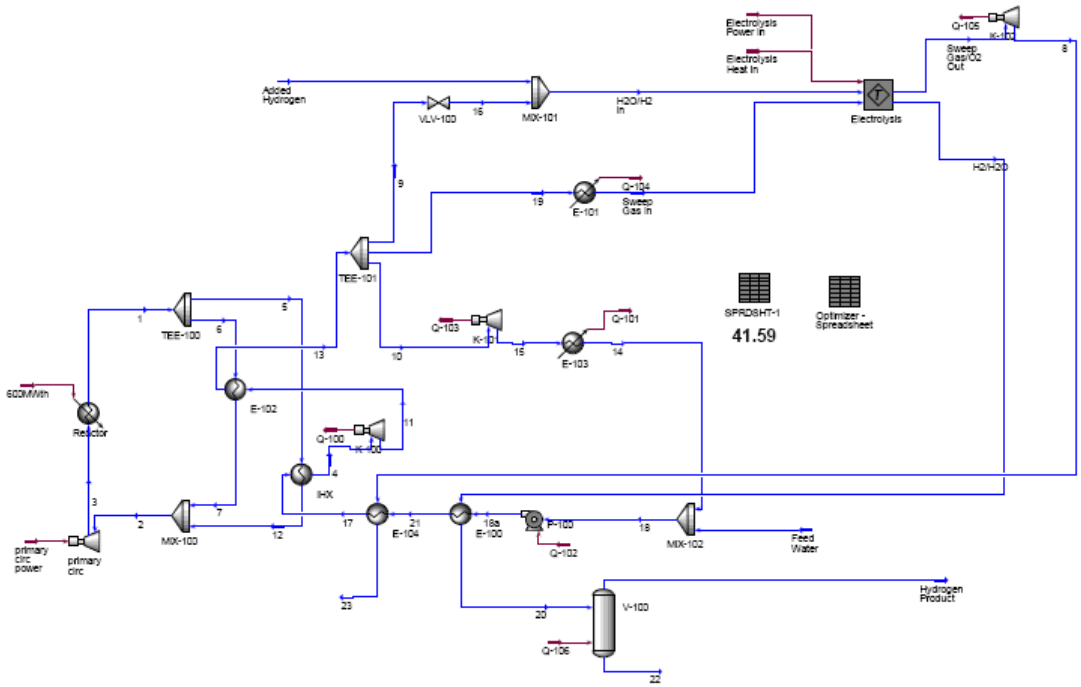

Figure 3-39. HTSR/HTSE Configuration 4 (41.59%).

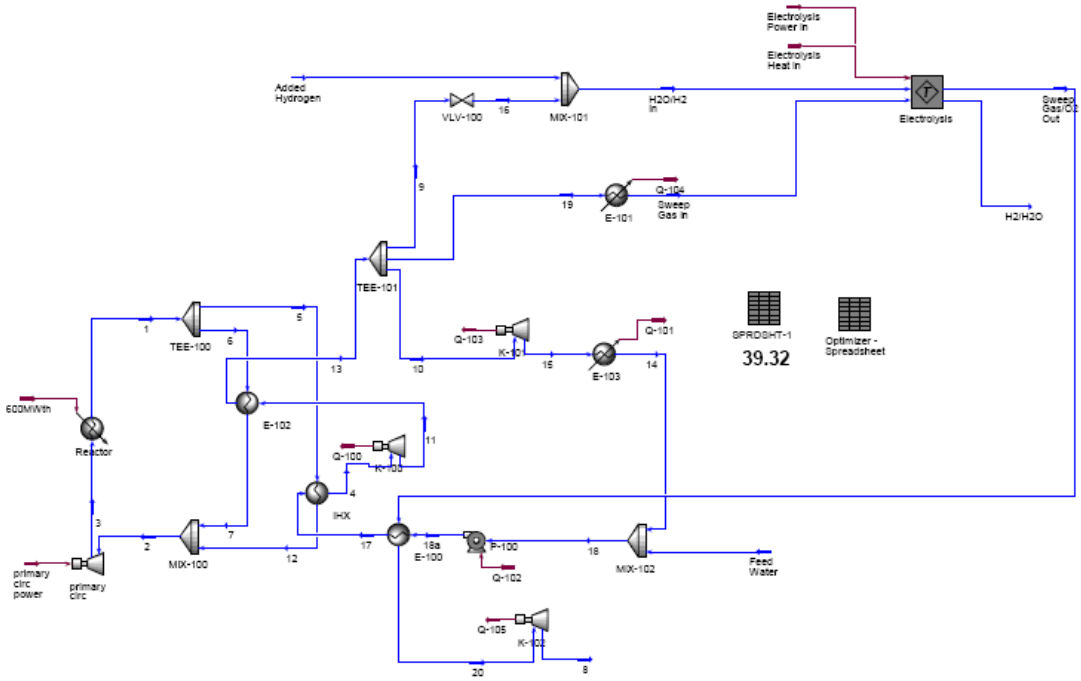

Figure 3-40. HTSR/HTSE Configuration 5 (39.32%).

Figure 3-41 shows the VHTR/HTSE system using helium as primary coolant. This system shows much higher efficiency than the HTRC/HTSE system, since it is adapting gas Brayton cycle. For the helium primary coolant, the efficiency is reached up to 48 %, and for the molten salt coolant, up to 50%. (Figure 3-42) It has a simple PCU configuration, but a complicated HTSE system, which is necessary to maximize heat recovery from high temperature H_2/H_2O mixture and sweep gas. Therefore, VHTR/HTSE

system is expected to require more capital cost than HTRC/HTSE system. For better estimation, more detail cost analysis is required.

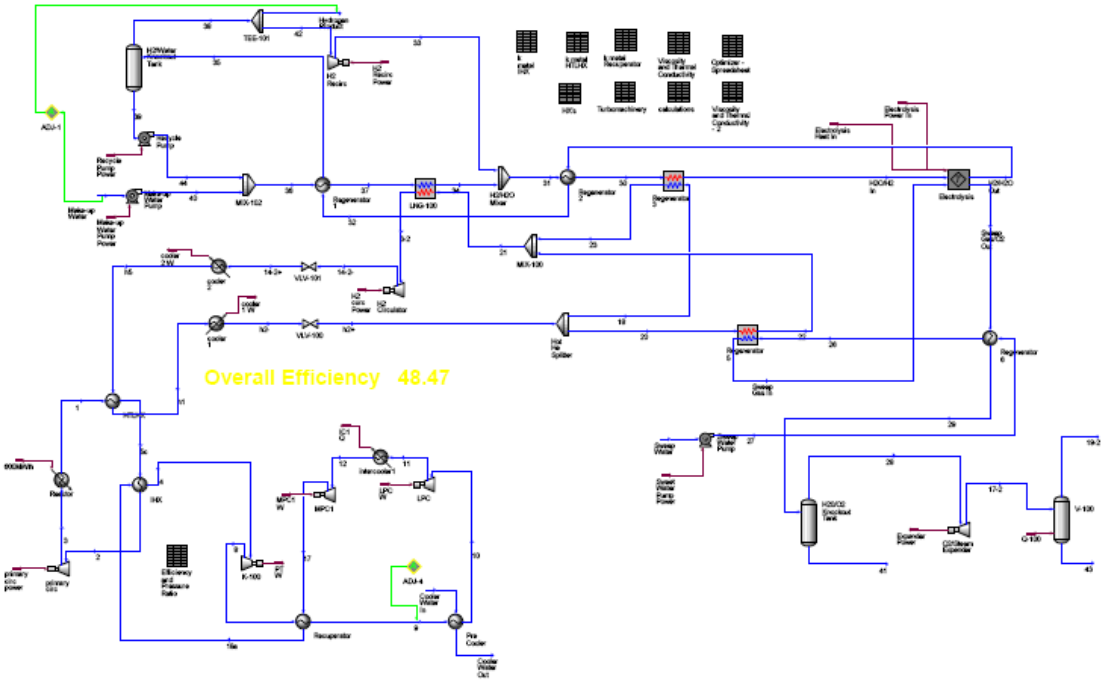

Figure 3-41. VHTR/HTSE Configuration 1 (48.47%).

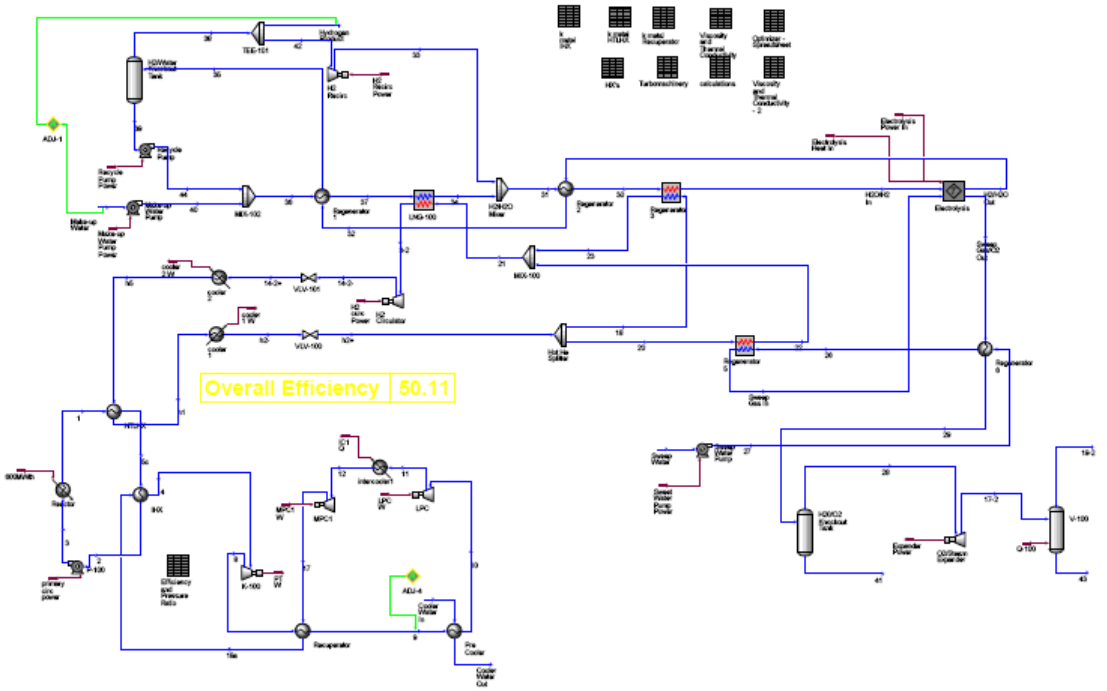

Figure 3-42. VHTR/HTSE Configuration 2 (50.11%)

3.3.9 Alternative Concepts and Preliminary Results

The five plant configurations studied have the common feature that the heat needed to close the energy balance on the HTSE process is provided by the VHTR. However, it is noted that there are other possibilities for providing this heat and that they should be explored for potential safety, reliability, and economic advantages. A simple analysis separates the heat requirements of the HTSE plant into high temperature (~900 °C) and low temperature (~260 °C) heat. The high temperature heat for the configurations in this report is delivered through a series of process heat loops that trace back to the reactor outlet. Inherent in this choice are a number of issues including material challenges associated with heat exchanger operation at high temperature, heat losses from pipe runs up to several hundred meters long, the need for higher-cost metal alloys to withstand the high temperatures and possibly pressures, the need for electrical heaters should the heat transfer coolant be a molten salt, the cycle inefficiency associated with mixing of the process heat return line coolant at a different temperature than the PCU return coolant, pumping losses, and in general an increase in operational complexity resulting from a dedicated heat transfer loop.

Thus, there may be incentives for using other means to deliver this heat in place of a high temperature process heat loop. A potentially attractive option is to recover the heat from ohmic losses in the electrolytic cell and substitute this in place of high temperature reactor heat. Such a scheme might involve running the electrolyzer at a higher voltage to obtain an increase in ohmic heat. Additionally, this might be augmented with heat from electrical heaters (or alternatively, hydrogen burners) to do away altogether with the need for high temperature process heat from the reactor. The recuperation of ohmic heat for raising reactant temperatures has been proposed in the context of hydrogen production using the S-CO_2 closed Brayton cycle [Yildiz 2006]. The tradeoff of course is increased plant inefficiency for reduced capital cost. Capital cost is reduced by not only simplifying a heat transport loop, but also by increasing electrolyzer H_2 production through increased electrical power.

There are other advantages as well. Shifting the source of high temperature heat from the nuclear plant to the chemical plant might significantly improve the safety and maintainability of the nuclear plant and simplify its operation. The safety requirements related to high temperature heat production in the chemical plant will likely be less stringent.

Even if the need for high temperature reactor heat is eliminated as described above, there is still a need for low temperature heat. But here also there is the prospect for reduced complexity and cost savings. The bulk of the low temperature heat is used to produce water vapor at 260 °C from liquid water at room temperature. For the VHTR there are copious amounts of heat available at 130 °C in the form of waste heat rejected to the ultimate heat sink. This heat is available at essentially zero cost. One possibility then is to use nuclear plant waste heat to boil water at this temperature and then compress the vapor to the required conditions of 260 °C and 5 MPa.

Finally, a more relevant plant economic performance index is cost per unit of hydrogen produced in place of plant efficiency. The latter does not reflect the underlying increase in capital costs when cell area or heat transfer area is increased to improve efficiency. This would need to be addressed.

One might also note that if high temperature heat needs were met exclusively through recuperation and from a heat source other than the reactor, then a lower temperature reactor concept could be used in place of the VHTR.

3.4 Optimum Heat Exchanger Sizing Model

In the integrated system of VHTR and HTSE, an intermediate heat exchanger (IHX), which transfers heat from the reactor core to the electricity or hydrogen production system is one key component, and its effectiveness is directly related to the system overall efficiency. In the VHTRs, the gas fluids used for coolant generally have poor heat transfer capability, so it requires very large surface area for a given conditions. For this reason, a compact heat exchanger (CHE), which is widely used in industry especially for gas-to-gas or gas-to-liquid heat exchange is considered as a potential candidate for an IHX replacing the classical shell and tube type heat exchanger. A compact heat exchanger is arbitrary referred to be a heat exchanger having a surface area density greater than 700 m^2/m^3. The compactness is usually achieved by fins and micro-channels, and leads to the enormous heat transfer enhancement and size reduction.

In the current study, we focused on the optimum sizing and cost for CHEs. The cost of a heat exchanger can be described as the summation of capital cost and operating cost. The capital cost is associated with the heat exchanger size, and the operating cost is associated with pumping power. Generally, the capital and operating costs are competitive. For example, if the size of a heat exchanger is reduced for lower capital cost, the more operating cost should be paid for due to the increased pressure drop. Therefore, the size of the heat exchanger should be carefully determined from the economic aspect. Until recently, research has been carried out for estimation of CHE heat performance and friction loss, but little attention has been given to the optimum size and cost in utilizing it in the real system. In this study, we developed an analytic model for the optimum size of the compact heat exchangers, and evaluated them for VHTR systems.

3.4.1 Determination of Characteristic Parameters

Kays and London [1984] characterized compact heat exchangers by the following geometrical parameters.

L : CHE length
H : CHE height and width
V : Volume of CHE ($V = H^2 \cdot L$)
A_f : Frontal area ($A_f = H^2$, $A_{f,h} = 0.5A_f$, $A_{f,c} = 0.5A_f$)
A : Flow area ($A_h = 0.5A$, $A_c = 0.5A$)
β : Surface area density
σ : Ratio of the free flow area to the frontal area ($\sigma = A / A_f$)
S : Heat transfer surface ($S = \beta \cdot V$, $S_h = 0.5S$, $S_c = 0.5S$)
d_e : Equivalent diameter ($d_e = 4AL / S$)

All the heat transfer and friction factor calculations are based on the above geometrical parameters. Among the various types of compact heat exchangers, the PCHE manufactured by HEATRIC was investigated in this study. A PCHE is a type of compact heat exchanger, which consists of many plates into which the channels are chemically etched, followed by diffusion bonding to form a monolithic block. Figure 3-43 shows the cut through cross section of the typical PCHE showing the shape of the channels.

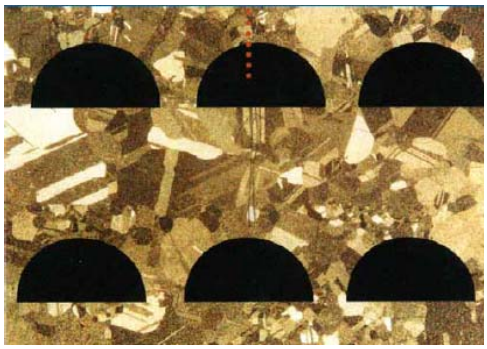

Figure 3-43 Picture of a PCHE cross section Dewson and Grady, 2003]

Main configuration parameters for PCHE, can be calculated by the basic geometrical variables as the typical heat exchangers [Kakac, 2002, Bajan and Klaus, 2003].

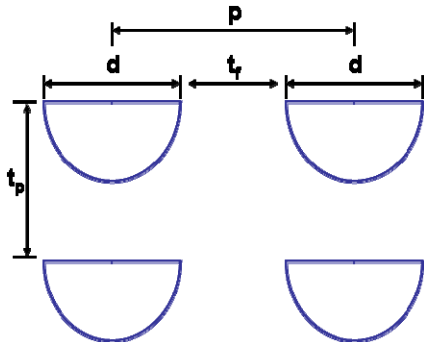

(a) cross section (front view)

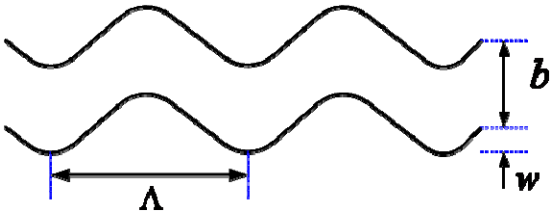

(b) channel side view

Figure 3-44 Illustration PCHE channels.

Figure 3-44 shows the front section and side view of PCHE channel. In this figure, each symbol represents the followings.

d : channel diameter (m)
p : pitch of channel (m)
t_p : plate thickness (m)
t_f : fin thickness (m)
Λ : wave length (m)
b : channel width (m) – ($b = d$ for PCHE)

Wall thickness (t_f) and pitch (p)

Hesselgreaves [2001] recommends the following formula for the minimum wall thickness.

$$t_f = \frac{1}{\left(\frac{\sigma_D}{\Delta P} + 1\right) N_f} \tag{3-16}$$

where:

t_f : minimum wall thickness

σ_D : maximum allowable stress

ΔP : pressure differential between hot and cold fluid

N_f : number of fins per meter

In the PCHE, the number of fins per meter means the number of channel walls per meter [Dostal et al. , 2004]. Therefore,

$$N_f = \frac{1}{p} \tag{3-17}$$

According to Figure 3-44, the pitch (p) of the heat exchanger channel can be expressed as follows,

$$p = d + t_f \tag{3-18}$$

By inserting Eq (3-18) and (3-17) into Eq (3-16), the following equation can be obtained.

$$t_f = \left(\frac{\Delta P}{\sigma_D}\right) \cdot d \tag{3-19}$$

This equation shows that the channel wall thickness is proportional to the design pressure and channel diameter.

Surface area density (β) and Ratio of free flow area to frontal area (σ)

The surface area density in the PCHE can be determined as follows.

$$\beta = \frac{S}{V} = \frac{(0.5 \cdot \pi \cdot d + d) \cdot L}{(d + t_f) \cdot (t_p) \cdot L} = \frac{(2 \cdot \pi \cdot d + d)}{(d + t_f) \cdot (t_p)} \tag{3-20}$$

The ratio of free flow area and frontal area is determined as follows.

$$\sigma = \frac{\frac{\pi}{8} d^2}{(d + t_f) \cdot (t_p)} \tag{3-21}$$

Hydraulic diameter (d_e)

The hydraulic diameter of PCHE can be determined by the following equation.

$$de = \frac{4A}{P} = \frac{4 \cdot \frac{\pi}{8} d^2}{\frac{\pi d}{2} + d} = \frac{\pi d}{\pi + 2} \tag{3-22}$$

Waviness ($\frac{b}{\Lambda}$)

The waviness of the PCHE can be determined by

$$Waviness = \frac{b}{\Lambda}. \tag{3-23}$$

For PCHE, b equals to channel diameter (d) in Figure 3-44.

Determination of the reference configuration parameters and properties

Table 3-7 summarizes the configuration parameters and properties for the reference PCHE. In this study, the reference diameter was selected to be 0.002 m, which is recommended by HEATRIC. They found for most application that the economic thermal performance optimum channel diameter to be 2 mm [Dewson et al., 2003, Dostal et al., 2004]. The pitch and plate thickness were determined by Eq. (3-16) through (3-19). For this calculation, the minimum plate thickness (t_p) between channels was determined to be 1.5 mm by recommendation of HEATRIC (Dewson et al., 2003). Finally, the calculated pitch and fin thickness were 0.0024 and 0.0015 m, respectively. Based on the basic geometrical parameters, the characteristic parameters for a compact heat exchanger were obtained. The surface area density and ratio of free flow to frontal area were calculated to be 1714 m^2/m^3 and 0.52 by Eq. (3-20) and (3-21), respectively. The allowable stress is assumed to be 10 MPa, which is approximately half of the rupture strength of Alloy 617 at 900 ^oC. Density of Alloy 617 is 7890 kg/m^3.

Table 3-7. Configuration parameters and properties for the reference PCHE.

Parameters	unit	Values
Diameter (d)	m	0.002
Pitch (p)	m	0.0024
Plate thickness (t_p)	m	0.0015
Fin thickness (t_f)	m	0.0004
Surface area density (β)	m^2/m^3	1714
Ratio of free flow to frontal area (σ)		0.52
Pins per meter (N_f)	#/m	417
Density (ρ_{metal})	Kg/m^3	7850
Allowable stress (σ_D)	MPa	10

3.4.2 Scaling Analysis of Compact Heat Exchanger Sizing and Cost

In the compact heat exchanger, two costs are competitive; (1) Capital cost, and (2) Operating cost. For example, the increase of flow area enhances the heat transfer capacity increasing flow velocity, but it requires more pumping power increasing the pressure drop. Therefore, the size of heat exchanger should be determined under consideration of various economic factors. In this section, we qualitatively investigated the relationship between the size and the total cost by scaling analysis. This qualitative study helps us understand how each thermal hydraulic and economic parameter is connected together.

Heat Transfer

To assess the cost of a heat exchanger, it is important fist to evaluate the heat transfer since it is highly related to its size. The heat transfer in the heat exchanger is expressed by the following equation.

$$Q = U \cdot S \cdot \theta_m \tag{3-24}$$

where:

Q : total transferred heat
U : overall heat transfer coefficient
S : heat transfer surface area
θ_m : log mean temperature

Therefore, the surface area is written as

$$S = \frac{Q}{U \cdot \theta_m}. \tag{3-25}$$

Since the values of Q and θ_m are fixed in the design condition, the surface area is proportional to the inverse of the overall heat transfer coefficient.

$$S \propto \frac{1}{U} \tag{3-26}$$

In the compact heat exchanger, since heat transfer surface area is proportional to the volume, the following relation is formed.

$$S \propto V \text{ and } U \propto h \propto h_h \propto h_c \tag{3-27}$$

where:

V : compact heat exchanger volume

h_h : heat transfer coefficient of hot channel

h_c : heat transfer of cold channel

Therefore, the volume is inversely proportional to the heat transfer coefficient.

$$V \propto \frac{1}{h} \tag{3-28}$$

Generally, the heat transfer correlation can be expressed as follows,

$$Nu = \frac{h \cdot d_e}{k} = b\,\mathrm{Re}^b\,\mathrm{Pr}^c \tag{3-29}$$

And, the Reynolds number and Prandtl number in the compact heat exchanger are defined by

$$\mathrm{Re} = \frac{d_e G}{\mu} = \frac{d_e \dot{m}}{A\mu}, \tag{3-30}$$

and

$$\mathrm{Pr} = \frac{C_p \cdot \mu}{k}. \tag{3-31}$$

Where

$\dot{m}$: Mass flow rate (kg/s)

A : flow area (m^2)

μ : Viscosity (Pa m)

C_p : Heat capacity (J/kg K)

k : Thermal conductivity (W/m K)

Therefore, the Eq (3-29) can be rearranged as follows,

$$h = \left[\left(\frac{bk}{d_e} \right) \left(\frac{d_e \cdot \dot{m}}{\mu} \right)^b \mathrm{Pr}^c \right] \cdot A^{-b} = F_1 \cdot A^{-b}. \tag{3-32}$$

It means that

$$h \propto A^{-b}. \tag{3-33}$$

If we relate Eq. (3-28) to Eq. (3-33), we obtain

$$V \propto \frac{1}{h} \propto A^{b}. \tag{3-34}$$

It means the total volume of the heat exchanger is proportional to A^b. The total volume is proportional to the flow area multiplied by the length of the heat exchanger,

$$V \propto A \cdot L, \tag{3-35}$$

$$L \propto \frac{V}{A} \tag{3-36}$$

Therefore,

$$L \propto \frac{V}{A} \propto \frac{A^b}{A} \propto A^{b-1}. \tag{3-37}$$

Friction Loss

The friction loss is an important factor because higher friction loss requires more pumping power consuming additional operating cost. The friction loss in the compact heat exchanger is generally expressed by

$$\Delta P = f \frac{G^2}{2\rho} \frac{S}{A} = f \frac{G^2}{2\rho} \frac{4L}{d_e}. \tag{3-38}$$

Where

ΔP : Pressure drop (Pa)
f : Friction factor
ρ : Density of flow (kg/m^3)

The general form of friction factor correlation is as follows,

$$f = e\,\mathrm{Re}^{i}. \tag{3-39}$$

Inserting Eq. (3-39) into Eq. (3-38), the friction loss correlation can be rearranged as follows,

$$\Delta P = \left[e\left(\frac{d_e \dot{m}}{\mu}\right)^{i} \left(\frac{\dot{m}^2}{2\rho}\right)\left(\frac{4}{d_e}\right) \right] \cdot \frac{L}{A^{i+2}}. \tag{3-40}$$

Therefore,

$$\Delta P \propto \frac{L}{A^{i+2}} \tag{3-41}$$

If the length (L) in Eq. (3-41) is replaced with Eq. (3-37), it becomes

$$\Delta P \propto \frac{L}{A^{i+2}} \propto \frac{A^{b-1}}{A^{i+2}}. \tag{3-42}$$

Finally we obtains the following relation,

$$\Delta P \propto A^{b-i-3}. \tag{3-43}$$

Cost of Compact Heat Exchanger

To assess the total cost of a heat exchanger, it is important first to evaluate the capital cost (C_c). Generally, the cost of heat exchanger can be estimated based on its weight, and since the weight is proportional to the volume of the compact heat exchanger, the capital cost and volume of the heat exchanger can be related as follows.

$$C_c \propto V \tag{3-44}$$

From Eq (4-18), it becomes

$$C_c \propto A^b \tag{3-45}$$

Eq (3-45) means that the capital cost increases with flow area.

From Eq. (3-37), the length of the heat exchanger is related to the flow area as follows.

$$L \propto A^{b-1} \tag{3-46}$$

It means that the variation of the length is dependent on the value of the index, b.

(i) b>1: L increases with flow area
(ii) b=1: L does not changes
(iii) b<1: L decreases with flow area

According to the heat transfer references or handbooks [Bajan, 2001], Heat Transfer Handbook), the index, b is generally no more than unity. Therefore, we can consider that the increase of flow area leads to the decrease of heat exchanger length.

Heat exchanger operating cost can be assumed to be proportional to the pumping power.

$$C_o \propto P_{pumping} \tag{3-47}$$

Since the pumping power is proportional to the pressure drop,

$$P_{pumping} \propto \Delta P, \tag{3-48}$$

It becomes

$$P_{pumping} \propto \Delta P \propto A^{b-i-3}. \tag{3-49}$$

It means that the operating cost is the relation of flow area and indices b and i.

$$C_o \propto A^{b-i-3} \tag{3-50}$$

According to this relation, the variation of the operating cost with the flow area is dependent on the two indices, b and i, as follows.

(i) b-i-3 > 0: C_o increases with the flow area

(ii) b-i-3 = 0: C_o is not dependent on the flow area

(iii) b-i-3 < 0: C_o decreases with the flow area

However, since the values of b and i are usually less than 1.00 according to the heat transfer references [Bajan , 2001], Heat Transfer Handbook), the value of (b-i-3) can be considered to be less than zero. It means the operating cost of heat exchanger decreases with flow area.

In summary, the increase of flow area at the given duty and operating conditions, qualitatively, leads to the following consequences.

$$A(\uparrow) \Rightarrow h(\downarrow) \Rightarrow U(\downarrow) \Rightarrow V(\uparrow) \Rightarrow L(\downarrow) \Rightarrow C_c(\uparrow) \Rightarrow \Delta P(\downarrow) \Rightarrow C_o(\downarrow) \tag{3-51}$$

This relation shows that the increase of flow rate increases the capital cost but reduces the operating cost. Therefore, it means that there exists an optimum flow area to minimize the total cost. The total cost of the heat exchanger can be expressed by the summation of the capital cost and the operating cost.

$$C_{total} = K_1 \cdot A^b + K_2 \cdot A^{b-i-3} \tag{3-52}$$

To find out the optimum flow area, differentiation of Eq. (3-52) was obtained.

$$\frac{dC_{total}}{dA} = K_1 \cdot b \cdot A^{b-1} + K_2 \cdot (b-i-3) \cdot A^{b-i-4} \tag{3-53}$$

At the optimum point, since the differentiation is zero, it satisfies

$$K_1 \cdot b \cdot {A_{opt}}^{b-1} + K_2 \cdot (b-i-3) \cdot {A_{opt}}^{b-i-4} = 0. \tag{3-54}$$

Therefore, the optimum surface area can be written as

$$A_{opt} = \left(\left(\frac{3-b+i}{b} \right) \cdot \left(\frac{K_2}{K_1} \right) \right)^{\frac{1}{3+i}}. \tag{3-55}$$

It means that the optimum flow area increases with the operating cost but decreases with the capital cost. If we determine K_1 and K_2, we can calculate the optimum surface area. The determination of those two parameters was explained in the next section.

3.4.3 Optimum Sizing Model for Minimum Cost of Compact Heat Exchanger

In this section, we developed the analytic model to determine the total cost and optimum heat exchanger size, and finally determined K_1 and K_2 in Eq. (3-52). In this study, it is assumed that the hot and cold channel has the same geometry and portion in the heat exchanger. So, the hot and cold channel properties can be expressed as follows.

(i) frontal area

$A_{f,h} = 0.5A_f$ (hot channel)

$A_{f,c} = 0.5A_f$ (cold channel)

(ii) flow area

$A_h = 0.5A$ (hot channel)

$A_c = 0.5A$ (cold channel)

(iii) heat transfer surface

$S_h = 0.5A_H$ (hot channel)

$S_c = 0.5A_H$ (cold channel)

(iv) equivalent diameter

$d_{e,h} = d_e$ (hot channel)

$d_{e,c} = d_e$ (cold channel)

From Eq (3-25),

$$S_h = 0.5A_H = \frac{Q}{U_h \cdot \theta_m} \tag{3-56}$$

The overall heat transfer coefficient can be expressed as follows,

$$U_h = \frac{1}{\frac{1}{h_h} + S_h R_w + \frac{S_h}{h_c S_c}} \tag{3-57}$$

If we assume that the heat resistance of the CHE wall is negligible compared to the convective heat resistance, (usually, the heat resistance in the flow area is much larger than the solid wall (Song (2005)),

$$U_h \approx \frac{1}{\frac{1}{h_h} + \frac{S_h}{h_c S_c}} \tag{3-58}$$

Then,

$$S_h = S_c = 0.5 A_H \tag{3-59}$$

Therefore, Eq (3-58) becomes

$$U_h \approx \frac{1}{\frac{1}{h_h} + \frac{1}{h_c}} . \tag{3-60}$$

The heat transfer coefficients is usually expressed as shown in Eq. (3-29),

$$Nu = \frac{h \cdot d_e}{k} = a \,\mathrm{Re}^b \,\mathrm{Pr}^c \tag{3-61}$$

Therefore,

$$h_h = \left[\left(\frac{ak_h}{d_e} \right) \left(\frac{d_e \cdot \dot{m}_h}{\mu} \right)^b \mathrm{Pr}_h{}^c \right] \cdot A_h{}^{-b} = \left[\left(\frac{ak_h}{d_e} \right) \left(\frac{d_e \cdot \dot{m}_h}{0.5\mu} \right)^b \mathrm{Pr}_h{}^c \right] \cdot A^{-b} = FACT1 \cdot A^{-b} \tag{3-62}$$

$$h_c = \left[\left(\frac{ak_c}{d_e} \right) \left(\frac{d_e \cdot \dot{m}_c}{\mu} \right)^b \mathrm{Pr}_c{}^c \right] \cdot A_c{}^{-b} = \left[\left(\frac{ak_c}{d_e} \right) \left(\frac{d_e \cdot \dot{m}_c}{0.5\mu} \right)^b \mathrm{Pr}_c{}^c \right] \cdot A^{-b} = FACT2 \cdot A^{-b} \tag{3-63}$$

If we insert Eq (3-62) and Eq (3-63) into Eq (3-60), the overall heat transfer coefficient can be expressed by

$$U_h = \frac{1}{\frac{A^b}{FACT1} + \frac{A^b}{FACT2}} = \left(\frac{1}{\frac{1}{FACT1} + \frac{1}{FACT2}} \right) \cdot A^{-b} = FACT3 \cdot A^{-b} . \tag{3-64}$$

From Eq (3-56), the heat transfer surface area of the compact heat exchanger is

$$S_h = 0.5A_H = \frac{Q}{U_h \cdot \theta_m}, \tag{3-65}$$

And

$$A_H = \frac{2 \cdot Q}{U_h \cdot \theta_m}. \tag{3-66}$$

From the definition of surface area density (Eq. (3-20)), the volume of the CHE can be expressed by

$$A_H = \beta \cdot V = \frac{2 \cdot Q}{U_h \cdot \theta_m}, \tag{3-67}$$

Therefore, the volume of the CHE volume becomes

$$V = \frac{1}{\beta} \cdot \frac{2Q}{FACT3 \cdot A^{-b} \cdot \theta_m} = \left(\frac{2 \cdot Q}{\beta \cdot FACT3 \cdot \theta_m} \right) \cdot A^b = FACT4 \cdot A^b. \tag{3-68}$$

If we only consider the metal volume, the volume of metal can be expressed by

$$V_{Material} = (1-\sigma) \cdot V = (1-\sigma) \cdot FACT4 \cdot A^b. \tag{3-69}$$

Since the volume of the heat exchanger is

$$V = A_{fr} \cdot L = \frac{A}{\sigma} \cdot L, \tag{3-70}$$

The length becomes

$$L = \frac{\sigma}{A} \cdot V = \frac{\sigma}{A} \cdot FACT4 \cdot A^b = \left(\sigma \cdot FACT4\right) \cdot A^{b-1}. \tag{3-71}$$

The friction loss of the heat exchanger is expressed by Eq. (3-38) and (3-39) as follows,

$$\Delta P = f \frac{G^2}{2\rho} \frac{S}{A} = f \frac{G^2}{2\rho} \frac{4L}{d_e} \tag{3-72}$$

where

$$f = f_2(\mathrm{Re}) = e\,\mathrm{Re}^i. \tag{3-73}$$

The hot channel pressure drop can be obtained by inserting Eq. (3-73) into Eq. (3-72),

$$\Delta P_h = \left[e\left(\frac{d_e \dot{m}_h}{\mu_h} \right)^i \left(\frac{\dot{m}_h{}^2}{2\rho_h} \right) \left(\frac{4}{d_e} \right) \right] \cdot \frac{L}{A_h^{i+2}} = \left[e\left(\frac{d_e \dot{m}_h}{0.5\mu_h} \right)^i \left(\frac{\dot{m}_h{}^2}{\rho_h} \right) \left(\frac{4}{d_e} \right) \right] \cdot \frac{L}{A^{i+2}} \tag{3-74}$$

Replacing L in Eq. (3-74) with Eq. (3-71), it becomes

$$\Delta P_h = \left[e\left(\frac{d_e \dot{m}_h}{0.5\mu_h}\right)^i \left(\frac{\dot{m}_h{}^2}{\rho_h}\right)\left(\frac{4}{d_e}\right)\right] \cdot \frac{(\sigma \cdot FACT4)\cdot A^{b-1}}{A^{i+2}}$$

$$= \left[e\left(\frac{d_e \dot{m}_h}{0.5\mu_h}\right)^i \left(\frac{\dot{m}_h{}^2}{\rho_h}\right)\left(\frac{4}{d_e}\right)\right] \cdot (\sigma \cdot FACT4)\cdot A^{b-i-3} = FACT5 \cdot A^{b-i-3}. \quad (3\text{-}75)$$

The pressure drop of the cold channel can be obtained by the same method.

$$\Delta P_c = \left[e\left(\frac{d_e \dot{m}_c}{0.5\mu_c}\right)^i \left(\frac{\dot{m}_c{}^2}{\rho_c}\right)\left(\frac{4}{d_e}\right)\right] \cdot (\sigma \cdot FACT4)\cdot A^{b-i-3} = FACT6 \cdot A^{b-i-3} \quad (3\text{-}76)$$

From the pressure drops, the pumping power can be approximately calculated as follows,

$$P_{power,h} = \frac{\dot{m}_h \cdot \Delta P_h}{\rho_h} = \frac{\dot{m}_h \cdot FACT5}{\rho_h} \cdot A^{b-i-3} \quad (3\text{-}77)$$

$$P_{power,c} = \frac{\dot{m}_c \cdot \Delta P_c}{\rho_c} = \frac{\dot{m}_c \cdot FACT6}{\rho_c} \cdot A^{b-i-3} \quad (3\text{-}78)$$

The cost of heat exchanger is the summation of the capital cost and operating cost. The capital cost of the compact heat exchanger is determined based on the mass. From Eq (3-70), the mass of the heat exchanger is

$$M_{CHE} = \rho_{Material} \cdot V_{Material} = \rho_{Materal} \cdot (1-\sigma) \cdot FACT4 \cdot A^b. \quad (3\text{-}79)$$

Therefore, the capital cost can be expressed by

$$CP = C_{CHEmass} \cdot M_{CHE} = C_{CHEmass} \cdot \rho_{Materal} \cdot (1-\sigma) \cdot FACT4 \cdot A^b \quad (3\text{-}80)$$

where:

CP : capital cost of CHE

$C_{CHEmass}$: price($) per CHE unit mass (kg)

The operating cost can be assumed to be proportional to the pumping power. Therefore,

$$OP = C_{op} \cdot (P_{power,h} + P_{power,c}) \cdot Y \quad (3\text{-}81)$$

where:

OP : operating cost of CHE

C_{op} : cost($) per watt-hour

Y : total duration of operation

Therefore,

$$OP = C_{op} \cdot Y \cdot (\frac{\dot{m}_h \cdot FACT5}{\rho_h} + \frac{\dot{m}_c \cdot FACT6}{\rho_c}) \cdot A^{b-i-3} \tag{3-82}$$

The total cost becomes

$$C_{total} = CP + OP = \left(C_{CHEmass} \cdot \rho_{Materal} \cdot (1-\sigma) \cdot FACT4\right) \cdot A^b + \left(C_{op} \cdot Y \cdot (\frac{\dot{m}_h \cdot FACT5}{\rho_h} + \frac{\dot{m}_c \cdot FACT6}{\rho_c}) \right) \cdot A^{b-i-3} \tag{3-83}$$

It can be simplified as follows

$$C_{total} = K_1 \cdot A^b + K_2 \cdot A^{b-i-3}. \tag{3-84}$$

This is the same correlation as Eq. (4-37), and K_1 and K_2 are determined as follows.

$$K_1 = C_{CHEmass} \cdot \rho_{Materal} \cdot (1-\sigma) \cdot FACT4 \tag{3-85}$$

$$K_2 = C_{op} \cdot Y \cdot (\frac{\dot{m}_h \cdot FACT5}{\rho_h} + \frac{\dot{m}_c \cdot FACT6}{\rho_c}) \tag{3-86}$$

where,

$$FACT1 = \left(\frac{ak_h}{d_e}\right)\left(\frac{d_e \cdot \dot{m}_h}{0.5\mu}\right)^b \mathrm{Pr}_h{}^c \tag{3-87}$$

$$FACT2 = \left(\frac{ak_c}{d_e}\right)\left(\frac{d_e \cdot \dot{m}_c}{0.5\mu}\right)^b \mathrm{Pr}_c{}^c. \tag{3-88}$$

$$FACT3 = \frac{1}{\frac{1}{FACT1} + \frac{1}{FACT2}} \tag{3-89}$$

$$FACT4 = \frac{2 \cdot Q}{\beta \cdot FACT3 \cdot \theta_m} \tag{3-90}$$

$$FACT5 = \left[e\left(\frac{d_e \dot{m}_h}{0.5\mu_h}\right)^i \left(\frac{\dot{m}_h{}^2}{\rho_h}\right)\left(\frac{4}{d_e}\right)\right] \cdot \left(\sigma \cdot FACT4\right) \tag{3-91}$$

$$FACT6 = \left[e\left(\frac{d_e \dot{m}_c}{0.5\mu_c}\right)^i \left(\frac{\dot{m}_c{}^2}{\rho_c}\right)\left(\frac{4}{d_e}\right)\right] \cdot \left(\sigma \cdot FACT4\right) \tag{3-92}$$

As derived in Eq. (3-55), the optimum flow surface is

$$A_{opt} = \left(\left(\frac{3-b+i}{b}\right) \cdot \left(\frac{K_2}{K_1}\right)\right)^{\frac{1}{3+i}}. \tag{3-93}$$

The optimum aspect ratio is

$$\left.\frac{H}{L}\right|_{opt} = \frac{\left(A_{opt}/\sigma\right)^{0.5}}{\sigma \cdot FACT4 \cdot A_{opt}^{\,b-1}} = \frac{A_{opt}^{\,1.5-b}}{\sigma^{1.5} \cdot FACT4}. \tag{3-94}$$

3.4.4 Reference IHX Conditions and Input Parameters

Figure 3-45 shows a reference design of 600 MWt VHTR/HTSE system. In this system, the core part and PCU are connected through an IHX. And VHTR and HTSE are integrated by a SHX at the ternary loop (intermediate heat exchange loop). It means that the heat generated in the reactor core is transferred to PCU through IHX, and it is re-transferred in the PCU to HTSE through SHX. The advantage of this configuration is for being able to achieve the highest temperature at both HTSE and PCU, maximizing the efficiency. For high efficiency, regenerating and inter-cooling systems are adapted. The heat in the turbine outlet could be effectively recovered to the turbine inlet. A total of 5 heat exchangers were used in this system, and the main focus has been on the IHX among them, which transfers 600 MWt heat from primary side to secondary side.

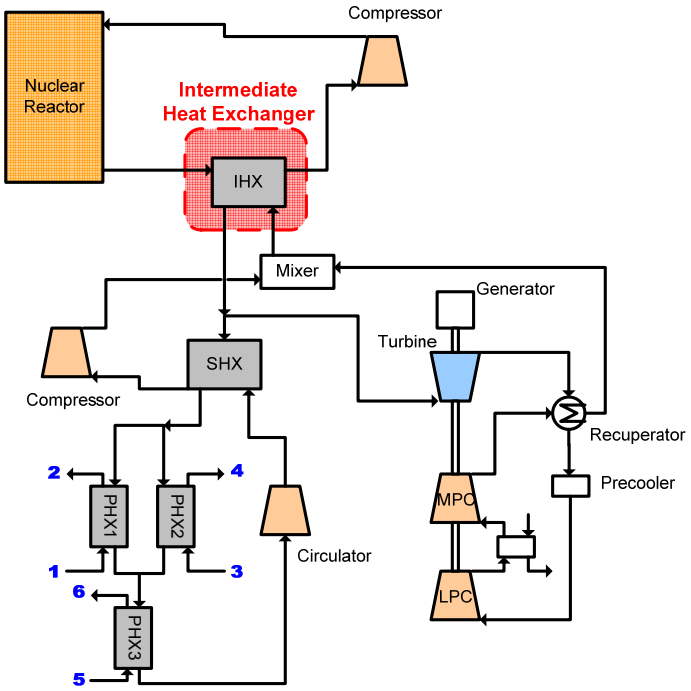

Figure 3-45 Reference configuration of a 600 MWt VHTR/HTSE system.

Table 3-8 summarizes the design conditions for the IHX. These design parameters were calculated and optimized by HYSYS 3.2, a process analysis code. The fluid properties such as density and viscosity were obtained from NIST Chemistry WebBook.

Table 3-8 IHX operating conditions for the reference system.

	Hot Channel (Primary)		Cold Channel (Secondary)	
	In	**Out**	**In**	**Out**
Fluid Type	Helium	Helium	Helium	Helium
Temperature (^oC)	900	594	579	885
Pressure (MPa)	7	6.95	7.97	7.92
Flow rate (kg/s)	385	385	385	385
Density (kg/m^3)	2.86	3.83	4.25	3.12
Heat Capacity (kJ/kg K)	5.19	5.19	5.19	5.19
Thermal Conductivity (W/m K)	0.4	0.33	0.326	0.4
Viscosity (Pa s)	5.17e-5	5.17e-5	4.13e-5	4.13e-5

INCONEL® Alloy 617 was selected for heat exchanger material. Alloy 617 is a solid-solution, strengthened nickel-chromium-cobalt-molybdenum alloy with an exceptional combination of high temperature strength and oxidation resistance. The alloy also has excellent resistance to a wide range of corrosive environments, and it is readily formed and welded by conventional techniques. The combination of high strength and oxidation resistance at temperature over 980 ^oC makes this an attractive material for VHTR/HTSE system. Melting range and some physical properties are summarized in Table 3-9.

Table 3-9 Properties of Alloy 617.

Properties	Values
Density (Mg/m3)	8.36
Melting Ranges (^oC)	1332~1380
Specific Heat (J/kg C) at 900 C	636
Thermal Conductivity (W/m C) at 900 C	27.1

Friction factor and heat transfer coefficients are very important parameters, which determine the size of the heat exchangers. In this study, PCHE type of compact heat exchanger was selected. Some correlations applicable for PCHE are summarized in Table 3-10 and 3-11. In this study, Oyakawa & Shinzato [1989]'s correlations were selected, which were originally developed for wavy channels. The main advantage of them is that the waviness effect of channel is considered. These considerations can lead to more physically acceptable consequences. Although Oyakawa & Shinzato's correlation showed reasonable agreement with wide ranges of wavy channel experimental data, as shown in Figure 3-46 and 3-47, they have still some deviation from the real PCHE experimental data from Nikitin et al. [2006] and Song [2005]. Therefore, the improvement of heat transfer and friction model for PCHE is required in the future.

Table 3-10 Friction factor (Fanning) correlations for compact heat exchanger.

Type	Correlations
Laminar Flow	$f = 16 \cdot \mathrm{Re}^{-1}$ (for circular straight pipe)
Blasius	$f = 0.0791 \cdot \mathrm{Re}^{-0.25}$
Song [2005]	$f = 4.17 \cdot \mathrm{Re}^{-0.76}$ (for PCHE)
Kays and London [1984]	$f = 0.6 \cdot \mathrm{Re}^{-0.425}$ (for wavy compact heat exchanger)
Oyakawa & Shinzato [1989]	$f = 2.0 \cdot \mathrm{Re}^{-0.4} \cdot \cdot \left(\frac{2b}{\Lambda}\right)^{0.25}$ (for wavy channel)
Hesselgreaves [2001]	$f = 11 \cdot \mathrm{Re}^{-0.53}$ (for PCHE)
Nikitin et al. [2006]	$f = 0.1 \cdot \mathrm{Re}^{-0.152}$ (for PCHE)

Table 3-11 Heat transfer correlations for compact heat exchanger.

Type	Correlations
Laminar Flow	$Nu = 4.089$ (for circular straight pipe)
Dittus-Boelter	$Nu = 0.021 \cdot \mathrm{Re}^{0.8}\ \mathrm{Pr}^{0.4}$ (for circular straight pipe)
Song [2005]	$Nu = 0.08 \cdot \mathrm{Re}^{0.74}\ \mathrm{Pr}^{2.69}$ (for PCHE)
Oyakawa & Shinzato [1989]	$Nu = 0.4 \cdot \mathrm{Re}^{0.6}\ \mathrm{Pr}^{0.33} \cdot \left(\frac{2b}{\Lambda}\right)^{0.25}$ (for wavy channel)
Hesselgreaves [2001]	$Nu = 0.125 \cdot \mathrm{Re}^{0.64}\ \mathrm{Pr}^{0.33}$ (for PCHE)

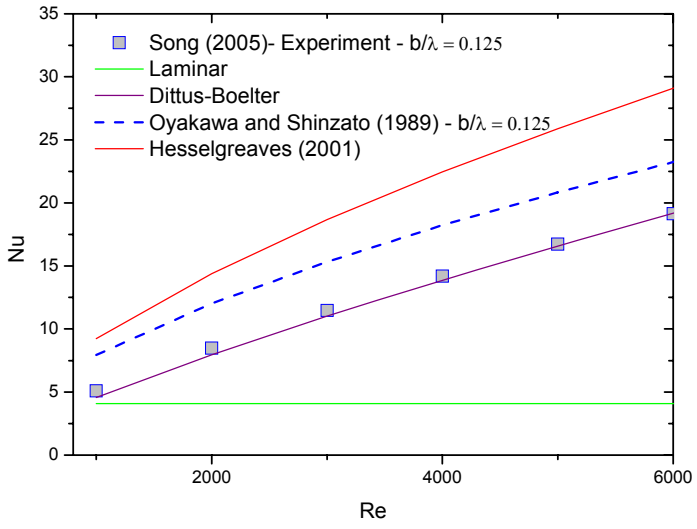

Figure 3-46. Heat Transfer correlations.

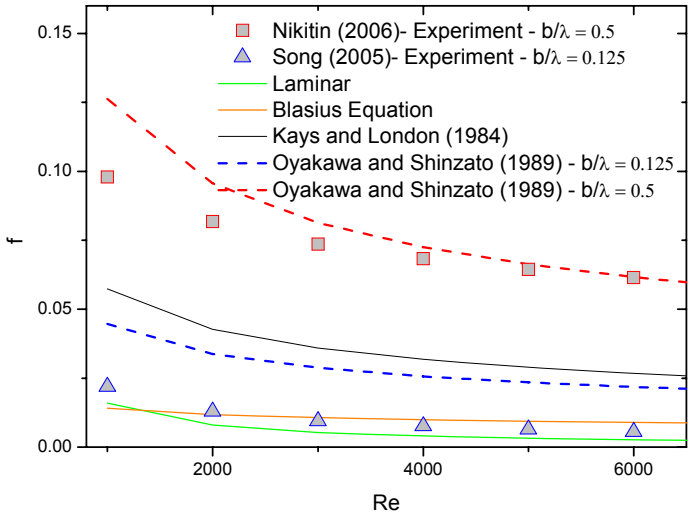

Figure 3-47. Friction factor correlations.

The two input parameters, $C_{CHEmass}$ and C_{op} should be determined for cost estimation. Currently, the PCHE is being sold on a $/kg basis. For non-nuclear applications, which is fabricated of chrome duplex, it costs approximately $50/kg. For nuclear application, Heatric estimates the price of standard product in stainless steel to be around 30 $. If environmental conditions exclude the use of stainless steel, the HXs may be manufactured of titanium, which will increase the price up to $120/kg [Dostal et al. (2004)].

The value of C_{op} can be obtained from consumer price index average price data [EIA, 2007]. According to this reference, the electricity cost is 0.0000612 $/watts-hour for the industrial sector. The reference operating period is assumed to be 20 years.

3.4.5 Optimum Sizing of Compact Heat Exchanger for Reference System

The optimum size of the IHX has been estimated. Figure 3-48 illustrates the cost variations with flow area for the reference IHX. As shown in this figure, the capital cost increases with flow area. It is due to the increase of volume. On the other hand, the operating cost exponentially decreases with flow area because of the decreased pumping power. The total cost is sharply decreasing at the beginning due to the operating cost effect and reaches minimum cost, and then gradually increases with the capital cost. For the reference IHX (600 MWt), the optimum flow area was estimated to be 28 m^2.

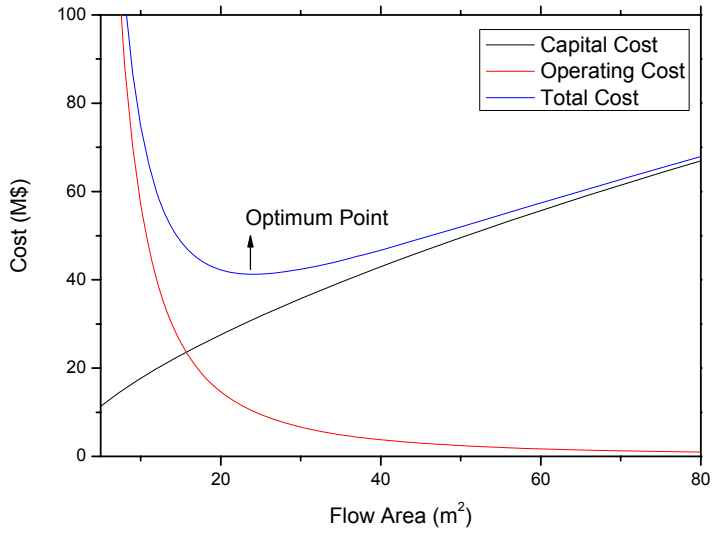

Figure 3-48 Optimum flow area for reference IHX.

Figure 3-49 shows that the total cost is very slightly increasing with the flow area when it is larger than the optimum size. It means that the size of IHX can be flexibly determined if the flow area is larger than the optimum. However, at the low flow area, especially lower than the intersection point between the capital cost and the operating cost, the total cost is dramatically increased, and the IHX becomes uneconomic. Therefore, the flow area of the IHX should not be reduced lower than this value. We named this surface area as the minimum allowable flow area, and it can be calculated from Eq. (3-84) and (3-93).

$$A_{\min} = \left(\frac{K_2}{K_1}\right)^{\frac{1}{3+i}} = \left(\frac{3-b+i}{b}\right)^{\frac{1}{3+i}} \cdot A_{opt} \tag{3-95}$$

$$\frac{A_{\min}}{A_{opt}} = \left(\frac{K_2}{K_1}\right)^{\frac{1}{3+i}} = \left(\frac{3-b+i}{b}\right)^{\frac{1}{3+i}} \tag{3-96}$$

For the reference IHX, the minimum allowable area is calculated to be 18.43 m^2. Therefore, we recommend that the flow area of the reference IHX should not be selected below 18.43 m^2.

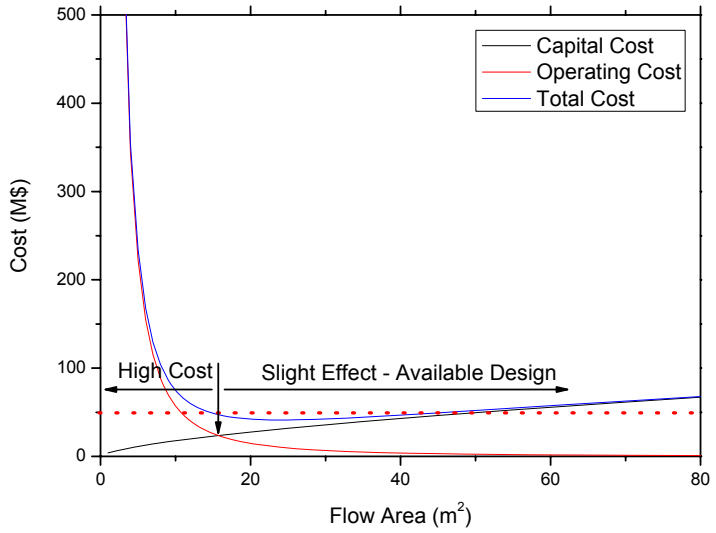

Figure 3-49 Minimum Allowable flow area for reference IHX.

Figure 3-50 shows the aspect ratio with flow area. The optimum aspect ratio for the reference IHX is estimated to be 13.5. It means that the length of the heat exchanger is much smaller than the height and width (length = 0.71 m, height and width = 9.59 m). This is very unrealistic design for heat exchangers. So, we tried to decrease the aspect ratio (below 1.00) by decreasing flow area. However, in this case, as mentioned above, the total cost is sharply increased more than 100 times. Therefore, it makes the design of the IHX very difficult.

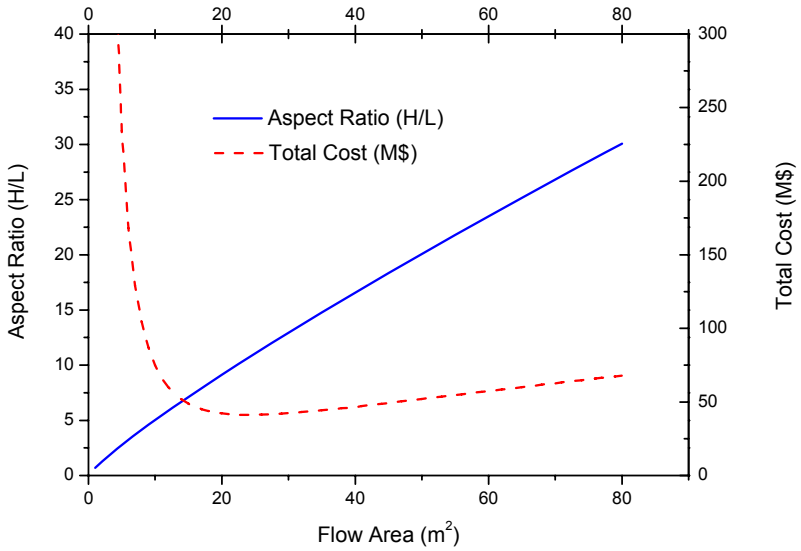

Figure 3-50 Aspect ratio variations with flow area.

Figure 3-51 shows the variation of the total cost with aspect ratio. As shown in this figure, the total cost sharply increases lower than the aspect ratio (=9.32) at the minimum allowable flow area (=18.43 m^2).

The unrealistic aspect ratio is mainly caused by the size of channel diameter. In the PCHE, the micro-size channel leads to high surface density and heat transfer. However, it also reduces the boundary layer thickness severely increasing the pressure drop. To reduce the pressure drop, we should reduce the length of the channels, but it finally results in the unrealistic aspect ratio. Figure 3-52 shows the effect of the pressure drop of the IHX on the overall system efficiency. As shown in this figure, the overall efficiency linearly decreases with the pressure drop. The system overall efficiency reaches up to 45 % at low pressure drop within 50 kPa, however it drops down to less than 40 % at the higher pressure drop more than 200 kPa (~2 atm). In the following sections, we discussed about this problem in more detail.

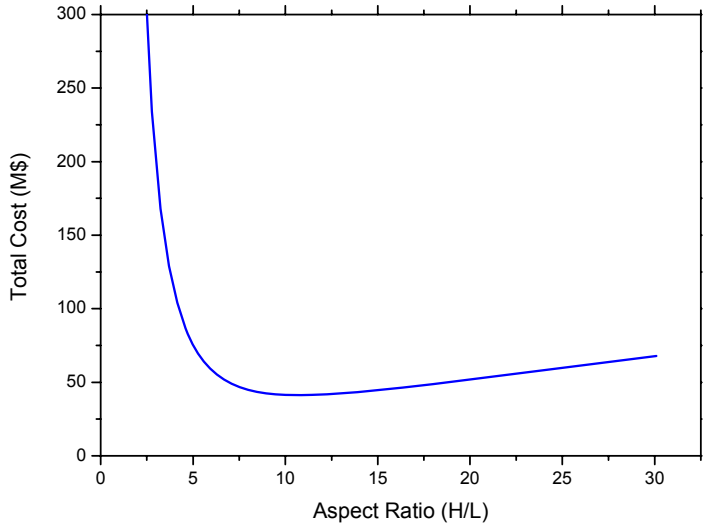

Figure 3-51 Aspect ratio vs. Total cost.

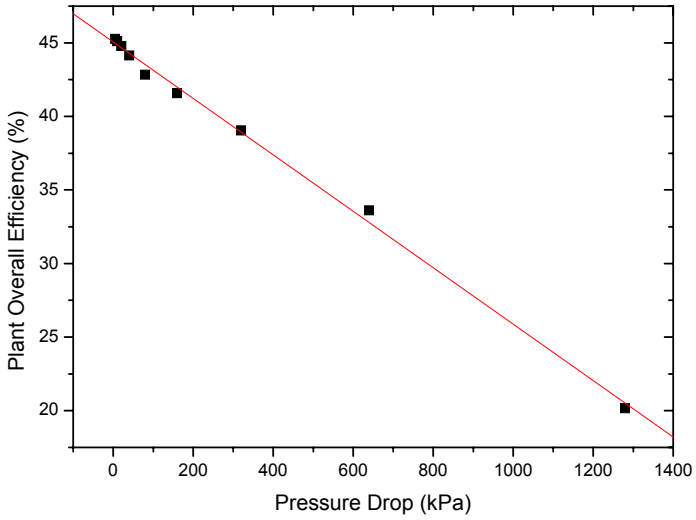

Figure 3-52 Effect of IHX pressure drop on the system overall efficiency.

3.4.6 Effect of Geometrical Parameters

As seen in the previous section, the compactness of PCHE reduces the IHX cost dramatically, but the quality of compactness can result in an unrealistic aspect ratio. In this section, we modified the basic channel configurations to include changes in channel diameter and waviness, and considered various changes to these parameters in order to achieve a more realistic design.

Figure 3-53 shows the effect of channel diameter on the optimum aspect ratio. As shown in this figure, the aspect ratio of PCHE exponentially decreases with channel diameter and becomes 1.00 at around d=0.010m, which is four times as large as the original size.

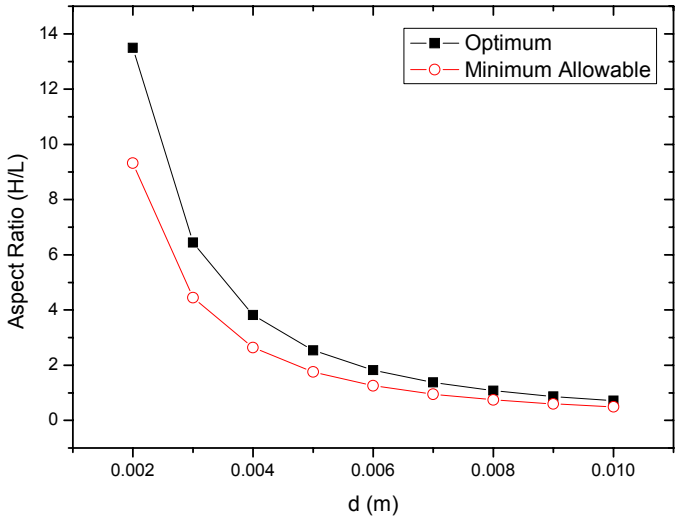

Figure 3-53 Effect of channel diameter (d) on optimum aspect ratio.

Figure 3-54 shows the effect of channel diameter on the volume of the optimum heat exchanger. As shown in this figure, the volume of the heat exchanger linearly increases with the channel diameter.

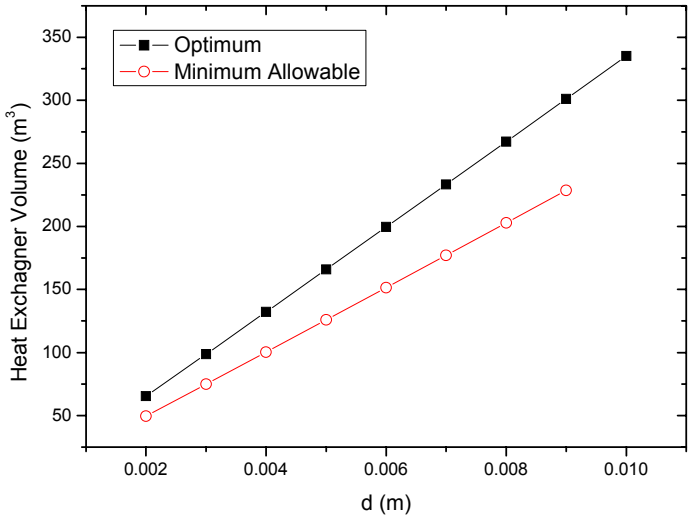

Figure 3-54 Effect of channel diameter (d) on optimum heat exchanger volume.

One notable result here is that the decreasing rate of the aspect ratio is diminished with the diameter size. As shown in Figure 3-53, the diameter effect on the aspect ratio is significant when the size is small. However, as the diameter is increased, the rate of decreasing of the aspect ratio becomes small, especially when the diameter is more than 0.005 m. On the other hand, the cost and volume are continuously increasing with increasing diameter (See Figure 3-54 and 3-55). It means that the channel diameter should be selected nearly or equally to 0.005 m from the economic point of view. According to the graph, at d=0.005 m, the minimum possible aspect ratio ranges around 2.00, which means the length of the heat exchanger becomes half of the width or height. This value (H/L=2) is an improvement over the reference cases (H/L=13.45), but is still relatively high aspect ratio. One good approach to solve this problem is to split the heat exchanger into several modules. In this case, we can divide the original heat exchanger into more than 4 independent modules, and maintain the aspect ratio below 1.00. However, since the large number of modules makes the system much complicated, the number of modules should be carefully determined. Though beyond the scope of this study, more work is needed to determine the optimum number and size of modular heat exchangers that would meet the same heat exchange requirements as the single heat exchanger examined here.

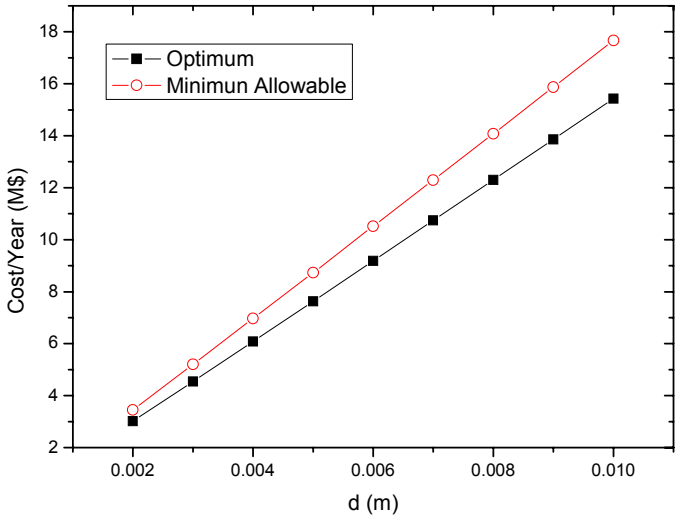

Figure 3-55 Effect of channel diameter (d) on the optimum cost/year.

If the lifetime cost of the heat exchanger is considered (i.e., the sum of the capital cost plus the total operating cost over the lifetime of the heat exchanger), different heat exchanger flow channel diameters can be calculated (via Eq. (3-55)) that optimize the capital and total operating costs. Different optimum points are realized because total operating costs increase with each additional year of service, while capital costs are not time-dependent. Operating costs per year can be reduced by decreasing pressure drop, but this may require increased flow surface area, increased channel diameter, and subsequently increased capital costs. The optimized total cost for any expected length of service can be normalized by dividing the total optimized cost by the expected service length to provide a basis of comparison, and this is what is plotted in Figure 3-55 in response to changing flow channel diameter.

Waviness is also an important geometrical parameter for PCHE design, because it greatly affects the heat transfer and friction loss. We studied the effect of varying the waviness factor from zero (for straight pipe) to 0.5 (for Nikitinn et al. (2005)), and estimated the effect of this change. Figure 3-56 through 3-58 show the variation in cost/year, the volume, and the aspect ratio with waviness, respectively. As a result, we found that the total cost was reduced by waviness, but the aspect ratio increased. It is because the increase of waviness enhanced the heat transfer coefficient, thus reducing the volume, but caused an increase in friction losses and higher pressure drops. Therefore, the waviness can be effectively used to increase heat exchanger compactness and reduce capital costs, but can lead to the unfavorable increase of the aspect ratio. According to the graphs, the waviness exponentially reduces the heat exchanger total cost, but linearly increases the aspect ratio. We think that the economically appropriate range of the waviness is 0.1 through 0.25. However, more detailed study of this effect is needed in future work.

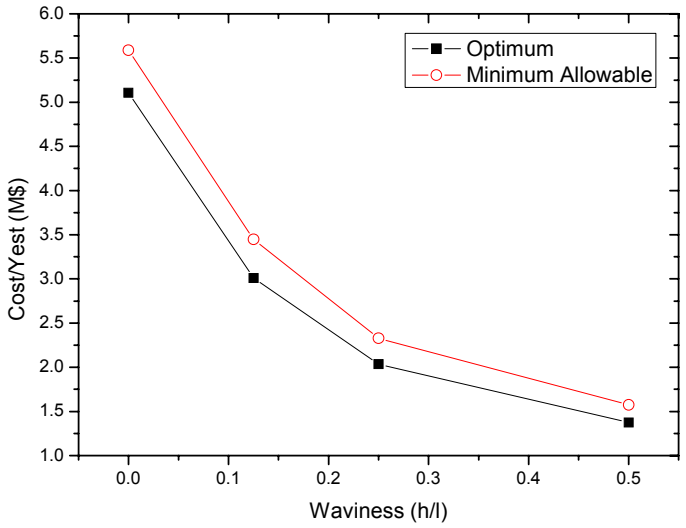

Figure 3-56 Effect of waviness ($\frac{b}{\Lambda}$) on the cost/year.

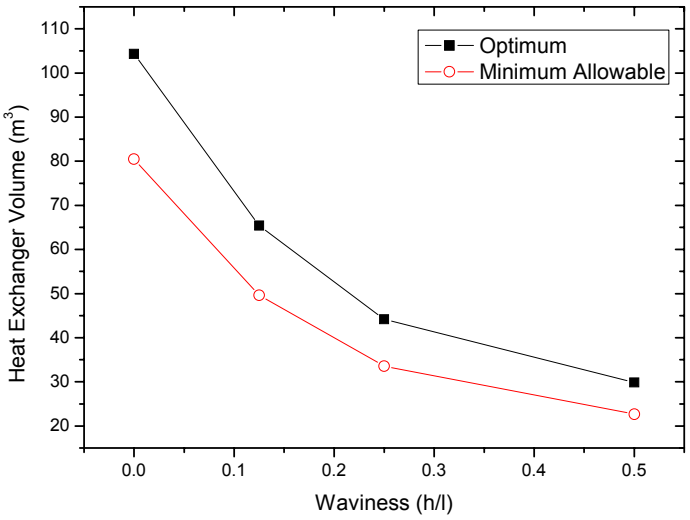

Figure 3-57 Effect of waviness ($\frac{b}{\Lambda}$) on the heat exchanger volume.

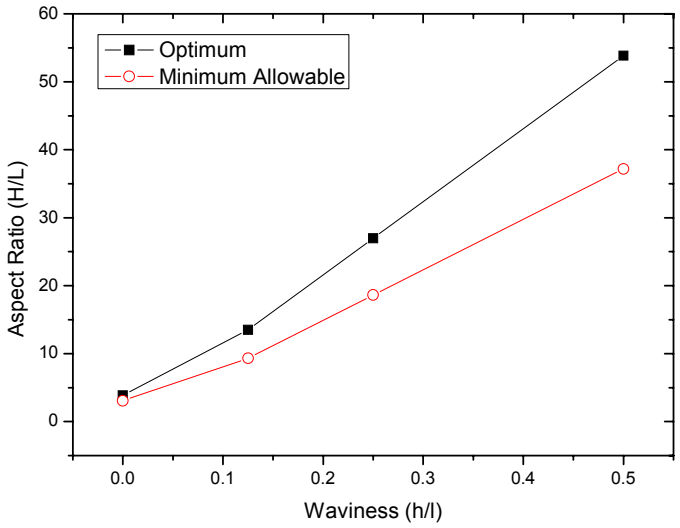

Figure 3-58 Effect of waviness ($\frac{b}{\Lambda}$) on the aspect ratio.

3.4.7 Effect of Duty and Operating Period

As described above, 600 MWt of heat is transferred from primary side to the secondary side in the reference IHX. In this case, if we reduce the reactor power while maintaining all design parameters except for flow rates, the overall system efficiency is preserved, but the IHX duty will be changed. Then we can compare the design of the heat exchanger with different duties. In this study, we changed the duties and estimated the sizes and aspect ratios of optimum heat exchangers. Figure 3-59 shows that aspect ratio rapidly decreases as the duty is reduced. When the duty drops down to 5 MWt, the optimum aspect ratio becomes lower than 1.0. Figure 3-60 gives more interesting results. In this figure, the effect of duty on heat exchanger length is plotted. As shown in this figure, the PCHE optimum length is hardly affected by duty. It means that for the fixed operating conditions, the optimum heat exchanger length is determined only by temperature and pressure conditions. Therefore, practical compact heat exchangers at optimum sizes can be constructed for low duty operation, but not for high duty operation.

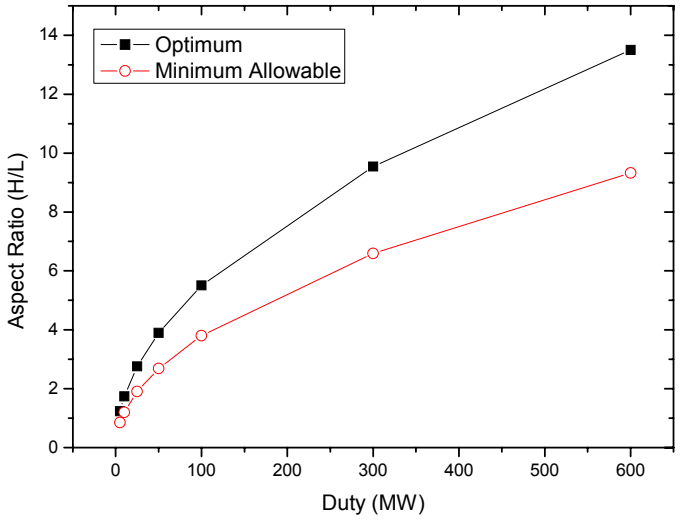

Figure 3-59 Effect of duty on the optimum aspect ratio.

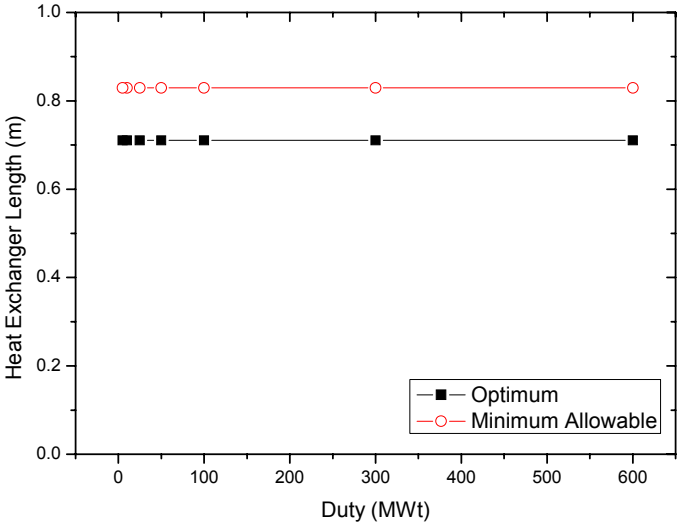

Figure 3-60 Effect of duty on the optimum heat exchanger length.

Figure 3-61 through 3-63 shows the effect of operating period on the cost /year and aspect ratio and heat exchanger volume, respectively. As shown in these figures, the operating period dramatically decreases the cost/year. It is a very obvious result, because the majority of the total cost is used for the heat exchanger manufacturing cost. However, it increases the aspect ratio and heat exchanger volume a little. The increase of the operating period increases the value of K_2 in Eq. (3-55), which is closely related to the operating cost. It means that the optimum flow area also should be increased, because the relative contribution of the operating cost is increased. It leads to the increase of the total heat exchanger volume and aspect ratio.

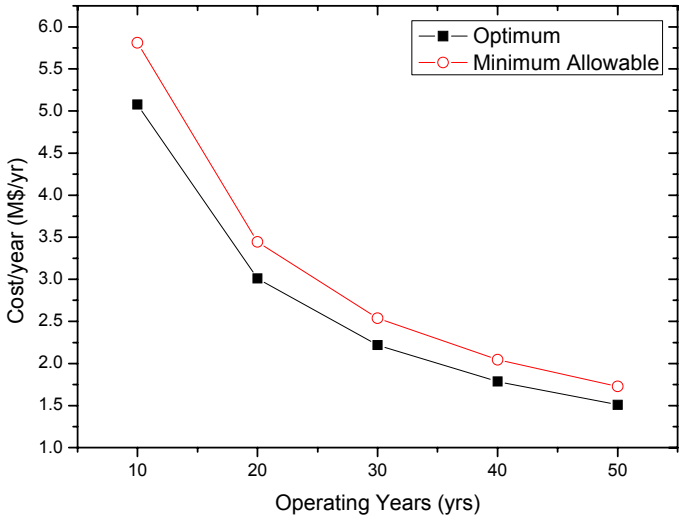

Figure 3-61 Effect of operating year on the cost/year.

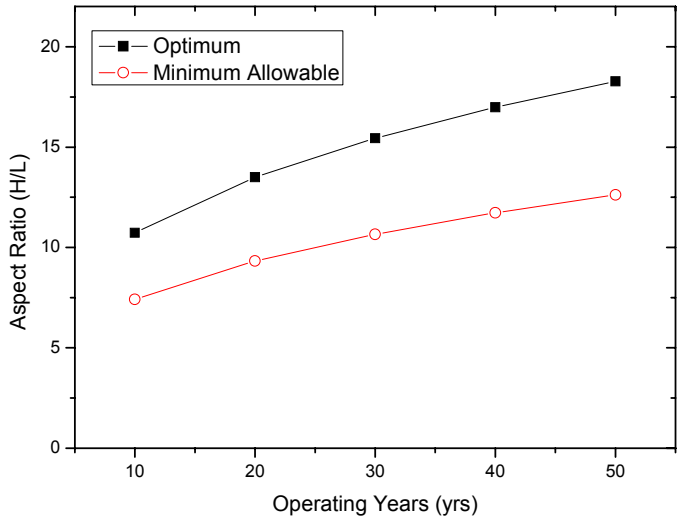

Figure 3-62 Effect of operating years on the aspect ratio.

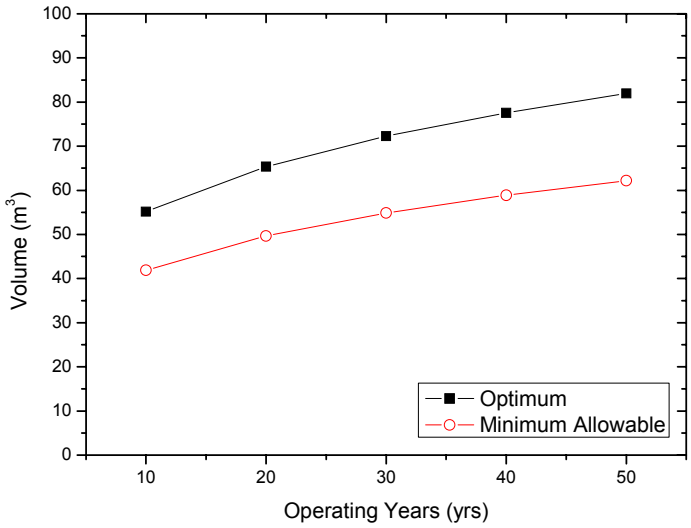

Figure 3-63 Effect operating years on the heat exchanger volume.

3.4.8 Effect of Working Fluids

The effect of working fluids on the IHX cost and size is summarized in Table 3-12. In all, four combinations of working fluids were estimated. Helium and Flinak (Molten Salt) were considered as primary coolants, and Helium and supercritical CO_2 as secondary coolants. According to the results, Helium to helium heat transfer shows the highest cost and volume of the heat exchanger at the optimum point. The lowest cost and size was observed for Flinak to supercritical CO_2 heat transfer. Generally, helium is known to be a more effective coolant for heat transfer than supercritical CO_2, but in our study, using supercritical CO_2 resulted in about 15~25% less total cost and heat exchanger volume than using helium. This result is due to the lower pumping power requirements of supercritical CO_2, which has gas-like viscosities but liquid-like densities. Although helium has excellent heat transfer properties, the smaller pressure drop of supercritical CO_2 allowed for a reduction in the optimum flow area and heat exchanger volume. Comparing the fluids at the same aspect ratio (H/L=1), supercritical CO_2 showed about 20% reduction of total cost and heat exchanger volume.

Table 3-12 Effect of working fluids on the IHX size and cost.

	Primary Secondary	**Helium Helium**	**Flinak Helium**	**Helium CO2**	**Flinak CO2**
Optimum	Total Cost (M$)	60.22	19.00	49.12	14.46
	Aspect Ratio (H/L)	13.50	28.61	13.21	15.50
	Volume (m3)	65.39	20.64	53.34	15.71
Minimum Allowable	Total Cost (M$)	68.92	21.75	56.23	16.56
	Aspect Ratio (H/L)	9.32	19.75	9.12	10.70
	Volume (m3)	49.64	15.67	40.50	11.92
H/L=1	Channel Diameter (m)	0.008	0.012	0.008	0.009
	Total Cost (M$)	246.07	117.23	200.74	66.63
	Volume (m3)	267.21	127.31	217.98	72.35

3.5 Integration of VHTR and SI Process

The US Department of Energy is investigating the use of a Very High Temperature Gas-Cooled Reactor (VHTR) to power the production of hydrogen via a thermo chemical Sulfur-Iodine Process (SI Process). Hydrogen production processes are still in the early stages of development and coupling this process to a nuclear reactor requires suffice separation between facilities to ensure abnormal behavior of the hydrogen production facility does not affect the safety of the nuclear power plant. An intermediate heat transfer loop is required to transport the energy from the nuclear plant's reactor to a series of reactions that constitute the SI process. The combination of a nuclear power plant with a hydrogen production facility is proposed as one of the designs for the Next Generation Nuclear Plant (NGNP).

The heat generation loop and the heat transfer loops were integrated into the Aspen Plus® SI model created by General Atomics (GA). Helium was used as the working fluid in the heat transfer loop from the nuclear reactor. The original model contained heaters, coolers, and other types of blocks with specified or calculated heat duties. The energy supplied to the system was ambiguously added through these blocks. Replacing the heaters and coolers with heat exchangers allowed the SI process model to also demonstrate the transfer of heat from the helium to the process streams. Hot helium was used to heat streams via heat exchangers in place of heaters while a combination of cool helium and cooling water was used to cool streams to the appropriate temperatures. Sensitivity analyses were used vigorously to minimize the heat lost to water and to increase the system's efficiency. The heat generation loop based off a HYSYS® example was created in Aspen Plus® to supply hot helium to the heat transfer loops. It also validated Aspen Plus® as a useful tool in modeling the SI process. Once the system is fully integrated and pieced together, the Balance of Plant (BOP) will be analyzed.

The original GA model was broken up into three sections, each focusing on a different step in the SI process. The project aims to create a heat generation loop and integrate it into the GA's SI process model. This report focuses on the creation of the Aspen Plus® heat generation, the integration of heat transport loops into the GA model, and some background research. Key milestones in this project are:

- ✓ SI Process Steps Heat of Reactions Research
- ✓ Development of the Heat Generation Loop in ASPEN PLUS®
- X Helium Heat Loop Integration into:
  - ✓ Sulfuric Acid Decomposition GA Model
  - X Section III GA Model
- X Combination of all parts into operating entire SI flow sheet
- X System Optimization
- X Balance of Plant Analysis Investigation

Key:
- ✓ Completed
- X Not Completed

This project thus far: (1) describes key assumptions regarding the high-temperature reactor and helium flow rates; (2) evaluates fundamental values for each step of the SI process to allow accurate efficiency calculations; (3) illustrates the construction of the heat generation loop in Aspen Plus®; (4) identifies strategies behind configurations for each section's heat transfer loop; (5) explains evaluations to find the most efficient setup for each section's heat transfer configuration; and (6) elaborates on the integration of helium heat transport into GA's sulfuric acid decomposition model.

Key Requirements and Assumptions

Three temperature assumptions were required for the results obtained thus far in this analysis. These include the outlet stream temperature of the high-temperature reactor, the outlet temperature of the heat generation loop, and the maximum temperature required by the hydrogen production facility. The NGNP was assumed to produce 600 MW of thermal power. The pressure assumed within the reactor was 7 MPa. The outlet temperature of the reactor was assumed to be 900°C. The heat generation loop provides extra safety by putting a buffer between the nuclear reactor and the hydrogen production plant. The helium in direct contact with the nuclear reactor is contained within its own loop, such that it is never mixed or interchanged with the helium used to transport energy between the NGNP and the hydrogen production facility. According to Davis et al. (2005), the heat generation loop is expected to have an output stream of helium headed to the hydrogen production facility at 875.1°C and 19 kg/s. Also from the literature, heat loss during transport accounts for the 850°C entrance temperature into the hydrogen production facility.

Table 3-13. Analysis Assumption.

Parameter	Nominal Value
NGNP:	
Power, MW	600
Outlet Temperature, ºC	900
Pressure, MPa	7
IHX Pressure Drop, MPa	0.05
IHX Temperature Drop, ºC	231.24
Heat Generation Loop:	
Outlet Temperature, ºC	875.1
Hydrogen Production	
Inlet Temperature, ºC	850

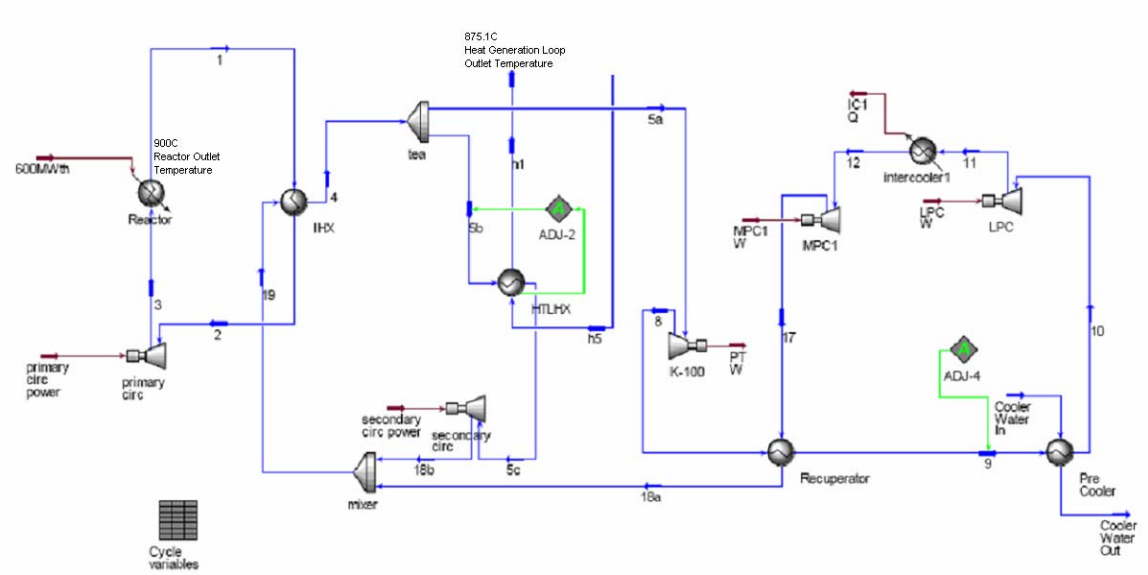

Figure 3-64. HYSYS® model of the Heat Generation Loop.

Heat Generation Loop

The heat generation loop's purpose is to transfer heat effectively and safely from the NGNP reactor to the streams to the SI process. The process heat that is eventually utilized by the SI process travels from the reactor through two heat exchangers before exiting the loop. There are two main circular streams within the heat generation loop. The reactor heats helium which is then transferred via a heat exchanger. Within this heat exchanger the heat is transferred to another closed-loop helium stream. Only heat is exchanged between these two internal loops. Both parts are closed cycles that separate the helium that comes in contact with the reactor core from the rest of the system.

The heat generation loop was also created to validate Aspen Plus® as an appropriate modeling program for the SI process. An accepted example created in HYSYS® code was readily available to build this model. Stream and block data comparisons proved that Aspen Plus® could be used as a simulation engine for the SI process. Some slight variations occurred between the two models, requiring further investigation.

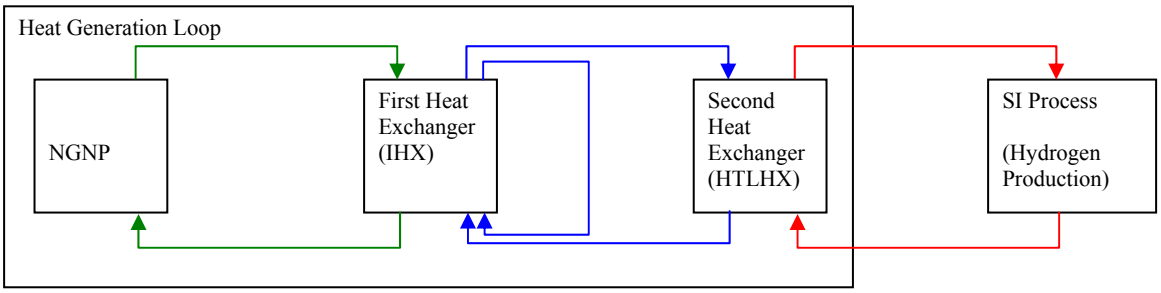

Figure 3-65. Simplified Heat Generation Loop Model.

The exiting stream from the NGNP is 900°C. The cool stream of the first heat exchanger is warmed to 885°C by the reactor's output which is cooled to 668.76 °C. The warmed stream now is split up such that

only 4.05% goes to the next heat exchanger. At the next heat exchanger, the stream headed for the SI process is heated to 875.1°C. Meanwhile, the other 95.95% heads to satisfy the other purpose of the NGNP. It goes to a turbine to produce 501100 kW (501.1 MW) of electrical power. The rest of the heat generation loop pressurizes the streams and sends them back to the first heat exchanger.

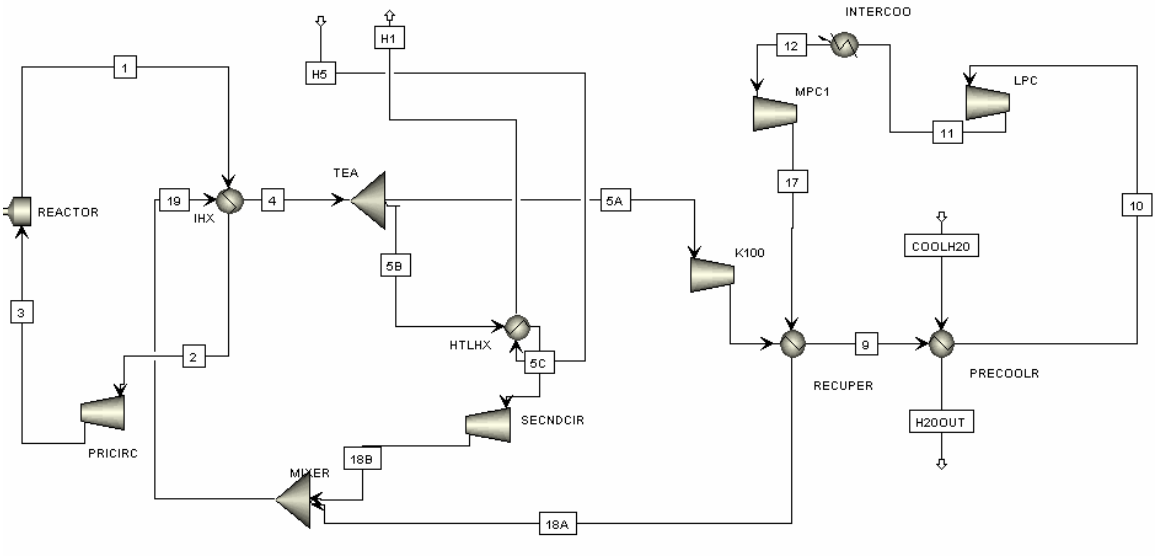

Figure 3-66. Aspen Plus® Heat Generation Loop Model.

Heat Transfer Models

The purpose of the heat transfer models is to modify the GA SI process models to reflect the use of hot helium as an energy supply. Basic strategies are implemented in order to add in the hot helium streams. The heat from the helium will be used to vary the temperatures in all three sections while supplying the driving force behind both endothermic decomposition reactions. For clarity in such a complex system, the helium heat streams were colored red and cooling water streams were colored blue while the original process streams were left black. Figure 3-67 shows the SI process helium heat transfer loop.

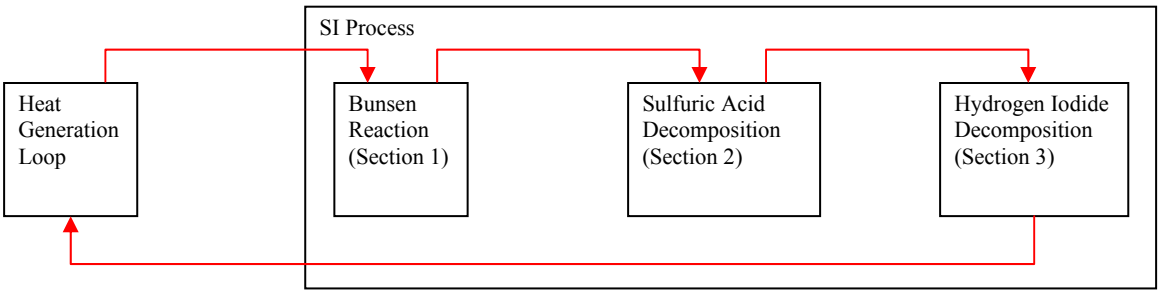

Figure 3-67. SI Process Helium Heat Transfer Loop.

In order to recover some of the heat lost during the cooler blocks, the helium streams were split up to have a lower mass flow. With this lower mass flow, the streams encountered a larger temperature change in heat exchangers where they are on the hot side. By adjusting the mass flow to reflect an appropriate temperature change, these streams were used on the cold side of the next heat exchanger they

encountered. There they reacquire heat that otherwise would have been lost from the system. If the stream had not been split up and still used to heat another fluid, the helium's exiting temperature would not be low enough to be able to acquire heat from a cooler.

Sulfuric Acid decomposition is the step in the SI process that produces the product oxygen and catalyst sulfur dioxide. It is an endothermic reaction that occurs at high temperatures. The GA sulfuric acid decomposition model was equilibrium based. It had input describing the K value at equilibrium based on temperature built into its Aspen Plus® code. The system ranged in temperature from 40°C to 900°C. This model was worked on first because of its relative simplicity and its priority for heat. The sulfuric acid decomposition step is by far the most endothermic of all of the SI process steps. Due to this need for high temperatures, this step was designed to be heated first. It required the hottest possible stream of helium directly from the heat generation loop.

The original GA flow sheet contained many heaters and coolers to change the thermodynamic properties of the streams. These blocks ambiguously added and removed heat from the streams based on their settings and heat duties. In order to make the heat transfer from the helium to the streams, the flow sheet was edited to include heat exchangers either before the blocks that contained heat duties or replaced the heaters and coolers altogether. In total, ten heat exchangers were added to facilitate the transfer of heat from the helium.

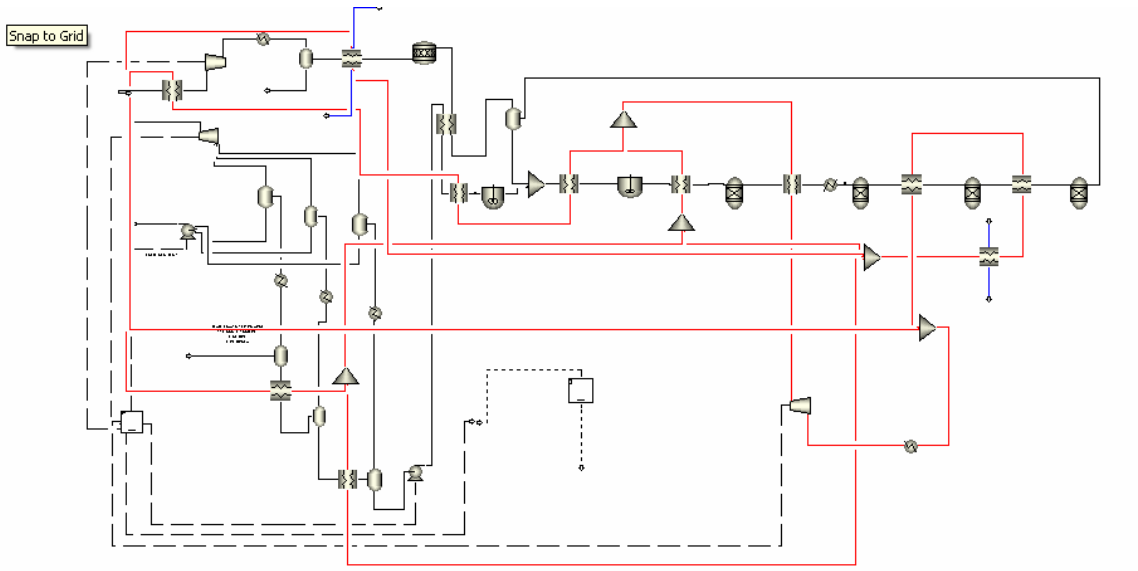

Figure 3-68. Completed GA Sulfuric Acid Decomposition Model with Helium Heating.

During the initial setup, the streams were sorted based on temperature, such that the streams requiring the hottest outlet temperatures were heated first. However, it was quickly realized that the 19 kg/s of 850°C helium sustained a negligible temperature changes as it lost heat to the process fluid. Nevertheless, the streams were still ranked from highest outlet temperature to lowest to allow an increase in molar flow of the process without having to redesign the heating/cooling system. If the system was amplified by increasing the molar feed flow and products, this design should be able to be finely tuned to account for the changes due to its priority heating order.

There remains one heater directly involved in heating the process fluid. According to Davis et al. (2005), the heat transfer loops can only deliver a maximum of 850°C to the hydrogen production plant. The GA

model requires 900°C for one of its equilibrium based reactors, meaning that the heater is required to increase the process fluid after a heat exchanger with the hottest helium by a minimum of 50°C.

The heat generation loop was constructed in Aspen Plus® considering the stream characteristics and block layout of a provided HYSYS® model. Benefits of creating an Aspen Plus® heat generation loop model include additional details on stream properties and its ability to be integrated into the entire GA SI system. The Aspen Plus® model was created also to validate Aspen Plus® as a legitimate program to use to model the SI process.

3.6 Summary

A combined VHTR/HTSE system is one promising technology to produce hydrogen efficiently. In this study, the thermodynamic overall plant efficiency of the integrated system is evaluated using various configurations and working fluids. For these calculations, the reactor outlet temperature was fixed at 900 °C, which is the most sensitive factor for system efficiency. Totally, 51 different systems were optimized and evaluated. As a result, the maximum system efficiency was obtained for the reheat cycle (Configuration 5) with a combination of Flinak-CO_2-Flinak working fluids in the primary, secondary and ternary loops. In this case, the system efficiency reached up to 50.64 %. Even though the reheat system can achieve high efficiencies, economic analysis is recommended to optimize the entire process, including the capital costs. The control characteristics of each system should also be studied.

The minimum efficiency was obtained for the steam combined system (Configuration 4). This result means that recuperation is a more effective way to recover the heat from turbine outlet due to the fact that the difference between turbine outlet temperature and the compressor inlet temperature is very large. Therefore, in all aspects, the steam combined cycle is not preferred in the configuration we investigated. However, with a different configuration, this conclusion might differ.

The important result of this study is that we obtained very high efficiency even for the simple regeneration system. In case of indirect serial configuration, the optimal efficiency was 48.38 % for Flinak-He-Flinak combination. In the serial system, since all the main components are independently separated, it may give much benefit for safety, maintenance and control problems. Although the parallel system resulted in a higher maximum temperature in the PCU, the maximum overall efficiency (47.24 %) was a little lower than for the serial system because of the addition of one extra circulator.

The use of liquid Flinak almost always resulted in the highest efficiency for each configuration evaluated because the liquid phase coolant (Flinak) requires much less circulation power than the high pressure gas phase coolant. The relative benefit of Flinak was larger in the primary loop than in the ternary loop, with an average increase of about 1.5% in overall cycle efficiency for the primary loop versus about 0.6% for the ternary loop. The smaller benefit of Flinak in the ternary loop was due to the relatively smaller pumping power requirements compared to the primary loop. It is not clear if the increased efficiency in either loop is worth the capital cost associated with the facilities required for keeping the salt molten during shutdown and the materials issues associated with using molten salts at high temperatures.

Direct integration methods of a high temperature Rankin cycle (HTRC) and HTSE system was thermodynamically estimated as alternatives for the VHTR/HTSE system. Despite of its lower efficiency, the direct combination of HTRC and HTSE systems has some advantages compared with VHTR/HTSE system. Firstly, it requires no additional steam generation loop because the steam generated in the secondary side to produce electricity is used for electrolysis as well. Therefore, the configuration of this system can be highly simplified reducing its size, complexity and capital cost. Secondly, the steam Rankin cycle is well proven technology. The system has been used for several decades in the most

commercial nuclear reactors. It means that we have lots of design and operating experiences on this reactor, even though high temperature application requires more severe operating conditions than the current one. It will cause the reduction of the uncertainties for the newly developed technology. In this work, the efficiency of this system has been estimated by HYSYS code, commercial process analysis software. As a result, 41.6 % of maximum efficiency was obtained for a specific configuration (Configuration 2). This efficiency looks much smaller than the reference VHTR/HTSE system (~49%). However, more investigations on the economical and technical aspects are necessary for better estimation.

Parametric studies indicate that the core inlet temperature is a very sensitive factor to the overall system efficiency. As the core inlet temperature is raised, the PCU flow rate can also be increased resulting in PCU efficiency increase. However, the increase of core inlet temperature requires higher flow rate in the primary side, requiring higher circulation power. The overall plant efficiency is also sensitive to the efficiencies of the compressor and turbine and the effectiveness of the heat exchanger, especially at low core inlet temperatures near 500 °C. Maintaining the performance of compressor, turbine and heat exchangers is essential for maintaining an efficient hydrogen production process.

The heat generation loop and the heat transfer loops were integrated into the Aspen Plus® SI model created by General Atomics (GA). Helium was used as the working fluid in the heat transfer loop from the nuclear reactor. The original model contained heaters, coolers, and other types of blocks with specified or calculated heat duties. The energy supplied to the system was ambiguously added through these blocks. Replacing the heaters and coolers with heat exchangers allowed the SI process model to also demonstrate the transfer of heat from the helium to the process streams. Hot helium was used to heat streams via heat exchangers in place of heaters while a combination of cool helium and cooling water was used to cool streams to the appropriate temperatures. Sensitivity analyses were used vigorously to minimize the heat lost to water and to increase the system's efficiency. The heat generation loop based off a HYSYS® example was created in Aspen Plus® to supply hot helium to the heat transfer loops. It also validated Aspen Plus® as a useful tool in modeling the SI process. Once the system is fully integrated and pieced together, the Balance of Plant (BOP) will be analyzed.

In this study, the optimum size of the compact heat exchanger has been investigated from an economic point of view. We analytically developed an optimum sizing model on the basis of heat exchanger weight and friction loss and then applied it to the reference 600 MWt VHTR system. As a result, we could obtain the optimum size and configuration for the reference IHX, but we found that it has an unrealistically large aspect ratio due to its small-sized channels. The flow area and channel diameter were then adjusted to achieve a realistic aspect ratio. Achievement of this realistic aspect ratio resulted in higher cost, but the cost increase was less than would have occurred by simply reducing the flow area by itself. The appropriate channel diameter is estimated to be 5.00 mm for the reference IHX. The effect of channel waviness enhanced the compactness and heat transfer performance, but unfavorable increased the aspect ratio. Therefore, the waviness should be carefully determined based on performance and economics. In this study, the waviness of the IHX is recommended to be between 1.0 and 2.5. We also found that reducing the duty dramatically decreases the aspect ratio. It means that the compact heat exchanger can be optimally designed for low duty, but multiple modules are required for high duty operation due to the unrealistic aspect ratio associated with a single module heat exchanger. Finally, we investigated the effect of working fluids, and found that using carbon dioxide instead of helium reduces the size and cost by about 20% due to the lower pumping power in spite of its lower heat transfer capability.

4. HYPEP V&V Plan

One of the most important parts in code development is validation and verification (V&V). This section describes the methods to validate and verify HyPEP code developed in the current research. The V&V process will be carried out divided into three parts. Firstly, the gas property models, the most basic parameters in thermal hydraulics analysis are validated by comparisons with reference data, and then the system component models like pump, turbine, reactor and etc. are validated. Finally, the integration of each system component will be validated. The details are described as follows.

4.1 Validation of Gas Property Model

The validation of gas property models is the first V&V process. The accuracy of the property models is the most fundamental part in thermal hydraulics analysis. Although we have very good component and system models, reliable analysis is impossible without accurate property models. The validation of gas properties are divided into two parts. One is the validation of single gas property model, and the other of mixture property model. Two gas properties, density and heat capacity are compared with the reference data since HyPEP code is basically a 1-D steady state code. In a 1-D steady state code, thermal conductivity and viscosity are not used for analysis. For single gas property validation, NIST chemistry database and HYSYS Peng-Robins Equation-of-State model will be used as the references. For mixture gas property, only HYSYS code mixture model is available since NIST does not provide mixture gas property data. Figure 4-1 shows the NIST fluid property database for validation of gas properties, respectively.

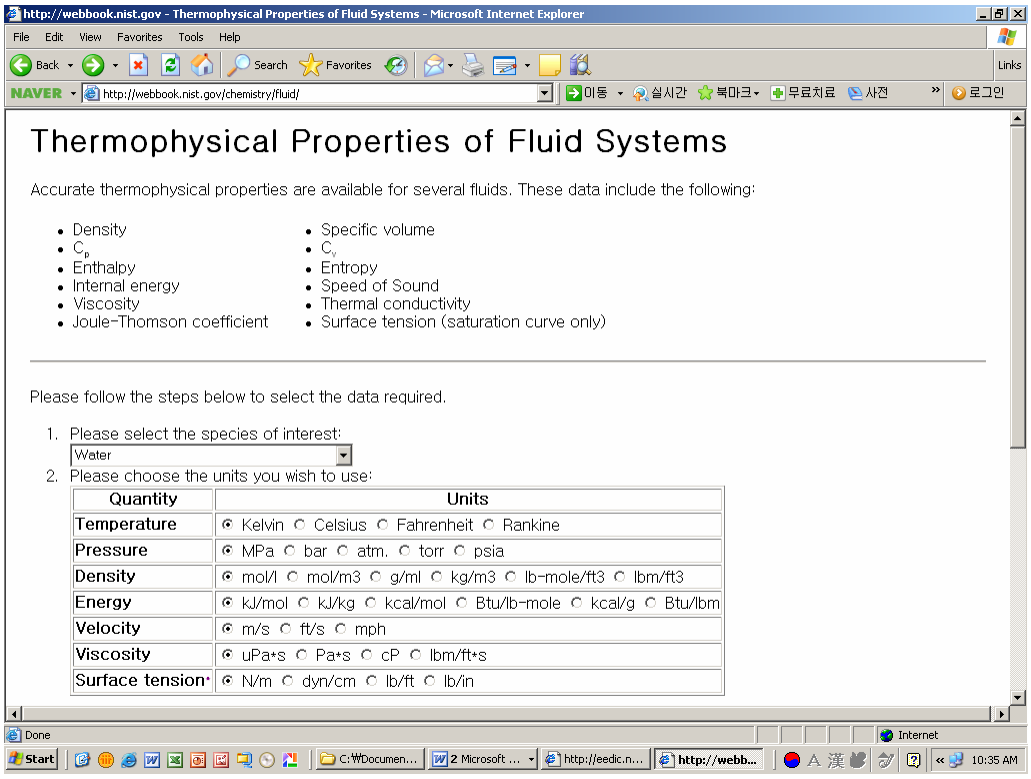

Figure 4-1. NIST chemistry webbook (http://webbook.nist.gov/chemistry/fluid/).

In this work, the properties of five gas species are compared with the reference data. The gases are He,CO_2, H_2, O_2 and H_2O. Helium is a favorable coolant material considered in VHTR due to its high heat capacity and thermal conductivity. It can be used all over the system components. Carbon dioxide is one alternative material for helium. It can be used for PCU system providing high efficiency even at lower operating temperature. However, it is not available for primary coolant because of its reactivity to the graphite materials in the reactor core. Hydrogen, oxygen and steam are the important gases to be validated for integrated VHTR/HTSE system, because their thermal properties are highly associated with the total hydrogen generation efficiency. The ranges of validations are 0.1~32 MPa in pressure and 300~1350 K in temperature. Therefore, the following gas species and properties are scheduled to be validated in the next work year. Figure 4-2 and 4-3 shows some sample reference data to be used for property validation.

a. Gas species and properties to be validated

i. Helium
- Density
- Heat Capacity

ii. CO_2
- Density
- Heat Capacity

iii. H_2
- Density
- Heat Capacity

iv. O_2
- Density
- Heat Capacity

v. H_2O
- Density
- Heat Capacity

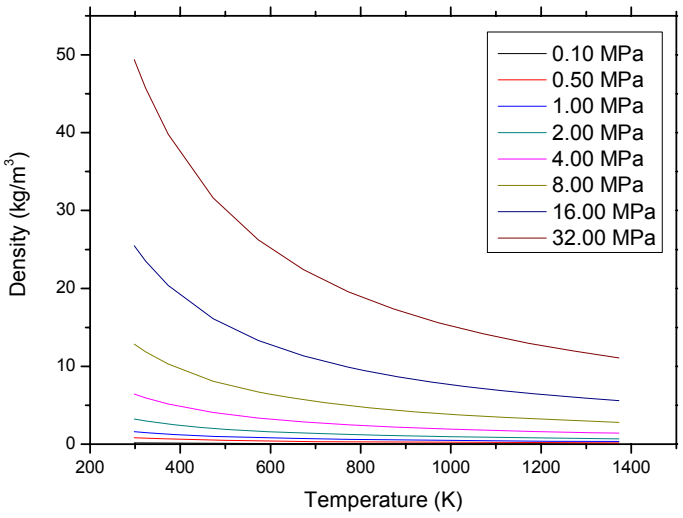

Figure 4-2. Reference density (Helium) calculated by Peng Robins EOS Model (HYSYS).

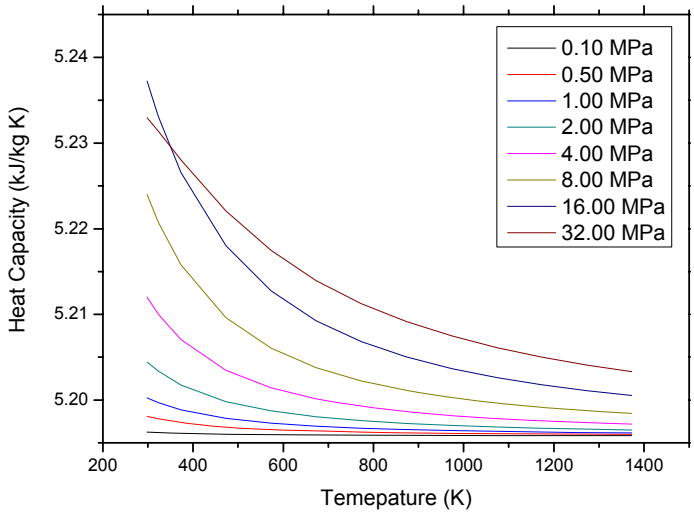

Figure 4-3. Reference heat capacity (Helium) calculated by Peng Robins EOS Model (HYSYS).

Once the single gas properties are validated, mixture gas properties should be validated. The mixture properties are determined by the mixing law used in the mixture model. HYSYS code calculation is used as the reference data to validate the HyPEP mixture property model, since the mixture property database is not provided by NIST chemistry webbook. Validation will be carried out on the binary and ternary mixture, and some selected gas combinations and concentrations will be used here because of the time and cost limitations. Helium/CO2, Helium/O2 and Helium/CO2/O2 mixtures will be validated as follows. Figure 4-4 through 4-8 show some reference data for mixture gas properties.

b. Multi-gas properties

i. Binary gas mixture
- Helium/CO_2 mixture
  - Density
  - Heat Capacity

- Helium/O_2 mixture
  - Density
  - Heat Capacity

ii. Ternary gas mixture
- Helium/CO_2/O_2 mixture
  - Density
  - Heat Capacity

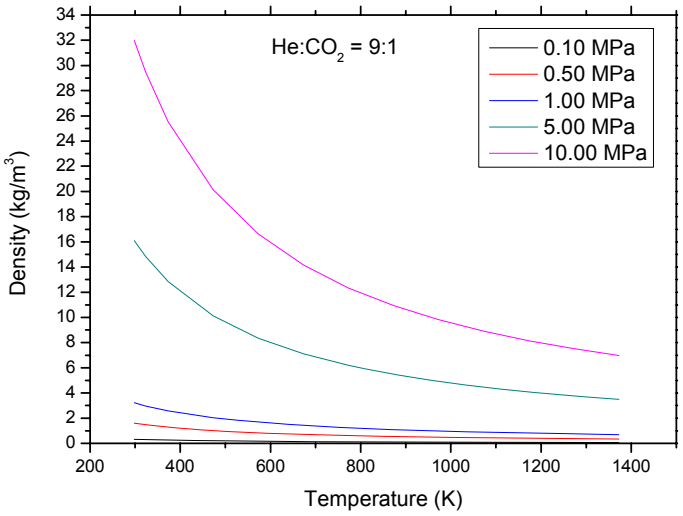

Figure 4-4. Reference density calculated for He/CO2 mixture (He:CO_2=9:1) by Peng Robins EOS Model (HYSYS).

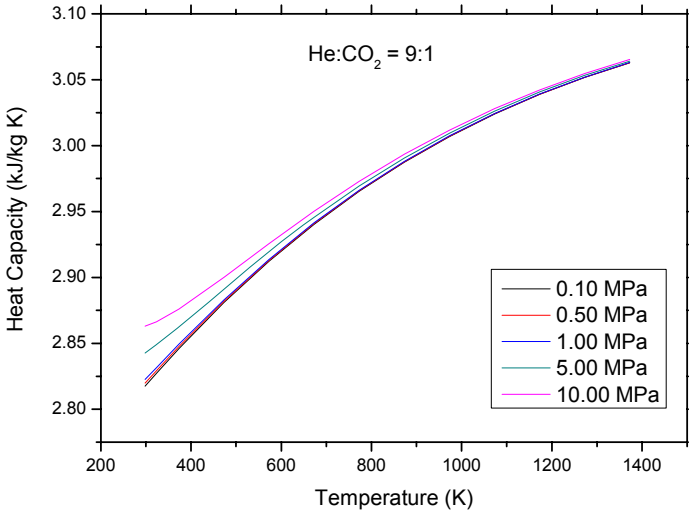

Figure 4-5. Reference heat capacity calculated for He/CO2 mixture (He:CO2=9:1) by Peng Robins EOS Model (HYSYS).

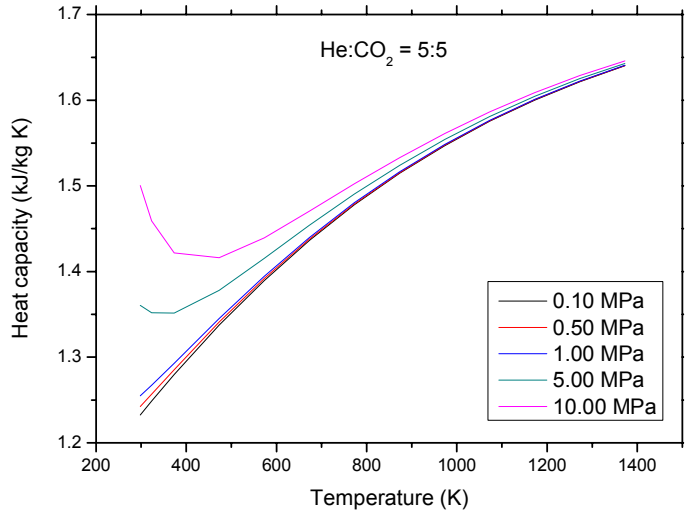

Figure 4-6. Reference heat capacity calculated for He/CO2 mixture (He:CO2=5:5) by Peng Robins EOS Model (HYSYS).

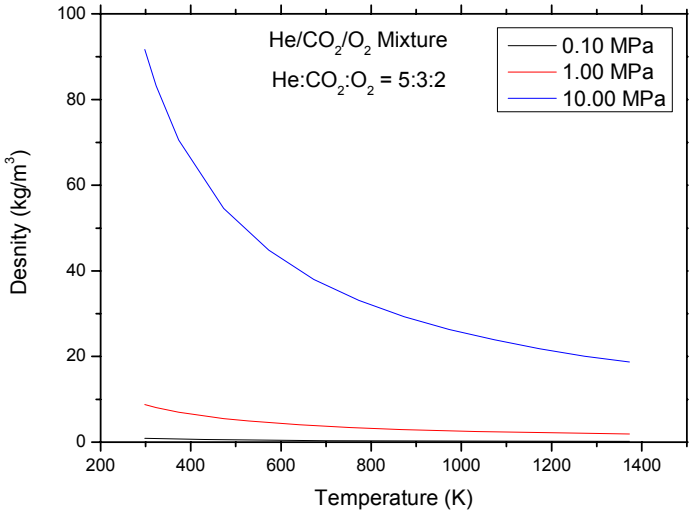

Figure 4-7. Reference heat capacity calculated for He/CO2 mixture ($He:CO_2:O_2$=5:3:2) by Peng Robins EOS Model (HYSYS).

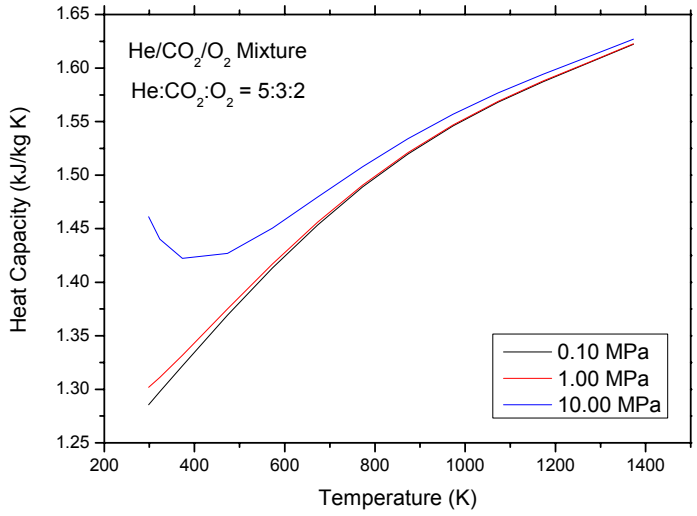

Figure 4-8. Reference heat capacity calculated for He/CO2 mixture ($He:CO_2:O_2$=5:3:2) by Peng Robins EOS Model (HYSYS).

4.2 Validation of System Component Model

Once the properties models are validated, the system component models should be validated next. To validate the component model, HYSYS code is used to generate the reference data. There are some important system components that should be validated in system modeling; heat exchanger, turbo machinery, reactor, heater/cooler and etc. Each component has different system parameters and they should be extensively tested.

a. Reactor System Components

The reactor system components will include the specialized components for the pebble bed reactors and the prismatic reactors. The reactor component models the nuclear reactor. For the hydrogen production efficiencies, the main differences of the reactor systems to consider are the core and vessel pressure drops. The pebble bed reactor component and the prismatic reactor component will have empirically derived correlations suitable to each design for estimating the core and vessel-wide pressure drop. The following parameters should be considered to validate reactor component model.

- Heat duty
- Pressure drop

b. Heat Exchanger Components

Heat exchanger is the most basic component in integration system. It transfers heat from one side to the other side making the heat used for generating electrical works and increasing hydrogen production system. Heat exchanger has the following essential parameters to be validated.

- Overall heat transfer coefficient
- Effectiveness
- Log mean temperature
- Heat transfer duty
- Minimum temperature approach

c. PCU Components

PCU components will include Brayton cycle component and Rankin cycle component. Reheats and the superheating circuits may be modeled using the base component of HyPEP. The PCU components will calculate the electricity generation efficiencies. Turbine and compressor are the most essential components in the PCU system. The following parameters should be validated here.

- Turbine and compressor efficiency (isentropic or polytropic)
- Pressure ratio

d. Electrolyzer

HTSE components will be provided to model the high temperature steam electrolysis. The HTSE will be formed by the electrolyzer, separator, condenser, heat exchanger, etc. Among these components, electrolyzer is the key component in this system. To validate these components, the following parameters should be considered.

- Electrical power input
- ASR
- Operating temperature and pressure

4.3 Validation of System Integration

After validation of the components models, the integration of the system components will be finally validated. The integration systems previously developed in this study will be used for this validation

work; a direct serial system, a direct parallel system, an indirect serial system, an indirect parallel system, a steam combined system, a reheat system and etc. This work will extensively confirm the validity of this code for application to the VHTR and hydrogen production systems by benchmark with the commercial process analysis codes such as HYSYS and ASPEN Plus.

5. SYSTEM INTEGRATION II – Quasi-static and dynamic analyses of the VHTR/HTSE for hydrogen production

5.1 Introduction

There are three performance-related aspects that must be addressed in studies aimed at commercialization of hydrogen generation using nuclear power. They are production, operability, and safety and their successful navigation will lead to a plant design that is viable in the commercial marketplace along with a set of Technical Specifications for operating the plant. Briefly, production is the task of obtaining hydrogen in an economical manner at full power operation. Operability is the ability to perform plant startup, load change, and shutdown without the need for complex control systems to maintain important process variables within limits. It also includes a measure of how stable the inherent response of the plant is during operational transients. Safety is the task of ensuring the plant can be shut down in a safe manner following an equipment failure or operator error. Engineering analyses are needed for assessing production, operability, and safety.

This section of the report focuses on operability. Operability is a function of the inherent characteristics of the plant and, hence, can be shaped at the design stage. An important objective is to ensure that values of process variables during operation do not overly constrain plant life through excessive mechanical stress or creep. Operability is addressed in the course of setting the plant load schedule and the plant response to step changes in load. The load schedule specifies values of important plant process variables at each power level over the normal operating range. For the VHTR process variables that have strict limits are fuel and reactor structure temperatures and coolant pressures and temperatures in heat transport piping. The load schedule takes in startup and shutdown as well as normal load changes associated with changes in production demand. There will be separate load schedules for startup/shutdown and for production. The plant response to a step change in load demand gives the magnitude of the deviation in plant variables from steady state and the rate at which deviations die away. A change in demand can arise from either the grid (change in power from the dispatcher) or an anticipated upset that requires shutting down the plant. The goal again is to ensure operational life is not overly limited by excessive time rates of change. In part this is achieved by having deviations naturally die away. Otherwise the plant is unstable and ability to adhere to design load schedule for safe operation will be compromised.

The other two goals, those of production and safety, are addressed elsewhere. Production appears in Section 3 and safety is the subject of ongoing research. The HyPEP code [Oh et al. 2006a] is being developed to address production in terms of efficiency and economics. Safety is to be examined in the future. This will involve determining the safety systems needed to maintain safe conditions following a failure of equipment or control systems. The GAMMA code [Oh et al. 2007b] has been proposed for use in the study of severe events such as air ingress.

The current work on operability is qualified here with respect to the future role of nuclear hydrogen in the national energy mix. The demand for electricity and/or hydrogen will place operational constraints on a particular plant. In an electricity-generating plant the product is not easily stored so operational flexibility to change power to meet varying electric grid demand must be provided. In a commercial nuclear power plant the production range needed is typically 25 to 100 percent of full power. In a chemical plant, however, the product can be more easily stored so there is not as great a need for partial power operation. The chemical plant typically runs at full power with short term variations in demand buffered by drawing from or adding to stored chemical inventory. What is an appropriate goal for product output and mix for a nuclear-hydrogen plant (i.e. hydrogen only or co-generation) is outside the scope of this work and will need to be addressed in future systems integration work. The optimum mix depends on the future markets for hydrogen and electricity on a daily, seasonal, yearly, and geographic basis. In absence of this

information it is assumed in this work that hydrogen is the sole product delivered at the plant fence. The appropriateness of this assumption depends on the outcome of future energy system studies.

In summary this section of the report investigates the operability of a nuclear-hydrogen plant. A plant control strategy is developed and the load schedule and the step response are examined. Identification of important phenomena that shape the operational behavior of the plant guides the work.

5.2 Methods

Operability is assessed by examining the behavior of the combined plant and control system for two types of operational maneuvers, a quasi-static load change and a step change in hydrogen production rate. The process variable values are examined to see that they remain within limits set for normal operation which includes both absolute value and time rate of change value. The methods for identifying important phenomena and for characterizing the plant response are described in this section.

5.2.1 Time Scale of Phenomena

The combined plant response is shaped by the time constants of the various components. The time constants and where they appear in the flowpaths for the transport of conserved quantities can provide insight into the time behavior of the overall plant.

The time response of a component is in the neighborhood of an operating point given by the ordinary differential equation

$$\frac{d}{dt}y = \frac{-1}{\tau}\left[\, y + F\left[u(t)\right] \,\right] \tag{5-1}$$

where $u(t)$ is the forcing function, y is the observed process variable, F is a function of u, and τ is the time constant. The role of the time constant is made evident by applying a step input to the component. The initial steady state satisfies from Eq. (5-1)

$$y\left(0^-\right) + F\left[u\left(0^-\right)\right] = 0 \ , \tag{5-2}$$

so the component response for a step in F applied at $t=0$ is

$$\frac{y(t) - y(\infty)}{y\left(0^-\right) - y(\infty)} = e^{\frac{-t}{\tau}}, \quad t > 0 \tag{5-3}$$

where $y(\infty)$ designates the new steady state. One sees that the observed variable moves to the new steady state with time constant τ.

Analytic expressions for time constants and energy capacitances for the major components in a coupled VHTR and HTSE plant are derived in this report.

5.2.2 Component Temperature Rates of Change

The plant operational behavior can be characterized to the first-order by the response to a step change in demand. Such changes may arise with the hydrogen distribution system or the electric grid. The time

taken to come into equilibrium with the new demand condition, termed the *response time*, and the interim deviation compared to that if the change were carried out quasi-statically, termed the *overshoot*, are important. The response time is important for meeting production goals while the overshoot is important for longevity-related integrity of structures.

Analyses based on component time constants and thermal capacitances can provide a measure of response time. Further, such analyses provide insight into what is controlling plant response and provide an adjunct to detailed transient simulation. The time constants and thermal capacitances control how long before the core and heat sink powers come back into equilibrium with each other after a change in conditions. A change in local conditions at the heat source (sink) flows through a series of processes each with a characteristic time constant before reaching the heat sink (source) where the temperature and flow changes create feedback effects that operate to bring all processes back to equilibrium. But until equilibrium is restored, a power generation imbalance gives rise to an energy imbalance approximated by

$$\delta E = \delta P \sum \tau_i \tag{5-4}$$

where δP is an initial step change in power and the τ_i are a series of process time constants through which the change must propagate before feedback effects occur to bring heat sink and core power back into equilibrium. The change in temperature caused by this power imbalance averaged among the i processes is

$$\delta T = \frac{\delta P \sum \tau_i}{\sum \left(\rho V C_p\right)_i} \tag{5-5}$$

If the original and terminal plant states are on the normal plant operating curve, as is the case for the instances we will look at, then the overshoot in temperature is given by

$$\delta T_{os} = \frac{\delta P \sum \tau_i}{\sum \left(\rho V C_p\right)_i} - \delta T_{load} \tag{5-6}$$

where δT_{load} is the change in temperature in going from the original to the new operating point on the plant operating curve or load schedule. To make use of the above expression, one first needs to identify the propagation path for the transient and to calculate the time constant and thermal capacitances of the processes along the propagation path.

The rate of change in temperature before equilibrium is reached is from Eq. (5-5)

$$\frac{d\delta T}{dt} = \frac{\delta P}{\sum \left(\rho V C_p\right)_i} . \tag{5-7}$$

5.2.3 Load Schedule

The full power operating point is set based on production goals while subject to material limits that include creep and thermal stress. Previous work [Oh 2006 and Oh 2007a] addressed the design of equipment for meeting these objectives. The simulation codes HYSYS and GAS-PASS [Vilim 2004]

were used to calculate the full power condition and identified active control elements including pump, compressor, turbine, and electrolyzer needed.

In moving from designing for production (i.e. full power operation) on to designing for operability (i.e. partial power operation) the task is to specify how the outputs of these elements change with load. The specification must satisfy the material limits mentioned where thermal stresses may now include those brought about by time rates of change.

The partial power operating point is a continuum over power and is given by the *load schedule*. The load schedule specifies the value of each process variable as a function of plant power. Good operability as represented by reduced thermal stresses during power change is achieved by developing a load schedule that maintains temperature constant at the hottest points in the plant (e.g. reactor outlet) over power while at load. A mathematical relation shows what can be achieved from the standpoint of the number of independently controllable actuators needed to achieve constant temperature at a given number of points and the values actuator outputs need to assume.

Each of the components in the plant in the steady state satisfies an equation of the form

$$0 = [\ y + F\ [\underline{u}(t)]\ ] \tag{5-8}$$

where

$\underline{u}(t)$	=	vector of input forcing functions,
F	=	function of $u(t)$,
y	=	component output.

Assume for the sake of exposition that there are three control variables: two flowrates, w_1 and w_2, and rod reactivity, ρ. Coupling the equations for all components leads to a system of equations for the plant state vector expressed in terms of the control variables (assuming constant properties)

$$[T_1\, T_2 \ldots T_n]^T = A_o(w_1, w_2, \rho\ )^{-1}\, b_o(w_1, w_2, \rho\ ) \tag{5-9}$$

where the T_i are temperatures, A_o is a matrix whose elements are functions of the control variables, and b_o is a vector.

The control variables are written as linear functions of the plant power

$$w_1 = m_1\, P + b_1$$
$$w_2 = m_2\, P + b_2$$
$$\rho\ = m_3 \left(P - P_0\right)$$

where m_1, m_2, m_3, b_1, and b_2 are constants.

Differentiating the above set of equations with respect to power gives a set of load schedule coefficients that defines the load schedule about an operating point

$$\left[\frac{dT_1}{dP}\,\frac{dT_2}{dP}\,\bullet\bullet\bullet\,\frac{dT_n}{dP}\right]^T = A_1(m_1, m_2, m_3, T_1, T_2, \ldots, T_n)^{-1}\, b_1(m_1, m_2, m_3) \tag{5-10}$$

One sees from the above equation that three load coefficients can be arbitrarily assigned through the three parameters m_1, m_2, and m_3. This expression holds at a particular power. It can be applied repeatedly at different power to achieve the load schedule desired for three temperatures. In general, assigning values to n temperatures over the load range will require n actuators.

It is apparent that a simulation code equipped with the proper features can be used to determine the output of each actuator as a function of load to achieve a desired load schedule. Essentially, for given values for the process variables on the left-hand side of Eq. (5-9) at a given power, the unknowns on the right-hand side are solved for. A load schedule is obtained by performing this calculation at each power. The GAS-PASS/H code has this capability.

5.2.4 Startup

The same concept of using actuators to manage temperatures also applies for design of the startup schedule. However, in any one component there may now be multiple physics regions that must be passed through one after the other. In the reactor, the core passes from being initially subcritical, then critical with delayed neutrons, and finally critical with delayed neutrons and temperature feedback. In a boiler the water is initially subcooled, then becomes saturated with unity quality at the exit, and finally possibly superheated at the exit. A condenser passes through analogous regions. A helium turbine may initially function as a compressor driven by the generator until temperatures and pressures reach the point where the turbine produces work.

Essentially a load schedule must be developed for each physics region the plant passes through during startup. Simulation of this requires model switching as each region is passed through. As a result calculation of plant startup is more complex. The need for model switching will need to be provided for in future simulations.

5.2.5 Stability Assessment

A stable combined plant is important for good operability. A physical system is stable if the transition to a new state, as driven by altered forcing function values, is marked by a smooth and non-oscillatory transition. Stability can be qualitatively assessed by examining the system response to a step change in an input variable. Since a step is composed of an infinite set of frequencies it excites all modes of the system. The stability can also be assessed by more formal methods that examine eigenvalues of the system linearized about an operating point. [Depiante, 1994] The physical processes that govern the response of the reactor to a change in the load are described and a simple expression that predicts how reactor stability trends with plant parameter values is given below.

There is a natural tendency for reactor power to follow a change in heat sink load. An increase in load reduces heat sink outlet temperature which propagates to reduce reactor core inlet temperature, adding reactivity which increases power. The resulting core outlet temperature increase propagates back to the heat sink providing additional heat to meet the increase in power. The potential for oscillations arises if the heat sink does not attenuate this temperature front. In this case the front moves on to the core where it raises inlet temperature and causes reactor power to decrease. One sees that there is the potential for core power to alternately increase and decrease as the reactor inlet and outlet temperatures change out of phase with each other. The degree to which core power oscillations are dampened is a function of the attenuation of the temperature front at the heat sink and the size of the reactivity inlet temperature coefficient.

A simple reactivity balance shows how stability trends with integral reactivity parameters. The reactor power in the asymptote is related to the flowrate and inlet temperature through

$$0 = A\,(P - 1) + B\,(\frac{P}{W} - 1) + \mathrm{C}\,\delta T_i \tag{5-11}$$

as derived in Section 5.3.4.2.6. The change in reactor outlet temperature expressed as a function of change in reactor inlet temperature is then

$$\delta T_{out} = \left(1 - \frac{C\,\Delta T_{c-100} / B}{\frac{A}{B} + 1} \right) \delta T_i \tag{5-12}$$

where A, B, and C are integral reactivity parameters, P and W are normalized power and flow, respectively, and δT_i is change in inlet temperature. If the expression within the parentheses is negative, then a change in inlet temperature in one direction leads to a change in outlet temperature in the opposite direction. Hence, to the extent the heat sink passes through without attenuation a primary hot leg temperature front associated with an increase in reactor power due to an initial reactivity addition, the reactor power will begin to decrease on negative temperature reactivity a time later equal to the propagation time around the primary system. For oscillations to occur, this time must be long enough that the initial reactor power increase (due to the original reactivity addition) begins to equilibrate before the temperature front makes it back to the reactor. Thus, oscillations are favored if 1) the heat sink weakly attenuates primary hot leg temperature fronts, 2) the loop propagation time is more than a few tens of seconds (making it greater than the core time constant), and 3) the expression in parentheses in Eq. (5-12) is negative. The amplitude of these oscillations will increase as $C\Delta T_{c-100} / B$ becomes a larger positive number and A/B a smaller positive number provided the ratio of the two is more than unity.

5.3 Models

Models for the dynamic behavior of system components are developed by writing the conservation balances in lumped parameter form. The resulting ordinary differential equations have been programmed in the GAS-PASS/H code where they are solved numerically to obtain a time-dependent solution. The ordinary differential equations are also linearized to obtain expressions for the time constant and energy capacitance of a component.

5.3.1 Electrolyzer

The electrolytic cell modeled has a planar rectangular geometry consisting of the following components. Listed from cell exterior and moving through the cell in a line normal to the cell plane to the opposite side we have: steel separator, edge rails, porous cathode, electrolyte, porous anode, edge rails, and separator. The two inlet streams enter at right angles to each other with each stream entering along the normal to a cell edge. Of these components only the electrodes and electrolyte are in close contact with the gas streams and are sites of significant energy deposition/generation.

In modeling the cell note that the electrochemical processes reach equilibrium at a much faster rate than the thermal processes. It is reasonable then to model them as quasi-static. It is assumed that the two flow

streams entering the cell do so at the same temperature. It is also assumed that the two flow streams within the interior of the cell are perfectly mixed and that each stream exits the cell at the same temperature. Further, the cell components listed above are all assumed to be in thermal equilibrium with each other and with the flow streams within the cell. Then an energy balance on the cell gives for the rate of change of cell temperature

$$\left[\left(\rho V C_p\right)_s + \left(\rho V C_v\right)_g\right] \frac{d}{dt} T =$$
$$\left[\begin{array}{c} m_{H_2O-i-cath}\, h_{H_2O}\left(T_i,P\right) + m_{H_2-i-cath}\, h_{H_2}\left(T_i,P\right) + m_{N_2-i-cath}\, h_{N_2}\left(T_i,P\right) + \\ m_{O_2-i-anode}\, h_{O_2}\left(T_i,P\right) + m_{N_2-i-anode}\, h_{N_2}\left(T_i,P\right) \end{array}\right] -$$
$$\left[\begin{array}{c} m_{H_2O-o-cath}\, h_{H_2O}\left(T,P\right) + m_{H_2-o-cath}\, h_{H_2}\left(T,P\right) + m_{N_2-o-cath}\, h_{N_2}\left(T,P\right) + \\ m_{O_2-o-anode}\, h_{O_2}\left(T,P\right) + m_{N_2-o-anode}\, h_{N_2}\left(T,P\right) \end{array}\right] + \qquad (5\text{-}13)$$
$$Q + W$$

where

ρ	=	density,
V	=	volume,
T	=	temperature,
m	=	species mass flow rate (kg/s),
h	=	specific enthalpy (joules/kg),
Q	=	rate of heat transfer to the electrolyzer,
W	=	rate of electrical work supplied to the electrolyzer, and
P	=	pressure,

and where subscripts *i* and *o* represent inlet and outlet, respectively, and *s* and *g* represent structure and gas, respectively. The electrical work is

$$W = V_{cell} \cdot A \cdot i \qquad (5\text{-}14)$$

$$W = V_{cell} \cdot A \cdot \left(\frac{V_{cell} - V_N}{ASR}\right) \qquad (5\text{-}15)$$

where

V_{cell}	=	voltage applied to cell,
i	=	current density,
A	=	electrolyte area, and
ASR	=	area specific resistance,

and where

$$V_N = \frac{-1}{2F}\left[\Delta G_f{}^0(T) + RT \ln\left[\left(\frac{f_{H_2}\, f_{O_2}{}^{\frac{1}{2}}}{f_{H_2O}}\right)\left(\frac{P}{P_{STD}}\right)^{\frac{1}{2}}\right]\right] \quad \text{and} \qquad (5\text{-}16)$$

$$ASR = \left(ASR\right)_0 + C_1 \exp\left(\frac{C_2}{T}\right) \tag{5-17}$$

where *C1* and *C2* are constants and *T* is in degrees K.

The characteristic times for how cell output quantities (species concentration, structure temperatures, and temperatures of gas streams) respond to changes in cell inlet conditions (current and inlet temperature) are derived for several simplifying and reasonable assumptions. The species concentrations and the gas stream temperatures respond much more quickly to changes in cell inlet conditions than do the temperatures of structures. These elements can be treated quasi-statically compared to the structures. Further, of the structures only the electrodes and electrolytes are in intimate contact with the changing thermal conditions in the cell. Assume that only water enters the cell and that only hydrogen and oxygen exit the cell. The heat capacity of the gas inside the cell is negligible and it is assumed the cell is operated adiabatically. Then from Eq. (5-13)

$$\rho V C_p \frac{d}{dt} T = m_{H_2O}\ h_{H_2O} - \left(m_{H_2} h_{H_2} + m_{O_2} h_{O_2}\right) + W \tag{5-18}$$

$$m_{H_2} = \frac{A_{H_2}}{A_{H_2O}} m_{H_2O} \qquad m_{o_2} = \frac{A_{O_2}}{2A_{H_2O}} m_{H_2O} \tag{5-19}$$

$$\rho V C_p \frac{d}{dt} T = m_{H_2O}\left[h_{H_2O}\left(T_i\right) - \frac{1}{A_{H_2O}}\left(A_{H_2} h_{H_2}\left(T\right) + \frac{A_{0_2}}{2}\left(T\right)\right)\right] + W \tag{5-20}$$

where ρ is the density and V is the volume and T is temperature of the electrodes and electrolyte (i.e. thermally active structures), m is species mass flow rate (kg/s), h is specific enthalpy (joules/kg), W is rate of electrical work supplied to the electrolyzer, A is atomic number, and subscript i represents inlet.

Suppose control on i (i.e. m_{H2}) and accept V_{cell}

$$m_{H_2O} = \frac{A_{H_2O} A}{2F} \tag{5-21}$$

Writing the electrical work in terms of current, i, Nernst voltage, V_N, cell area, A, and area specific resistance, ASR,

$$\begin{aligned} W &= V_{cell}\ A\ i \\ &= \left(V_N + i \cdot ASR\right) A\ i \\ &= A V_N\ i + A \cdot ASR\ i^2 \\ &= A V_N\left(T\right) i + A \cdot ASR\ i^2 \end{aligned} \tag{5-22}$$

$$\rho V C_p \frac{d}{dt} T = \frac{A_{H_2O} A}{2F}\, i \left[h_{H_2O}(T_i) - \frac{1}{A_{H_2O}} \left(A_{H_2}\, h_{H_2}(T) + \frac{A_{O_2}}{2} h_{O_2}(T) \right) \right] + A V_N(T)\, i + A \cdot ASR\, i^2 \tag{5-23}$$

and then linearizing the equation

$$\begin{aligned} \rho V C_p \frac{d}{dt} \delta T = {} & \frac{A_{H_2O} A}{2F} \left[i_o\, C_{\rho_{H_2O}} \delta T_i + h_{H_2O}(T_{i_o}) \delta i \right] \\ & - \frac{A A_{H_2}}{2F} \left[i_o\, C_{\rho_{H_2}}\, \delta T + h_{H_2}(T_o) \delta i \right] \\ & - \frac{A A_{O_2}}{4F} \left[i_o\, C_{\rho_{O_2}}\, \delta T + h_{O_2}(T_o) \delta i \right] \\ & + A \left[i_o \frac{\partial V_N(T)}{\partial T} \delta T + V_N(T_o) \delta i \right] \\ & + A \left[ASR_o \left(i_o^2 + 2 i_o \delta i + (\delta i)^2 \right) + i_o^2 \frac{\partial}{\partial T} ASR\ \delta T \right] \end{aligned} \tag{5-24}$$

where subscript *o* represents the linearization point. The above equation gives the change in cell temperature (electrodes, electrolyte, and outlet gas streams) in terms of changes in cell current and temperature of the inlet gas streams. Collecting terms gives

$$\begin{aligned} \rho V C_P \frac{d}{dt} \delta T = {} & -\frac{i_0 A}{2F} \left[A_{H_2} C_{pH_2} + A_{O_2} C_{pO_2} - 2F \frac{\partial V_N(T)}{\partial T} - 2F i_0 \frac{\partial ASR}{\partial T} \right] \delta T \\ & + \frac{A}{2F} \left[A_{H_2O} h_{H_2O}(T_i) - A_{H_2} h_{H_2}(T_0) - \frac{A_{O_2}}{2} h_{O_2}(T_0) + 2F V_N(T_0) + 4F \cdot ASR\, i_0 \right] \delta_i \\ & + \left[\frac{A_{H_2O} A}{2F} i_0 C_{pH_2O} \right] \delta T_i \end{aligned} \tag{5-25}$$

and from the above according to Eq. (5-1) the cell time constant is

$$\tau^{-1} = \frac{i_o A}{2F (\rho V C_\rho)_s} \left[A_{H_2}\, C_{\rho_{H_2}} + A_{O_2}\, C_{\rho_{O_2}} - 2F\, \partial \frac{V_{N(T)}}{\partial T} - 2F\, i_o\, \frac{\partial}{\partial T} ASR \right] \tag{5-26}$$

where the various terms in this equation are given by

$$V_N = +\frac{1}{2F}\left[\Delta G_f^o(T) + RT\ ln\left\{ \left(\frac{f_{H_2} f_{o_2}^{1/2}}{f_{H_2O}} \right) \left(\frac{P}{P_{STD}} \right)^{1/2} \right\} \right] \tag{5-27}$$

$$\partial \frac{V_N}{\partial T} = +\frac{1}{2F}\left[\frac{\partial \Delta G_f^o}{\partial T} + R\ ln\left\{ \left(\frac{f_{H_2} f_{o_2}^{1/2}}{f_{H_2O}} \right) \left(\frac{P}{P_{STD}} \right)^{1/2} \right\} \right] \tag{5-28}$$

$$ASR = ASR_o + C_1\ exp\left(\frac{C_2}{T} \right) \tag{5-29}$$

$$\partial \frac{ASR}{\partial T} = -\frac{C_1 C_2}{T^2}\ exp\left(\frac{C_2}{T} \right) = -\frac{C_2}{T}(ASR). \tag{5-30}$$

5.3.2 Heat Exchanger

The efficiency of the closed Brayton cycle is very sensitive to pressure losses and so there is an incentive to use heat exchangers with a high effectiveness/low pressure drop characteristics. Generally, this implies plate and fin or printed circuit heat exchangers (PCHE) in a counter flow configuration. This section develops models for the PCHE.

The construction of a typical PCHE is shown in Figure 5-1. The design consists of alternating hot and cold plates with semi-circular parallel flow channels etched into the lower face of each plate with the channels carrying the respective hot and cold streams. The hot and cold streams flow in opposite directions.

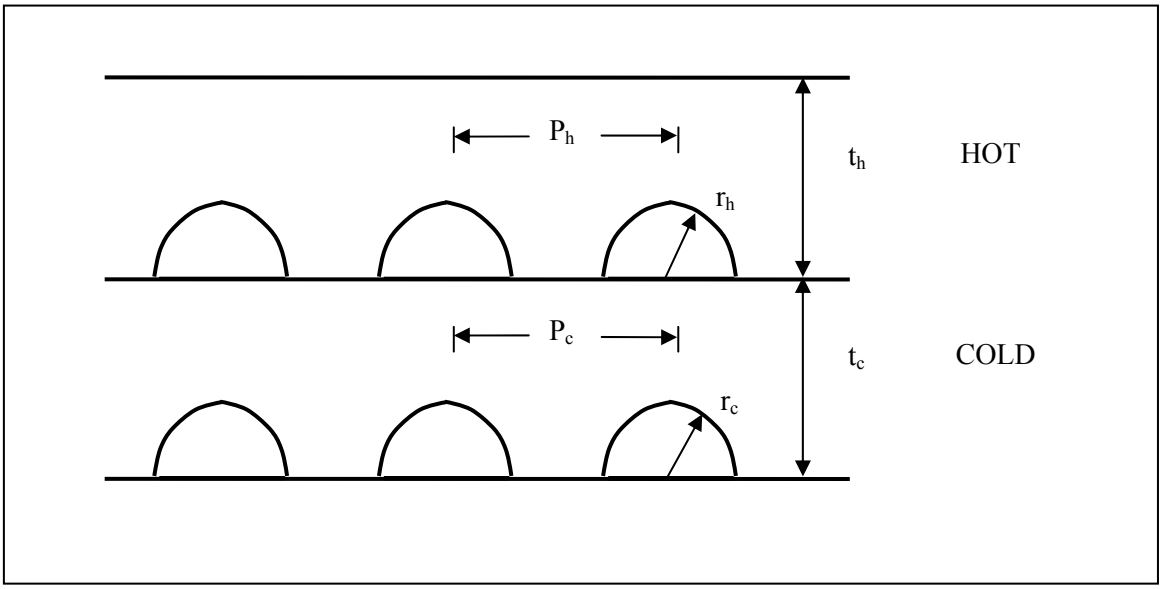

Figure 5-1 View of Printed Circuit Heat Exchanger in Cross Section.

The energy equation for the hot side coolant node is

$$V\frac{d(\rho h)_{h_o}}{dt} = -Q_{h-t} + w_{h_i}h(T,P)_{h_i} - w_{h_o}h(T,P)_{h_o} \tag{5-31}$$

where $Q_{h\text{-}t}$ is the rate of total heat transfer from the hot side coolant to the heat transfer media which we refer to as a tube and h is enthalpy. Similarly, the energy equation for the cold side coolant is

$$V\frac{d(\rho h)_{c_o}}{dt} = Q_{t-c} + w_{c_i}h(T,P)_{c_i} - w_{c_o}h(T,P)_{c_o} \tag{5-32}$$

where $Q_{t\text{-}c}$ is the rate of total heat transfer from the tube to the cold side coolant. The energy equation for the tube is

$$V\frac{d(\rho C_p T)_t}{dt} = -Q_{t-c} + Q_{h-t}\,. \tag{5-33}$$

In the case where the tube metal is lumped with one of the coolants rather than solving separately for its temperature, the heat transfer rate from hot to cold fluid is for constant fluid properties

$$Q = AU\frac{(T_{ho}-T_{ci})-(T_{hi}-T_{co})}{\ln((T_{ho}-T_{ci})/(T_{hi}-T_{co})}\,. \tag{5-34}$$

A unit cell delineated by four boundaries across each of which there is zero net energy flow is defined for characterizing the different heat transfer processes. Figure 5-2 shows two adjacent unit cells contained in the cross section of an infinite array of alternating hot and cold plates. We consider the upper unit cell in Figure 5-2. Both unit cells are similar enough that this one suffices for obtaining representative time constants. Heat flows from the hot channel on the bottom to the cold channel on the top. The dashed horizontal lines drawn through each channel identify cell boundaries across which there is not net flow of energy. Of course, the energy flow in the cell shown is two dimensional and it is assumed this distribution is known so that the cell boundaries can be drawn as the dashed lines shown. This establishes dimension *t'* shown in the figure.

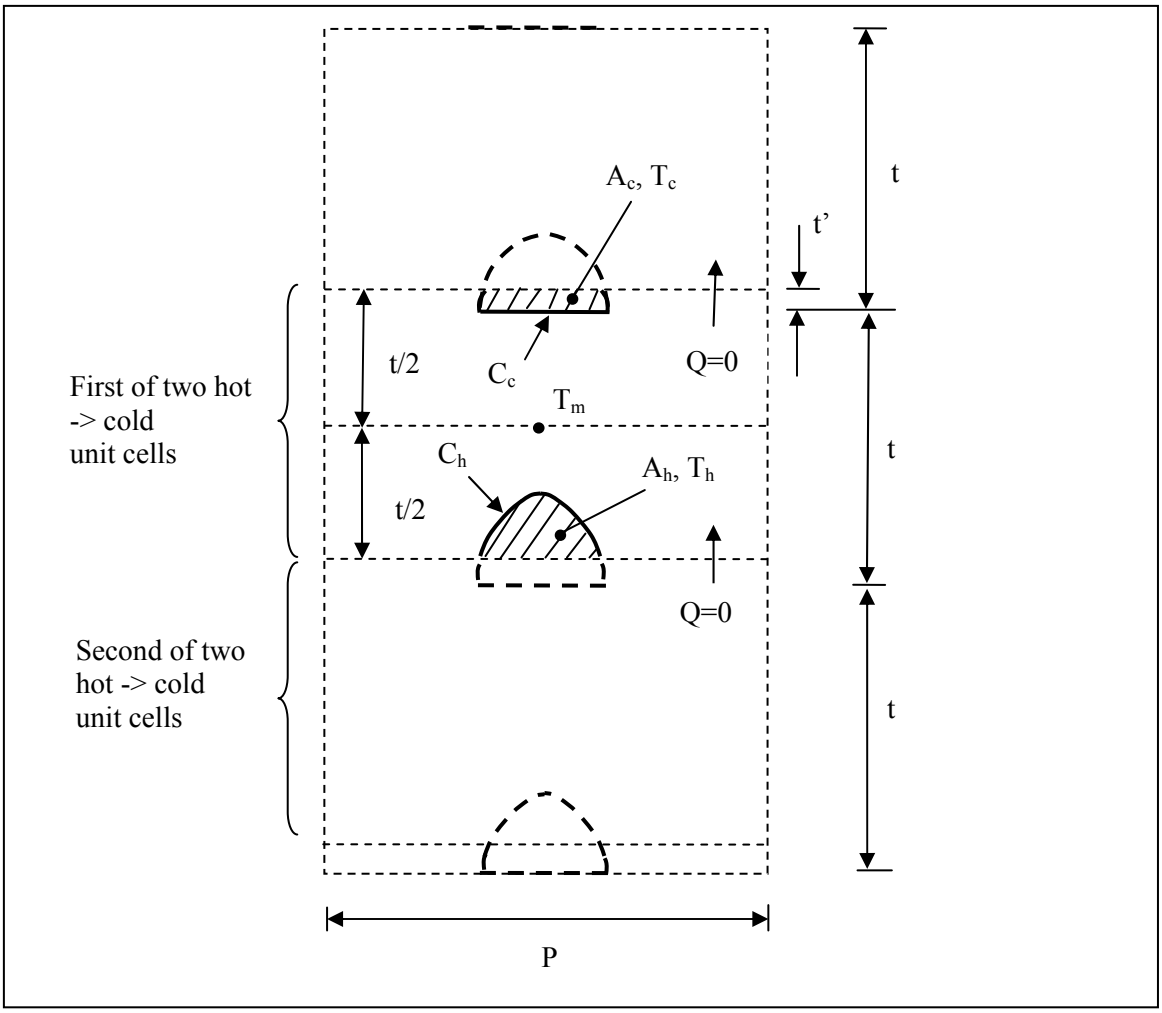

Figure 5-2 Unit Cells Defined for Infinite Array of Hot and Cold Channels.

A one-dimensional representation of heat flow between the channels in the top unit cell is shown in Figure 5-2. This is of course an approximation to a multidimensional heat flow problem but captures to the first order the energy storage mechanisms and heat flow resistances of the three regions: the hot channel, the cold channel, and the intervening heat transfer media. The coolant in the channels that interacts with the heat transfer media in the cell is marked by the hash lines in the channels. This fluid has a cross sectional area denoted by A and it makes contact with the media through circumference C. The circumference is the solid line that abuts the hash lines. The hot stream, media, and cold stream have average temperatures T_h, T_m, and T_c, respectively, shown in Figure 5-2. The heat transfer between the hot stream and the media is approximated by

$$T_h - T_1 = \frac{Q/l}{C_h h_h} \tag{5-35}$$

where T_1 is the temperature at the surface of the media in contact with the hot stream, h_h is the heat transfer coefficient between the hot stream and the surface of the media, and k is the thermal conductivity of the media. Similarly, the heat transfer through the media is approximated by

$$T_1 - T_m = \frac{Q/l}{\frac{kP}{t/2}\ \frac{(t/2*P - A_h)}{t/2*P}} \tag{5-36}$$

where A_h is the hot fluid cross sectional area of the unit cell. The factor on the right in the denominator attempts to correct for the reduction in the cross section of the media caused by the hot channel and its subsequent effect on average conductivity. Alternatively, this correction factor could be obtained from the solution to the two-dimensional conduction equation for the media. The above two equations yield

$$Q = \bar{h}_{h-m}\, l\, (T_h - T_m) \tag{5-37}$$

where

$$\bar{h}_{h-m} = \left(\frac{1}{C_h h_h} + \frac{1}{\frac{kP}{t/2}\ \frac{(t/2*P - A_h)}{t/2*P}} \right)^{-1} . \tag{5-38}$$

Similarly, the heat flow between the media and the cold channel is given by

$$Q = \bar{h}_{m-c}\, l\, (T_m - T_c) \tag{5-39}$$

where

$$\bar{h}_{m-c} = \left(\frac{1}{C_c h_c} + \frac{1}{\frac{kP}{t/2}\ \frac{(t/2*P - A_c)}{t/2*P}} \right)^{-1} . \tag{5-40}$$

An energy balance on the hot channel coolant in thermal contact with media over a length l gives

$$(\rho A l C_v)_h \frac{dT_h}{dt} = -(C_p w)_h (T_h - T_i) - \bar{h}_{h-m}\, l\, (T_h - T_m) \tag{5-41}$$

where ρ is density, C_p is specific heat, w is flow rate, and subscript i refers to inlet. Similarly, for the media

$$(\rho A l C_p)_m \frac{dT_m}{dt} = -\bar{h}_{h-m}\, l\, (T_m - T_h) - \bar{h}_{m-c}\, l\, (T_m - T_c) . \tag{5-42}$$

Rewriting these two equations in terms of time constants,

$$\frac{dT_h}{dt} = -\frac{1}{\tau_{i-h}}\left(T_h - T_i\right) - \frac{1}{\tau_{h-m}}\left(T_h - T_m\right) \tag{5-43}$$

and

$$\frac{dT_m}{dt} = -\frac{1}{\tau_{m-h}}\left(T_m - T_h\right) - \frac{1}{\tau_{m-c}}\left(T_m - T_c\right) \tag{5-44}$$

where

$$\tau_{i-h} = \frac{\left(\rho A l C_v\right)_h}{\left(C_p w\right)_h}, \qquad \tau_{h-m} = \frac{\left(\rho A C_v\right)_h}{\bar{h}_{h-m}}, \qquad \text{and} \tag{5-45}$$

$$\tau_{m-h} = \frac{\left(\rho A C_p\right)_m}{\bar{h}_{h-m}}, \qquad \tau_{m-c} = \frac{\left(\rho A C_p\right)_m}{\bar{h}_{m-c}}. \tag{5-46}$$

Three nodes representing the hot side coolant, heat transfer media, and cold side coolant. A lumped parameter energy storage equation is written for each of the nodes. When writing these equations it is assumed from the standpoint of energy storage that there is perfect mixing of the energy that enters a node so that the node is at a uniform temperature.

General expressions are developed for the parameters C_h, A_h, C_c, and A_c that appear above. The location of the zero heat flow boundaries in Figure 5-2 is referenced in terms of the displacement *t'*. In the absence of a solution to the two-dimensional conduction equation, we assume the zero net heat flow line is located where one-half of the channel perimeter lies above the line and the other half below. The total channel perimeter is $r*(\pi+2)$. Let the angle between the base of the semi-circle and the radius that intersects the zero heat flow line be θ. Then θ satisfies

$$\frac{1}{2}C = \frac{1}{2}r\left(\pi + 2\right) = 2r + 2r\theta \quad \text{or} \qquad \theta = \frac{1}{4}\left(\pi - 2\right) \tag{5-47}$$

where C is the total perimeter of the channel. We have then for the hot channel in the unit cell (i.e. hashed region) of Figure 5-2

$$C_h = r\left(\frac{\pi}{2} + 1\right), \quad A_h = r^2\left(\frac{\pi}{2} - \theta - \sin\theta\cos\theta\right), \text{ and } \quad A_m = P\frac{t}{2} - A_h \tag{5-48}$$

where θ is given by Eq. (5-47). From Eq. (5-47) and (5-48) one obtains for the data in Table 5-1 $\theta = 0.285$ rads, $C_h = 2.57$r, and $A_h = 1.016$r^2. For the cold channel

$$C_c = C_h \qquad \text{and} \qquad A_c = \frac{\pi}{2}r^2 - A_h \tag{5-49}$$

Table 5-1. Design Data for Helium Printed Circuit Heat Exchangers.

	IHX	HTLHX	PCU Recuperator
Channel Diameter, *2r* (m)	1.5e-03	1.5e-03	1.5e-03
Channel Pitch, *P* (m)	1.8e-03	2.25e-03	2.56e-03
Plate Thickness, *t* (m)	8.55e-04	1.17e-03	1.79e-03
Channel Length, *l* (m)	2.34	1.089	1.62
Number of Channels, $N_{channels}$ (one side)	7.33e06	4.36e05	4.264e06
In Width Direction	2639	673	2443
In Height Direction	2778	648	1745
Hot Side Flow, *w* (kg/s) - Total	289	32.1	260
$w_{channel}$ - Per Channel	3.94e-05	7.36e-05	5.10e-05
Cold Side Flow, *w* (kg/s) - Total	292	27.5	260
$w_{channel}$ - Per Channel	3.98e-05	5.31e-05	5.10e-05
Width (m)	4.75	1.52	5.23
Height (m)	4.75	1.52	5.23
Volume (m^3)	52.8	2.5	62.9

5.3.3 Boiler

The response of the two-phase mixture temperature in a counterflow heat exchanger to changes in boundary conditions is derived. It is assumed the hot side is single phase liquid and that the cold side has saturated liquid water entering and saturated steam exiting. If we assume the water is on the shell side, then the energy equation for the water is

$$\frac{d}{dt} M_{H_2O}\, i \;+\; \left(\rho V C_p\right)_{shell} \frac{d}{dt} T_{sat} = Q + w_{fw} h_{fw} - w_s h_g \;. \tag{5-50}$$

The above equation lumps the heat capacity of the shell in with the water mixture.

If we assume no change in mass so that the feedwater flow equals steam flow, then

$$\frac{d}{dt} M_{H_2O} = 0 = w_{fw} w_s \,, \tag{5-51}$$

and Eq. (5-50) becomes

$$\frac{di}{dt} + \frac{\left(\rho V\, C_p\right)_{shell}}{M_{H_2O}} \frac{d}{dt} T_{sat} = \frac{1}{M_{H_2O}} \left[Q - w_{fw} \left(h_g - h_{fw} \right) \right] . \tag{5-52}$$

The first term in Eq. (5-52) can be expanded into

$$\frac{d}{dt} i = c \frac{dT_{sat}}{dt} + i_{fg} \frac{d}{dt} x \tag{5-53}$$

where

$$c = \left(1 - x\right)\frac{d}{dT} i_f + x\frac{d}{dt} i_g \ . \tag{5-54}$$

Then Eq. (5-52) becomes

$$\left[c + \frac{\left(\rho V C_\rho\right)_{shell}}{M_{H_2O}}\right]\frac{d}{dt} T_{sat} + i_{fg}\frac{d}{dt} x = \frac{1}{M_{H_2O}}\left[Q - w_{fw}\left(h_g - h_{fw}\right)\right] . \tag{5-55}$$

The derivative of the quality with respect to time in this equation is eliminated next.

Writing the conservation of volume equation for the mixture

$$M_{H_2O}\frac{d}{dt} v = 0 \ , \tag{5-56}$$

where we have made use of Eq. (5-50). Expanding Eq. (5-51) leads to

$$0 = \phi\frac{d}{dt} T_{sat} + v_{fg}\frac{d}{dt} x \ , \tag{5-57}$$

where

$$\phi = x\frac{d}{dT} v_g + \left(1 - x\right)\frac{d}{dT} v_f \ . \tag{5-58}$$

The equation for the saturation temperature is obtained by combining Eqs. (5-55) and (5-57) which gives

$$\frac{d}{dt} T_{sat} = \frac{1}{M\left[c + \dfrac{\left(\rho V C_p\right)_{shell}}{M} - \dfrac{\phi i_{fg}}{v_{fg}}\right]}\left[Q - w_{fw}\left(h_g - h_{fw}\right)\right] . \tag{5-59}$$

If the change in T_{SAT} is small, then one can solve Eq. (5-59) with the properties and quality taken to be constant.

An expression for the heat transfer rate, Q, is obtained by assuming that the coolant axial temperature profiles are those that would result in the steady state given the instantaneous values of the boundary conditions. Then the log mean temperature model gives

$$\frac{T_{hi}-T_{sat}}{T_{ho}-T_{sat}} = exp\left[\frac{UA}{\left(wC_p\right)_h}\right] = K^{-1} \ . \tag{5-60}$$

and

$$Q = UA\,\frac{\left(T_{ho}-T_{sat}\right)-\left(T_{hi}-T_{sat}\right)}{\ln\left(\left(T_{ho}-T_{sat}\right)/\left(T_{hi}-T_{sat}\right)\right)} \tag{5-61}$$

where the subscript *h* refers to the hot side, *i* to the inlet, and *o* to the outlet. Using the above equation and neglecting the thermal inertia of the hot side coolant, a hot side energy balance gives

$$Q = \left(w\ C_p\right)_h \left(1-K\right)\left(T_{hi}-T_{sat}\right) . \tag{5-62}$$

The final equation for the saturation temperature in terms of the time dependent boundary conditions of hot side inlet temperature, feedwater enthalpy, and steam flowrate is obtained by substituting Eq. (5-61) into Eq. (5-59) which gives,

$$\frac{d}{dt}T_{sat} = \frac{-1}{\tau}\left[T_{sat} + F\left(t\right)\right] \ , \tag{5-63}$$

where

$$\frac{1}{\tau} = \frac{\left(wC_p\right)_h\left(1-K\right)}{M_{H_2O}\left[c + \dfrac{\left(\rho V C_\rho\right)_{shell}}{M_{H_2O}} - \dfrac{\phi\, i_{fg}}{v_{vg}}\right]} \ . \tag{5-64}$$

5.3.4 Reactor Core

This section describes the model developed for the reactor core and its application for simulating the response of the core to temperature perturbations that originate in the hydrogen plant.

5.3.4.1 Temperatures

The reactor core is a collection of fueled hexagonal columns with each column having axial coolant holes that connect the inlet plenum to the outlet plenum. The distribution of coolant flow among the columns is influenced by the presence of leakage paths between adjacent columns. A detailed prediction of the distribution of coolant is the subject of other work. [Vilim 2007a] In the present work we note that the flow of coolant is predominantly axially through the column holes. Then a one-dimensional representation of the core provides the main dependence of core temperatures on coolant inlet temperature and flowrate.

An averaged thermal-hydraulic behavior of the graphite column with its array of coolant holes and fuel holes is obtained by transforming into a unit cell annular geometry. This cell is shown in Figure 5-3. The radii of the three regions in the annular model are selected to preserve the areas in the original fuel element matrix and the number of unit cells is set equal to the number of coolant holes so that

$$n_{cl}\ A_{cl} = n_{cl}\ \pi(r_{cl}^{\ 2} - r_{gr}^{\ 2}) \qquad n_{cl}\ A_{gr} = n_{cl}\ \pi(r_{gr}^{\ 2} - r_{f}^{\ 2}) \qquad n_{cl}\ A_{f} = n_{cl}\pi r_{f}^{\ 2} \tag{5-65}$$

where the left-hand side of each equation is the area in the original fuel element and the right side is an equal area distributed across a number of unit cells (i.e. annular fuel elements) equal to the number of coolant channels. Here

A	=	cross-sectional area in the original fuel element on a per unit cell basis,
n	=	number of holes in the original fuel element, and
r	=	equivalent outer radius for annular pin representation

and *f*, *gr*, *cl* represent fuel, graphite, and coolant, respectively. This transformation yields an effective one-dimensional conduction distance for the graphite.

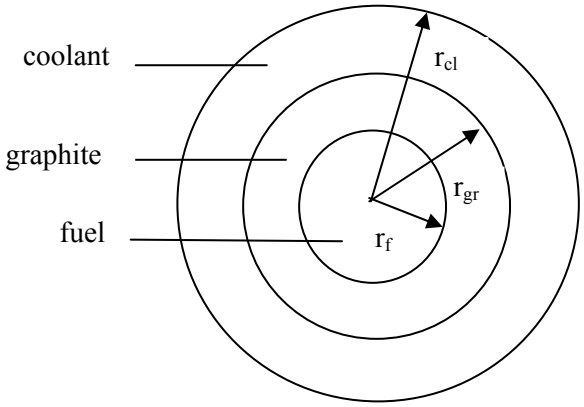

Figure 5-3 Transformed Fuel Element Geometry.

Adopting this annular geometry the energy equation for the fuel in contact with the graphite is

$$(\rho C_p)_f \frac{dT_f}{dt} = Q_f - \frac{h_{f-gr} 2\pi r_f}{A_f}(T_f - T_{gr}) \tag{5-66}$$

where

T_f	=	fuel temperature,
Q_f	=	volumetric heat generation rate,
$h_{f\text{-}gr}$	=	fuel to graphite heat transfer coefficient,
r_f	=	radius of fuel,
A_f	=	cross sectional area of fuel, and
T_{gr}	=	graphite temperature.

An expression for the heat transfer coefficient is obtained as follows. The analytic solution to the steady-state one-dimensional heat conduction problem gives the heat flux at the graphite-fuel interface as one-half of the graphite and fuel temperature rise times the heat transfer coefficient

$$\frac{1}{h_{f-gr}} = \frac{r_f}{4k_f} + \frac{\Delta r_{gr}}{2k_{gr}} + \frac{1}{h_{gap}} \tag{5-67}$$

where

k_f = fuel conductivity,
Δr_{gr} = graphite thickness, and
h_{gap} = gap conductivity.

But one-half the graphite and fuel temperature rise is approximately the difference between the average fuel and average graphite temperature, $T_f - T_{gr}$. Thus, the heat transfer coefficient given above will result in Eq. (5-66) being very nearly satisfied at steady state.

The energy equation for the graphite is

$$(\rho C_p)_{gr} \frac{dT_{gr}}{dt} = \frac{h_{f-gr} 2\pi r_f}{A_{gr}} (T_f - T_{gr}) - \frac{h_{gr\text{-}cl} 2\pi r_{gr}}{A_{gr}} (T_{gr} - T_{cl}) \tag{5-68}$$

where

T_{cl} = coolant temperature,
$h_{gr\text{-}cl}$ = cladding to coolant heat transfer coefficient,
r_{gr} = outer radius of graphite, and
A_{gr} = cross sectional area of graphite.

The graphite to coolant heat transfer coefficient is given by

$$\frac{1}{h_{gr\text{-}cl}} = \frac{\Delta r_{gr}}{2k_{gr}} + \frac{1}{h_{cl}} \tag{5-69}$$

where Δr_{gr} is the graphite thickness,

$$h_{cl} = \frac{k_{cl}}{D_{h-cl}} Nu_{cl} \tag{5-70}$$

and where

$D_{h\text{-}cl}$ = hydraulic diameter of the coolant channel, and
Nu_{cl} = Nusselt number.

The values of engineering parameters that appear in the above equations are given for the VHTR based on the GT-MHR design given in Table 5-2 and 5-3.

The fuel and graphite temperature during a transient are obtained by solving Eq. (5-66) and (5-68) with the coolant temperature treated as a forcing function. The coolant temperature is assumed to be given by

$$T_{cl} = \frac{T_{in} + T_{out}}{2} \tag{5-71}$$

where T_{in} is the core inlet temperature and T_{out} is the outlet temperature. These two quantities are obtained from an energy balance on the core solved in parallel with the conservation equations for the rest of the primary system. Implicitly differencing Eq. (5-66) gives

$$T_f^{n+1} - T_f^{n} = \frac{\Delta t\, Q_f^{n+1}}{(\rho C_p)_f} - \Delta t A_{11} T_f^{n+1} + \Delta t A_{11} T_{gr}^{n+1} \tag{5-72}$$

where

$$A_{11} = \frac{h_{f-gr} 2\pi r_f}{A_f (\rho C_p)_f} \ .$$

In the steady state the left-hand side is zero and the equation simplifies to

$$- A_{11} T_f + A_{11} T_{gr} + \frac{Q_f}{(\rho C_p)_f} = 0$$

Rearranging Eq. (5-72)

$$C_{11}\, T_f^{n+1} + C_{12}\, T_{gr}^{n+1} = D_1 \tag{5-73}$$

where

$$C_{11} = 1 + \Delta t A_{11}$$

$$C_{12} = - \Delta t A_{11}$$

$$D_1 = T_f^{n} + \Delta t \frac{Q_f^{n+1}}{(\rho C_p)_f} .$$

Implicitly differencing Eq. (5-68) gives

$$T_{gr}^{n+1} - T_{gr}^{n} = \Delta t\, A_{21} (T_f^{n+1} - T_{gr}^{n+1}) - \Delta t\, A_{23} (T_{gr}^{n+1} - T_{cl}^{n+1}) \tag{5-74}$$

where

$$A_{21} = \frac{h_{f-gr} 2\pi r_f}{A_{gr} (\rho C_p)_{gr}}$$

$$A_{23} = \frac{h_{gr-cl} 2\pi r_{gr}}{A_{gr} (\rho C_p)_{gr}} \ .$$

In the steady state the left-hand side is zero and the equation simplifies to

$$A_{21}\,T_f - (A_{21} + A_{23})\,T_{gr} + A_{23}\,T_{cl} = 0$$

Rearranging Eq. (5-75)

$$C_{21}\,T_f^{\,n+1} + C_{22}\,T_{gr}^{\,n+1} = D_2 \qquad (5\text{-}75)$$

where

$$C_{21} = -\Delta t A_{21}$$

$$C_{22} = \Delta t A_{21} + \Delta t A_{23} + 1$$

$$D_2 = \Delta t A_{23} T_{cl}^{\,n+1} + T_{gr}^{\,n}$$

These two equations for fuel and graphite temperature (either steady-state or transient case) are solved simultaneously with a coolant energy equation where T_{cl} appears as an unknown and a fuel nuclear power equation where Q_f appears as an unknown.

Table 5-2 Values of Design Parameters for Annular Unit-Cell Representation of Fuel Element.

Coolant	n_{cl}	$A_{cl}\,n_{cl}$ (m^2)	A_{cl} (m^2)	r_{cl} (m)	$C_{p\text{-}cl}$ (j/kg-C)	k_{cl} (w/m-C)	-
	106	$102\,\frac{\pi}{4}\,0.016^2 = 0.022$	2.1E-04	26E-03	5200	0.37	
Graphite	-	$A_{gr}\,n_{cl}$ (m^2)	A_{gr} (m^2)	r_{gr} (m)	$C_{p\text{-}gr}$ (j/kg-C)	k_{gr} (w/m-C)	ρ_{gr} (kg/m^3)
		$\sqrt{3}(0.360)^2$ -0.022-0.027=0.175	1.7E-03	25E-03	1100	80	1,740
Fuel	-	$A_f\,n_{cl}$ (m^2)	A_f (m^2)	r_f (m)	$C_{p\text{-}f}$ (j/kg-C)	k_f (w/m-C)	ρ_f (kg/m^3)
		$210\,\frac{\pi}{4}\,0.0127^2 = 0.027$	2.5E-04	8.9E-03	160 ($Cp_{UC_2} \sim Cp_{UC}$)	20 (UC)	13,600

Table 5-3 Values of Design Parameters for Coolant Channel in Fuel Element.

Coolant Mass Flow Rate	Number of Coolant Holes per Fuel Element	Number of Fuel Element Columns	Coolant Mass Flow Rate in Fueled Elements (kg/s)	Coolant Mass Flow Rate per Coolant Channel (kg/s)
	106	72+30=102	288*0.85=244	0.023
Coolant Heat Transfer Coefficient	$(Re)_{He}$	$(Pr)_{He}$	D_{cl} (m)	$h_{cl} = \frac{k_{He}}{D_{cl}} 0.023\ \mathrm{Re}^{0.8}\ \mathrm{Pr}^{0.3}$ (W/m^2-C)
	41,000	-1	0.016 (coolant channel diameter)	2600

5.3.4.2 Reactivity Feedback

The net reactivity is expressed as a sum of individual reactivities. A reference state is defined and with it individual component temperatures. For convenience this state is taken as the full power steady-state condition. With respect to this state the reactivity introduced by a change in temperature of a component is given by

$$\rho = \frac{d\rho}{dL} L\, \beta\, \delta T \tag{5-76}$$

where is L is length, β is the coefficient of linear expansion, and δT is the temperature change. Of course, the individual component reactivities are dependent on the arrangement of components within the reactor vessel. We develop these for the GT-MHR upon which the VHTR is based. For this particular design 1) the reactor inlet coolant enters the core at the top and flows vertically down, 2) the control rod drive mechanisms are fixed to the top of the vessel and the rods enter at the top of the core, 3) the core rests on the bottom of the vessel, 4) the vessel wall is cooled by the coolant entering the reactor vessel, 5) the physical dimensions of the core are large compared to the neutron mean free path such that reactivity chage associated with a change in leakage due to core temperature expansion is insignificant, and 6) the reactivity feedback associated with coolant density is negligible.

5.3.4.2.1 Control Rods

Temperature changes in the core introduce control rod reactivity in two ways. First, the vessel temperature is assumed equal to the reactor inlet temperature so the vessel length changes in response to reactor inlet temperature resulting a change in control rod position relative to the top of the core. Second, the temperature of the graphite moderator blocks are assumed equal to the coolant temperature so the core length changes in response to the coolant temperature resulting in a change in control rod position relative to the top of the core. The net change in reactivity is then given by

$$\delta\rho = (-(L\beta)_v\, \delta T_i + (L\beta)_m\, \delta T_m) \left(\frac{d\rho}{dL}\right)_{cr} \tag{5-77}$$

where

T_i = reactor inlet coolant temperature and
T_m = reactor midplane moderator temperature, and

where the last term is the change in reactivity per unit change in the position of the rods with respect to the top of the core. Insertion into the core is taken as the positive direction. The subscripts *v*, *m*, *cr* represent vessel, moderator, and control rod, respectively. The above expression is rewritten as

$$\delta\rho = \alpha_{cr-v}\,\delta T_i + \alpha_{cr-m}\,\delta T_m \tag{5-78}$$

where $\alpha_{cr-v} = -(L\beta)_v \left(\frac{d\rho}{dL}\right)_{cr}$ and $\alpha_{cr-m} = (L\beta)_m \left(\frac{d\rho}{dL}\right)_{cr}$.

5.3.4.2.2 Graphite Moderation

The neutron flux spectrum and neutron leakage change with graphite temperature creating a source of reactivity. Assuming the fuel temperature is maintained constant, the reactivity introduced relative to a reference graphite temperature is represented by

$$\delta\rho = \alpha_{gr-m}\,(T_{gr} - T_{gr,0}) \tag{5-79}$$

where T_{gr} is the graphite midplane temperature. An estimate for the graphite moderator temperature coefficient of reactivity, $\alpha_{gr\text{-}m}$ for the VHTR is given in Table 5-4.

Table 5-4 Integral Reactivity Coefficients for VHTR.

Operating Control Rods - Vessel, $\alpha_{cr\text{-}v}$ (\$/°C)	[0,+5.2e-4][a], mean=2.6e-04
Operating Control Rods - Moderator, $\alpha_{cr\text{-}m}$ (\$/°C)	-0.74e-4
Moderator, α_m (dk/dT) @ 770° C [b] (Fig. 37 [MacDonald 2003])	[-1.0e-5, +4.0e-5]
α_m (\$/°C)	[-1.67e-3, +6.67e-3], mean=2.5e-03
Fuel, α_f (dk/dT) @ 820° C [b] (Fig. 35 [MacDonald])	[-5.5e-5, -4.4e-5]
α_f (\$/°C)	[-9.2e-3, -7.3e-3], mean= - 8.25e-03
Average moderator temperature rise[b], $\Delta T_{m\text{-}100}$ (°C)	100
Average fuel temperature rise[b], $\Delta T_{f\text{-}100}$ (°C)	50
Coolant temperature rise, $\Delta T_{c\text{-}100}$ (°C)	510
$A = \alpha_f\ (\Delta T_{m\text{-}100} + \Delta T_{f\text{-}100})$, (\$)	- 1.2
$B = (\alpha_m + \alpha_{cr\text{-}m} + \alpha_f)/2 * \Delta T_{c\text{-}100}$, (\$)	- 1.5 [d]
$C = \alpha_{cr\text{-}v} + \alpha_m + \alpha_{cr\text{-}m} + \alpha_f$	-5.6e-03 [d]
A+B, (\$)	- 2.7 [d]
$1 - \frac{C\Delta T_{c-100}/B}{\frac{A}{B}+1}$	- 0.042 [d]
$C\Delta T_{c-100}/B$	0.90 [d]
$\frac{A}{B}$	0.83 [d]

[a] Vessel time constant is large at six inch thickness. Range covers time that varies from instantaneous to infinite.
[b] Average moderator and fuel temperatures from Table 11 of [MacDonald 2003].
[c] $\beta_{eff} \sim 6x10^{-3}$.
[d] based on mean values

5.3.4.2.3 Coolant Density

A coolant density reactivity coefficient, α_{He} , is defined through

$$\rho_{void} - \rho_0 = \alpha_{He} (\theta_{void} - \theta_0) \tag{5-80}$$

where

ρ = reactivity, and
θ = density.

The subscript *void* denotes the core with no coolant present and the subscript *0* denotes the full power reference condition. At the reference condition ρ_0 is taken as zero. The ideal gas law gives for the coolant at the core midplane,

$$\theta = \frac{P}{RT_{cl,K}} \tag{5-81}$$

where T_{cl} is the reactor midplane coolant mixed-mean temperature in degrees Kelvin and P is the gas pressure. The reactivity change relative to the reference state for a change in temperature and pressure is then from Eqs. (5-80) and (5-81)

$$\rho = \frac{\alpha_{He}}{R} \left(\frac{P}{T_{cl}} - \left(\frac{P}{T_{cl}} \right)_0 \right). \tag{5-82}$$

The coolant density reactivity coefficient can be solved for using Eqs. (5-80) and (5-82) is

$$\alpha_{He} = - R \left(\frac{T_{cl}}{P} \right)_0 \rho_{void} . \tag{5-83}$$

Typically, the coolant density reactivity coefficient is negligible in the thermal gas reactor and is set to zero in this work.

5.3.4.2.4 Fuel Doppler

The change in k-effective with the temperature of the fuel at the core midplane, T_f , is given by

$$\frac{dk_{eff}}{dT_f} = \frac{K_D}{T_f} \tag{5-84}$$

where the left-hand side is the *Doppler coefficient* and K_D is the *Doppler constant*. Integrating the above expression gives

$$\delta k_{eff} = K_D \ln \left(\frac{T_f}{T_{f,0}} \right) \tag{5-85}$$

where the subscript *0* denotes the full power steady-state condition. At this condition the net reactivity of the core is zero and k_{eff} is unity. For a change from this state the new values of ρ and k_{eff} are related by

$$\rho = \frac{k_{eff} - 1}{k_{eff}} \approx \delta k_{eff} \tag{5-86}$$

where δk_{eff} is the change in k-effective in going from full power steady state to the new state. Then from Eqs. (5-85) and (5-86), the reactivity in dollars from the change in fuel temperature is

$$\rho = \frac{K_D}{\beta_{eff}} \ln\left(\frac{T_f}{T_{f,0}}\right) \approx \alpha_D \, (T_f - T_{f,0}) \tag{5-87}$$

where

$$\alpha_D = \frac{K_D}{\beta_{eff} \; T_{f,0}} . \tag{5-88}$$

An estimate for the Doppler temperature coefficient of reactivity, α_D for the VHTR , is given in Table 5-4,

5.3.4.2.5 Net Reactivity

The net reactivity is the sum of the individual components given by Eqs. (5-78), (5-79), (5-82), and (5-87), plus any reactivity added through control rod motion not related to thermal expansion,

$$\rho = \alpha_{cr-v} \, (T_i - T_{i,0}) + (\alpha_{cr-gr} + \alpha_{gr-m}) \, (T_{gr} - T_{gr,0})$$

$$+ \frac{\alpha_{He}}{R}\left(\frac{P}{T_{cl}} - \left(\frac{P}{T_{cl}}\right)_0\right) + \alpha_D \, (T_f - T_{f,0}) + \rho_{rod} . \tag{5-89}$$

5.3.4.2.6 Net Reactivity in Quasi-Static Case

In the case where coolant, moderator, and fuel temperature are in equilibrium with the instantaneous power and flow, the above expression can be simplified. The total change in reactivity due to temperature change is the sum of that associated with the control rods, the moderator, and the fuel and is given by

$$\delta\rho = \alpha_{cr-v} \, \delta T_i + \alpha_m \, \delta T_m + \alpha_{cr-m} \, \delta T_m + \alpha_f \, \delta T_f \tag{5-90}$$

where

T_m = average moderator temperature.

Note that the moderator and fuel temperature changes are related to the reactor power-to-flow ratio and the reactor power through the expressions,

$$\delta T_m = \delta T_i + \frac{\Delta T_{c-100}}{2}\left(\frac{P}{W} - 1\right) + \Delta T_{m-100}(P-1), \tag{5-91}$$

$$\delta T_f = \delta T_i + \frac{\Delta T_{c-100}}{2}\left(\frac{P}{W} - 1\right) + (\Delta T_{m-100} + \Delta T_{f-100})(P-1), \tag{5-92}$$

where

P	=	fission plus decay power normalized to full power condition,
W	=	flowrate normalized to full power condition,
ΔT_{c-100}	=	mixed mean reactor coolant temperature rise at full power condition,
ΔT_{m-100}	=	average moderator temperature rise at full power condition, and,
ΔT_{f-100}	=	average fuel temperature rise at full power condition.

If the feedback components in Eq. (5-90) are linear, then substituting the above expressions into Eq. (5-90) and collecting terms gives

$$\rho = (\alpha_{cr-v} + \alpha_m + \alpha_{cr-m} + \alpha_f)\,\delta T_i + (\alpha_m + \alpha_{cr-m} + \alpha_f)\frac{\Delta T_{c-100}}{2}\left(\frac{P}{W} - 1\right) + \alpha_f(\Delta T_{m-100} + \Delta T_{f-100})\,(P-1) \tag{5-93}$$

or

$$\delta\rho = A(P-1) + B\left(\frac{P}{W} - 1\right) + C\,\delta T_i \tag{5-94}$$

where

$$A = \alpha_f(\Delta T_{m-100} + \Delta T_{f-100}) \tag{5-95}$$

$$B = (\alpha_m + \alpha_{cr-m} + \alpha_f)\frac{\Delta T_{c-100}}{2},$$

$$C = \alpha_{cr-v} + \alpha_m + \alpha_{cr-m} + \alpha_f .$$

5.3.4.2.7 Neutronic Time Constant

For the transients of interest the reactivity is always much less than β so that the prompt jump approximation can be made. If also the number of precursor groups is taken as one, then the normalized fission power is given by

$$\left[\rho(t) - 1\right]\frac{dP}{dt} + \left[\lambda_f \rho(t) + \frac{d\rho}{dt}\right]P(t) = 0 . \tag{5-96}$$

where the reactivity has been normalized to β and has units of dollars. The above equation is rearranged as

$$\frac{d}{dt}P = \frac{1}{\tau}P \tag{5-97}$$

and has solution

$$P = Ke^{t/\tau} \tag{5-98}$$

where

$$\tau = \frac{1-\rho}{\lambda\rho + \frac{d}{dt}\rho} \,. \tag{5-99}$$

The solution reveals the neutron population response has characteristic short and long term behavior. For a near step change in reactivity, in the short term as the reactivity is being added

$$\tau \approx \left(\frac{d}{dt}\rho\right)^{-1} \,. \tag{5-100}$$

Once the near step reactivity has been added, assuming $\rho << 1$, then

$$\tau \approx \frac{1}{\lambda\rho} \,. \tag{5-101}$$

which shows the approach to equilibrium proceeds initially with a time constant longer than that of the delayed neutron time constant followed by a continual lengthening?

An expression for the time constant of the core power when reactivity enters through reactivity feedbacks is obtained as follows. The reactivity is given by

$$\rho = A\left(P-1\right) + B\left(\frac{P}{W}-1\right) + C\delta T_i + \rho_{rod} \tag{5-102}$$

where the power, P, and flowrate, W, are normalized to some equilibrium condition. Here we have assumed that the core temperatures remain in equilibrium as power and flow change (in fact they will lag according to the thermal time constants of the structures that provide the reactivity feedback). From Eq. (5-97) and (5-101), if we let $P=1+\delta P$, $W=1+\delta W$, and drop other than first-order terms, then the power is given by

$$\frac{d}{dP}\delta P = \frac{1}{\tau}\delta P + \lambda\left[-B\delta W + C\delta T_i + \rho_{ext}\right], \quad \tau = \frac{-1}{\lambda\left(A+B\right)} \,. \tag{5-103}$$

5.4 Integrated Plant Power Control System

5.4.1 Reference Plant

The integrated system studied is described in [Davis 2006] as Case 6. In [Oh 2006a] this design was selected as the reference case for the current project and in subsequent reports [Oh 2007b] the design of the HTSE process was expanded upon to include specification of configuration of components and individual component sizes. In the present report a GAS-PASS/H code [Vilim 2004] model developed for the reference case and described in [Oh 2007b] is used to calculate the full power condition and the partial power load schedule. That model is represented by the network diagrams shown in Figures 5-4 through 5-6.

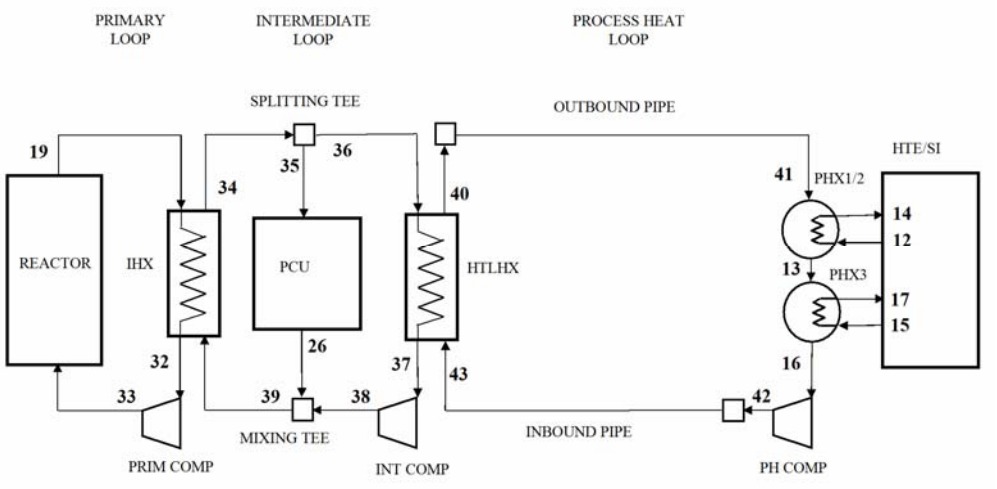

Figure 5-4 Overall Equipment Configuration for VHTR-HTSE Plant.

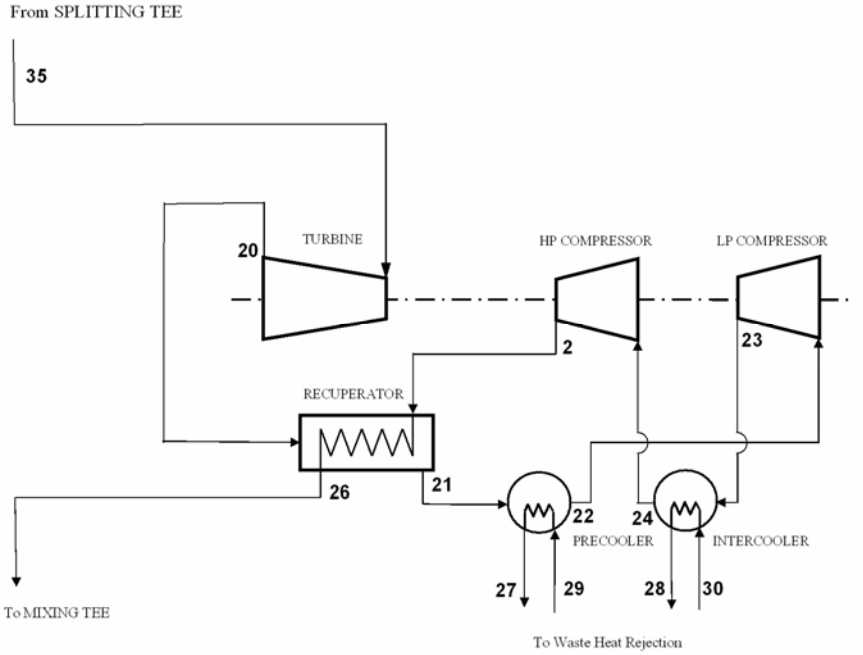

Figure 5-5 Power Conversion Unit Equipment Configuration.

The first figure shows how the reactor, PCU, process heat loop, and HTSE plant are configured. The second figure shows the details of equipment layout for the PCU and the third figure the details of equipment layout for the HTSE plant.

The values of engineering parameters used in the simulation of the reference plant are given in Tables 5-1, 5-5 and 5-6. Heat exchanger dimensions are given in Table 5-1. Compressor and turbine operating characteristics are given in Table 5-5. Electrolyser dimensions and operating characteristics are given in Table 5-6.

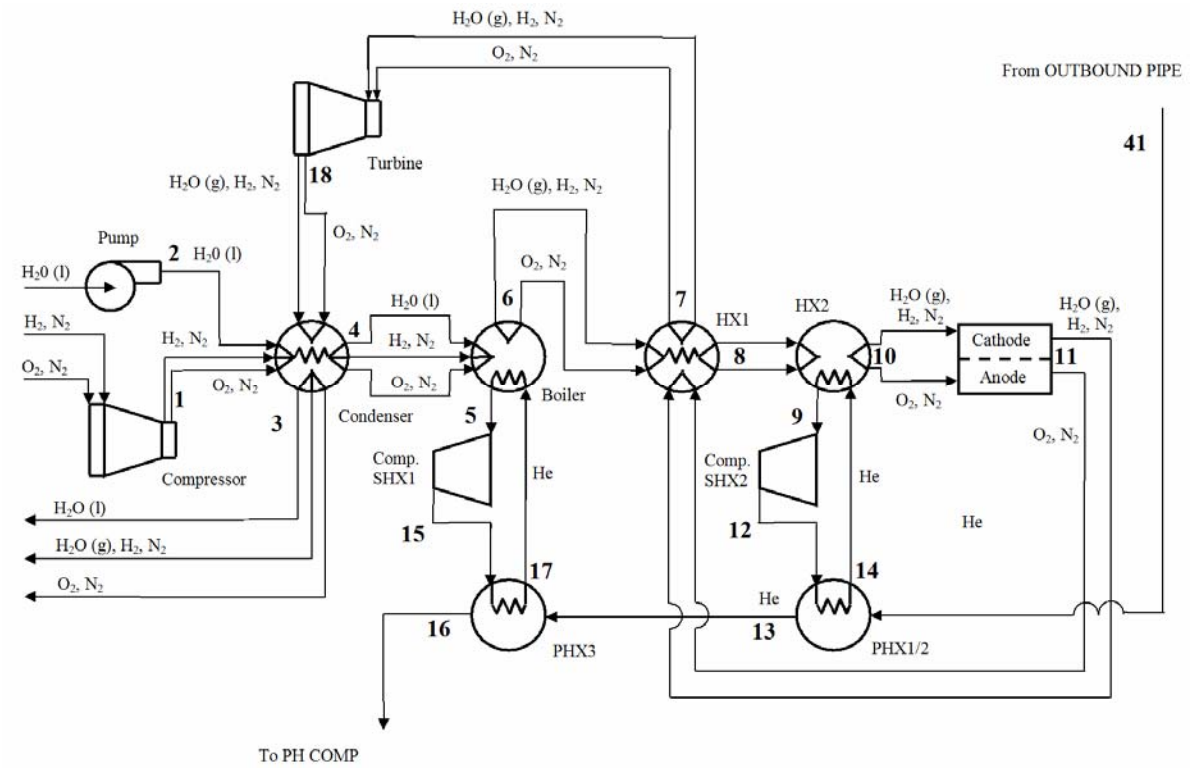

Figure 5-6 High Temperature Steam Electrolysis Equipment Configuration.

5.4.2 Full-Power Design Point

A steady-state full power operating point was calculated with the GAS-PASS/H code model. The boundary conditions used are given in Table 5-7 and were selected based on consideration of the GT-MHR design as described in [Shenoy 1996], the operation of an HTSE plant as described in [Stoots 2005], and the integrated operation of the plants as described in [Davis 2006]. The values of process variables are given in Table 5-8 through 5-11. Conditions in the primary system are given in Table 5-8, conditions in the intermediate system in Table 5-9, conditions in the PCU in Table 5-10, and conditions in the HTSE plant in Table 5-11. The GAS-PASS/H code provides for a sweep gas but none was used in this model. The product stream into the electrolyzer was a boundary condition set to 0.95 and 0.05 mode fractions of H_20 and H_2, respectively. The value for the current boundary condition was selected to give a electrolyzer product output of 0.05 and 0.95 mode fractions of H_20 and H_2, respectively

Table 5-5. Full Power Turbine and Compressor Operating Characteristics.

		Pressure Ratio	Efficiency
Turbine -	HTSE	3.2	0.93
	PCU	3.1	0.94
Compressor -	Primary Loop	1.014	0.89
	Intermediate Loop	1.014	0.89
	Process Heat Loop	1.17	0.89
	PCU Low Pressure	1.83	0.89
	PCU High Pressure	1.82	0.89

Table 5.6. Electrolyzer Dimensions and Operating Characteristics [Vilim 2006a].

	H_2O	H_2	O_2			
A_w (kg/mol)	18.0e-03	2.02e-3	32.0e-3			
C_ρ @ 950°C (J/kg-K)	2.45e03 @50 atm	15.1e3 @ 1 atm	917 @ 1 atm			
A (m^2)	i (amps/m^2)	$(\rho V)_s$ [a] (kg)	$(C\rho)_s$ (J/kg-K)	P/P_{STD}	T (C)	
64e-4	1880	13.9e-3	400	50	816	
F (coul/mol)	R (J/mol-K)	$\frac{(\partial \Delta G)^o}{\partial T}$ [b] (J/mol-K)	ASR[o c] (ohms-cm^2)	C_1 [c] (ohms-m^2)	C_2 [c] (K)	ΔG^o [b] (J/mol)
96,485	8.31	-55.5 @ 1 atm, 950°C	0	8.39E-4	8,030	2.02e5 @ 1 atm, 950°C

[a] [Hartivigsen 2006], [b] [Ohta 1979], [c] [Pradhan 2006]

Table 5-7. Boundary Conditions Used to Determine Full Power Operating Point.

Power (MW)	Reactor	Generator					
	594	280					
Temperature (°C)	HTSE Reactant Inlet	Precooler Cold Side Inlet	Intercooler Cold Side Inlet				
	21	21	21				
Flowrate (all species) (kg/s)	Electrolyzer Inlet	Compressor SHX1	Compressor SHX2	Precooler Cold Side Inlet	Intercooler Cold Side Inlet	Primary Compressor	Process Heat Loop Compressor
	21.5	51.8	10.4	21	21	288	25.1
Mode Fractions	Electroyzer Inlet – H_2O	Electrolyzer Inlet – H_2					
	0.95	0.05					
Current (amps)	Electrolyzer						
	217						

Table 5-8. Primary System Full Power Conditions.

	Reactor	IHX Hot Side	Primary System Compressor
Power (MW)	594	601	7
Outlet Temperature (°C)	887	485	490
Outlet Pressure (MPa)	7.09	7.04	7.13
Mass Flowrate (kg/s)	288	288	288

Table 5-9. Intermediate System Full Power Conditions.

	IHX Cold Side	HTLHX Hot Side	Mixing T	Intermediate Compressor
Power (MW)	601	436	0	0.9
Outlet Temperature (°C)	485	611	478	617
Outlet Pressure (MPa)	7.04	7.27	7.37	7.37
Mass Flowrate (kg/s)	288	32.4	291	32.4

Table 5-10. Power Conversion Unit Full Power Conditions.

	Turbine	Recuperator Hot Side	Recuperator Cold Side	HP Compressor	LP Compressor	Precooler Hot Side	Inter-cooler Hot Side
Power (MW)	534	462	462	126	127	151	127
Outlet Temperature (°C)	479	141	461	123	124	30	30
Outlet Pressure (MPa)	2.36	2.31	7.37	7.43	4.13	2.26	4.08
Mass Flow Rate (kg/s)	263	263	263	263	263	263	263

Table 5-11. High Temperature Steam Electrolysis Plant Full Power Conditions.

		Condenser	Boiler	HX1	HX2	Turbine	Cell	PHX1/2	PHX3
Power (MW)	Hot Side	18.8	43.2	24.9	5.32	11.5	288	5.3	43.2
	Cold Side	18.8	43.2	24.9	5.32			5.3	43.2
Outlet Temperature (°C)	Hot Side	43	328	545	725	340	968	800	469
	Cold Side	184	247	712	817			842	488
Outlet Pressure (MPa)	Hot Side	1.53	5.0	5.0	5.0	1.56	5.0	1.76	1.71
	Cold Side	5.00	5.0	5.0	5.0			5.0	5.0
Mass Flowrate - All Species (kg/s)	Hot Side	21.5	51.8	21.5	10.4	21.5	21.5	25.1	25.1
	Cold Side	21.5	21.5	21.5	21.5			10.4	51.8

5.4.3 Power Control Scheme

The integrated system must be capable of operating to meet production demands that originate beyond the plant fence, most likely from the operator of a hydrogen pipeline or storage facility. This necessarily implies the plant must be able to startup and shutdown and meet partial production demands. In this section control schemes for operating the plant at partial production levels are described. It considers the quasi-static case where production levels are changed in a slow enough manner that dynamics are not excited. More rapid changes in load are addressed in the next section. Control schemes are developed for meeting hydrogen production rates that lie in the range 30 to 100 percent of full power production. It is possible that yet to be performed research on energy systems and their mix in the U.S. may conclude that there is no requirement for partial load operation. Perhaps operation between only 80 and 100 percent full power, as is typical for a chemical plant, will be all that is needed. Modeling and simulating startup and shutdown is more complex as described in Section 5.2.4. This task will be performed later in this project.

A main objective in developing a control strategy for partial load operation is to maintain temperatures, particularly hot end temperatures (~ 900 C), constant with power over the 30-100 percent power range. Another consideration is that peak efficiency occurs at full power since the plant is to operate there for the largest fraction of life. While partial load efficiency is important, maintaining constant temperatures over load at the hot end is probably more important since material capabilities at 900 C are a limiting factor in plant lifetime. Development of a control strategy is therefore focused on maintaining constant hot end temperatures.

The first control strategy examined makes use of the principle that the temperature change from inlet to outlet in a heat exchanger remains constant when the mass flowrate and power are varied in the same proportion. This is true for ideal-like gases such as helium, hydrogen, oxygen, and nitrogen and for the liquid and gas phases of water. It is not true, however, for water when there is a phase change. In the HTSE plant and its process heat loop there are a total of five

compressor and pumps with which to manage mass flowrate in response to power in heat exchangers (to the first order heat exchanger power varies linearly with hydrogen production rate). In the PCU and primary system there is only one compressor to manage mass flowrate while there are several different circuits. To achieve the desired control of mass flowrate helium inventory control is used. Essentially because density is proportional to pressure for fixed temperature, by varying pressure and maintaining constant speed turbomachinery, gas velocity remains constant and mass flowrate (proportional to the product of density and velocity) is linear with pressure. Thus, pressure is manipulated through coolant mass inventory so that it is proportional to heat exchanger power so that in turn mass flowrate is proportional to heat exchanger power. The result for this control scheme is described below.

A load schedule was formulated to give the value of all process variables in terms of fraction of full power hydrogen production rate. The control scheme that realizes this prescribes all controlling process variables (i.e. forcing functions) as a function of fraction of full power hydrogen production rate which is taken as the independent variable (or equivalently, electrolyzer electrical current where it has been assumed all current goes to decompose water). The following controlling process variables were selected: reactor power, eight mass flowrates, plus the electrolyzer current, for a total of ten forcing functions. The need for ten forcing functions follows from the number of equations in the model and the dictate that there be a unique solution. As a cross check, the number of forcing functions needed was independently derived from consideration of the physics alone. Other sets of ten could be used but this set was appealing based on the discussion above. Each of these ten forcing functions was linearly ramped from its full power value at one end to a value of 30 percent of this at the other end. Hence, the load schedule covers the range of operation from 30 to 100 percent of the full power hydrogen production rate.

The load schedule is assessed primarily on the degree to which temperatures on the hot side of the combined plant are maintained constant. Also of interest are the pressures on the helium side for assessment of creep under pressure load. The pressures in the HTSE plant were maintained at 5 MPa over the load schedule from downstream of where the reactant water in fed in up to the point where the products enter the pressure-work recovery turbine.

The temperatures in the hot side of the coupled plant are shown in Figures 5-7 and 5-8. The first figure shows the temperatures in the HTSE plant and the second figure shows temperatures in the VHTR plant. The temperatures in the latter vary by no more than 30 C over the load range. However, in the HTSE plant, the electrolyzer outlet varies by more than 400 C over the load range. The inlet to the electrolyzer is essentially constant temperature. Other temperatures in the HTSE plant vary by 100 to 200 C. These temperature changes with load, especially at the electrolyzer outlet are probably not acceptable since they will limit the rate at which the plant could change power. Cold side temperatures in the combined plant are shown in Figure 5-9. The largest temperature change is about 150 C in the process heat loop inbound pipe. Helium loop pressures are shown in Figure 5-10. Pressure is to a first order proportional to hydrogen production rate, a consequence of inventory control. The production and consumption of power by major system components is shown in Figure 5-11. Essentially all the thermal power produced by the VHTR is consumed by thermal loads in the HTSE plant and in generating electricity to power electrical loads which include the electrolyzer and pumps and compressors. But as described in [Vilim 2007], there is a potential for supplanting some of the thermal load with waste heat so that the combined plant could be a net exporter of electricity to the grid.

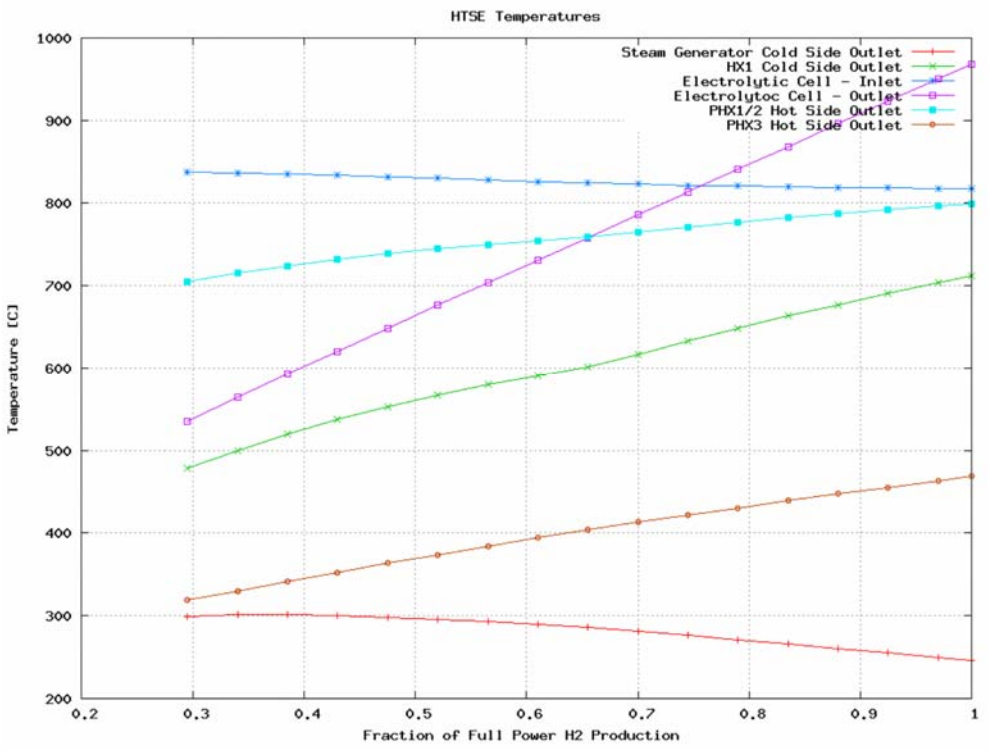

Figure 5-7 Temperatures in High Temperature Steam Electrolysis Plant.

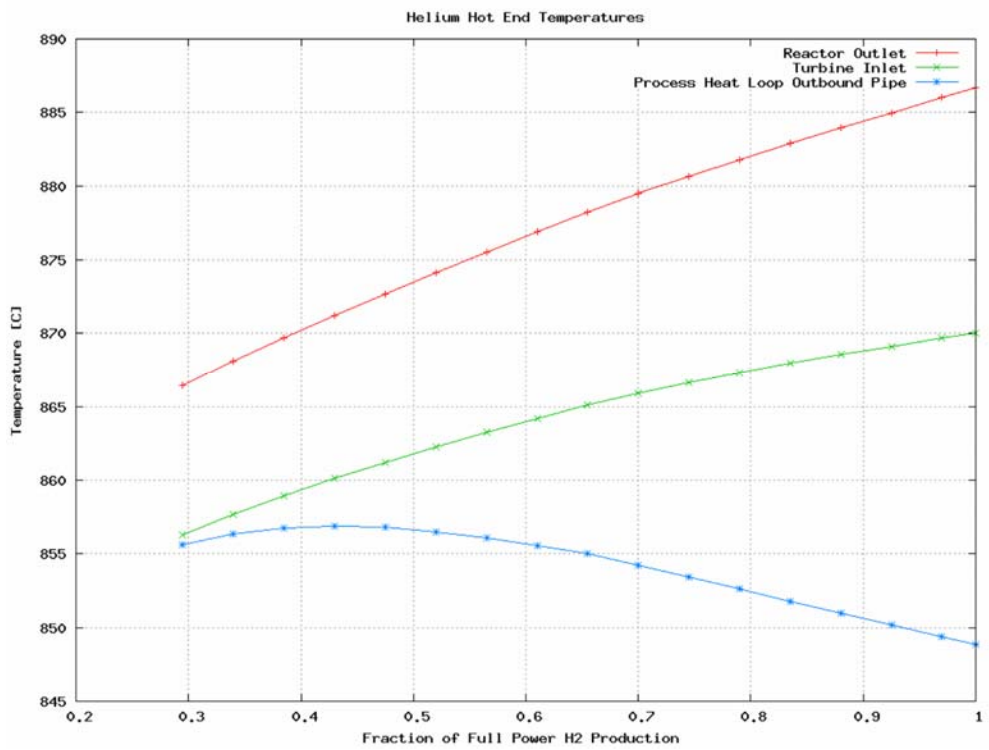

Figure 5-8 Temperatures in Hot End of VHTR Plant.

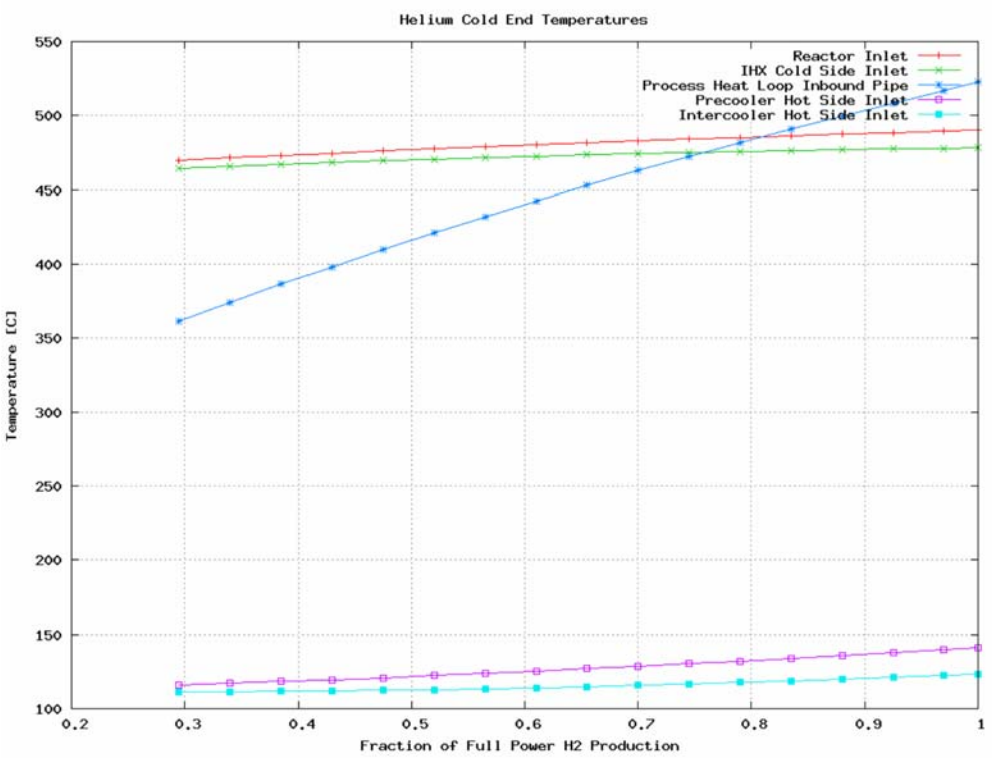

Figure 5-9 Temperatures in Cold End of VHTR Plant.

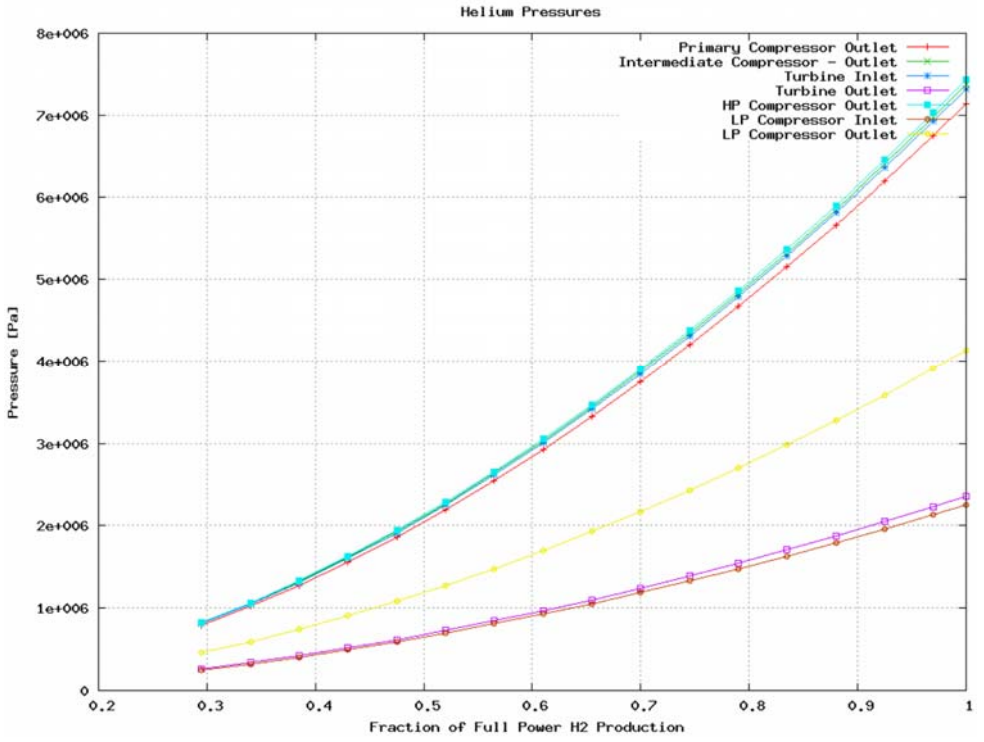

Figure 5-10 Pressures in Helium Loops.

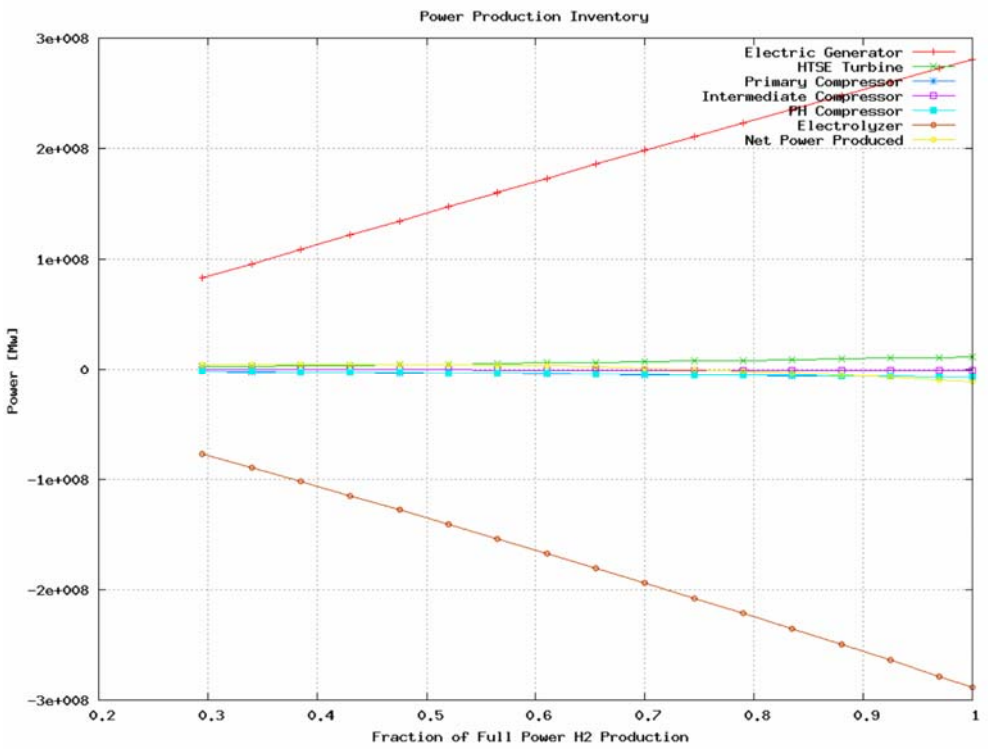

Figure 5-11 Power Production and Consumption in Major System Components.

Because the electrolyzer sensible heat is recuperated externally at the exit of the recuperator, there is a significant temperature rise in the electrolyzer during full power operation. If the resulting spatial temperature gradient is unacceptable, then either internal recuperation or operating the cell at a current density where there is no sensible heat generated along the length between inlet and outlet can be used to reduce the size of the gradient. The latter option has the disadvantage that the required current density will be lower resulting in an increase in cell area per unit hydrogen production rate and poorer economics. Internal recuperation would seem to be the preferred solution since it involves only passing a counter current gas flow over the individual cells lined up from inlet to outlet.

There is an additional disadvantage associated with the control strategy just described. Because the sensible heat available for external recuperation depends nonlinearly with hydrogen production rate, the inlet temperature to the electrolyzer varies significantly (~ 400 C) over the 30-100 percent hydrogen production range. One solution to this problem is to increase the current density at lower powers and generate more sensible heat per unit product mass flowrate. This can be achieved by reducing the active cell area per unit hydrogen production (i.e. operate fewer cells). This scheme was explored with GAS-PASS/H to see how effective it might be. The results are shown in Figure 5-12 through 5-14. Clearly, this is effective as seen in Figure 5-12 where the ranges of electrolyzer inlet and outlet temperature have been significantly reduced.

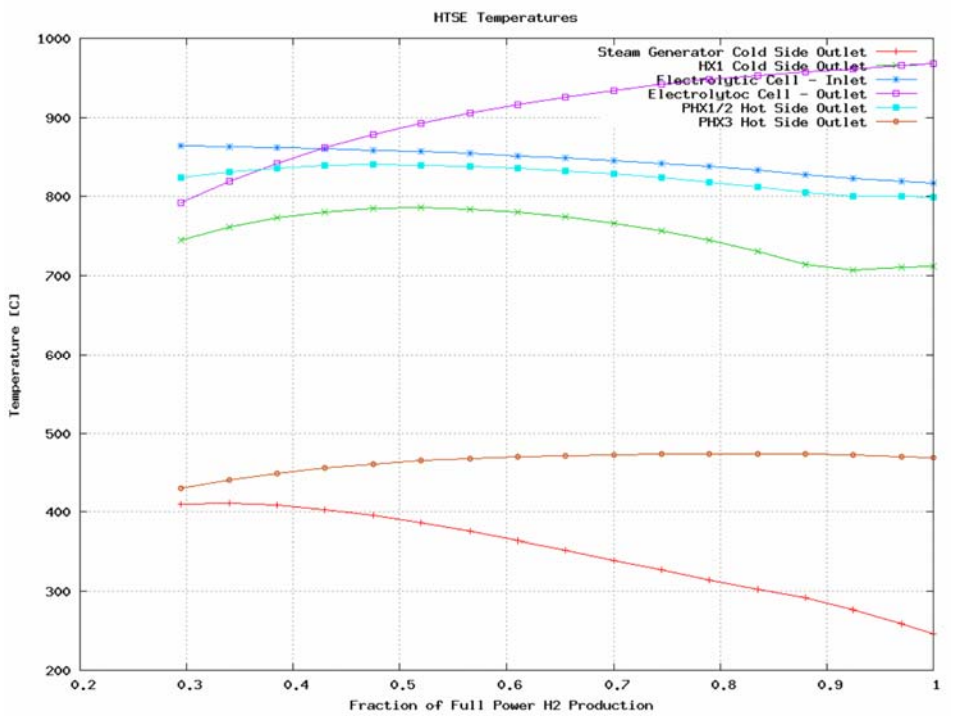

Figure 5-12 Temperatures in High Temperature Steam Electrolysis Plant for Reduced Cell Area.

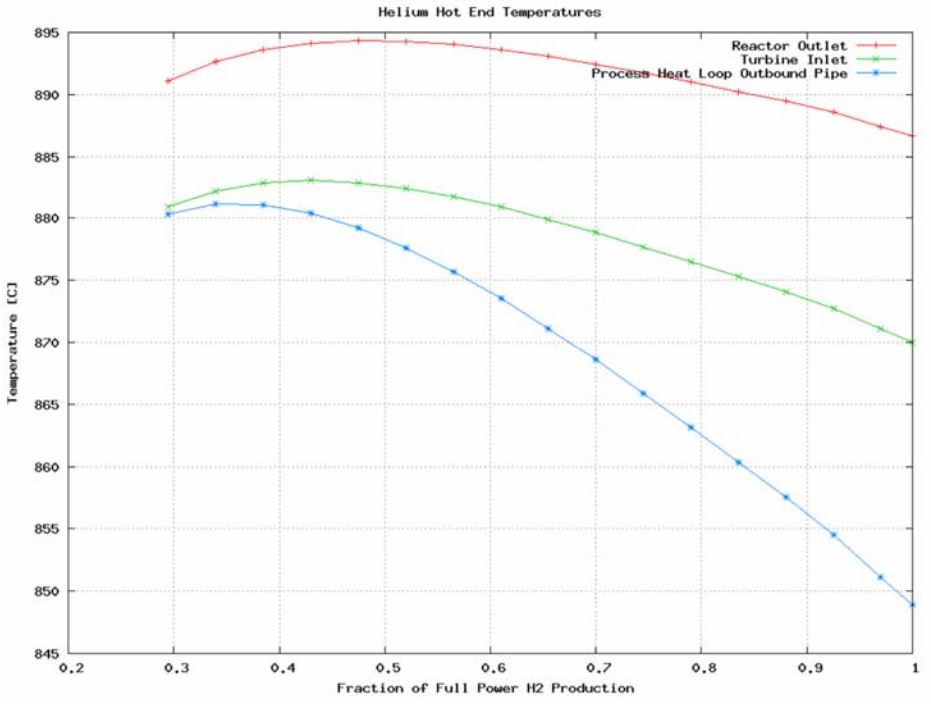

Figure 5-13 Temperatures in Hot End of VHTR Plant for Reduced Cell Area.

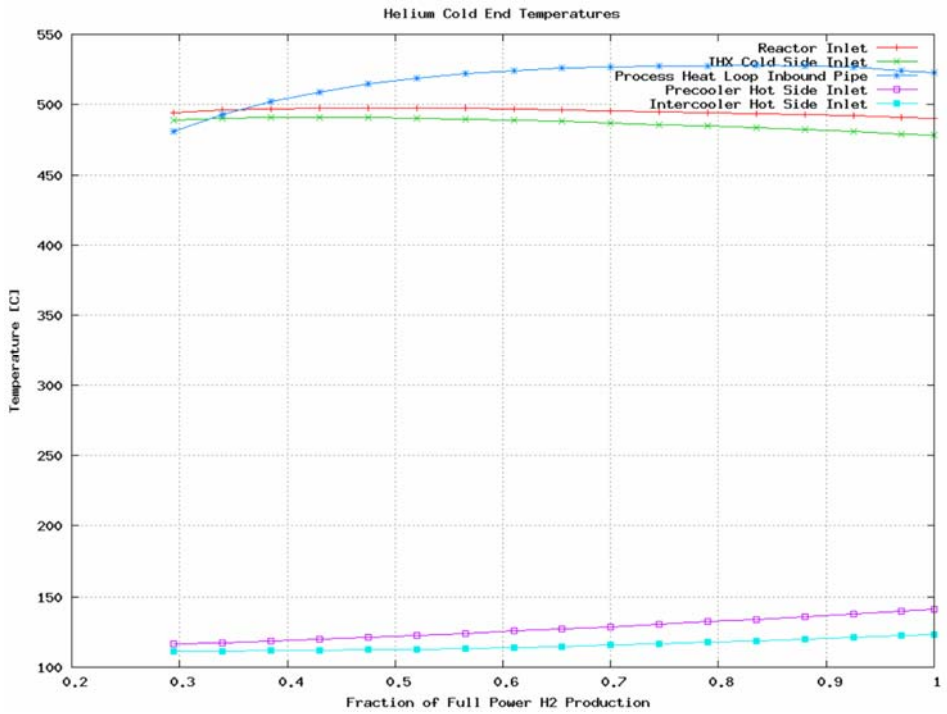

Figure 5-14 Temperatures in Cold End of VHTR Plant for Reduced Cell Area.

The electrolyzer outlet temperature range is now 180 C, down from over 400 C. These results were obtained for a linear ramp in cell area starting with the previous value at full power value down to a fraction 0.4 at 30 percent hydrogen production rate. There is also a reduction in the temperature variation in the process heat inbound pipe as seen by comparing Figure 5-9 with Figure 5-14. In general then, managing active cell area during load change can lead to a reduction in temperature swings seen in components.

In Section 5.2.3 the mathematical basis for obtaining a desired load schedule is given. From this development it is clear that a combination of flowrate (compressor and pump) and current density control should permit the results in Figures 5-12 through 5-14 to be refined so that hot end temperature changes with load are further reduced. This is left for future work.

5.5 Plant Transient Behavior

5.5.1 Time Constants and Energy Capacitances

5.5.1.1 Electrolyzer

The cell time constant of Section 5.3.1 is evaluated for representative VHTR/HTSE cell conditions. For simplicity it was assumed the reactant stream is pure water vapor and that it is completely decomposed in the cell. The data input to the calculation are shown in Tables 5-12 through 5-14. It is assumed the reactant stream is pure water vapor and that it is completely decomposed by the cell as shown in Table 5-12. Representative operating conditions are given in Table 5-13. The values for cell mass and specific heat include only the electrodes and the

electrolyte and not the separators, edge rails, or flow forms according to the rationale given earlier. The cell mass is from [Hartvigsen 2006]. The ASR data is from [Pradhan 2006]. The expression for the cell time constant (Eq. (5-26)) yielded a value of 206 s for this data.

The cell energy capacitance of Section 5.3.1 is also evaluated for representative VHTR/HTSE cell conditions. The mass of a cell of electrode area 64 cm^2 as obtained from [Hartvigen 2006] was multiplied by the estimated specific heat of the cell material and the number of such cells to obtain the energy capacitance. The number of cells was obtained by taking the total electrode area in Table 5-15 and dividing by 64 cm^2. The calculation is shown in Table 5-15 and yields a value of 270 MJ/K. It should be noted, however, that design optimization has not yet been performed and so electrode area is subject to some uncertainty. More aggressive operation of the cell could reduce total electrode area by up to a factor of ten compared to the value given in Table 5-15. The estimated thermal capacitance would decrease by this same factor. The time constant and energy capacitance values have been entered in Table 5-18.

The validity of assumptions made in the derivation of the one-dimensional model of Section 5.3.1 has been examined. The model ignores the two-dimensional nature of the temperature distributions in the electrodes, electrolyte, and gas streams that arise as a consequence of the planar rectangular geometry of the cell and the 90 degree difference in angle of incidence between the two gas streams. In addition the heat capacity of the steel separators and edge rails is neglected since their temperature state is thought to be not tightly thermally coupled to the electrodes and electrolyte.

An experiment [Pradhan 2006] provided an opportunity to validate the expression for the time constant given by Eq. (5-26). In the experiment the identical Cerametec cell that is being used for water splitting SOEC studies at Idaho National Laboratory (INL) was run in fuel cell mode. The conditions are the same as in Table 5-12 through 5-14 with the exception that the pressure was atmospheric and that hydrogen and oxygen were fed into the cell rather than removed from the cell. The cell was operated at atmospheric pressure and hydrogen and oxygen were fed into rather than removed from the cell. The mole fractions of hydrogen, oxygen, and water estimated from [Pradhan 2006] were 0.46, 0.2, and 0.85. The water-splitting model in Section 5.3.1 was modified to describe a fuel cell by a change of sign on the Nernst potential and the Gibbs standard free energy of formation (to account for interchange of products and reactants). With these adjustments and for the conditions in [Pradhan 2006] Eq. (5-26) yields a cell time constant of 279 s.

A value for the time constant of the cell was derived from data in [Pradhan 2006] by empirical curve fitting. In the experiment the fuel cell was at a steady state prior to a step change in the cell current. The measured cell outlet temperature during the subsequent transient appears in Figure 5-15. The description in [Pradhan 2006] indicates there was an initial power supply problem and, hence, the appearance of a saw tooth on the ramp up in temperature. We have attempted to adjust for this by backward extrapolating in time after the occurrence of the sawtooth. Figure 5-15 shows the back calculation of a value for the time constant from the experiment data. The value from Eq. (5-26) (i.e. 279 s as given above) differs by 19 percent from the value of 235 s obtained from Figure 5-15 by curve fitting. This suggests that the assumptions underlying the derivation in Section 5.3.1 are reasonable from the standpoint of estimating an approximate measure of cell outlet temperature time response.

Table 5-12 Species Data for Electrolytic Cell Time Constant Estimate.

	H_2O	H_2	O_2
A_w (kg/mol)	18.0e-3	2.02e-3	32.0e-3
C_ρ @ 950°C (J/kg-K)	2.45e+3 @50 atm	15.1e3 @1 atm	917 @1 atm
F	1.0	0.67	0.33

Table 5-13 Operating Data for Electrolytic Cell Time Constant Estimate.

A (m^2)	i (amps/m^2)	$(\rho V)_s$ [c] (kg)	$(C_\rho)_s$ (J/kg-K)	P/P_{STD}	T (C)
64e-4	1880	13.9e-3	400	50	816

[a] [Hartivigsen 2006]

Table 5-14 Other Data for Electrolytic Cell Time Constant Estimate.

F (coul/mol)	R (J/mol-K)	$\frac{(\partial \Delta G)^{o\ a}}{\partial T}$ (J/mol-K)	ASR_o [b] ($ohms\text{-}cm^2$)	C_1 [b] ($ohms\text{-}m^2$)	C_2 [b] (K)	$\Delta G^{o\ a}$ (J/mol)
96,485	8.31	-55.5 @1 atm, 950°C	0	8.39e-4	8,030	2.02e5 @1 atm, 950°C

[a][Ohta 1979] [b][Pradhan 2006] [c][Hartvigsen 2006] (electrodes and electrolyte)

Table 5-15 Electrolytic Cell Time Constant and Energy Capacitance.

T (s)	Cell area = 225 cm^2		Cell area =64 cm^2		
	No. of cells[b]	Stack Electrode Area (m^2)	No. of Cells	$(\rho V)_s (C_\rho)_s$ per Cell (J/K)	Total[a] $(\rho V)_s (C_\rho)_s$ (J/K)
206	14e06	0.0225*14e06= 3.15e5	3.15e5/0.0064= 49.2e06	13.9e-03*400= 5.56	5.56*49.2e06= 270e06

[a] Electrodes and electrolyte only

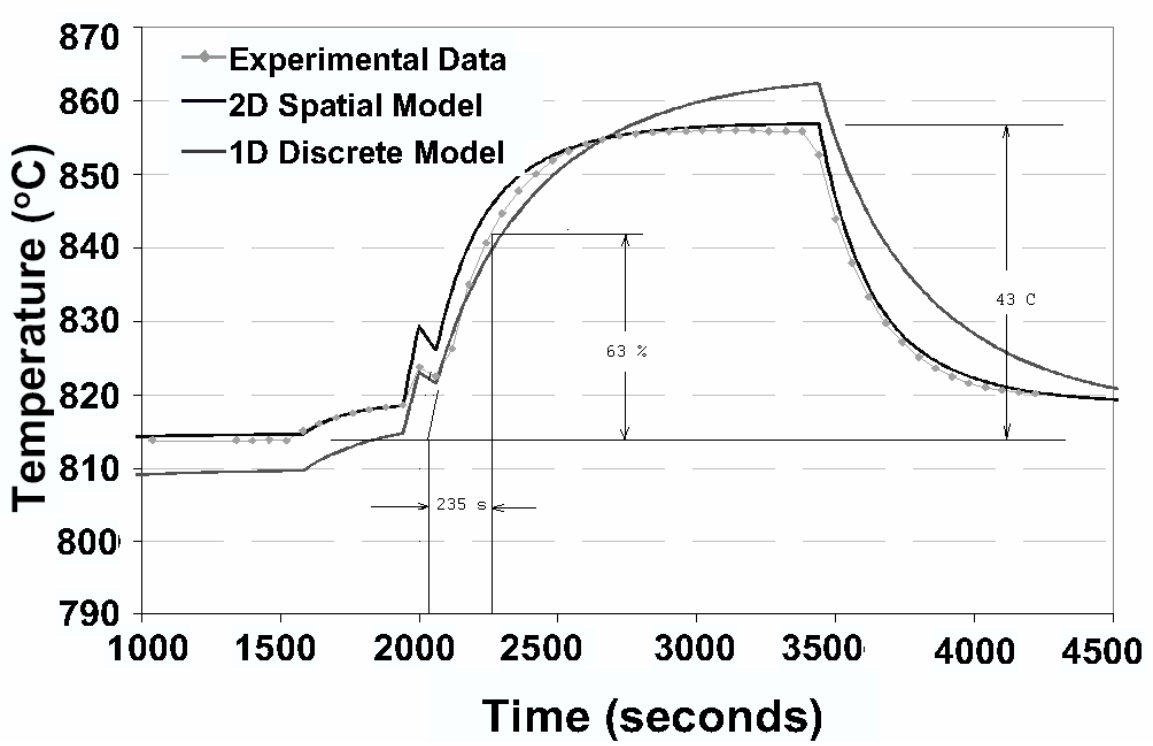

Figure 5-15 Time Constant for an Electrolytic Cell Operating in the Fuel Cell Model.

5.5.1.2 PCHE Heat Exchangers

As described previously there are incentives to choose printed circuit type heat exchangers for heat transfer circuits that use a gas coolant. In the reference configuration for the combined plant shown in Figure 5-4 the recuperator in the PCU and heat exchangers IHX and HTLHX are assumed to be PCHEs. Time constants and energy capacitances are calculated for these units from the models developed in Section 5.3.2.

Design data for these heat exchangers are taken from [Oh 2006c] and are reproduced in Table 5-16. Thermo-physical properties used in the calculation are given in Table 5-17. Values for heat transfer parameters associated with the models of Section 5.3.2 are given in Table 5-19. The three time constants associated with the hot side of the PCHE are shown in Table 5-20. Note that there are corresponding time constants not shown for the cold side. They were not calculated as their values will be similar to those for the hot side.

Inspection of Table 5-20 shows that the heat exchanger metal has an energy capacitance at least five times greater than the next highest source of capacitance. The time constants associated with the other capacitances are at least a factor of ten faster than for the metal. Thus, the heat exchanger response is dominated by the metal behavior. Table 5-21 shows the calculation of the metal capacitance. The cold side metal is accounted for by doubling the capacitance of the hot side metal. The time constants shown are those for the metal taken from Table 5-20. This data is reproduced in Table 5-18.

Table 5-16 Design Data for Helium Printed Circuit Heat Exchangers [Oh 2006c].

	IHX	HTLHX	PCU Recuperator
Channel Diameter, $2r$ (m)	1.5e-03	1.5e-03	1.5e-03
Channel Pitch, P (m)	1.8e-03	2.25e-03	2.56e-03
Plate Thickness, t (m)	8.55e-04	1.17e-03	1.79e-03
Channel Length, l (m)	2.34	1.089	1.62
Number of Channels, $N_{channels}$ (one side)	7.33e06	4.36e05	4.264e06
In Width Direction	2639	673	2443
In Height Direction	2778	648	1745
Hot Side Flow, w (kg/s) - Total	289	32.1	260
$w_{channel}$ - Per Channel	3.94e-05	7.36e-05	6.10e-05
Cold Side Flow, w (kg/s) - Total	292	27.5	260
$w_{channel}$ - Per Channel	3.98e-05	6.31e-05	6.10e-05
Width (m)	4.75	1.52	6.23
Height (m)	4.75	1.52	6.23
Volume (m^3)	52.8	2.5	62.9

Table 5-17 Thermo-Physical Properties for Helium Printed Circuit Heat Exchangers.

	IHX	HTLHX	PCU Recuperator
$(C_p)_m$ (J/kg-K)	500	500	500
$(C_v)_h = (C_p)_h - R$ (J/kg-K)	3114	3114	3114
$(C_p)_h$ (J/kg-K)	5200	5200	5200
ρ_h (kg/m^3)	3.59	3.47	2.18
ρ_m (kg/m^3)	8000	8000	8000
k_m (J/m-s-K)	22	23	16.4

Table 5-18 Summary of Thermal Time Constants and Capacitances.

	Time Constant (s)	Energy Capacitance (MJ/°C)	Ref.	Notes
Reactor Vessel				
Active Core				
Fuel Elements	9.5	200		
Neutronics	3.7	-		
He Coolant	2.8[a]	4.7		Assumes 0.2 void fraction
Internals	unknown	unknown		
Wall	4000	1000		< 500 C
Intermediate System				
IHX	0.28	27		
Flow Paths	unknown	unknown		
Power Conversion Unit				
Turbine	-	8.0[b]		
Recuperator	1.9	95		
Vessel Wall	2300	1000		< 500 C
Coolers	-	-		< 200 C
Compressors	-	-		< 200 C
HTSE Plant				
HTLHX	0.96	2.8		
Outbound Pipe				
Pipe Wall	21	2.3		100 m; molten salt
Coolant	12	4.3		100 m; molten salt
Inbound Pipe				
Pipe Wall	21	2.3		100 m; molten salt
Coolant	12	4.3		100 m; molten salt
Condenser	30	7		
Boiler	20	2.3		
Superheater HX1	35	4.5		
Electrolytic Cells	206	270		

[a] Mixing [b] Based on mass of rotor and static structure estimated to be 16,000 kg

Table 5-19 Hot-Side Heat Transfer Parameters for Helium Printed Circuit Heat Exchangers.

	IHX	HTLHX	PCU Recuperator
θ (rads), Eq. (13)	0.285	0.285	0.285
C_h (m), Eq. (14)	0.00193	0.00193	0.00193
A_h (m^2), Eq. (14)	5.71e-07	5.71e-07	5.71e-07
h_{h-m} (J/m-s-K) (Ref. C. Oh, 2006a)	1660	1715	2089
$\overline{h}_{h-m}$ (J/m-s-K), Eq. (4)	2.82	3.1	3.61
A_m (m^2)	1.98e-07	7.45e-07	1.72e-06

Table 5-20 Time Constants for Helium Printed Circuit Heat Exchangers.

	IHX	HTLHX	PCU Recuperator
$(\rho A l C_v)_h$ (joules/^{o}C)	0.0150	0.00672	0.00628
$(C_p w)_h$	2.05e-01	3.83e-01	3.17e-01
$(\rho A C_v)_h$	0.00638	0.00617	0.00388
$(\rho A C_p)_m$	7.94e-01	2.98	6.88
$\tau_{i-h} = \frac{(\rho A l C_v)_h}{(C_p w)_h}$ (s)	0.07	0.02	0.02
$\tau_{h-m} = \frac{(\rho A C_v)_h}{\bar{h}_{h-m}}$ (s)	0.002	0.002	0.001
$\tau_{m-h} = \frac{(\rho A C_p)_m}{\bar{h}_{h-m}}$ (s)	0.28	0.96	1.9

Table 5-21 PCHE Time Constant and Energy Capacitance.

	IHX	HTLHX	PCU Recuperator
Metal Energy Capacitance $(\rho A C_p)_m$ per channel (J/C-m)	7.94e-01	2.98	6.88
Channel Length, l (m)	2.34	1.089	1.62
Number of Channels, $N_{channels}$ (one side)	7.33e06	4.36e05	4.264e06
Total Capacitance, $2\ (\rho A C_p)_m\ l\ N_{channels}$ (MJ/C)	27	2.8	95
Dominant Time Constant	0.28	0.96	1.9

5.5.1.3 Boiler

The expression for the boiler time constant given by Eq. (5-64) is dependent on the internal geometry and dimensions of the heat exchanger. At this time the boiler design is known only to the level of thermal power and UA. Rather than perform a detailed design effort to obtain this additional data, engineering scaling principles are applied to a unit for which a complete design is available. The unit is the 300 MWt Oconee once-through steam generator for which a dynamic model was developed in [Vilim 2001]. The temperatures and pressure conditions used in this model are similar to those in the HTSE plant while the heat transfer rate is based on heat transfer correlations. So it is expected the numbers obtained should be representative for the purposes of scoping calculations.

The Oconee unit and related model [Vilim 2001] additionally have subcooled and superheat regions. It is advantageous then not limit to limit treatment of the time constant to just the boiler, but to set up a similar correspondence between HTSE superheater and condenser components with once-through steam generator superheated and subcooled regions, respectively. Note that since the condensation heat rate in

the HTSE condenser is a small fraction of the component heat load, it will be ignored. The condenser can then be treated as a heat exchanger with subcooled water on one side and vapor on the other and data obtained from the subcooled region of the once-through steam generator.

In obtaining the heat exchanger data from the correspondences defined above, the assumption is made that the heat transfer coefficient in each of the superheater (HX1), boiler, and condenser in Figure 5-6 has the same value as in the corresponding regions of the Oconee model. This is a reasonable assumption since the underlying heat transfer mechanisms are the same between corresponding regions. In this case, individually for each region

$$\left(\frac{Q}{A\,\Delta T}\right)_{OT} = \left(\frac{Q}{A\,\Delta T}\right)_{HTSE} \tag{5-104}$$

where Q is the thermal power, A is the heat transfer coefficient, and ΔT is the log mean temperature difference and subscript OT represents once-through. The heat transfer areas are then related through

$$\frac{A_{HTSE}}{A_{OT}} = \left(\frac{Q}{\Delta T}\right)_{HTSE}\left(\frac{\Delta T}{Q}\right)_{OT}. \tag{5-105}$$

This scaling law is used to obtain HTSE design data from the once-through design.

The area scaling factor on the left-hand side of the above equation is calculated for each of the HTSE condenser, boiler, and superheater. These components appear in Figure 5-6 and the data used are from the HTSE plant data in Table 5-11 and the once-through unit in [Vilim 2001]. Note that the HTSE plant contains superheaters HX1 and HX2 having thermal power 26 and 5 MWt, respectively. For the purposes of computing time constants and energy capacitances, HX2 is ignored because its effect on time behavior is second order. The input data and the calculated values of the area scaling factor are shown in Table 5-22. Note the expression for the log mean temperature difference, ΔT, differs between the single phase and two-phase cases.

In applying the area scaling factor to compute heat exchanger dimensions, it is assumed the adjusted area in going from once-through to HTSE plant is achieved by changing only the number of heat exchanger tubes. Then the parameters shown in Table 5-23 are assumed to remain constant. The number of tubes and the areas on either side of a HTSE heat exchanger are shown in Table 5-24 as derived by applying the scaling factor to the values of these same parameters in the once-through design. The energy capacitances are assumed to scale similarly. Values are given in Table 5-25.

The values of the time constants for each of the superheater, boiler, and condenser in the HTSE plant are given in Table 5-26. These values are from the once-through steam generator in [Vilim 2001]. It has been assumed that in adjusting the areas from once-through to HTSE the mass of coolant and structure and the flowrates change by the same factor. This will be true when the flowrates scale proportionally with power which would be the case if the log mean temperature difference remains unchanged. Since this is not exactly the case the time constant values from the once-through unit provide only approximate values.

The representative time constant and energy capacitance finally used for each HTSE component was obtained as follows. Identified in Table 5-25 in bold is the energy capacitance with the largest value among the four energy capacitances for each component. Note that each value is at least twice as big as the next largest value. To the first order then the time constant of the associated capacitance dominates.

These time constants are taken as representative of the components and are shown in Table 5-26 in bold. The bolded values are shown reproduced in summary in Table 5-18.

Table 5-22 Area Factor for Scaling from 300 MWt Oconee Once-Through Steam Generator to HTSE Water Heat Exchangers

Region-to-Component Correspondence		Q (MWt)		T_{hi} (C)		T_{ho} (C)		T_{ci} (C)		T_{co} (C)		ΔT (C)			$\frac{A_{HTE}}{A_{OT}}$
OT Region	HTSE Component	OT[b]	HTSE[c]	OT	HTSE	OT	HTSE	OT	HTSE	OT	HTSE	Eq.()	OT	HTSE	
Subcooled	Condenser[a]	16	15.4	303	304	293	68	266	21	286	182	18a	21	79	0.26
Two-Phase	Boiler	244	43.4	452	500	303	339	286	257	286	257	19a	65	148	0.078
Superheated	HX1	40	26	476	989	452	540	286	257	347	742	18a	147	264	0.36

[a] Vapor condensing on hot side is small part of total heat load so hot side behaves very nearly as a single phase coolant
[b] [Vilim 2001]
[c] Table 4-8

Table 5-23 Dimensions Preserved in Scaling from Once-Through Steam Generator to HTSE Water Heat Exchangers

Parameter	Value [Vilim 2001]
Tube Length (m)	
Subcooled/Condenser	1.14
Two-Phase/Boiler	0.86
Superheater/HX1	1.00
Tube Outside Diameter (m)	1.67E-02
Tube Inside Diameter (m)	1.27E-02
Tube Pitch-to-Diameter ratio	1.355
Shell Thickness	2.0E-02

Table 5-24 HTSE Water Heat Exchanger Dimensions Scaled from 300 MWt STAR-LM Once-Through Steam Generator.

Water Phase Region-to-Component Correspondence		Number of Tubes		Flow Area on Water Side (m^2)		Flow Area on Non-Water Side (m^2)*	
STAR-LM Region	HTSE Component	STAR-LM	HTSE	STAR-LM	HTSE	STAR-LM	HTSE
Subcooled	Condenser	26720	6900	5.99	1.6	3.39	0.88
Two-Phase	Boiler	26720	2100	5.99	0.47	3.39	0.26
Superheated	HX1	26720	9600	5.99	2.2	3.39	1.2

* Based on coolant with specific heat and heat transfer properties of PbBi

Table 5-25 HTSE Water Heat Exchanger Energy Capacitances Scaled from 300 MWt STAR-LM Once-Through Steam Generator.

Water Phase Region-to-Component Correspondence		Energy Capacitance of Shell Structure on Water Side (MJ/C)		Energy Capacitance of Tube Structure on Non-Water Side (MJ/C)		Energy Capacitance of Water in Contact with Shell (MJ/C)		Energy Capacitance of Coolant in Contact with Tube (MJ/C)*	
STAR-LM Region	HTSE Component	STAR-LM	HTSE	STAR-LM	HTSE	STAR-LM	HE	STAR-LM	HTSE
Subcooled	Condenser	7	1.8	14	3.6	27	**7.0**	6	1.6
Two-Phase	Boiler	5	0.40	11	0.86	29	**2.3**	4	0.31
Superheated	HX1	6	2.2	12.4	**4.5**	1.4	0.50	5	1.8

*Based on coolant with specific heat and heat transfer properties of PbBi

Table 5-26 HTSE Water Heat Exchanger Time Constants from 300 MWt STAR-LM Once-Through Steam Generator.

	Shell Structure (s)	Tube Structure (s)	Water in Contact with Shell (s)	Coolant in Contact with Tube* (s)
Condenser	179	14	**30**	0.4
Boiler	42	1.8	**20**	0.4
HX1	417	**35**	1.3	0.4

*Based on coolant with specific heat and heat transfer properties of PbBi

5.5.1.4 Reactor Core

The thermal response behavior of the VHTR core is represented by the model for heat transfer of Section 5.3.4.1. This model assumes the annular unit cell shown in Figure 5-3. Two types of calculations were performed. The first calculation estimates the thermal time constant and the energy capacitance of the core. It is based on the values of unit cell geometry parameters calculated from design data in Table 5-2. The calculation of heat transfer coefficient from solid to coolant is then calculated in Table 5-27. From this Table 5-27 shows the calculation of a core thermal time constant of 9.5 s and an active core region energy capacitance of 200 MJ/C. These values are reproduced in Table 5-18.

The second calculation of core thermal response is that performed in the GAS-PASS/H dynamic simulations described in Section 5.5.5.2. The code solves the dynamic fuel pin model of Section 5.3.4.1. The data input to that calculation are taken from Tables 5-2 and 5-3.

The neutronic response of the VHTR core is represented by the models for reactivity feedback of Section 5.3.4. Two types of calculations were performed. The first calculation estimates the neutronic time constant of the core based on the model of Section 5.3.4.2.7. This calculation requires an estimate for the integral feedback parameters A, B, and C which in turn require estimates for the differential worth of control rods and for individual reactivity coefficients. The differential rod worth is calculated in Table 5-28 and control rod reactivity coefficients in Table 5-29. The remaining reactivity coefficients and the integral feedback parameters are calculated in Table 5-4. Given these values and a one-group precursor half life of $\lambda = 0.1\ s^{-1}$ and $A+B = -2.7\ \$$ from Table 5-4, the long term time constant for core power is 3.7 s. This vale is reproduced in Table 5-18.

The second calculation of reactivity feedback is that performed in the GAS-PASS/H dynamic simulations described in Section 5.5.5.2. The code solves the six-group point kinetics equations for the core power using the expression for net reactivity given by Eq. (5-89) of Section 5.3.4.2.5. The values for individual reactivity coefficients are taken from Tables 5-4 and 5-29.

Table 5-27 Thermal Time Constant and Capacitance of Fuel Element as Represented by Solid Cylinder.

Volume per Fuel Element	Exterior Volume (m^3)	Coolant Volume (m^3)	Fuel Matrix Volume, (m^3)	Graphite Volume, (m^3)
	$\sqrt{3}(0.360)^2\ 0.79 = 0.177$	$108 \cdot 0.79 \cdot \frac{\pi}{4} \cdot 0.016^2 = 0.017$	$210 \cdot 0.79 \cdot \frac{\pi}{4} \cdot 0.0127^2 = 0.021$	0.177-0.017-0.021 = 0.139
Volume per Coolant Hole	Coolant Volume, V_{cl} (m^3)	Fuel Matrix Volume, V_f (m^3)	Graphite Volume, V_c (m^3)	
	0.017/108 = 0.157e-3	0.021/108 = 0.194e-3	0.139/108 = 1.29e-3	
Mass per Fuel Element	UO_2 Mass (Kg)	UC_2 Mass (Kg)	C Mass (Kg)	
	~2350/720 = 3.26	~2350/720 = 3.26	0.139·1740 = 242	
Mass per Coolant Hole	m_{UO_2} (Kg)	m_{UC_2} (Kg)	m_C (Kg)	
	3.26/108 = 0.030	3.26/108 = 0.030	242/108 = 2.24	
Density	$\rho_{UO_2}\left(Kg/m^3\right)$	$\rho_{UC_2} \sim \rho_{UC}\left(Kg/m^3\right)$	$\rho_C\left(Kg/m^3\right)$	
	11,000	13,600	1,740	
Specific Heat	Cp_{UO_2} (J/Kg-c)	$Cp_{UC_2} \sim Cp_{UC}$ (J/Kg-C)	Cp_C (J/Kg-C)	
	300	160	1100	
Conductivity	k_C (W/m-K)	k_{He} (W/m-K)		
	80	0.37		
Thermal Capacitance per Coolant Hole	$(mC_\rho)_{UO_2} + (mC_\rho)_{UC_2} + (mC_\rho)_C$ (J/°C)			
	0.03·300+0.03·160+2.24·1100 = 2500			
Equivalent Radius of Solid per Coolant Hole	L (m)	$V = V_C + V_f$ (m^3)	$r = \left(\frac{V}{\pi L}\right)^{1/2}$ (m)	
	0.79	(1.29+0.194)e-3 = 1.48e-3	0.024	

Table 5-27 Thermal Time Constant and Capacitance of Fuel Element as Represented by Solid Cylinder (cont'd).

Coolant Heat Transfer Coefficient	$(Re)_{He}$	$(Pr)_{He}$	D_{cl} (m)	$h_{cl} = \frac{k_{He}}{D_{cl}} 0.023\ \mathrm{Re}^{0.8}\ \mathrm{Pr}^{0.3}$ (W/m^2-C)
	41,000	-1	0.016	2600
Effective Heat Transfer Coefficient (J/s-m-C)	$h = \left(\frac{r}{4k_C} + \frac{1}{h_{cl}} \right)^{-1}$			
	$\left(\frac{0.024}{4.80} + \frac{1}{2600} \right)^{-1} = 2200$			
Fuel Element Time Constant (s)	$\tau = \frac{\rho V C_p}{2\pi\, rhL}$, (s) Eq.(x)			
	$\frac{2500}{2\pi \cdot 0.024 \cdot 2200 \cdot 0.79} = 9.5$			
Active Core Energy Capacitance (J/C)	$\left[\left(mC_\rho\right)_{UO_2} + \left(mC_\rho\right)_{UC_2} + \left(mC_\rho\right)_C \right] \cdot N_{holes} \cdot N_{elements}$			
	$2500 \cdot 108 \cdot 720 = 200\text{e}6$			

Table 5-28 Upper Bound for Differential Worth of Operating Control Rods for GT-MHR.

Number of Operating Control Rods[a] i.e., outer neutron control	36
Upper limit on worth per rod[b] ($)	0.5
Absorber length of Operating Control Rod[c] (in/m)	229/5.8
Worth per absorber per unit absorber length ($/m)	0.5/5.8=0.086
Combined worth of Operating Control Rods per unit absorber length ($/m)	0.086(36) = 3.1

[a] Startup control rods are withdrawn before criticality: p.4-5 and p. 4-12 of [Shenoy 1996].
Operating control rods are inserted to varying heights during operation: p.4-22 of [Shenoy 1996].
[b] Each control rod has its own independent drive: p.4-26 of [Shenoy 1996]. Any single drive, for safety reasons, should be limited to less then one dollar.
[c] Figs. 4.1-12, 4.1-13, and 4.2-2 [Shenoy 1996]. Scaled from these figures.

Table 5-29 Deviation of Control Rod Reactivity Coefficients for VHTR.

Operating Control Rods -Vessel Length, L (m) (hot duct to top of core) Steel coefficient of thermal expansion, β (m/m/C) Differential worth, dρ/dL ($/m) [Table 5-28] $\alpha_{cr\text{-}v}$ [Eq. (3-67)] ($/°C)	437·2.54e-2 =11.1 1.5e-5 3.1 11.1·1.5e-5 ·3.1 = 5.2e-4
Operating Control Rods - Moderator Length[a], L (m) (active core height), Graphite coefficient of thermal expansion, β (m/m/C) Differential worth, dρ/dL ($/m) [Table 5-28] $\alpha_{cr\text{-}m}$ [Eq. (3-67)] ($/°C)	7.93 0.3e-5 3.1 -7.93·0.3e-5 ·3.1 = -0.74e-4

[a] p.30 of [MacDonald 2003]

5.5.1.5 Process Heat Pipes

Dimensions for the pipes to and from the HTSE process are for FLINAK and a distance of 90 m.[Lillo 2005] Data is given in Table 5-30. Time constant and energy capacitance values calculated there are reproduced in Table 5-18.

Table 5-30 Time Constants and Energy Capacitances of Coolant and Wall of Pipes to/from HTSE Plant.
FLINAK and separate hot/cold legs.

Pipe Dimensions	Length, L (m)	Inner Radius, r_i (m)	Outer Radius, r_o (m)	Flowrate, w (kg/s)	Velocity, v (m/s)		
	90	0.065	0.079	133	5.3		
Coolant	μ (Pa-s)	C_p (J/C-kg)	k (W/m-C)	ρ (kg/m^3)	*Re*	*Pr*	$h_{cl} = \frac{k_{He}}{D_{cl}} 0.023\ \mathrm{Re}^{0.8}\ \mathrm{Pr}^{0.3}$ (W/m^2-C)
	1.62E-03	1905	0.8	1880	8.0E05	3.9	1.1E04
Structure	k (W/m-C)	C_p (J/C-kg)	ρ (kg/m^3)				
	25	500	8000				
$\frac{1}{h} = \frac{\Delta t}{2k} + \frac{1}{h_{cl}}$ (W/m^2-C)	2700						
Time Constants and Energy Capacitances	$\tau_s = \left(\frac{\rho \Delta t C_p}{h} \right)_s$ (s)	$\tau_{cl} = \frac{\left(\rho V C_p\right)_{cl}}{\left(w C_p\right)_{cl} + hA}$ (s)	$\left(\rho V C_p\right)_s$ (MJ/C)	$\left(\rho V C_p\right)_{cl}$ (MJ/C)			
	21	12	2.3	4.3			

5.5.1.6 Overall Plant

Expressions for time constants and energy capacitances were derived in Section 5.3 and evaluated for the major components in Section 5.5.1. The results are summarized in Table 5-18 and are used in the following subsections to draw some preliminary conclusions.

Some simple observations are made. The reactor and PCU vessel walls have very large thermal capacitances (1000 MJ/C) but the time constant for these components as they interact with the helium coolant is almost an hour. Thus, upset events of the order of several minutes, these capacitances will not be particularly active. However, during startup this capacitance will be important. It will not be important for operational transients since the vessel walls are maintained at constant temperature.

The overall time response of the contents of the reactor vessel is largely a function of the fuel. The neutronics are essentially quasi-static compared to the fuel (3.7 s versus 9.5 s) while the fuel energy capacitance (200 MJ/C) is large. Judging from the physical space occupied by the fuel in the reactor vessel, it would appear to be greater than all other structure energy capacitances that are faster than a few tens of seconds. The helium coolant is insignificant (4.7 MJ/C) compared to the fuel.

In the HTSE plant the energy capacitance of the electrolytic cells (270 MJ/C) is almost a factor of ten greater than all the other components combined (~30 MJ/C). The time constant (206 s) is also roughly ten times greater than the other components (12-35 s). However, since the electrolytic cells are essentially downstream of the process heat components of the HTSE this heat capacity will have little effect in dampening a transient there. It does mean that rapid transients (seconds) in that part of the plant will be muted in their impact on electrolytic cell temperature. Essentially, with the process heat components operating at a power level of 50 MW small transients will be limited in the rates of temperature change they can induce in the electrolytic cells. Similarly, with the electrolysis process depositing only about 10 MW of thermal energy in the cells, transients in the electric generating part of the plant will result in limited rates of temperature change in the cells.

5.5.2 Plant Startup

A preliminary procedure for bringing the combined plant up to full power from cold subcritical is given in Table 5-31.

The time taken to reach full power is limited by the reactor power input to the combined plant and the heat capacity of the combined plant. Table 5-18 suggests that the total heat capacity is of the order 3000 MJ/C. Suppose the reactor power is raised linearly from 0 to 600 MWt and half of the heat is rejected to the heat sink. If the plant is at room temperature and on average is raised to the core mid-plane temperature at full power, then the time taken is

$$3000E06(J/C) * 700 (C) / (600E6(J/s) * 0.5 * 0.5) = 14{,}000 \text{ s}$$

or about four hours.

However, the time rate of change of temperature in thick structures such as the wall of the reactor and PCU vessels may have to be limited to achieve acceptable thermal stresses. There may be a similar consideration for the pressure boundary for the electrolytic cells which operate at high temperature and pressure. Thus, a startup time of four hours is a lower bound.

Table 5-31 Preliminary Startup Procedure for Representative VHTR/HTSE Plant Configuration.

Combined Plant Operating Mode	Sequence of Control Actions	Terminal condition
Reactor to Hot Critical	-	Subcritical core, cold and atmospheric pressure primary system
	Add inventory	Subcritical core, cold and uniform partially pressurized primary system
	Turning gear on	Subcritical core, hot and non-uniform partially pressurized primary system
	Add rod reactivity	Critical core, hot and non-uniform partially pressurized primary system
Ascend to House Electric Load	Add rod reactivity, turn on coolers, decouple turning gear	Plant self-sustaining as a heat engine
	Add rod reactivity	Increase turbomachine speed to match grid frequency
	Synchronize to grid and raise power to equal house load	Reactor at about 3 % load
	Turn on molten salt heaters	Thawed hydrogen plant heat transport loop
Ascend to House Thermal Load	Startup PH and SHX1 compressors	Two-phase region in boiler
	Increase reactor power, increase flow of PH and SHX1 compressors, turn on water pump	Saturated steam delivered to electrolyzer
Ascend to Bottom of Operating Range	Startup SHX2 compressor	Superheated steam delivered to electrolyzer
	Increase reactor power. Deliver electric power to electrolyzer.	Electrolyzer at temperature at bottom of operating range
Ascend to Full Power	Follow combined plant load schedule to full power condition: Inventory Control for reactor, Flowrate Control for HTSE plant	HTSE plant at full power hydrogen production

5.5.3 Step Change in Hydrogen Production

5.5.3.1 Electrolyzer Response

The electrolyzer output quantities (species concentration, structure temperatures, and temperatures of gas streams) respond to changes in cell inlet conditions (current and inlet temperature) to the first order on a time scale given by the cell time constant. An expression for the time constant is given in Section 5.3.1 and an estimate for its value is given in Table 5-15. One sees that it would take about ten minutes for the cell to reach a new equilibrium state if equilibrium conditions were defined as being reached three time constants after a step change in input conditions. However, this is the inherent response of the cell. The adjustment of the output conditions to a change in inputs could be accelerated through manipulation of the inputs by a controller.

5.5.3.2 HTSE Plant Response

In addition to partial power steady-state operation, a power reactor is typically designed to be able to meet an instantaneous change in generator power of ten percent. The initial and final states are given by the load schedule. However, in the interim, dynamics are excited and the plant deviates from equilibrium. The transient behavior is obtained from a dynamic simulation. However, a measure of the deviation can be estimated using the method of Section 5.2.2.

The load change considered is a ten percent step increase in hydrogen demand for the HTSE plant of Figure 5-6. It is assumed that the reactants from Compressor 1 and Pump 2 up to the Cell 11 inlet and the products from the Cell 1 output to Condenser 3 increase by this amount. All other flowrates in the combined plant and the electric power to the cell are assumed to remain constant. Of interest is the rate at which temperatures in the HTSE plant change before the control system acts to bring control variables into agreement with the load schedule for the new hydrogen production level.

Inspection of Figure 5-6 reveals that the HTSE equipment components containing either water and/or cell products are all tightly coupled thermally to each other. The two recuperating heat exchangers are responsible. An approximate estimate for the rate of temperature change throughout these components (condenser, boiler, HX1, HX2, cell, and turbine) is obtained from Eq. (5-7). Before the load change the thermal power provided by PHX1 and PHX2 is 50 MWt while the thermal output from the electrolyzer is about 10 MWt. The energy capacitance from Table 5-18 is 270 MJ/C for the electrolyzer and about 30 MJ/C for the other components. The temperature rates of change amongst the components for a ten percent change in power will from Eq. (5-7) range from 0.02^{o} C/s (=0.1*60/300) to 0.17^{o} C/s (=0.1*50/30).

In summary, the rate of temperature change in each component will be limited to less than 0.2^{o} C/s. This is about a factor of five below rates (1^{o} C/s) that might lead to accumulated fatigue at the tube sheet in a large (hundreds of MW) tube and shell heat exchanger operating at 500^{o} C. The HTSE heat exchangers are smaller (tens of MW) so temperature rates of change would have to be greater yet than 1^{o} C/s to create a fatigue problem. The exception may, however, be HX2 which operates at an outlet temperature of 850^{o} C.

5.5.4 Reactor Trip

A reactor trip would be followed by an automatic runback in primary flowrate to avoid thermal shock to the hot side components in the primary loop and intermediate loop. The generator would automatically disconnect from the grid since it would not be able to meet grid demand. The result is that the electrical power to the electrolyzer and the thermal power to the HTSE plant would drop to near zero. In the

scenario envisioned the molten salt line to the HTSE plant would no longer be heated but would still be in thermal contact with the boiler water inventory. Unless isolated, the water would continue to boil draining heat from the lines possibly causing the salt to freeze.

5.5.4.1 Molten Salt Process Heat Loop Response

The issue is how much margin to freezing would remain if the boiler were not isolated? A simple calculation provides some insight. For the boiler volume computed from data in Tables 5-23 and 5-24 and an assumed void fraction of 0.667, the resulting inventory is capable of removing approximately 300 MJ of energy through the latent heat of vaporization. Based on an initial sizing of the boiler the latent heat of vaporization of the water inventory is approximately 300 MJ. (Note this differs from the value in Table 5-18 which applies only about an operating point.) Table 5-18 shows the molten salt lines represent about 14 MJ/C of heat capacity. Thus, the water inventory could lower the average temperature of the molten salt lines by about 20^{o} C, probably not enough to freeze all the salt. Depending on the nature of the gravity head in the molten salt line, local freezing near the boiler might be averted by maintaining natural circulation in the molten salt circuit with the boiler acting as a heat sink.

5.5.5 Loss of HTSE Heat Sink

5.5.5.1 Reactor Response

General stability criteria for an at-power core coupled to a heat sink were developed in Section 5.2.5. Essentially three criteria must be met, one of which relates the perturbation to core outlet temperature resulting from a temperature perturbation at the inlet. A necessary condition for the reactor to tend toward stable operation is that the core temperature feedback processes attenuate the effect of an inlet temperature perturbation on the outlet temperature of the core. Eq. (5-12) provides an expression for the degree of attenuation.

The magnitude and sign of the attenuation of inlet temperature perturbation was calculated for the VHTR core. The quantity in parenthesis in Eq. (5-12) was evaluated at full power conditions. Table 5-28 presents the estimate for rod differential worth. Normally the Operating Control Rods are inserted into the top of the core to maintain criticality. An increase in vessel temperature causes the rods to be move upward relative to the top of the core adding reactivity. An increase in fuel element temperature causes the core length to increase effectively causing the rods to move further into the core adding negative reactivity. The reactivity coefficients associated with these differential expansions are derived in Table 5-29. The attenuation coefficient of Eq. (5-12) is calculated in Table 5-4. It has a value of -0.042 indicating near complete attenuation at the outlet of temperature perturbations arising at the inlet. On the basis of this one would expect the VHTR core coupled to a heat source to be very stable with respect to neutronic power.

Another stability assessment was made by comparing the values of two parameters identified in [Depiante 1994] as being important for controlling stability. These parameters and their values appear as the last two entries in Table 5-4. Figure 5-16 shows these values plotted on a stability map taken from [Depiante 1994]. According to this map the core power again is stable with respect to coupling to a heat sink. Note that in Figure 5-16 the x and y axis parameters are the same as the second last and last entries, respectively, in Table 5-4.

These stability criteria are probably of greater significance for coupling to the Sulfur Iodine (SI) plant compared to the HTSE plant. Consider first the case of the HTSE plant. More than 90 percent of the VHTR core thermal power is delivered to the PCU. The coupled neutronic and thermal feedback processes in the core have a combined time constant of about 10 s (Table 5-18) while the transit time from the core outlet through the IHX and through the turbine and recuperator of the PCU and back to the

core inlet is estimated to be about 10 s based on an estimated helium volume of 700 m^3 and a mass flowrate of 320 kg/s. This comparatively short transit time means the opportunity for out of phase behavior is minimized. While the thermal power delivered to the HTSE plant has a propagation time through the outbound and inbound pipes of the order 25 s (Table 5-18) and thus would tend to promote oscillations, the power is only a few percent of the total core power. Hence, the reactor inlet temperature perturbation introduced through this path will be small and not a strong source of instability. Next consider the SI plant. This heat sink consumes almost all the core thermal power while the propagation time through the outbound and inbound pipes to the hydrogen plant cited above is significantly longer than the 10 s core time constant. Thus, stability issues will be more pronounced for the VHTR coupled to the SI process compared to the HTSE process.

Future work should examine the more general case of reduced primary flowrate to characterize how attenuation represented by Eq. (5-12) is changed. The transit time through the PCU will increase to a value that exceeds the core power time constant violating one of the three stability criteria.

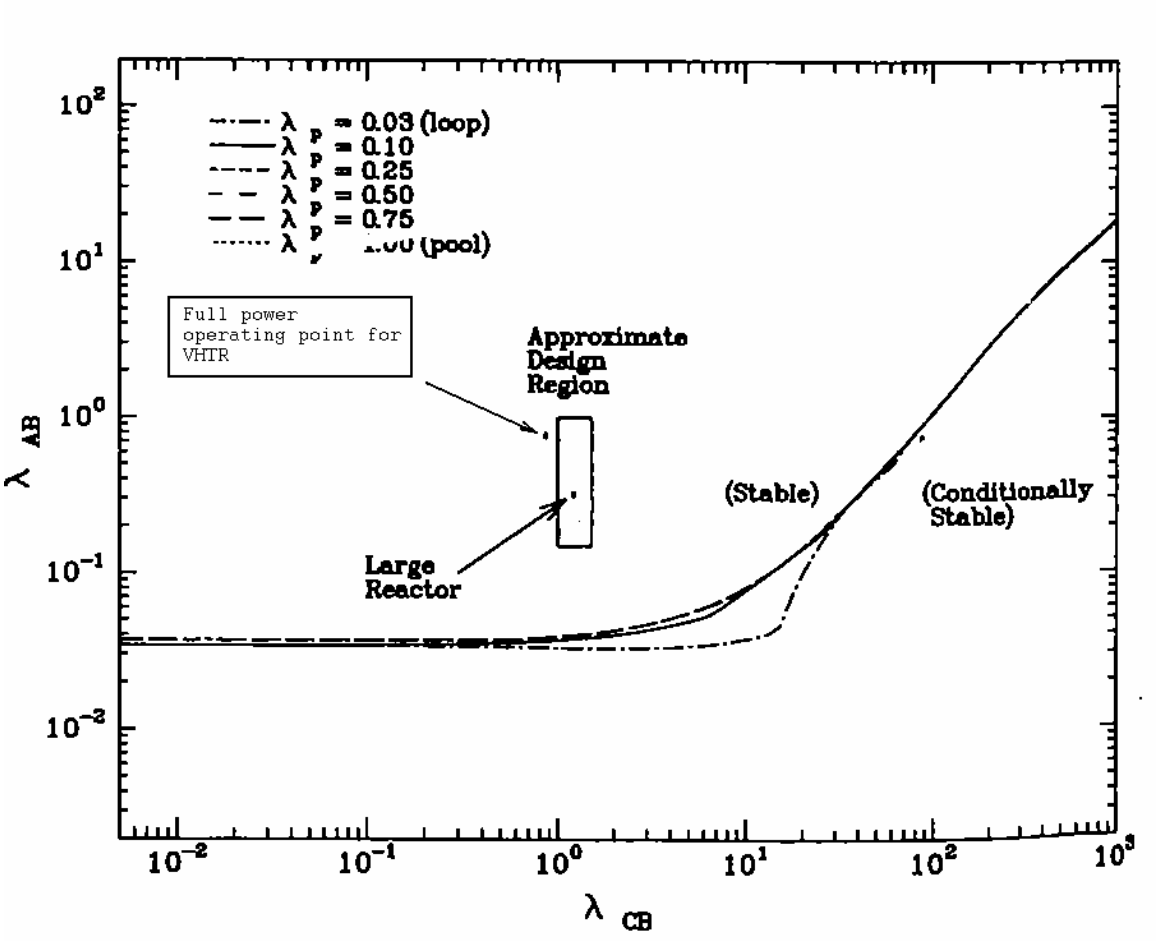

Figure 5-16 Stability Map for Inlet Temperature Perturbations Showing Location of VHTR Core.

5.5.5.2 Indirect Cycle Primary System Response

As described earlier the stability of the combined reactor-chemical plant depends on several factors. These include the dependence of core neutronic power on temperature reactivity feedbacks, the coupling of the core to the heat sink via the intermediate heat, and the time for a perturbation in core outlet temperature to propagate back to the inlet to the core. The analysis of the Section 5.2.5 addressed only temperature feedback, in a quasi-static setting, and the accompanying tendency to either attenuate or amplify the passage of perturbations in reactor inlet temperature through the core. A more complete indication of plant stability for the VHTR-HTSE is obtained by including all three phenomena in a dynamic simulation. This section describes results obtained using the GAS-PASS/H dynamic systems code.[Vilim 2004]

In developing an understanding of the time behavior of the plant the manner in which the time lag is represented in the simulation is important. In the VHTR-HTSE reference design there are three components to the propagation of a temperature front from core outlet to inlet. They are, starting at the reactor outlet,: the circulation time around the primary system, the circulation time out through the IHX and through the PCU and the return back through the IHX, and a similar circulation path through the IHX but this time through the hydrogen process heat loop. With all three time lags acting simultaneously, the role attributable to each of these paths in the integrated plant behavior is somewhat obscured. A clearer picture is obtained by introducing a simplified representation. A single time lag between the core outlet and inlet captures the essence of all three components. A measure of stability is obtained by varying this parameter and observing the tendency for outlet temperature and power time variations to be naturally damped.

The plant configuration simulated is shown in Figure 5-17. It contains the main features of the closed-loop indirect Brayton cycle of the reference design which are a closed-loop primary system coupled to a heat sink through an intermediate heat exchanger. In the simulation the inlet to the cold side of the heat exchanger is driven by a temperature forcing function used to represent a perturbation that originates in the PCU or HTSE plant. The perturbation upon reaching the heat exchanger passes through it, enters the core, and potentially initiates under-damped oscillations at the reactor outlet. The outlet temperature perturbation makes its way to the core through the three different paths described above. Each has a characteristic time. A single mixing volume between the core outlet and inlet to the hot side of the heat exchanger is used to represent the associated delay.

In addition to the transport time delay, other phenomena important for reactor-heat sink dynamic behavior are included in the simulation. These include 1) the storage of mass and energy in the coolant in the core channels and the hot and cold sides of the intermediate heat exchanger. Data used in the simulation for this heat exchanger are given in Table 5-16. 2) The storage of energy in the fuel and graphite. Data used in the simulation are given in Table 5-2. 3) Reactivity as a function of temperature. Data used in the simulation are given in Table 5-4. 4) A six-group point kinetics model driven by individual temperature feedback components.

Simulations were performed for a near-step increase in temperature at the inlet to the cold side of the intermediate heat exchanger. The forcing function is shown in Figure 5-18. The magnitude of the temperature increase resulted in an asymptotic decrease in core power of 50 MWt without active reactivity addition (i.e. control rod movement) which equals the full power heat input to the HTSE plant. The temperature increase was purposely selected to correspond to a complete loss of the HTSE plant as a heat sink. The results for a 20 s mixing volume time constant appear in Figure 5-19 through 5-23. The coolant, graphite, and fuel average temperature are shown in Figure 5-19. The reactivity components are shown in Figures 5-20. The reactor power appears in Figure 5-21. The outlet temperature of the core and of the mixing volume is shown in Figure 5-22. Figure 5-23 shows the change in core outlet temperature

versus change in core inlet temperature. The inherent stability of the reactor is reflected in the change in reactor outlet temperature versus the change in reactor inlet temperature. The reactor response is considered stable if the outlet temperature is damped and in-phase with the inlet temperature.

Propagation of H_2 Plant Temperature Disturbance in Combined Plant

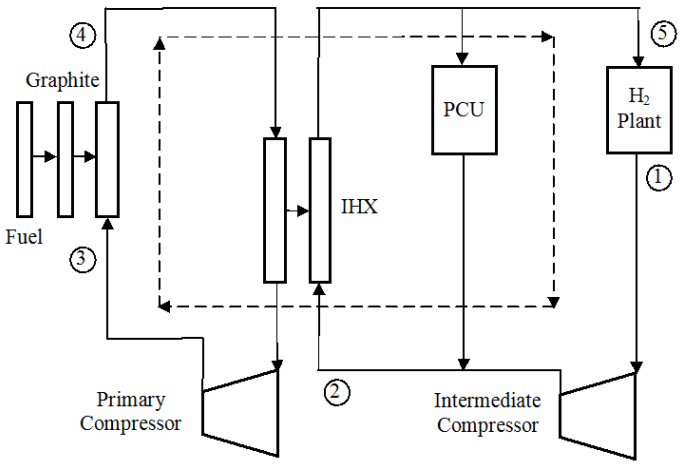

Canonical Representation of Combined Plant with Surrogate Path Delay

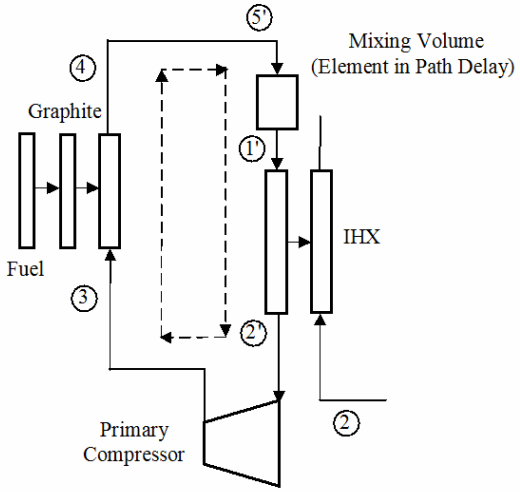

Points along Path of Propagation

① Initial temperature perturbation

② Perturbation enters IHX

③ Perturbation enters core

④ Phased-lagged perturbation exits core

⑤ Perturbation returns to H2 plant

Path Delay with Potential to Create Instability

④ - ⑤ - ① - ② - ③

Surrogate Path Delay for Investigation of Stability

④ - ⑤' - ①' - ②' - ③

Figure 5-17 Plant Configurations Appearing in Assessment of Combined-Plant Stability

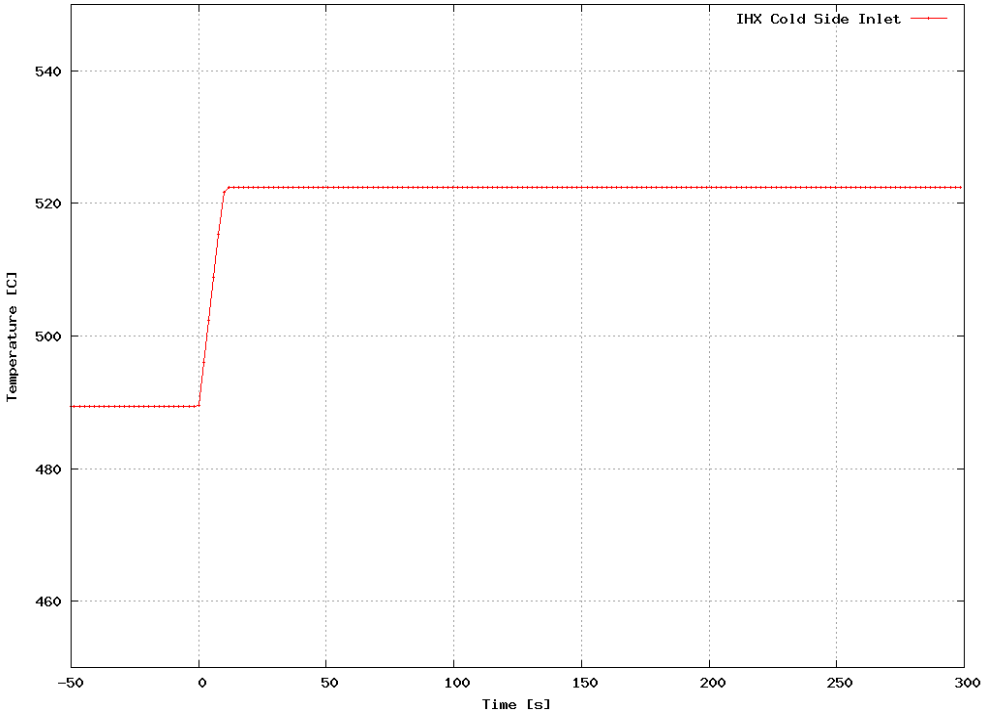

Figure 5-18 Inlet Temperature to Cold Side of IHX – Forcing Function for Stability Investigation.

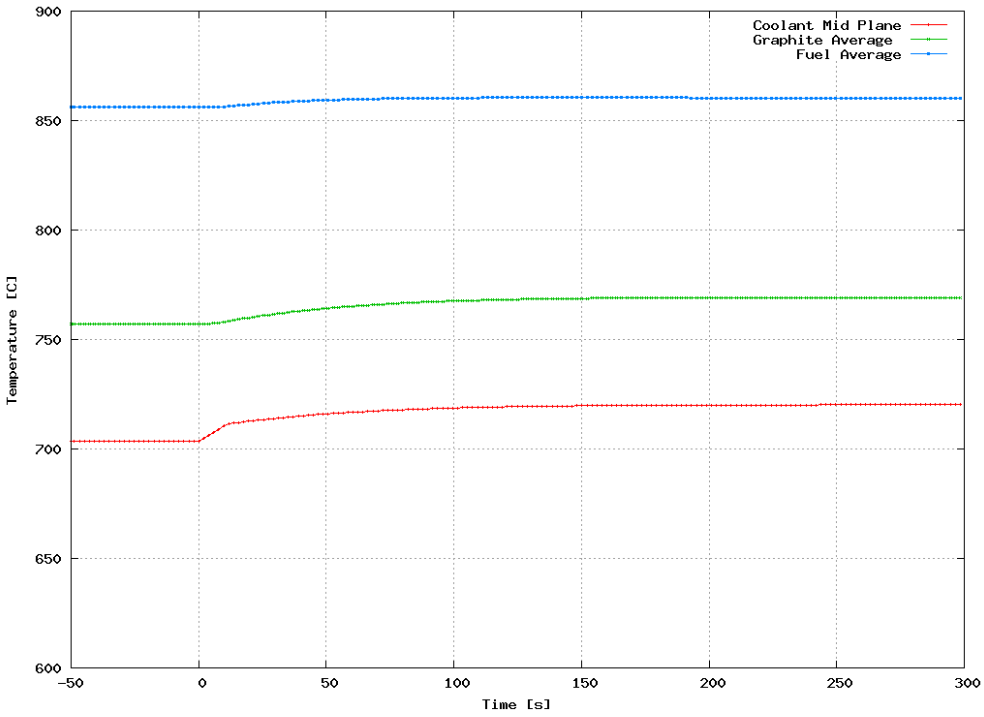

Figure 5-19 Core Temperatures for 20 s Mixing Time Constant.

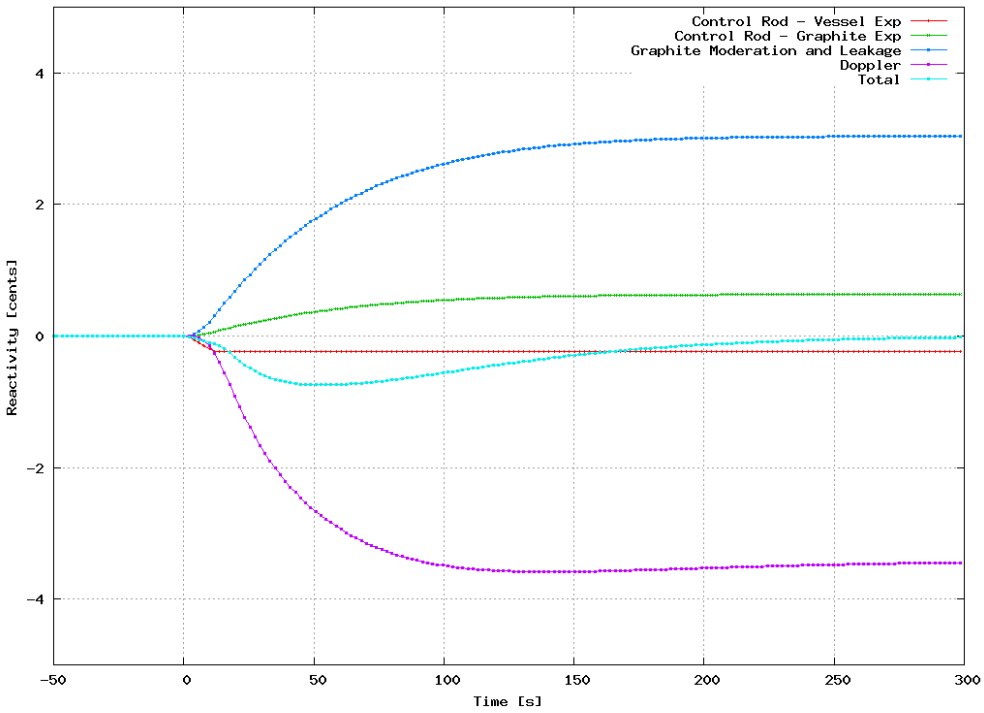

Figure 5-20 Reactivity Components for 20 s Mixing Time Constant.

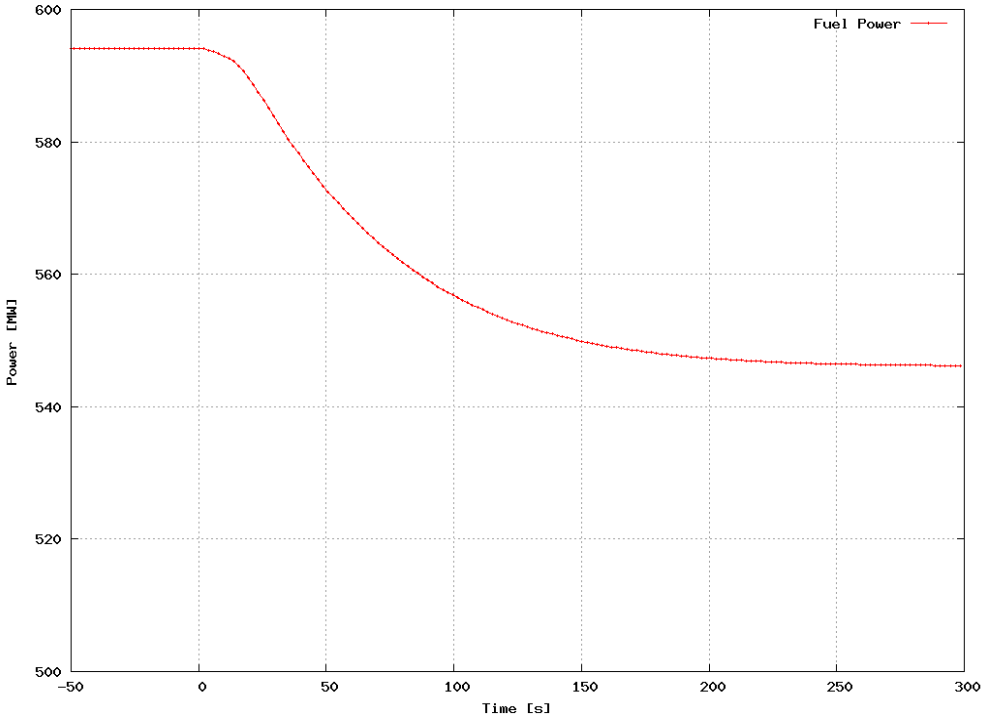

Figure 5-21 Reactor Power for 20 s Mixing Time Constant.

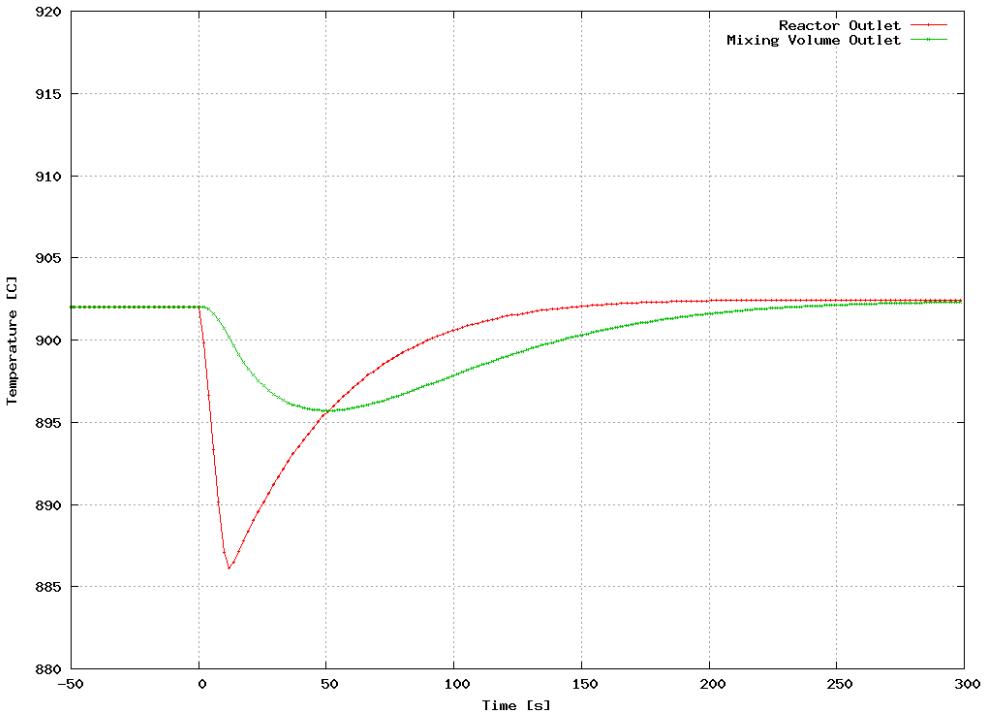

Figure 5-22 Core Outlet and Mixing Volume Outlet Temperatures for 20 s Mixing Time Constant.

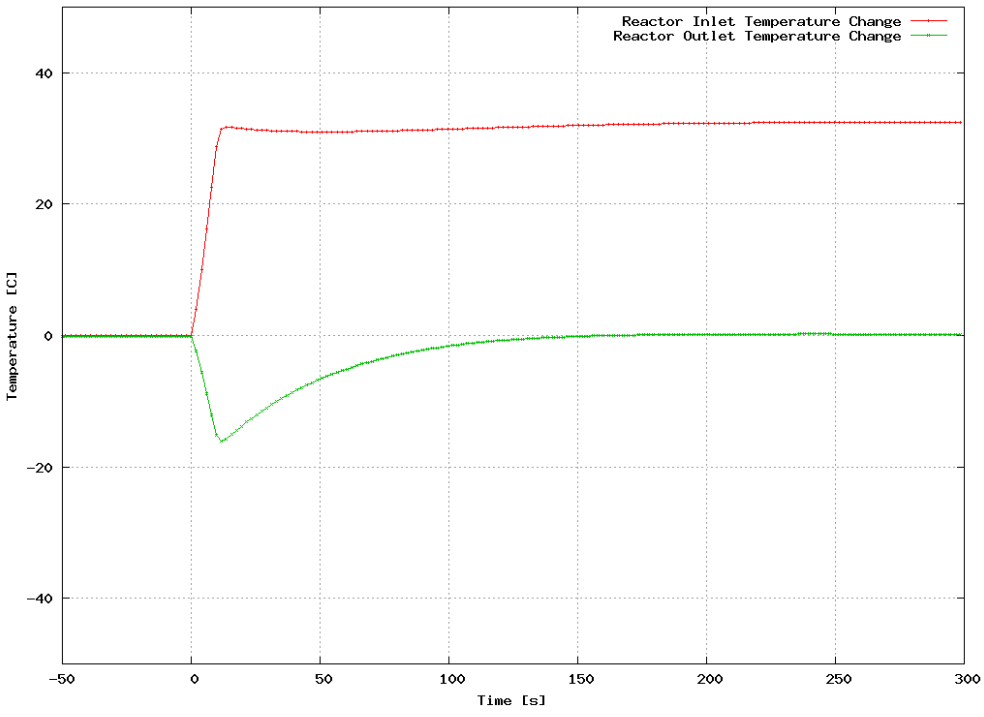

Figure 5-23 Change in Core Inlet and Outlet Temperatures for 20 s Mixing Time Constant.

The potential for instability was investigated across a broad range of outlet-to-inlet transport delays. Simulations of the VHTR response to the forcing function in Figure 5-18 were performed for mixing volume time constant values of 5, 50, and 500 s. Figure 5-24 shows the change in core outlet temperature versus change in core inlet temperature for these three values. The corresponding inherent power response (i.e. not control rod motion) appears in Figure 5-25.

The dynamic simulation results indicate temperature perturbations originating in the HTSE plant will not give rise to unstable reactor behavior. Instead, the reactor response is very stable. Figure 5-24 shows that in the long term the reactor outlet temperature reverts back to its original value before a step change in cold side IHX inlet temperature was imposed. In the short term, Figure 5-24 shows the temperature perturbation at the core inlet is attenuated by at least a factor of two in passing through the core and that the resulting perturbation exiting the core is almost completely attenuated by the IHX before return to the core inlet. This is true for delay times of five through 500 seconds. Figure 5-25 shows the core power is essentially unaffected by the size of the delay. Thus, sustained out-of-phase oscillations between core inlet and outlet temperature do not appear likely in the VHTR-HTSE at full power conditions for nominal values of reactivity feedback coefficients. A large Doppler reactivity component, three times greater than next reactivity component per unit temperature, is mainly responsible. Future work should investigate the sensitivity of this result to variation in the values of reactivity feedback parameters and for partial power conditions, particularly at low mass flow rates.

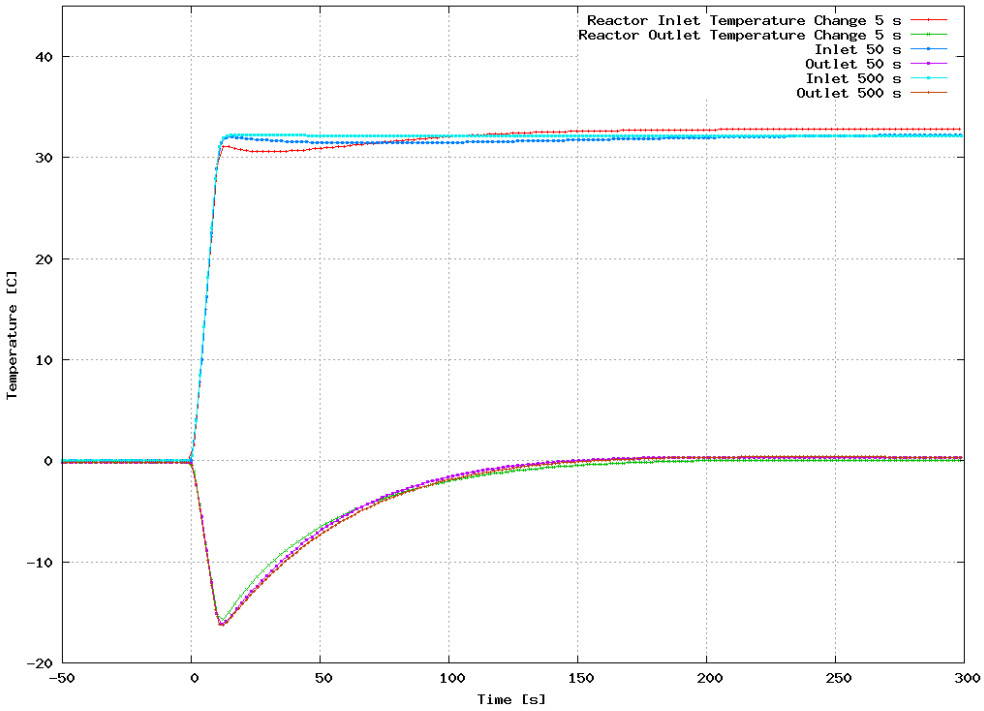

Figure 5-24 Change in Core Inlet and Outlet Temperatures as a Function of Mixing Time Constant.

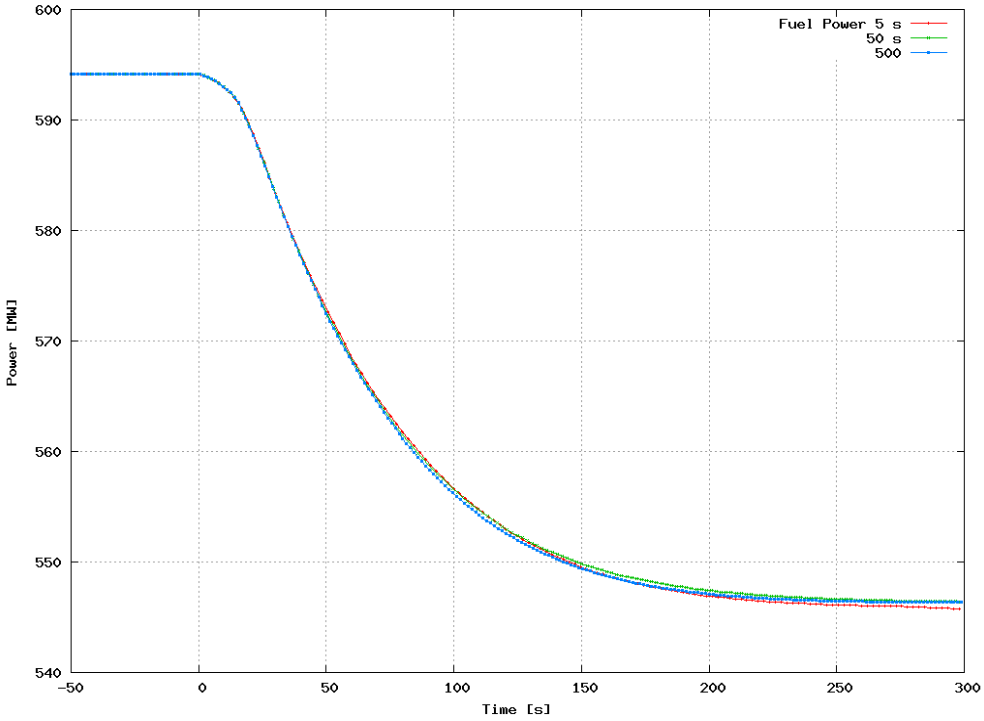

Figure 5-25 Power in Fuel as a Function of Mixing Time Constant.

5.6 Summary

Nuclear-hydrogen will need to compete on three fronts: production, operability, and safety to be viable in the energy marketplace of the future. In this section we examined the operability of a nuclear-hydrogen plant while production was examined in Section 3. Safety is to be addressed in future work. Plant operability is the degree to which time varying production demands can be met while staying within equipment limits. Criteria for gauging operability were developed and applied to one of the two reference DOE/INL plants for hydrogen production, the Very High Temperature Reactor coupled to the High Temperature Steam Electrolysis process.

The degree of operability inherent in the reference plant was characterized in terms of the underlying physical processes. The description included the role of individual component time constants and energy capacitances and the inherent relationships among process variables including reactivity versus temperature and properties of near-ideal gas coolants. It was shown how each of these phenomena acts to shape operability.

Prior to performing dynamic simulations some simple analytic methods involving component time constants and energy capacitances were used to characterize the dynamic behavior of the VHTR coupled to the HTSE plant. First, the time needed to start up the combined plant based on heat capacity considerations alone and assuming a linear ramp up of reactor power is about four hours. This is less than a typical startup time of 24 hours for a nuclear plant. However, in the analysis there was no consideration given for exceeding limiting thermal stresses. Second, temperature rates of change during a load change were estimated. A ten percent step change in hydrogen production rate would result in a maximum average rate of change in temperature in the hydrogen plant of less than 0.2 C/s before the control system

began to re-establish equilibrium with the rest of the combined plant. Given the relatively small size of the components in the HTSE plant and, hence, a small wall and tube sheet thickness, this rate of change does not appear to present a thermal fatigue problem. Third, the failure to thermally isolate the HTSE boiler from the molten salt process heat loop coming from the reactor following a reactor trip and its consequence for the state of the molten salt coolant was investigated. It is important to avoid freezing the salt. It appears that the temperature of the salt might be reduced by as much as 20 C. Given that there might be a couple of hundred degrees margin between the coldest point in the loop and the salt freezing temperature no large-scale freezing appears possible. Whether local freezing occurs would depend on the natural circulation characteristics of the molten salt loop. Fourth, it was found through a study of time constants and energy capacitances that rates of temperature change in the HTSE plant are largely determined by the thermal characteristics of the electrolyzer. It's comparatively large thermal mass and the presence of recuperative heat exchangers result in a tight thermal coupling between the electrolyzer and other HTSE components.

A control strategy for meeting changes in hydrogen demand at the plant fence was developed and evaluated using the GAS-PASS/H dynamic simulation code. It was assumed that the demand for hydrogen could vary from 30 to 100 percent of the full power production rate. The strategy uses inventory control in the VHTR plant and flow control in the HTSE plant to attempt to maintain constant hot side temperatures. The control scheme requires no additional pumps or compressors beyond those needed for full power operation. Active electrolyzer cell area is varied with power to counter non-linear dependence of electrolyzer joule heat on hydrogen production rate and its consequent effect on heat recuperation. In this initial simulation controlled flows were assumed to vary linearly with hydrogen production rate. The simulations show that hot side temperatures can likely be maintained near constant. However, nonlinearities in the HTSE plant will require that each controlled flow be its own function of hydrogen production rate. To the first order, this function will be linear. The means for determining these non-linear relationships was described. In future work the GAS-PASS/H code should be used to calculate them.

A dynamic simulation confirmed earlier work that suggested thermal transients arising in the chemical plant are strongly damped at the reactor making for a stable combined plant. The large Doppler reactivity component, three times greater than next reactivity component per unit temperature, is mainly responsible. This is the case even for long process heat transport times which create the potential for out-of-phase oscillations in temperature at the reactor inlet and outlet.

It is noted that plant specifications for meeting hydrogen production demand rates at the plant fence will dictate the operational control strategy. Thus, a good understanding of the hydrogen market that the plant will serve is needed. Systems integration studies should in the future attempt to define a set of demand requirements a plant must meet. These would be based on projections for hydrogen demand on a daily, weekly, yearly, and geographic basis; and the role of local storage in mitigating the impact of temporal swings in hydrogen demand on plant operation.

6. Conclusions

In the HyPEP project we are investigating the production, operability, and safety aspects of using nuclear power for generating hydrogen. Two DOE/INL reference systems serve as baselines for comparing design options and features with respect to these three elements. In FY07 production and operability were investigated for one of these designs, the Very High Temperature Reactor coupled to the High Temperature Steam Electrolysis process. Modeling work was initiated for the second design; the Very High Temperature Reactor coupled the Sulfur Iodine process.

To facilitate the characterization of production the HyPEP code is being developed. Efficiency and capital cost estimates will be generated by this code permitting an assessment of the economics of production. The beta version is scheduled to be completed in October 2007. Major work completed includes development and installation of the numeric scheme for the flow network and the component model developments. Testing of various basic aspects of the numerical scheme are being carried out such as the test of correct system build-up and pressure matrix set-up, smoothness of the property calculation routines, and the accuracy of the matrix solver, etc. A number of independent programs, such as Gauss elimination accuracy testing program, and 3-dimensional gas property visualizer, and HyPEP imbedded programs such as SolverDisplay unit and the LayoutInformation unit have been developed. These programs will be useful in the verification and validation of HyPEP in the third year. Currently all the major concepts for GUI have been explored, demonstrated, and installed in the HyPEP program.

A number of calculations were performed with the HYSYS code to determine the dependence of hydrogen production efficiency on plant configuration and working fluids. Of the 51 different systems studied, the maximum system efficiency was obtained for a reheat cycle with Flinak-CO_2-Flinak in the primary, secondary and ternary loops, respectively. A system efficiency of 50.64 percent was calculated. However, an economic analysis is needed to balance high efficiency against capital costs.

The calculations also show the use of liquid Flinak almost always results in the highest efficiency for each configuration evaluated. Because the liquid phase coolant (Flinak) requires much less circulation power than a high pressure gas phase coolant the primary system pumping power is significantly reduced. The relative benefit of Flinak was larger in the primary loop than in the ternary loop, with an average increase of about 1.5% in overall cycle efficiency for the primary loop versus about 0.6% for the ternary loop. The smaller benefit of Flinak in the ternary loop was due to the relatively smaller pumping power requirements compared to the primary loop. It is not clear if the increased efficiency in either loop is worth the capital cost associated with the facilities required for keeping the salt molten during shutdown and the materials issues associated with using molten salts at high temperatures.

The direct combination of HTRC and HTSE systems was investigated as an alternative to the VHTR/HTSE system. It requires no additional steam generation loop because the steam generated in the secondary side to produce electricity is used for electrolysis as well. Therefore, the configuration of this system can be highly simplified reducing its size, complexity and capital cost. In addition the steam Rankine cycle is well proven technology. The maximum efficiency of the configurations examined was 41.6 %. This efficiency is significantly smaller than the 49 percent of the reference VHTR/HTSE system.

Parametric studies indicate that system efficiency is very sensitive to core inlet temperature. Raising core inlet temperature raises average hot-side temperature but the increase in efficiency comes at the cost of greater flow rate in the primary side, requiring higher circulator power. The overall plant efficiency is also sensitive to the efficiencies of the compressor and turbine and the effectiveness of the heat exchanger, especially at low core inlet temperatures near 500 °C. Maintaining the performance of compressor, turbine and heat exchangers is essential for maintaining an efficient hydrogen production process.

The optimum size of the intermediate heat exchanger was investigated from an economic point of view. We analytically developed an optimum sizing model on the basis of heat exchanger weight and friction loss and then applied it to the reference 600 MWt VHTR system. The effect of channel waviness enhanced the compactness and heat transfer performance, but unfavorable increased the aspect ratio. Therefore, the waviness should be carefully determined based on performance and economics. In this study, the waviness of the IHX is recommended to be between 1.0 and 2.5. Finally, we investigated the effect of working fluids, and found that using carbon dioxide instead of helium reduces the size and cost by about 20% due to the lower pumping power in spite of its lower heat transfer capability.

Prior to performing dynamic simulations some simple analytic methods involving component time constants and energy capacitances were used to characterize the dynamic behavior of the VHTR coupled to the HTSE plant. First, the time needed to start up the combined plant based on heat capacity considerations alone and assuming a linear ramp up of reactor power is about four hours. This is less than a typical startup time of 24 hours for a nuclear plant. However, in the analysis there was no consideration given for exceeding limiting thermal stresses. Second, temperature rates of change during a load change were estimated. A ten percent step change in hydrogen production rate would result in a maximum average rate of change in temperature in the hydrogen plant of less than 0.2 C/s before the control system began to re-establish equilibrium with the rest of the combined plant. Given the relatively small size of the components in the HTSE plant and, hence, a small wall and tube sheet thickness, this rate of change does not appear to present a thermal fatigue problem. Third, the failure to thermally isolate the HTSE boiler from the molten salt process heat loop coming from the reactor following a reactor trip and its consequence for the state of the molten salt coolant was investigated. It is important to avoid freezing the salt. It appears that the temperature of the salt might be reduced by as much as 20 C. Given that there might be a couple of hundred degrees margin between the coldest point in the loop and the salt freezing temperature no large-scale freezing appears possible. Whether local freezing occurs would depend on the natural circulation characteristics of the molten salt loop. Fourth, it was found through a study of time constants and energy capacitances that rates of temperature change in the HTSE plant are largely determined by the thermal characteristics of the electrolyzer. It's comparatively large thermal mass and the presence of recuperative heat exchangers result in a tight thermal coupling between the electrolyzer and other HTSE components.

A control strategy for meeting changes in hydrogen demand at the plant fence was developed and evaluated using the GAS-PASS/H dynamic simulation code. It was assumed that the demand for hydrogen could vary from 30 to 100 percent of the full power production rate. The strategy uses inventory control in the VHTR plant and flow control in the HTSE plant to attempt to maintain constant hot side temperatures. The control scheme requires no additional pumps or compressors beyond those needed for full power operation. Active electrolyzer cell area is varied with power to counter non-linear dependence of electrolyzer joule heat on hydrogen production rate and its consequent effect on heat recuperation. In this initial simulation controlled flows were assumed to vary linearly with hydrogen production rate. The simulations show that hot side temperatures can likely be maintained near constant. However, nonlinearities in the HTSE plant will require that each controlled flow be its own function of hydrogen production rate. To the first order, this function will be linear. The means for determining these non-linear relationships was described. In future work the GAS-PASS/H code should be used to calculate them.

A dynamic simulation confirmed earlier work that suggested thermal transients arising in the chemical plant are strongly damped at the reactor making for a stable combined plant. The large Doppler reactivity component, three times greater than next reactivity component per unit temperature, is mainly responsible. This is the case even for long process heat transport times which create the potential for out-of-phase oscillations in temperature at the reactor inlet and outlet.

It is noted that plant specifications for meeting hydrogen production demand rates at the plant fence will dictate the operational control strategy. Thus, a good understanding of the hydrogen market that the plant will serve is needed. Systems integration studies should in the future attempt to define a set of demand requirements a plant must meet. These would be based on projections for hydrogen demand on a daily, weekly, yearly, and geographic basis; and the role of local storage in mitigating the impact of temporal swings in hydrogen demand on plant operation.

Acknowledgement

This work was supported through the Department of Energy's ROK/US-INERI and Power Conversion Program under DOE Idaho Operations Office Contract DE-AC07-99ID13727.

References

Aspen Technology, HYSYS User's Manual, Version 2.2.2, 2001.

Bajan, A., Klaus, A.D., Heat Transfer Handbook, John Wiley & Sons, 2003.

Bertrand and Meyer, Object-Oriented Software Construction, second edition, Prentice Hall, January, 1997.

Boyack, B., et al., Quantifying Reactor Safety Margins, Application of Code Scaling, Applicability, and Uncertainty Evaluation Methodology to Large-Break, Loss-of-Coolant Accident, NUREG/CR-5249, Nuclear Regulatory Commission, December 1989.

Carstens, N., "Control Studies for Supercritical Carbon Dioxide Power Conversion Systems," Ph.D. thesis, Department of Nuclear Engineering, Massachusetts Institute of Technology, June 2007.

Davis, C.B., Oh, C.H., Barner R.B., Sherman S.R., and Wilson D.F., Thermal-Hydraulic Analyses of Heat Transfer Fluid Requirements and Characteristics for Coupling a Hydrogen Production Plant to a High-Temperature Nuclear Reactor, INL/Et-05-00453, June 2006.

Depiante, E.V., "Stability Analysis of a Liquid-Metal Reactor and Its Primary Heat Transport System," Nuclear Engineering and Design, 152, pp.261-377, 1994.

Dewson, J. J., Grady, C., HEATRICTM Workshop at MIT, Cambridge, Ma, USA., October 2nd, 2003.

Dostal, V., Driscoll, M.J., Hejzler P., A Supercritical Carbon Dioxide Cycle for Next Generation Nuclear Reactor, MIT-ANP-TR-100, 2004.

Energy Information Administration (EIA), Average Retail Price of Electricity to Ultimate Consumers by End-Use Sector, www.eia.doe.gov, 2007.

Hartvigsen J., personal communication, Ceramatec, November 28, 2006.

Hesselgreaves, J.E., Compact Heat Exchangers, Selection, Design and Operation, 1st edition, Pergamon, 2001.

Independent Technology Review Group, Design Features and Technology Uncertainties for the Next [2] Generation Nuclear Plant, INEEL/EXT-04-01816, June 30, 2004.

Kakac, S., Liu H., Heat Exchangers - Selection, Rating, and Thermal Design, CRC Press, 2002.

Kays, W.M. and London, A.L., Compact Heat Exchangers, 3rd ed., McGraw-Hill, New York, 1984

Lillo, T. M., et al., "Engineering Analysis of Intermediate Loop and Process Heat Exchanger Requirements to Include Configuration Analysis and Materials Needs," INL/EXT-05-00690, September 2005.

MacDonald, P., NGNP Point Design - Results of the Initial Neutronics and Thermal-Hydraulics Assessments during FY-03, INEEL/EXT-03-00870 Ref. 1, September 2003.

Mckellar, M.G., Optimization of a Household Refrigerator Considering Alternative Refrigerants, Ph.D. Thesis, Department of Mechanical Engineering, Purdue University, August 1992.

Nikitin, K., Kato Y., Ngo L., Printed circuit heat exchanger thermal-hydraulic performance in supercritical CO2 experimental loop, International Journal of Refrigeration, Vol. 29, pp. 807-814, 2006.

NIST Chemistry WebBook, http://webbook.nist.gov/chemistry.

Oh, C.H., Davis C.B., Han J., Barner R., Sherman S., Vilim R., Lee Y., and Lee W., HyPEP FY06 Report: Models and Methods, INL/EXT-06-11725, September 2006a.

Oh, C.H., T. Lillo, W. Windes, T. Totemeier, B. Ward, R. Moore, and R. Barner, Development of a Supercritical Carbon Dioxide Brayton Cycle: Improving VHTR Efficiency and Testing Material Compatibility, Final Report, INL/EXT-06-01271, March 2006b.

Oh, C.H., personal communication, Idaho National laboratory, November 2006c.

Oh, C.H., Kim E.S., Sherman S.R., and Vilim R.B., HyPEP FY-07 Report: System Model Integration Model Development, INL/EXT-07-12470, April 2007a.

Oh, C.H., et al., "Development of GAMMA Code and Evaluation for a Very High Temperature Gas-Cooled Reactor," 2007 International Topical Meeting on Safety and Technology of Nuclear Hydrogen Production, Control, and Management," Boston, Massachusetts, June 2007b

Ohta, T., Solar-Hydrogen Energy Systems, Pergamon Press, 1979.

Oyakawa, K., Shinzato, T. and Mabuchi I., The effect of the channel width on heat transfer augmentation in sinusoidal wave channel, JSME International Journal, Series II, Vol. 32, no. 3, pp 403-410, 1989.

Patankar, S. V., "Numerical Heat Transfer and Fluid Flow," Hemisphere Publishing, 1980.

Pradhan, S., et al., Effects of Electrical Feedbacks on Planar Solid-Oxide Fuel Cells, ASME Transactions on Fuel Cell Science and Technologies, vol. 3, issue 4, November 2006.

Shenoy, A., Gas Turbine-Modular Helium Reactor (GT-MHR) Conceptual Design Report, Report number 910720/1, General Atomics, July 1996.

Song ,Sung Chu, Thermal-hydraulic performance of a printed circuit heat exchanger in an air test loop, M.S. Thesis of Korea Advanced Institute of Science and Technology (KAIST), 2005.

Stoots, C.M., Engineering Process Model for High-Temperature Electrolysis System Performance Evaluation, Idaho National Laboratory, June 2005.

The MathWorks, Inc., Matlab User's Manual, Version 7.3, 2006.

Vilim, R. B., "Transient Response of a Natural Circulating Liquid-Metal Reactor from Time Constants and Energy Capacitances," Monitoring and Control Technologies for the Secure, Transportable, Autonomous Reactor (STAR), Nuclear Energy Research Initiative Field Work Proposal 24441, September 2001.

Vilim, R.B., "Dynamic Modeling Efforts for System Interface", ANL-07/16, Argonne National Laboratory, December 2006a.ANL-07/16,

Vilim, R.B., "GAS-NET: A Two-Dimensional Network Code for Prediction of Core Flow and Temperature Distribution in the Prismatic Gas Reactor," ICAPP 2007 International Congress on Advances in Nuclear Power, Nice, France, May 13-18, 2007a.

Vilim, R.B., "Power Requirements at the VHTR/HTE Interface for Hydrogen Production," Proceedings of ICAPP 2007 Nice, France, May 13-18, 2007.

Vilim, R.B., Argonne National Laboratory, private communication, October 2006.

Vilim, R.B., Cahalan J., and Mertyurek, U., GAS-PASS/H: A Simulation Code for Gas Reactor Plant Systems, ICAPP 2004, Pittsburgh, PA, June 2004.

Yildiz, B., K. J. Hohnholt, and M. S. Kazimi, "Hydrogen Production Using High-Temperature Steam Electrolysis Supported by Advanced Gas Reactors with Supercritical CO2 Cycles," Nuclear Technology, Vol. 155, July 2006.